XVIII CONGRESSO NAZIONALE DI SCIENZE PLANETARIE

6-10 Febbraio 2023
Sala dei Notari, Palazzo dei Priori Perugia

ABSTRACTS Book
Oral Presentations

Società Italiana Scienze Planetarie
INAF Istituto Nazionale di Astrofisica
Agenzia Spaziale Italiana
A.D. 1308 unipg Dipartimento di Chimica, Biologia e Biotecnologie
A.D. 1308 unipg Dipartimento di Fisica e Geologia
A.D. 1308 unipg Dipartimento di Ingegneria
A.D. 1308 unipg Dipartimento di Ingegneria Civile e Ambientale
PRIN 2020 BEYOND-2p
Città di Perugia
Leonardo

PROGRAMMA

6 Febbraio, Lunedì

14:00 – 15:00	**Interventi Istituzionali** Prof. Alceo Macchioni Direttore Dip. di Chimica e Biologia Prof. Diego Perugini Direttore Dip Fisica e Geologia Prof. Ermanno Cardelli Direttore Ingegneria Prof. Giovanni Gigliotti Dipartimento di Ingegneria Civile ed Ambientale Prof. Fausto Elisei Prorettore Helios Vocca Rappresentanza del Rettore Marco Tavani Presidente INAF Leonardo Varasano Assessore alla Cultura Comune di Perugia	
15:00 – 15:30	Prospettive delle scienze planetarie in Italia	Barbara Negri ASI
15:30 – 15:55	Il Programma di Esplorazione dell'ESA	Raffaele Mugnuolo ASI
15:55 – 16:10	Paving the way for the Italian community towards Mars Sample Return (MSR), the next step in Martian exploration	Francesca Altieri

16:10 – 16:45 Coffee Break

16:45 – 18:30 Sessione 1: Astrochimica - Astrobiologia 1

Chair: Maria Teresa Muscari Tomajoli

16:45 – 17:15	**INVITED TALK: From Interstellar Clouds to Planetary Systems: the Astrochemical Thread**	Cecilia Ceccarelli IPAG
17:15 – 17:30	Theoretical investigation of formation routes leading to S-bearing species in space via the reactions of electronically excited atoms	Andrea Giustini
17:30 – 17:45	Rotational spectroscopy of pyrrole: a model for astrophysical searches	Assimo Maris
17:45 – 18:00	A laboratory investigation of the reactions N(2D) + benzene and N(2D) + toluene and implications for the atmospheric chemistry of Titan	Gianmarco Vanuzzo
18:00 – 18:15	Detectability of aromatic organics in Sulfates by the Mars 2020 Perseverance rover	Teresa Fornaro
18:15 – 18:30	Survivability of Xhantoria Parietina in simulated Mars conditions for 30days	Christian Lorenz

7 Febbraio, Martedì

9:00 – 10:30 Sessione 1: Astrochimica - Astrobiologia 2

Chair: Teresa Fornaro

09:00 – 09:30	**INVITED TALK: Open questions about the origin of life: where to go in Solar System studies**	Giovanni Vladilo INAF - OaTs
09:30 – 09:45	Desert cyanobacteria: Lesson learned from astrobiology experiments in low Earth orbit and implications for future missions	Daniela Billi
09:45 – 10:00	Worldwide distribution of acidophilic extremophiles provides insight into future space biology applications	Luca Tonietti
10:00 – 10:15	Eukaryotic organisms exposed to space environment: a focus on the physiological adaptions of the brine shrimps A. Salina to astrobiological studies	M. Teresa Muscari Tomajoli
10:15 – 10:30	Evolution of climate and observational properties of a habitable rocky planet: Earth.	Laura Silva

10:30 – 11:00 Coffee Break

11:00 – 12:00 Sessione 2: Pianeti e Satelliti: Analisi Dati e Modellistica

Chair: Giovanni Munaretto

11:00 – 11:15	Microwave thermal emission from Solar System Planets and CMB calibration	Michele Maris
11:15 – 11:30	Mineralogical mapping of Ceres as revealed by the 1 µm absorption	Giacomo Carrozzo
11:30– 11:45	Volatile emission from a fracture on a planetary surface: a Smoothed-Particle-Hydrodynamics approach	Matteo Teodori
11:45– 12:00	Roughness of planetary surfaces: Hapke theory and statistical multi-facet algorithm. preliminary analysis	Andrea Raponi

12:00 – 14:00 Pausa Pranzo

14:00 – 15:30 Sessione 3: Esopianeti

Chair: Aldo Bonomo / Riccardo Claudi

14:00 – 14:15	Search for and occurrence rate of Jupiter analogues in planetary systems with short period sub-Neptunes	Aldo Bonomo
14:15 – 14:30	Cold Jupiter shaping the formation of Super-Earths	Matteo Pinamonti

	around M dwarfs	
14:30 – 14:45	Responses of Eukaryotic photosynthetic organisms from different systematic groups to a simulated M dwarf starlight	Mariano Battistuzzi
14:45 – 15:00	The GAPS Program at TNG: That strange case of the young planetary system V1298 Tau	Riccardo Claudi
15:00 – 15:15	An Exoplanet Atmosphere as Never Seen Before.	Luigi Mancini
15:15 – 15:30	The HADES Program with HARPS-N@TNG. HADES: THE HArps-n red Dwarf Exoplanet Survey	Laura Affer

15:30 – 16:00 Coffee Break

16:00 – 17:30 Sessione 4: Mercurio

Chair: Cristina Re

16:00 – 16:30	**INVITED TALK: BepiColombo first results of the Cruise phase and Fly-Byes**	Anna Milillo INAF-IAPS
16:30 – 16:45	Ca and CaO Mercury exosphere as product of micro-meteoroids and comet stream particles impact	Martina Moroni
16:45 – 17:00	Remote sensing of Mercury Sodium emission and relationship with magnetospheric activity	Stefano Orsini
17:00 – 17:15	Permanent Shadowed regions of Mercury: new hypothesis about water ice origin	Silvia Bertoli
17:15 – 17:30	Spectral detection of Water ice, S-bearing ad organic species in Mercury's PSR by SIMBIO-SYS-VIHI on the BepiColombo Mission	Gianrico Filacchione

17:45 – 18:45 Assemblea Generale della Società Italiana di Scienze Planetarie

19:30 Cena Sociale Ristorante del Sole – Via della Rupe 1

8 Febbraio, Mercoledì

9:00 – 10:30 Sessione 5: Piccoli Corpi – Results of the DART/LICIACube Mission 1

Chair: Davide Perna

09:00 – 09:30	**INVITED TALK: The Light Italian Cubesat for Imaging of Asteroids in support to the NASA mission DART**	Elisabetta Dotto and the LICIACube Team
09:30 – 09:45	Modelling the ejecta plume after the DART impact	Alessandro Rossi
09:45 – 10:00	Color analysis of Dimorphos plume produced by DART impact using Liciacube-Luke data	Giovanni Poggiali
10:00 – 10:15	Towards reconstructing the Dimorphos ejecta plume by means of non-spherical dust simulations and DART-Liciacube data	Stavro Ivanovski
10:15 – 10:30	The shape of Dimorphos as seen by Liciacube-Luke images	Angelo Zinzi

10:30 – 11:00 Coffee Break

11:00 – 12:00 Sessione 5: Piccoli Corpi – Results of the DART/LICIACube Mission 2

Chair: Angelo Zinzi

11:00 – 11:15	Bouncing Boulders: A "secondary plume" from Didymos surface observed by Liciacube-Luke camera after DART impact on Dimorphos's surface	Elena Mazzotta Epifani
11:15 – 11:30	After DART: The Didymos system in the aftermath of the DART event	Simone Ieva
11:30– 11:45	A first assessment on the origin of Didymos and Dimorphos, NASA's DART mission targets	Fabio Ferrari
11:45– 12:00	The boulder size-frequency distribution derived from DART/DRACO images of Dimorphos: Preliminary results	Maurizio Pajola

12:00 – 14:00 Pausa Pranzo

14:00 – 15:30 Sessione 6: Piccoli Corpi – Artificiali e Naturali 1

Chair: Alessandro Rossi

14:00 – 14:30	**INVITED TALK: On the synergy between Planetary Science and Space engineering in the study and exploitation of natural routes**	Elisa Maria Alessi CNR - IMATI
14:30 – 14:45	The LICIACube extended mission as an imminent	Ettore Perozzi

	impactor sentinel	
14:45 – 15:00	The NEOROCKS "Rapid-Response Experiment"	Davide Perna
15:00 – 15:15	NEOROCKS: Investigating the physical nature of the small asteroid population	Vasiliki Petropoulou
15:15 – 15:30	Analysis of spectral variability of asteroid 3200 Phaethon in preparation to DESTINY+ space mission.	Marianna Angrisani

15:30 – 16:00 Coffee Break

16:00 – 16:45 Sessione 6: Piccoli Corpi – Artificiali e Naturali 2

Chair: Simone Ieva

16:00 – 16:15	VIS-IR imaging spectroscopy of Martian Meteorites	Simone De Angelis
16:15 – 16:30	Spectroscopic and nanoscale mineralogical investigation of Ryugu returned samples	Marco Ferrari
16:30 – 16:45	ProDisCo: A Systematic Comparison Between Measured Molecular Abundances in Comets and Protoplanetary Disks	Manuela Lippi

16:45 – 18:00 Sessione 7: Meteore e Meteoriti 1

Chair: Anna Barbaro

17:00 – 17:15	Water reactivity on Schreibersite: from Phosphites to Posphates	Stefano Pantaleone
17:15 – 17:30	Multi-collector ^{40}Ar-^{39}Ar dating in planetary geosciences: dating terrestrial impact structures	Gianfranco Di Vincenzo
17:30 – 17:45	Early differentiation of planetesimals: insights from melting experiments of an L6 ordinary chondrite	Matteo Masotta
17:45 – 18:00	Glass of possible impact origin from Pica (Chile)	Gabriele Giuli

9 Febbraio, Giovedì

9:00 – 9:45 Sessione 7: Meteore e meteoriti 2

Chair: Matteo Masotta

09:00 – 09:15	Cavezzo: fall, recovery and analysis of the first Italian meteorite found by PRISMA	Daniele Gardiol
09:15 – 09:30	Carbon phases in Ureilites with increasing the degree of shock: the example of five frontier mountain Ureilites.	Anna Barbaro
09:30 – 09:45	The chondritic impactor origin of the Ni-rich component in australasian tektites/microtektites	Luigi Folco
9:45 – 10:00	The Brachinites and Brachinite-like ungrouped achondrites connection: insights from Spinels mineral-chemistry	Tiberio Cuppone

10:00 – 10:30 Sessione 8: Dischi Protoplanetari e fasi primordiali

Chair: Manuela Lippi

10:00 – 10:15	Protoplanetary disks around solar-analogues: factories of pre-biotic molecules?	Claudio Codella
10:15 – 10:30	Kinematics perturbation in the protoplanetary disk of AS 209:signature of a giant protoplanets at 100 au	Davide Fedele

10:30 – 11:00 Coffee Break

11:00 – 12:00 Sessione 9: Marte 1

Chair: Ilaria Di Pietro

11:00 – 11:15	Buried faults, Sedimentary sequences and Playa environments	Gene Walter Schmidt
11:15 – 11:30	Methane on Mars: possible geomorphic indicators of Methane emission in three impact craters	Elettra Mariani
11:30– 11:45	Application of the Minimum Noise Fraction technique to Exomars/TGO-NOMAD LNO channel nadir data: SNR enhancement evaluation	Fabrizio Oliva
11:45– 12:00	Water cycle and aerosols at Mars with the NOMAD spectrometer onboard ExoMars TGO	Giuliano Liuzzi

12:00 – 14:00 Pausa Pranzo

14:00 – 15:15 Sessione 9: Marte 2

Chair: Simone Silvestro

14:00 – 14:15	Structural mapping and stress analysis to unravel the polyphasic tectonic history of the Claritas Fossae, Mars	Evandro Balbi
14:15 – 14:30	Did MARSIS find liquid water beneath the Martian south polar layered deposits?	Roberto Orosei
14:30 – 14:45	High-resolution compositional map and subsurface investigation of a martian valley close to Olympia Planum	Nicole Costa
14:45 – 15:00	debate of the large martian ripples	Hezy Yizhaq
15:00 – 15:15	Study of the dust lifting and electrification physics by means of martian analogues	Gabriele Franzese

15:15 – 15:45 Coffee Break

15:45 – 17:00 Sessione 10: Il Sistema Gioviano

Chair: Mauro Ciarniello

15:45 – 16:00	A preliminary study of Ganymede's energetic ion environment to be investigated with JUICE	Christina Plainaki
16:00 – 16:15	Observability of Callisto's exosphere with MAJIS/JUICE	Emiliano D'Aversa
16:15 – 16:30	Combining remote sensing and laboratory analysis to search for organics on the surface of Europa	Silvia Pagnoscin
16:30 – 16:45	The Jupiter's hot spots as observed by Juno-JIRAM: limb-darkening in thermal infrared	Davide Grassi

16:45 – 17:45 Sessione Europlanet a cura di Stavro Ivanovski e Federica Duras

18:00 – 20:30 Sessione Poster – Apericena e Premiazione Poster

10 Febbraio, Venerdì

9:00 – 10:30 Sessione 11: Planetologia Sperimentale 1

Chair: Alessandro Pisello

09:00 – 09:15	Water desorption from lunar sample analogues to support the ESA PROSPECT instrument development	John Brucato
09:15 – 09:30	Dielectric spectroscopy analyses of lunar regolith simulants for the radar detection of water ice on the Moon	Chloe Helena Martella
09:30 – 09:45	Alteration of organic matter on Ceres: results from laboratory studies on the complex geo-chemical history of the innermost dwarf planet	Maria Cristina De Sanctis
09:45 – 10:00	Preliminary results on the infrared H2-H2 and H2-He experimental collision induced absorption coefficients	Stefania Stefani
10:00 – 10:15	Hypervelocity impacts on Comet Interceptor dust impact sensor and counter for dust shield and detection system assessment	Stefano Ferretti
10:15 _ 10:30	The spectral and chemical changes of atmosphere-less surfaces induced by ion bombardment	Riccardo Urso

10:30 – 11:00 Coffee Break

11:00 – 11:45 Sessione 11: Planetologia Sperimentale 2

Chair: Eliana La Francesca

11:00 – 11:15	Low temperature reflectance spectra of NH4+ minerals in the VNIR: effect of phase trasitions for planetary investigation	Maximiliano Fastelli
11:15 – 11:30	UV irradiation experiments of organo-sulfate martian analog samples to support detection of organics on Mars by the NASA MARS2020 and ESA ExoMars rovers	Andrew Alberini
11:30– 11:45	Simulating icy-world surfaces in the laboratory: NIR spectra of natron, mirabilite and epsomite dissolved in water	Daniele Fulvio

11:45 – 12:30 Candidature Consiglio Direttivo SISP; Candidature Sede Edizione 2024; Premiazione della migliore presentazione

12:30 Fine Congresso

Poster Session
Giovedì 9 Febbraio ore 18:30 – 20:30

1	The key role of silicon in astrochemistry	Matteo Michielan
2	Photo-processing and thermal desorption of acetaldehyde, acetonitrile, and water ice mixtures on olivine grains: TPD and mass spectra analyses	Maria Angela Corazzi
3	Thermal desorption of PA(N)Hs-water ice mixtures from dust grains	Valeria Lino
4	The use of the correlation matrix for Martian life detection	Andrea Meneghin
5	Combined crossed-beams and theoretical investigation of the O(3p,1d) + acrylonitrile reactions and implications for Extraterrestrial environments	Giacomo Pannacci
6	Computed binding energies distribution of relevant S-bearing species at interstellar icy grains	Vittorio Bariosco
7	Testing alternative theories of gravity with the Bepicolombo mission: the case of Brans-Dicke theory	Miriam Falletta
8	Discovery of the TOI-411 system: a super-Earth and two sub-Neptunes orbiting a bright, nearby, sun-like star	Laura Inno
9	SETI within 30 parsecs from Earth	Graziano Chiaro
10	Dart-vetter: a deep learning tool for automatic vetting of TESS candidates.	Stefano Fiscale
11	Petro-mineralogical and geochemical study of lunar meteorite NWA 13859	Riccardo Avanzinelli
12	Early differentiation of planetesimals: insights from melting experiments of an L6 ordinary chondrite	Matteo Masotta
13	The NWA12800: an extremely interesting CV3 carbonaceous chondrite	Andrea Vitrano
14	The LUMIO cubesat: detecting meteoroid impacts on the lunar farside	Fabio Ferrari
15	Meteorite-dropping bolides observation with the PRISMA fireball network	Dario Barghini
16	MIDIR spectral characterization of Ol-bearing ungrouped achondrites	Cristian Carli
17	Microscopic impactor debris at Kamil crater, Egypt: the origin of the Fe-Ni oxide spherules	Luigi Folco
18	Mineralogical characterization of the fusion crust of the Cavezzo L5 chondrite	Marianglona Rondinelli
19	Mineralogical characterization and microchemical analysis of the Alfianello, Monte Milone, and Siena ordinary chondrites.	Valeria De Santis
20	First find of ringwoodite in the Alfianello L6 ordinary chondrite	Laura Carone
21	Preliminary characterization of two Rantila fall fragments.	Anna-Irene Landi
22	Alteration fronts in reckling peak 17085 CM carbonaceous chondrite: an investigation of the aqueous alteration process in the CMs parent asteroid.	Anna Musolino
23	Geochemical characterisation and Cr isotope composition of libyan desert glasses and ordinary chondrites: preliminary data	Martina Casalini

24	VIS–MIR spectral characterization of the NWA 12184 meteorite and modifications induced by solar wind irradiation experiment	Anna Galiano
25	New impact crater catalogue of the moon based on the deep learning approach	Riccardo La Grassa
26	Martian surface photometry with TGO/Cassis: current results and future perspectives	Giovanni Munaretto
27	Dielectric properties of sodium chloride doped ice for the characterization of Europa's ice shell	Alessandro Brin
28	Unvealing the chemistry of nitriles in titan's atmosphere: the reaction of excited atomic nitrogen, N(2d), with cyanoacetylene (HC3N), acrylonitrile (C2H3CN) and acetonitrile (CH3CN)	Luca Mancini
29	Aeolian landforms in the exomars landing site, a regional perspective	Simone Silvestro
30	Ubiquity of landslides in the solar system	Maria Teresa Brunetti
31	Geological mapping and preliminary spectral analysis of mare Ingenii basin.	Gloria Tognon
32	Possible volcanic origin for "mounds" of the Hypanis fan system, Mars: magmatic vs sedimentary.	Agnese Caramanico
33	On the nature of the dark resistant unit (DRU) in the oxia planum area, Mars	Michelangelo Formisano
34	Terrestrial and martian paleo-hydrologic environments: systematic comparison by means of prisma and crism hyperspectral data	Angelo Zinzi
35	A grid of climate models for the Noachian Mars using EOS-ESTM	Paolo Simonetti
36	MESSENGER grand finale at Mercury: surface age and property characterization	Elena Martellato
37	Geological and structural mapping of the Michelangelo (H-12) quadrangle of Mercury: preliminary results	Salvatore Buoninfante
38	Geological studies with MATISSE: a Mercury surface study case	Veronica Camplone
39	Landing site characterization of Marius Hills pit (Moon): a feasibility evaluation for the ESA lunar caves CDF study.	Riccardo Pozzobon
40	The planetary mapping and GIS laboratory at INAF-IAPS.	Alessandro Frigeri
41	Geological mapping of sedimentary sequences of impact craters in Arabia Terra: a test site for standardized planetary maps.	Lucia Marinangeli
42	Clay-rich deposits in Oxia Planum and north Xanthe terra: an updated overview of the infrared data in context with ExoMars rover mission	Jeremy Brossier
43	Improvement of the MARSIS on-board SW, on the Mars Express mission. Preliminary scientific results on Phobos and Mars.	Andrea Cicchetti
44	Eolo megaripple archive: mapping the recent aeolian deposits to support the luminescence investigation on Mars	Lucia Marinangeli
45	The surface of mercury investigated by means of principal component analysis on MASCS/MESSENGER data.	Anna Galiano
46	Structural analysis of the Discovery quadrangle (H-11), Mercury.	Antonio Sepe
47	Segmentation analysis of selected lobate scarps on Mercury	Luigi Ferranti

48	LICIACube activities at ASI-SSDC: processing, calibration, archiving and analysis of images	Angelo Zinzi
49	Visible spectroscopic survey of near earth objects from the Asiago observatory in the framework of the NEOROCKS project	Monica Lazzarin
50	A database for the thermal analysis of the comet 67p	Edoardo Rognini
51	NEOROCKS: the EU H2020 programme for NEO rapid observation, characterization, and key simulations.	Elisabetta Dotto
52	Future perspectives of the NEO physical properties database by the NEOROCKS EU project	Ilaria Di Pietro
53	Search and study for meteorites analogues to Didymos in preparation to the Milani/HERA investigation.	Giuseppe Massa
54	Laboratory investigation of icy surface analogs of some solar system objects	Alessandra Migliorini
55	Visible and near-infrared spectroscopy of Mars analogues in support of the ESA's ExoMars rover mission.	Simone Filomeno
56	Reflectance spectra of mascagnite and salammoniac minerals by varying viewing geometry.	Maximiliano Fastelli
57	Using the DAVIS laboratory setup to simulate and test MA_MISS surveys on rock samples.	Lorenzo Rossi
58	Stereo validation activities for the new stereo hyperspectral pushbroom camera: HYPSOS	Cristina Re
59	Dust detector on-board Milani cubesat: VISTA FM calibration and instrument main goals in the framework of HERA mission.	Chiara Gisellu
60	The PVRG spectral database of lab-made volcanic products on the SSDC infrastucure: a new catalog of reference spectra to characterize volcanic terrains on planetary bodies.	Alessandro Pisello
61	DAEDALUS Cam: an immersive stereoscopic camera to explore lunar caves	Claudio Pernechele
62	Astroinformatic and digital planetology laboratory in INAF	Romolo Politi
63	Making Janus ready to launch: on ground calibration campaign	Livio Agostini
64	TRIS: transmission and illumination system.	Eliana La Francesca
65	Ma_Miss and scientific activities in support of the exploration of the martian surface and subsurface in the next decade	Cristina De Sanctis
66	SHRK the high-contrast imager and spectrograph for LBT	Dino Mesa
67	Contamination-free manipulation of extraterrestrial dust particles using acoustic tweezers	Stefano Ferretti
68	Comparison of infrared spectral features from planetary surfaces and laboratory rock samples	Matteo Bisolfati
69	Finding long-period solar system or interstellar objects with machine learning in LSST.	Antonio Vanzanella
70	The age of Saturn's Rings: Clues from Ring-Moon composition	Mauro Ciarniello

PAVING THE WAY FOR ITALIAN COMMUNITY TOWARDS MARS SAMPLE RETURN (MSR), THE NEXT STEP IN MARS EXPLORATION. F. Altieri[1] and J. R. Brucato[2], [1]INAF, Istituto di Astrofisica e Planetologia Spaziali (IAPS), via del Fosso del Cavaliere 100, 00133 Roma, Itay, francesca.altieri@inaf.i, [2]INAF, Osservatorio Astrofisico di Arcetri L.go E. Fermi 5, 50125 Firenze, Italy, john.brucato@inaf.it

Introduction: Next step in the Mars exploration is to return samples from the Red Planet. Its success involves unprecedented technical challenges and complex international collaborations. Samples are identified and cached by the NASA Mars2020 rover Perseverance, landed in Jezero Crater on February 2021. NASA and ESA are currently defining concepts for a joint campaign to bring the samples back to the Earth by 2033.

Samples returned from Mars will be the most precious specimen ever collected, with a high astrobiological interest. To stimulate the widest contribution from the Italian community and to guarantee the best possible representation of the Italian scientists to this key long-term program, a series of workshops has been promoted by INAF gathering scientists involved in planetology, geochemistry, mineralogy, chemistry, microbiology and space technology. The ultimate goal is to build solid collaborations among Italian scientific and technologic communities interested in MSR to be internationally competitive for the next frontier in the exploration of Mars.

MSR Sample-Related Objectives and Planning: Sample-related objectives for MSR campaign have been defined in the report iMOST (International MSR Objectives/ Samples Team) [1] prepared by an international team. Specifically, these are:

1. Geological Environments: Interpret the primary geologic processes and history that formed the Martian geologic record, with an emphasis on the role of water.

2. Life: Assess and interpret the potential biological history of Mars, including assaying returned samples for the evidence of life.

3. Geochronology: Determine the evolutionary timeline of Mars.

4. Volatiles: Constrain the inventory of Martian volatiles as a function of geologic time and determine the ways in which these volatiles have interacted with Mars as a geologic system.

5. Planetary-scale geology: Reconstruct the history of Mars as a planet, elucidating those processes that have affected the origin and modification of the crust, mantle and core.

6. Environmental hazards: Understand and quantify the potential Martian environmental hazards to future human exploration and the terrestrial biosphere.

7. IRSU: Evaluate type and distribution of in situ resources to support potential future Mars Exploration.

Perseverance carries 38 sample tubes to be filled over the course of the mission. Samples to be cashed are selected accordingly to the iMOST report guidelines and the caching strategy guidance have been discussed in [2]. High priority outcrops are identified using the rover's instruments. The characteristics of each acquired sample and its surroundings are investigated and documented [3, 4]. A mosaic, composed of multiple images, showing the robotic arm of NASA's Perseverance rover conducting composition analysis on a rocky outcrop called "Skinner Ridge" in Mars' Jezero Crater is reported in Figure 1. The layered sedimentary rocks are in the face of a cliff in the Jazero carter delta and are thought to be a top prospect for finding signs of ancient microbial life on Mars. Figure 2 shows an image captured by Perseverance' Mastcam-z camera during the collection of a sample to be chased.

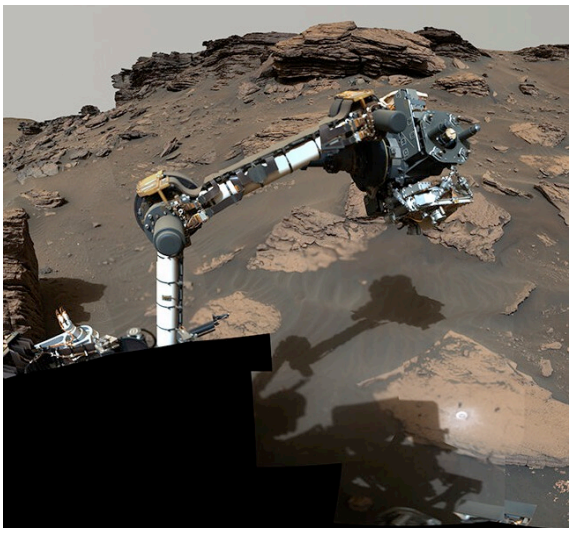

Figure 1- Perseveance investigating rokcs in the Jazero cater delta.
Credits: NASA/JPL-Caltech/MSSS
https://mars.nasa.gov/news/9261/nasas-perseverance-rover-investigates-geologically-rich-mars-terrain/

The investigation of the Martian samples would offer unique science pluses that cannot be achieved through orbital or landed missions that rely only on remote sensing and in situ measurements, respectively. Ensuring that all required scientific activities are properly designed, managed, and executed would require significant planning and coordination [5, 6].

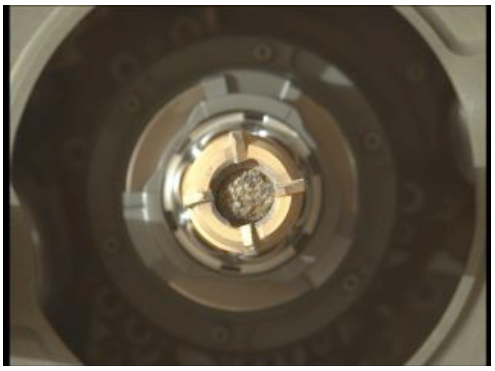

Figure 2 - Image of a sample collected by Perseverance on Jan. 31 2022. Credits: NASA/JPL-Caltech/ASU

Italian Involvement in MSR: In the framework of the MSR Science Program, key milestones are:
- Finalize in 2024 the science input for the Sample Receiving Project (SRP) to account for sample curation, safety assessment, as well as time and sterilization critical objective driven science.
- Issue the first competitive Announcement of Opportunity (AO) in 2026 for MSR objective driven science investigations on the samples.

To update the wide Italian community on the status of MSR Program and to be ready for the next key milestones, a series of workshops were organized by INAF. The 1st workshop was held virtually on 30th October 2020, few months before the landing of Perseverance in Jazero crater. The purpose was to inform the Italian community about the NASA-ESA join campaign to return the sample and on the scientific objective of iMOST. The 2nd workshop was held in person on 26-27 October 2023 in Rome, where key Italian academic organizations and industries were involved. During the first day delegates from ESA, NASA and ASI informed the Italian community about the status and the programmatic approach to MSR. In the second day of the workshop presentations from key speakers of the Italian scientific and technological community showed the high potentiality of the Italian community in this field. A discussion on how to strength the Italian participation to MSR was carried out in the final session of the workshop.

Participants acknowledged that this kind of workshops are very useful for the Italian community to be updated on the status of the art and to be aware of the next milestones. The need of a collective effort to consolidate the Italian participation to this topic was recognized and discussed.

Final Remarks: The overall Italian community interested in MSR has a big potentiality for conducting scientific analysis on the samples that will be returned to the Earth. However, more focused activities and technological equipment are needed to consolidate this potentially and overcome the gaps to be worldwide competitive for the next milestones.

The AO will be issued by NASA-ESA in 2026 to conduct the science investigations once the samples will be returned on Earth (currently planned for 2033). To be ready for the 2026, a series of activities needs to start soon to consolidate the Italian community, discussing the appropriate protocols and laboratory environments where to manipulate and analyze the samples.

Activities necessary for the MSR Science Program will cover a period of about a decade. A long-term vision is mandatory for properly identify, evaluate and plan the future activities.

The MSR objective is in its intimate nature interdisciplinary. It will be crucial to form a new generation of Italian scientists and to be ready with the necessary technological equipment. Italian community believes that Italian Universities, Research Centers, Space Agency and Research Ministry should play a crucial role in such a big leap towards the exploration of Mars and the search of signs of life beyond Earth.

References: [1] iMOST (2018), The Potential Science and Engineering Value of Samples Delivered to Earth by Mars Sample Return, (co-chairs D. W. Beaty, M. M. Grady, H. Y. McSween, E. Sefton-Nash; documentarian B.L. Carrier; plus 66 co-authors), 186 p. white paper. Posted August, 2018 by MEPAG at https://mepag.jpl.nasa.gov/reports.cfm [2] Kminek G. et al., 2021. MSR CSSC (2021) Mars Sample Return Caching Strategy Steering Committee Report. Prepared by the MSR Caching Strategy Steering Committee. Unpublished Report, available at https://mepag.jpl.nasa.gov/reports/Caching%20Strategy%20Report-Final.pdf. [4] Farley, K.A. et al., (2022). Acqueosely altered igneous rocks sampled on the floor of Jazer crater, Mars, Science, DOI: 10.1126/science.abo2196. [3] Farley, K.A. et al., (2022). Mars2020 Initial Report, Crater Floor Campaign August 11, 2022, available at PDS node. [5] Meyer, M.A., et al., (2022), Final Report of the MSR Science Planning Group 2 (MSPG2), Astrobiology, 22, 1, DOI: 10.1089/ast.2021.012.1 [6] Haltigin, T., et al., (2022), Rationale and Proposed Design for a Mars Sample Return (MSR) Science Program, Astrobiology, 22, 1, DOI: 10.1089/ast.2021.0122

Acknowledgements: This activity is supported by INAF, Grant: PRIN INAF Mainstream 2018.

THEORETICAL INVESTIGATION ON FORMATION ROUTES LEADING TO SULPHUR-BEARING SPECIES IN SPACE VIA THE REACTIONS OF ELECTRONICALLY EXCITED ATOMS

Andrea Giustini[1], Gabriella Di Genova[1], Nadia Balucani[1], Cecilia Ceccarelli,[2] and Marzio Rosi[3]
[1]Dipartimento di Chimica, Biologia e Biotecnologie, Università degli Studi di Perugia, Via Elce di Sotto 8, 06123, Perugia, Italy (giustiniandrea@gmail.com, gabriella.digenova@studenti.unipg.it, nadia.balucani@unipg.it)
[3]Univ. Grenoble Alpes, CNRS, Institut de Planétologie et d'Astrophysique de Grenoble (IPAG), F-38100 Grenoble, France; cecilia.ceccarelli@univ-grenoble-alpes.fr
[3]Dipartimento di Ingegneria Civile ed Ambientale, Università degli Studi di Perugia, Via G. Duranti 93, 06125, Perugia, Italy (marzio.rosi@unipg.it)

Introduction: The main goal of astrochemistry is to investigate formation and destruction pathways of molecules found in extraterrestrial environments, such as planetary atmospheres, comets or the interstellar medium (ISM) [1]. In the last decades or so, there have been important advances in the understanding of formation and destruction routes of interstellar complex organic molecules (iCOMs), most of them being characterized by the presence of oxygen or nitrogen atoms [2]. However, there is still an important lack of knowledge concerning the chemistry of other minor species, often due to the limited amount of both laboratory and computational data. Therefore, astrochemical models, implemented to simulate the chemical evolution of interstellar clouds, star-forming regions, circumstellar envelopes, cometery comae or planetary atmospheres are still far from being complete [3].

The chemistry leading to sulphur-bearing organic molecules is still in need to be characterized. Sulphur is present in space with an abundance of 16 ppm, and it is an interesting element for prebiotic chemistry since it is present in amino acids and several other biomolecules. In spite of some unanswered questions (in particular, see the sulphur depletion problem [4]), S-containing species, such as COS, CS, HNCS, CH_3SH, H_2CS, as well as cummulenes C_2S and C_3S, have been detected in a variety of objects [5]. Many sulphur species (H_2S, OCS, SO, S_2, SO_2 and CS_2) have also been identified in the coma of the comet 67P/Churyumov-Grasimenko [6] while for other more complex species only the gross formulas could be retrieved (C_nH_mS, C_nH_mOS, $C_nH_mO_2S$) [7].

In this contribution, we present a theoretical investigation of two reactions involving atomic sulphur in the first electronically excited state, ^1D, with two molecules, water and methanol, which are widely spread both in the gaseous phase of the interstellar medium as well as in interstellar/cometary ice. S(^1D) is produced by UV-induced photodissociation of precursor molecules, such as OCS [8] and CS_2 [9], which are present in extraterrestrial environments. In particular, OCS is among the few molecules for which a secure identification in interstellar ice has been provided [10–11]. Since the transition from the excited state (^1D) to the ground state (^3P) is spin-forbidden, the lifetime of the excited state (^1D) is long enough (36 s) for S(^1D) atoms to react with other gaseous species in relatively dense extraterrestrial environments, preventing radiative relaxation. Those conditions are not common in space, but S(^1D) can be formed by photodissociation of its precursors present in the ice surface and then immediately react with surrounding molecules. For this reason, the two systems we have been investigating can clarify some sulphur chemistry occurring on interstellar or cometary ice exposed to UV irradiation. Interestingly, the role of electronically excited metastable atoms have been recently considered in the research groups of Oberg and Herbst to address the complexity of interstellar ice chemistry [12–14].

Previous work from our laboratory has focused on the reactions of S(^1D) atoms with saturated and unsaturated hydrocarbons [15–17]. As expected, S(^1D) resulted to be much more reactive with respect to sulphur atoms in their ground ^3P state. In all cases, new molecular products holding a novel C-S bond were observed. In addition, the capability of S(^1D) of inserting into sigma bonds (already observed for the isovalent species O(^1D)) was confirmed.

Theoretical methods: The reactive potential energy surface (PES) of two reactions involving S(^1D) and CH_3OH or H_2O (two abundant species in cometary and interstellar ice) have been characterized by electronic structure calculations. All stationary points of the PES were optimized at the DFT level of theory, using the aug-cc-pVTZ [18] basis set. Frequencies analysis were carried out in order to determine the nature of the stationary points. If one single imaginary frequency emerges, the presence of a transition state is ascertained, whereas the absence of negative frequencies identifies local minima of the PES. When a transition state was found, an intrinsic reaction coordinate (IRC) calculation was executed. Subsequently, single-point calculations at the CCSD(T) method [19] were performed with the same basis set in order to refine the energy of each stationary point. All energies were corrected with the zero-point energies computed at the DFT level of theory. Statistical RRKM calculations of

the product branching fractions are also conducted when more than one reaction channel is open.

S(^{1}D) + CH_3OH: CH_3OH is an abundant species both in interstellar and cometary ice. According to our theoretical investigation, there are five open reaction channels

$$S(^1D) + CH_3OH \rightarrow CH_3O + H_2S$$
$$\rightarrow HSCOH + H_2$$
$$\rightarrow H_2CS + H_2O$$
$$\rightarrow HCSH + H_2O$$
$$\rightarrow HCOH + H_2S$$
$$\rightarrow CH_2OH + SH$$

The reaction starts with the S(^{1}D) insertion into a C–H bond of methanol leading to the formation (CH_2OHSH) of a bound intermediate which undergoes dissociation to the above mentioned sets of bimolecular products because of its high internal energy content. We are determing the product branching fractions with statistical methods. Interestingly, the same intermediate can be formed by the reaction involving atomic oxygen in its electronically excited ^{1}D state with mercaptane. We are therefore in the process of characterizing this reaction as well.

S(^{1}D) + H_2O: Water is the most abundant component of interstellar and cometary ice. The presence of precursors of S(^{1}D) like OCS in interstellar ice is also documented. Therefore, if formed on the surface of ice, S(^{1}D) will certainly react with water. According to our calculations, the reaction proceeds either by S(^{1}D) addition to one of the lone pairs of O or via insertion into one of two O–H bonds. Two different intermediates can be formed: H_2OS and HOSH. Among the various possible sets of reaction channels, the only exothermic channel is the one leading to $SO + H_2$.

Conclusions: Both reactions proceed without an activation energy, as expected from similar reactions involving S(^{1}D) and already characterized before [16,17]. In the case of the reaction with CH_3OH, several exothermic channels are open, while in the case of the reaction with H_2O only one channel is exothermic. However, if these reactions take place on the surface of cometary or interstellar ice, the ice matrix can help in stabilizing the reaction intermediates (that is, CH_2OHSH, H_2OS and HOSH) as already proved by the experiments on O(^{1}D) + hydrocarbons [12–13]. In particular, the S(^{1}D) + CH_3OH reaction could be responsible for the formation of the S/O-containing organic molecules detected in the coma of comet 67P/Churyumov–Gerasimenko with gross formula CH_4OS.

Aknowledgments: This work was supported by the Italian Space Agency (ASI, DC-VUM-2017-034, Grant n° 2019–3 U.O Life in Space), and has received funding from the Italian MUR (PRIN 2020, "Astrochemistry beyond the second period elements", Prot. 2020AFB3FX)

References:

[1] Caselli P. and Ceccarelli C. (2012) *Astron. Astrophys. Rev.,* 56, 20
[2] Herbst E. and van Dishoeck F. (2009) *Annu. Rev. Astron. Astrophys.*, 427–480, 47
[3] Ceccarelli C. et al. (2022) arXiv e-prints, [arXiv: astro- 310ph.SR/2206.13270].
[4] Vidal T. H. G. and Wakelam V. (2018) *Mon. Not. R. Astron. Soc.*, 5575–5587, 474
[5] Yamada et al. (2002) *A&A*, 1031–1044, 395
[6] Calmonte U. et al. (2016) *Mon. Not. R. Astron. Soc.,* S253–S273, 462
[7] Hänni N. et al. (2022) *Nat. Commun.*, 3639, 13
[8] Kim, M. H. et al. (2004) *Can. J. Chem.* 880-884, 82
[9] Black, G. and Jusinski, L.E. (1986) *Chem. Phys. Lett.*, 90–92, 124
[10] Gibb E. L., et al. (2000) *Astrophys. J.,* 347, 536
[11] Gibb E. L., et al. (2004) *Astrophys. J. S. S.,* 35, 151
[12] Bergner J. B. et al. (2017) *Astrophys. J.,* 29, 845
[13] Bergner J. B. et al. (2019) *Astrophys. J.,* 115, 874
[14] Carder J. T. et al. (2021) *MNRAS,* 1526–1532, 508
[15] McKee M. L. (1986) *J. Am. Chem. Soc.*, 5059–5064, 108
[16] Leonori F. et al. (2009) *J. Phys. Chem. A,* 15328–1534, 113
[17] Berteloite C. (2011) *Phys. Chem. Chem. Phys.*, 8485–8501, 13
[18] Dunning T. H. (1989) *J. Chem. Phys.,* 1007-1023, 90
[19] Purvis C. D. (1982) *J. Chem. Phys*., 1910, 76

Rotational spectroscopy of pyrrole: a model for astrophysical searches.

Assimo Maris[1], Cleo Whitcombe[2], Sonia Melandri[3], Luca Evangelisti[4], Dipartimento di Chimica G. Ciamician, Università di Bologna, via Selmi 2, 40126 Bologna, Italia, [1]assimo.maris@unibo.it, [2]cleoamber.whitcombe@studio.unibo.it, [3]sonia.melandri@unibo.it, [4]luca.evangelisti6@unibo.it.

Introduction: Pyrrole or azacyclopendiene is a five-member heterocyclic aromatic ring with point group symmetry C_{2v}. Pyrrole itself is not naturally occurring, but it is the building block of tetrapyrrole macrocycles, which are common cofactors in biochemistry, i.e. chlorophyll and porphyrins of heme. The recent detection of aromatic systems in the quiescent molecular cloud Taurus Molecular Cloud 1 (TMC-1) suggest that also pyrrole could be present.

Here we summarize the state of the art of laboratory research aimed to provide reliable data for the analysis of astronomical surveys. Hopefully, at the time of the conference new data measured in the 60-78 GHz frequency region with a free-jet absorption Stark modulated spectrometer will be also implemented.

Background: Spectroscopic methods allow extending the human capacity to observe the world beyond visible radiation. Actually, the whole spectral range, from the radiofrequency (longer wavelengths) to the X and gamma rays (shorter wavelengths), is used to achieve knowledge of the intrinsic properties of the matter as well as to detect and quantify the compounds of a mixture, to inspect matter at a microscopic level as well as to identify substances from very far distances by remote sensing. Every spectral region requires appropriate techniques and unveils special information. Molecular resonance rotational (MRR) spectroscopy in particular is related to the structure of the molecules and provides a unique signature for every species. Moreover, the specificity is so high that every variation in the status of a molecule is reflected in the spectrum and no different species exist with the same spectral features. This means that rotational spectroscopy can distinguish between isomers, conformers, isotopologues, vibronic states and neutral, ion and radical states. Using particular techniques even enantiomers can be identified. However, the application of MRR-spectroscopy is limited by two conditions: (i) the sample must be in the gas phase in order to allow the rotation motion and (ii) the target species must be polar since the signal intensity grows with the permanent electric dipole moment.

MRR-spectroscopy works in the radiofrequency region (microwave, millimeter and sub-millimeter spectral regions) and it is used to explore the cosmos with the purpose to recognize molecular species. Actually, most of the about 270 molecules that have been detected in the interstellar medium or circumstellar envelopes have been identified by their MRR signals [1,2]. Most of these species are linear or contain three-member rings, but since 2018 a series of aromatic compounds have been detected in TMC-1. Most of them contain the cyano group which confers a high electric dipole moment: benzonitrile (*c*-C_6H_6CN) [3], 1-cyanocyclopentadiene [4] and 2-cyanocyclopentadiene [5] (*c*-C_5H_5CN), 1- and 2-cyanonaphtalene (*c*-$C_{10}H_{10}CN$) [6] and 2-cyanoindene (*c*-C_9H_7CN) [7], but also unsubstituted hydrocarbon compounds have been determined: indene (*c*-C_9H_8) [8,9], cyclopentadiene (*c*-C_5H_6) [9] ethenylidenecyclopentadiene (*c*-$C_5H_4C_2H_2$) [10] and 1- and 2-ethynylcyclopentadiene (*c*-C_5H_5CCH) [11]. The next step is to consider heterocyclic aromatic organic compounds, in which one or more carbon atoms have been substituted by a heteroatom. While both N- and O-heterocycles have been identified in carbonaceous chondrites [12,13], they have never been detected in the gas phase. A recent search of furan (*c*-C_4H_4O) towards TMC-1 using the GOTHAM collaboration survey fixed an upper limit for the column density of 1.0×10^{12} cm^{-2}, which is very low [14]. As regards pyrrole (*c*-C_4H_4NH), previous research fixes an upper limit for the column density of 4× and 0.6×10^{12} cm^{-2} towards TMC-1 and Sgr-B2, respectively [15]. Despite these results suggesting that chemical processes in these clouds favor the formation of chains over rings of comparable molecular weight, the availability of accurate rest frequencies for the molecules under consideration remains an essential step for their search. Moreover, the electric dipole moment of pyrrole (μ=1.74(2) D [16]) is 2.6 times that of furan (μ=0.661(6) D [17]) and this could help its observation.

Results: The rotational spectrum of pyrrole and its isotopologues has been investigated since 1952 in different spectral regions and with different resolution powers [16,18-22]. Here we present a unique fit for the parent species in the ground state which collects all the available information, the achieved spectroscopic parameters are given in Table 1.

It is worth noting that several high-resolution infrared spectra have been detected and disentangled through vibrorotational analysis [23-27 and references therein]. In order to improve the reliability of the predictions, we plan to measure additional intrastate transition lines in the 60-78 GHz frequency range and include selected interstate transitions in the fit.

Table 1: Experimental spectroscopic parameters of pyrrole (*S*-reduction, *III*^{l} representation).

A/MHz	9130.6352(7)[a]
B	9001.3644(6)
C	4532.1081(6)
$D_J\times10^3$	2.9289(7)
$D_{JK}\times10^3$	-4.653(1)
$D_K\times10^3$	2.021(1)
$d_1\times10^3$	0.0614(4)
$d_2\times10^3$	0.0225(3)
$H_{JK}\times10^9$	-4.4(2)
$1.5\chi_{cc}$	-4.042(11)
$(\chi_{bb}-\chi_{aa})/4$	-0.027(1)
N[b]	175
rms[c]	0.054

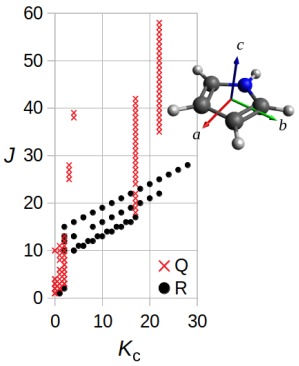

Data set distribution plot of the upper state *J* and K_c quantum numbers of the fitted transitions

[a] Error in the unit of the last digit. [b] Number of μ_a-type lines in the fit. [c] Standard deviation of the fit. Derived parameters: χ_{aa}=1.402(7), χ_{bb}=1.293(7), χ_{cc}=-2.695(7) MHz, $\eta=(\chi_{aa}-\chi_{bb})/\chi_{cc}$=0.040 almost symmetric nuclear quadrupole tensor, $\kappa=(2B-A-C)/(A-C)$=0.944 almost oblate rotor.

References: [1] C.P. Endres, S. Schlemmer, P. Schilke, J. Stutzki, H.S.P. Müller. The Cologne Database for Molecular Spectroscopy, CDMS, in the Virtual Atomic and Molecular Data Centre, VAMDC. *J. Mol. Spectrosc*. 327 (2016) 95-104. **https://doi.org/10.1016/j.jms.2016.03.005** [2] B.A. McGuire, 2021 Census of Interstellar, Circumstellar, Extragalactic, Protoplanetary Disk, and Exoplanetary Molecules. *Astrophys. J., Suppl. Ser.* 259 (2022) 30. **https://doi.org/10.3847/1538-4365/ac2a48** [3] B.A. McGuire, A.M. Burkhardt, S. Kalenskii, C.N. Shingledecker, A.J. Remijan, E. Herbst, M.C. McCarthy. Detection of the aromatic molecule benzonitrile (c-C6H5CN) in the interstellar medium. *Science* 359 (2018) 202-205. **https://doi.org/10.1126/science.aao4890** [4] M.C. McCarthy, K.L.K. Lee, R.A. Loomis, A.M. Burkhardt, C.N. Shingledecker, S.B. Charnley, M.A. Cordiner, E. Herbst, S. Kalenskii, E.R. Willis, C. Xue, A.J. Remijan, B.A. McGuire. Interstellar detection of the highly polar five-membered ring cyanocyclopentadiene. *Nature Astronomy* 5 (2021) 176-180. **https://doi.org/10.1038/s41550-020-01213-y** [5] K.L.K. Lee, P.B. Changala, R.A. Loomis, A.M. Burkhardt, C. Xue, M.A. Cordiner, S.B. Charnley, S. M.C. McCarthy, B.A. McGuire. Interstellar detection of 2-cyanocyclopentadiene, C5H5 CN, a second five-membered ring toward TMC-1. *Astrophys. J. Lett.* 910 (2021) L2. **https://doi.org/10.3847/2041-8213/abe764** [6] B.A. McGuire, R.A. Loomis, A.M. Burkhardt, K.L.K. Lee,C.N. Shingledecker, S.B. Charnley, I.R. Cooke, M.A. Cordiner, E. Herbst, S. Kalenskii, M.A. Siebert, E.R. Willis, C. Xue, A.J. Remijan, M.C. McCarthy. Detection of two interstellar polycyclic aromatic hydrocarbons via spectral matched filtering. *Science* 371 (2021) 1265-1269. **https://doi.org/10.1126/science.abb7535** [7] M.L. Sita, P.B. Changala, C. Xue, A.M. Burkhardt, C.N. Shingledecker, K.L.K. Lee, R.A. Loomis, E. Momjian, M.A. Siebert, D. Gupta, E. Herbst, A.J. Remijan, M.C. McCarthy, I.R. Cooke, B.A. McGuire. Discovery of Interstellar 2-Cyanoindene (2-C9H9CN) in GOTHAM Observations of TMC-1. *Astrophys. J. Lett*. 938 (2022) L12. **https://doi.org/10.3847/2041-8213/ac92f4** [8] A.M. Burkhardt, K.L.K. Lee, P.B. Changala, C.N. Shingledecker, I.R. Cooke, R.A. Loomis, H. Wei, S.B. Charnley, E. Herbst, M.C. McCarthy and B.A. McGuire. Discovery of the pure polycyclic aromatic hydrocarbon indene (c-C9H8) with GOTHAM observations of TMC-1. *Astrophys. J. Lett.* 913 (2021) **https://doi.org/L18. 10.3847/2041-8213/abfd3a** [9] J. Cernicharo, M. Agúndez, C. Cabezas, B. Tercero, N. Marcelino, J.R. Pardo, and P. de Vicente. Pure hydrocarbon cycles in TMC-1: Discovery of ethynylcyclopropenylidene, cyclopentadiene, and indene. *Astron. Astrophys.* 649 (2021) L15 (2021). **https://doi.org/10.1051/0004-6361/202141156** [10] J. Cernicharo, R. Fuentetaja, M. Agúndez, R.I. Kaiser, C. Cabezas, N. Marcelino, B. Tercero, J.R. Pardo, and P. de Vicente. Discovery of fulvenallene in TMC-1 with the QUIJOTE line survey. *Astron. Astrophys.* 663 (2022) L9. **https://doi.org/10.1051/0004-6361/202244399** [11] J. Cernicharo, M. Agúndez, R.I. Kaiser, C. Cabezas, B. Tercero, N. Marcelino, J.R. Pardo, and P. de Vicente. Discovery of two isomers of ethynyl cyclopentadiene in TMC-1: Abundances of CCH and CN derivatives of hydrocarbon cycles. *Astron. Astrophys.* 655 (2021) L1. **https://doi.org/10.1051/0004-6361/202142226** [12] M. Komiya, A. Shimoyama, K. Harada. Examination of organic compounds from insoluble organic matter isolated from some Antarctic carbonaceous chondrites by heating experiments. *Geochim. Cosmochim. Acta* 57 (1993) 907-914. **https://doi.org/10.1016/0016-7037(93)90177-X** [13] Z. Martins, O. Botta, M.L. Fogel, M.A. Sephton, D.P. Glavin, J.S. Watson, J.P. Dworkin, A.W. Schwartz, P. Ehrenfreund. Extraterrestrial nucleobases in the Murchison meteorite. *Earth Planet. Sci. Lett.* 270 (2008) 130-136. **https://doi.org/10.1016/j.epsl.2008.03.026** [14] T.J. Barnum, K.L.K. Lee, B.A. McGuire. Chirped-Pulse Fourier Transform Millimeter-Wave Spectroscopy of Furan, Isotopologues, and Vibrational Excited States. *ACS Earth Space Chem.* 5 (2021) 2986-2994. **https://doi.org/10.1021/acsearthspacechem.1c00182** [15] M.L. Kutner, D.E. Machnik, K.D. Tucker, R.L. Dickman. Search for interstellar pyrrole and furan. *Astrophys. J.*, 242 (1980) 541-544. **https://adsabs.harvard.edu/pdf/1980ApJ...242..541K** [16] L. Nygaard, J. Tormod Nielsen, J. Kirchheiner, G. Maltesen, J. Rastrup-Andersen, G. Ole Sørensen, Microwave spectra of isotopic pyrroles. Molecular structure, dipole moment, and 14N quadrupole coupling constants of pyrrole. *J. Mol. Struct.* 3 (1969) 491-506. **https://doi.org/10.1016/0022-2860(69)80031-1** [17] M. H. Sirvetz. The Microwave Spectrum of Furan. *J. Chem. Phys.* 19 (1951) 1609-1610. **https://doi.org/10.1063/1.1748135** [18] W.S. Wilcox, J.H. Goldstein. Evidence for a Completely Planar Structure of Pyrrole from Its Microwave Spectrum. *J. Chem. Phys.* 20 (1952) 1656-1657 **https://doi.org/10.1063/1.1700250** [19] B. Bak, D. Christensen, L. Hansen, J. Rastrup-Andersen. Microwave Determination of the Structure of Pyrrole. *J. Chem. Phys.* 24 (1956) 720. **https://doi.org/10.1063/1.1742597** [20] K. Bolton, R.D. Brown. Study of Potential Interstellar Molecules: Nuclear Quadrupole Coupling Constants of the Nitrogen Atom in Pyrrole. *Aust. J. Phys.* 27 (1974) 143-146. **https://doi.org/10.1071/PH740143** [21] L. Gaines, P. Thaddeus, G. Tomasevich, K. Tucker. Molecular beam maser spectroscopy. *NASA Technical Report* (1974) 79-86. **https://ntrs.nasa.gov/api/citations/19750002200/downloads/19750002200.pdf** [22] G. Wlodarczak, L. Martinache, J. Demaison, B.P. Van Eijck. The millimeter-wave spectra of furan, pyrrole, and pyridine: Experimental and theoretical determination of the quartic centrifugal distortion constants. *J. Mol. Spectrosc.* 127 (1988) 200-208. **https://doi.org/10.1016/0022-2852(88)90019-7** [23] A. Mellouki, R. Georges, M. Herman, D.L. Snavely, and S. Leytner. Spectroscopic investigation of ground state pyrrole (12C4H5N): the N-H stretch. *Chem. Phys.* 220 (1997) 311. **https://doi.org/10.1016/S0301-0104(97)00136-5.** [24] A. Mellouki, J. Vander Auwera, M. Herman. Rotation-Vibration Constants for the v1, v22, v24, v22+v24 and Ground States in Pyrrole (12C4H5N). *J. Mol. Spectrosc.* 193 (1999) 195-203. **https://doi.org/10.1006/jmsp.1998.7724** [25] A. Mellouki, J. Liévin, M. Herman. The vibrational spectrum of pyrrole (C4H5N) and furan (C4H4O) in the gas phase. *Chem. Phys.* 271 (2001) 239-266. **https://doi.org/10.1016/S0301-0104(01)00447-5** [26] F. Hegelund, R. Wugt Larsen, M.H. Palmer. The high-resolution infrared spectrum of pyrrole between 900 and 1500 cm-1 revisited. *J. Mol. Spectrosc.* 252 (2008) 93-97. **https://doi.org/10.1016/j.jms.2008.06.010** [27] D.W. Tokaryk, J.A. van Wijngaarden. Fourier transform spectra of the v16, 2v16, and 2v16-v16 bands of pyrrole taken with synchrotron radiation. *Can. J. Phys.* 87 (2009) 443-448. **https://doi.org/10.1139/P09-013**

A laboratory investigation of the reactions N(^{2}D) + benzene and N(^{2}D) + toluene and implications for the atmospheric chemistry of Titan

G. Vanuzzo[1], A. Caracciolo[1], M. Rosi[2], D. Skouteris[3], P. Casavecchia[1] and N. Balucani[1]
[1]Dip. Chimica, Biologia e Biotecnologie, via Elce di Sotto 8, Università Perugia, 06123 Perugia, IT, [2] Dip. Ingegneria Civile Ambientale, Via G. Duranti 93, Università di Perugia, 06125 Perugia, IT, [3] Master-Tec s.r.l., Via Sicilia 41, 06128 Perugia, IT

Introduction: The habitat offered by most planets of the Solar System appears to be not suitable for life [1]. However, in addition to Earth, other bodies can be promising. In particular, two moons, Europe and Titan, the most important moons of Jupiter and Saturn, respectively, are very interesting to understand the chemistry that might have preceded the appearance of life. In particular, Titan is characterized by a nitrogen-rich and dense atmosphere, the orange colour of which is due haze particles formed by N-rich organic macromolecules [2]. The Cassini-Huygens mission provided a detailed look at the composition of the atmosphere of Titan and we now know that, in addition to molecular nitrogen (~94-97%) and methane, many other saturated hydrocarbons and unsaturated hydrocarbons, as well as nitriles, are present in trace amount [3]. The observation of nitriles and N-rich organic macromolecules clearly indicates the involvement of nitrogen chemistry promoted either by the photoionization or photodissociation of N_2 [3-5]. Other processes, induced by cosmic rays, solar wind and energetic electrons from the magnetosphere of Saturn, can also dissociate or ionize nitrogen [3-6].

From a chemical point of view, an important role is played by nitrogen atoms in their first electronically excited state, ^{2}D, a metastable state with a long radiative lifetime which is produced in the upper atmosphere by a number of processes involving N_2 and high-energy photons or particles [3-6]. N(^{2}D) can react with the other components of the atmosphere of Titan, including the abundant CH_4 and H_2, as well as with other saturated (C_2H_6) and unsaturated aliphatic hydrocarbons (C_2H_2, C_2H_4). These reactions have been characterized in dedicated laboratory experiments and we now know that they bring to the formation of N-containing organic species [7-13]. In particular, the CRESU (an acronym of Cinétique de Réaction en Ecoulment Supersonique Uniforme) technique has been employed to derive low temperature rate coefficients (encompassing those of interest for the atmosphere Titan) for the most important reactions [7-9]. In addition, in our laboratory in Perugia we have investigated a series of N(^{2}D) reactions with aliphatic hydrocarbons by means of the crossed molecular beam (CMB) technique with mass spectrometric (MS) detection [10-15]. This experimental method provides a wealth of information on bimolecular reactions, including the nature of the primary products and their relative yields, i.e., the product *branching fractions* (BFs). Additional information is gained on the reaction mechanism and also the product energy partitioning. Since in CMB-MS experiments the reactions are investigated under single collision conditions, primary products are clearly established also when they are very reactive radicals.

After the success in the investigation of N(^{2}D) reactions with aliphatic hydrocarbons, more recently we have turned our attention to the case of reactions involving other species present in the upper atmosphere of Titan. In particular, we have investigated the reactions N(^{2}D) with H_2O [16,17], nitriles (HCCCN and C_2H_3CN) [18,19] and pyridine [20], a simple heteroaromatic compound containing an N atom (pyridine was alleged to be present in the atmosphere of Titan after Ion Neutral Mass Spectrometer (INMS) measurements, but spectroscopic detection has failed so far). In the case of the reaction with nitriles, we have observed the formation of products holding an additional N atom [18,19]. In the case of pyridine, instead, we have verified that the aromatic ring can be partially destroyed by the reaction with N(^{2}D) [20].

In this contribution, we present an experimental investigation of the reactions of N(^{2}D) with two other aromatic compounds: benzene (C_6H_6) and toluene ($C_6H_5CH_3$). Benzene, the simplest aromatic hydrocarbon, has been identified in the atmosphere of Titan by several instruments onboard Cassini-Huygens. In particular Cassini INMS derived a significant mole fraction of 1.31×10^{-6} at 950 [21], a region where N(^{2}D) is formed in a significant amount by photodissociation of N_2. Along with benzene, toluene has also been tentatively identified INMS. Therefore, at those altitude the reactions N(^{2}D) + C_6H_6 and N(^{2}D) + $C_6H_5CH_3$ can play a role

The interpretation of our experimental results has been supported by dedicated electronic structure calculations of the relevant potential energy surfaces and statistical estimates of product branching fractions. According to our study, the N(^{2}D) + benzene and N(^{2}D) + toluene are characterized by a similar reaction mechanism, with the addition of N(^{2}D) to the aromatic ring and the formation of a seven-atom ring. However,

our experimental results corroborated by the theoretical predictions have shown that, in the case of the reaction with benzene, the dominant channel (BF > 90%) is the one leading to HCN + C_5H_5 (cyclopentadienyl radical) in a ring-contraction channel. In the case of the reaction with toluene, instead, the analogous channel accounts only for one third of the reaction. Our results, accompanied by CRESU kinetic measurements performed by Kevin Hickson (Université de Bordeaux, Institut des Sciences Moléculaires), will be incorporated in the photochemical model developed by M. Dobrijevic (Laboratoire d'Astrophysique de Bordeaux, Université de Bordeaux).

Acknowledgments: The authors wish to thank the Italian MUR (PRIN 2017 – Grant 2017PJ5XXX), and the Italian Space Agency for the co-funding the Life in Space project (ASI N. 2019-3-U.0).

References:

[1] Shaw, A. M. (2007) Astrochemistry: From Astronomy to Astrobiology. Wiley.

[2] Israel, G.et al. (2005) Nature, 438, 796.

[3] Vuitton, V. et al. (2019), Icarus, 324, 120-197.

[4] Dutuit, O. et al. (2013) Astrophysical Journal Supplement Series, 204 (2013) 20; doi: 10.1088/0067-0049/204/2/20

[5] Loison, J. et al. (2015), Icarus, 247, 218 – 247.

[6] Dobrijevic, M., Loison, J.C. (2018), Icarus, 307, 371–379.

[7] Nuñez-Reyes, D. et al. (2019) Phys. Chem. Chem. Phys., 21, 6574-6581.

[8] Nuñez-Reyes, D. et al. (2019) Phys. Chem. Chem. Phys., 21, 22230-22237.

[9] Hickson, K. M. et al. (2020) Phys. Chem. Chem. Phys., 22, 22, 14026-14035.

[10] Balucani, N. et al. (2009) J. Phys. Chem. A, 113, 11138-11152; doi: 10.1021/jp904302g

[11] Balucani, N. et al. (2000) J. Am. Chem. Soc. 122, 4443-4450.

[12] Balucani, N. et al. (2012) J. Phys. Chem. A, 116, 10467-10479; doi:10.1021/jp3072316

[13] Balucani, N. et al. (2010) Faraday Discuss. 147, 189-216.

[14] Mancini, L. et al. (2021) J. Phys. Chem. A 125, 8846–8859.

[15] Vanuzzo, G. et al. (2022) ACS Earth Space Chem. 6, 2305–2321.

[16] Homayoon, Z. et al. (2014) J. Phys. Chem. Lett., 5, 3508−3513.

[17] Balucani, N. et al. (2015) Mol. Phys., 113, 2296−2301.

[18] Liang, P. et al. (2022) Mol. Phys. 120 (1-2), e1948126.

[19] Vanuzzo, G. et al. (2022) J. Phys. Chem. A 126, 6110–6123.

[20] Recio, P. et al. (2021) Chem. Phys. Lett. 779, 138852.

[21] Vuitton, V., Yelle, R.V., Cui, J. (2008) J. Geophys. Res.113, E05007.

DETECTABILITY OF AROMATIC ORGANICS IN SULFATES BY THE MARS 2020 PERSEVERANCE ROVER.

T. Fornaro[1], J. R. Brucato[1], G. Poggiali[1,2], A. Alberini[1,3], C. Garcia Florentino[1,4], R. S. Jakubek[5], M. Fries[5], S. Sharma[6], A. E. Murphy[7], R. Bhartia[8], A. Ollila[9], S. Clegg[9], G. Lopez-Reyes[10], J. A. Manrique[10], O. Beyssac[11], R. Wiens[12], [1]INAF-Astrophysical Observatory of Arcetri, largo E. Fermi 5, 50125 Florence, Italy (teresa.fornaro@inaf.it), [2]LESIA – Observatoire de Paris PSL, Université PSL, CNRS, Sorbonne Université, Université de Paris, 5 place Jules Janssen, 92190 Meudon, France, [3]Department of Physics and Astronomy, University of Florence, Via Giovanni Sansone 1, 50019 Sesto Fiorentino (Florence), Italy, [4]Department of Analytical Chemistry, University of the Basque Country UPV/EHU, P.O. Box 644, 48080 Bilbao, Basque Country, Spain, [5]NASA Johnson Space Center, 2101 NASA Parkway, Houston, TX 77058, USA, [6]Jet Propulsion Laboratory, California Institute of Technology, CA, USA, [7]Planetary Science Institute, 1700 E. Ft. Lowell, Tucson, AZ 85719, USA, [8]Photon Systems Incorporated, CA, USA, [9]Los Alamos National Laboratory, New Mexico, USA, [10]Astrobiology Research Group ERICA – Universidad de Valladolid, Valladolid, SPAIN, [11]IMPMC UMR 7590 CNRS-UPMC-MNHN-IRD, Place Jussieu 75005 Paris, France, [12]Purdue University, West Lafayette, Indiana, USA.

Introduction: Detection of organic matter by the Mars 2020 Perseverance rover can provide hints about habitability and possible presence of past life at Jezero crater, thus informing us about the astrobiological relevance of the samples collected by the rover to be returned to Earth.

The instruments onboard Perseverance capable of detecting organic matter are SHERLOC, a deep UV (248.6 nm) resonance Raman and fluorescence spectrometer, and SuperCam, which combines Laser Induced (1064 nm) Breakdown Spectroscopy, Time Resolved Raman (532 nm) and Luminescence, visible and Near InfraRed (400 - 900 nm, 1.3 - 2.6 µm) reflectance spectroscopy.

To date, SHERLOC detected the strongest fluorescence signatures interpreted as possible aromatic organics in materials associated with aqueous processes, i.e. sulfate- and carbonate-bearing materials [1], both in the igneous rocks of the Jezero Crater Floor and the sedimentary rocks at the Jezero Delta Front.

Unraveling the nature of the organics in the Jezero samples is quite challenging for a number of reasons. First, organics at relatively low concentration give very weak signals in Raman, but they can be detected with a more sensitive technique like fluorescence, which, however, is not very specific to molecular structure. Second, molecule-mineral interactions can affect spectroscopic signals with respect to the pure organics changing the spectral region where organics features should be expected [2][3][4]. Therefore, assignment of spectroscopic features cannot be based solely on databases for pure minerals and pure molecules, but it is indispensable to analyze organo-mineral complexes with laboratory instruments analogous to the ones onboard Perseverance in order to have much better databases to use as reference dataset for interpreting mission data.

Methods: To get insights into the nature of the possible organics detected on Mars in association with sulfates, we prepared analog samples composed of magnesium sulfate doped with 1-ring, 2-ring aromatics and polycyclic aromatic hydrocarbons, and we used them to perform detectability and sensitivity tests with instruments analogous to SuperCam and SHERLOC. Specifically, as SHERLOC-like instruments we used the SHERLOC Brassboard located at the Jet Propulsion Laboratory and the ACRONM instrument located at NASA-JSC, while as SuperCam-like instruments we used the SimulCam instrument located at University of Valladolid for Raman and a Bruker VERTEX 70v interferometer integrated with a Harrick Praying Mantis for DRIFT analysis for VISIR characterization.

Results: As expected, deep UV Raman and fluorescence appear to be the best techniques for detecting aromatic organics in sulfates even at very low organics concentrations (Fig. 1). Fluorescence, in particular, appears to be very sensitive to molecule-mineral interactions, which highlights the importance of acquiring data for molecule-mineral complexes as reference datasets. In addition, characterization of the samples with VISIR demonstrated that SuperCam VISIR can be used to detect some of the tested organics adsorbed on sulfates even at 1 wt% concentration (Fig. 2). Analysis with SimulCam also suggests that additional evidence for presence of organics may be found in variations of the background in the Raman spectrum.

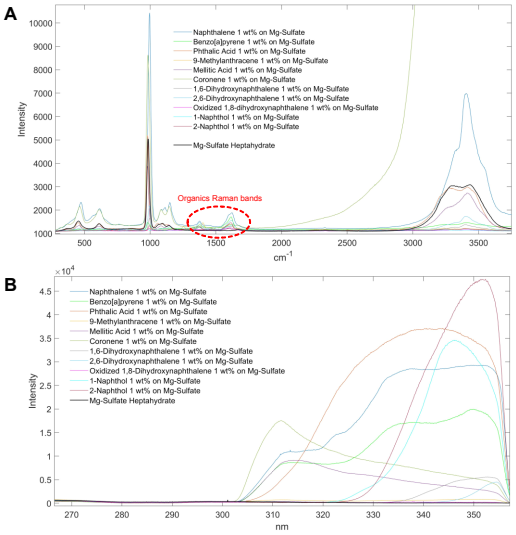

Fig. 1. A) Deep UV Raman spectra measured with ACRONM using 1200 ppp. B) Fluorescence spectra measured with Brassboard using 400 ppp.

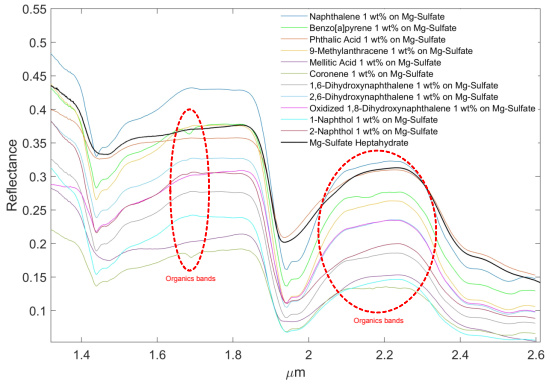

Fig. 2. VISIR spectra resampled on the 256 IR channels of SuperCam.

Conclusions: This work provides a key reference dataset for interpreting Mars 2020 mission data, and shows the complementarities of the techniques onboard Perseverance to detect high preservation potential minerals (e.g., sulfates) and organic molecules (e.g., PAHs) and aromatic carboxylic acids adsorbed on sulfates.

This work will also support interpretations of spectroscopic observations by future missions like ExoMars.

References: [1] Scheller E. L. et al. (2022) *Science*, eabo5204. [2] Fornaro T. et al. (2018) *Icarus*, *313*, 38-60. [3] Fornaro T. et al. (2020) *Front. Astron. Space Sci.*, *7*, 91. [4] Fornaro T. et al. (2018) *Life*, *8*, 56.

SURVIVABILITY OF XANTHORIA PARIETINA IN SIMULATED MARS CONDITIONS FOR 30 DAYS.

C. Lorenz[1], E. Bianchi[1], G. Poggiali[2,3], G. Alemanno[4], R. Benesperi[1], J. R. Brucato[3], S. Garland[4], J. Helbert[4], S. Loppi[5], A. Lorek[4], A. Maturilli[4], A. Papini[1], J. P. de Vera[6] and M. Baqué[4], [1]Department of Biology, University of Florence, Via La Pira 4, 50121 Florence, Italy, [2]LESIA-Observatoire de Paris, Université PSL, CNRS, Sorbonne Univerisité, Univerisité de Paris, 5 place Jules Janssen, 92190 Meudon, France, [3]INAF-Astrophysical Observatory of Arcetri, Largo E. Fermi 5, 50125 Florence, Italy, [4]Planetary Laboratories Department, Institute of Planetary Research, German Aerospace Center (DLR), Rutherfordstraße 2, 12489 Berlin, Germany, [5]Department of Environmental Sciences, University of Siena, Via P. A. Mattioli 4, 53100 Siena, Italy, [6]Microgravity User Support Center (MUSC), Space Operations and Astronaut Training, German Aerospace Center (DLR), Linder Höhe, 51147 Cologne, Germany.

Introduction: *Xanthoria parietina* (L.) Th. Fr. is a wide-spread foliose lichen that grows on barks and rocks [1]. This species shows high tolerance to air pollutants, heavy metals [2], and resistance to UV-radiation thanks to the shielding properties of the secondary metabolite parietin [3]. Several astrobiological studies involving lichens - that are symbiotic association between a fungus and an *alga* and/or a *cyanobacterium* - proved the ability of these organisms to be resistant and thrive in extreme environments such as space and Mars' surface simulated conditions [4, 5]. We have already tested the lichen species *X. parietina* in simulated space conditions, that was able to survive and to reactivate after exposure [6].

Methods: This experiment was performed aiming (i) to assess the survivability of *X. parietina* under simulated Mars conditions [7, 8] for 30 days, monitoring the lichen vitality through chlorophyll *a* fluorescence (F_V/F_M) as photoefficiency parameter, carrying out *in situ* and after treatment analyses; (ii) to evaluate the oxidative stress due to the extreme conditions, highlighting eventual changes in the lichen carotenoids' Raman signatures and (iii) to check for possible variations in the lichen photobiont's ultrastructure through TEM analysis. Eight samples were exposed to the simulated atmospheric conditions of Mars of which four were UV-irradiated with day-night cycles (FM, Full-Mars) and the other four kept in darkness (DM, Dark-Mars). A three gases mixture of 95% CO_2, 4% N_2 and 1% O_2 was used as best approximation of Mars-like atmospheric conditions, with a constant pressure of 600Pa [7, 8]. Temperature and humidity were subjected to day-night cycles, reaching during daytime 15°C and 0% RH, and during night -55°C and 100% RH (Fig. 1) according to Martian thermophysical conditions at mid-latitudes [7, 8]. UV-radiation for FM samples was simulated using a Xenon UV-lamp (spectral range 200 nm – 2200 nm) that was automatically turned on for 16 h (day) and turned off for 8 h (night) daily [7, 8]. The total average radiation dose for FM was 2452.32 J/cm^2 and the average instantaneous irradiance on the sample spots was 14.2 W/m^2 [9]. Four other samples were kept in control conditions during the experiment, at the constant temperature of 25°C, daily wetted and 12h dark and 12h light (ca. 50 µmol m^{-2} s^{-1} PAR photons).

Results: The photoefficiency results showed significant differences between the FM and DM samples. Yield values were found to correlate with temperature and humidity day-night cycles. The yield recovery values showed significant differences between the treatments, highlighting that UV irradiation caused stronger effects on fluorescence values. Raman spectroscopy showed that carotenoids' signals from UV exposed samples decreased significantly after the exposure. TEM analyses confirmed that UV exposed samples were the most affected by the treatment, showing chloroplastidial disorganization in photobionts' cells. Overall, *X. parietina* was able to survive to the simulated Mars conditions, and for this reason it may be considered a candidate for space long exposure and evaluations on the parietin photodegradability under UV-radiation.

References: [1] Nimis P.L., 2016. ITALIC 5.0. University of Trieste (http://dryades.units.it/italic). [2] Silberstein, L. *et al*. (1996). *The Lichenologist*, 28:355-365. [3] Solhaug, K. A., and Gauslaa, Y. (1996). *Oecologia*, 108:412-418. [4] Onofri, S. *et al*. (2012). *Astrobiology*, *12*(5), 508-516. [5] De Vera, J. P. *et al*. (2010). *Astrobiology*, *10*(2), 215-227. [6] Lorenz, C. *et al*. (2022). *IJA*, 1-17. [7] Lorek, A., and Koncz, A. (2013). *Habitability of Other Planets and Satellites* (pp. 145-162). Springer, Dordrecht. [8] De Vera, J. P. *et al*. (2014). *Planetary and Space Science*, *98*, 182-190. [9] Cockell, C. S. *et al*. (2000). *Icarus*, *146*(2), 343-359.

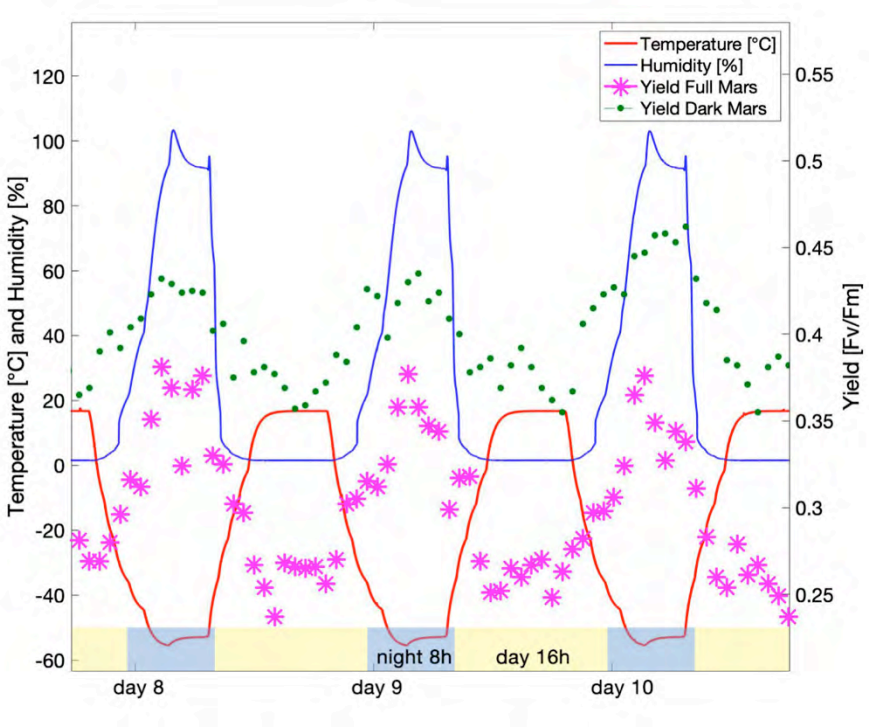

Figure 1 - Detail of the day-night cycles of the simulated Mars conditions (temperature, red thick line; humidity, blue thin line) and fluorescence variation values for both the treatments (FM and DM).

OPEN QUESTIONS ABOUT THE ORIGIN OF LIFE: WHERE TO GO IN SOLAR-SYSTEM STUDIES

G. Vladilo[1], [1]INAF-Osservatorio Astronomico di Trieste – Via G.B. Tiepolo 11, 34131 - Trieste

Introduction: The search for life beyond Earth is one of the main motivations for the exploration of the Solar System and for spectroscopic studies of exoplanetary atmospheres. The potential presence of life in remote environments depends not only on their habitability (e.g. the presence of liquid water), but also on the existence of (past) conditions suitable for the emergence of life. These conditions are poorly understood, but we should try to identify them in order to predict if life can actually be present in a planet or moon that is considered to be habitable. In this general context, I will review a few open questions about the origin of life and examine which indications they may give for future astrobiological studies. First, I will contrast the capability of surface and sub-surface planetary environments to support the emergence of life. I will then discuss the potential prebiotic contribution of different natural sources of ionizing radiation in the archean Earth. Finally, I will examine the possibility that the β− decays originated by the radioactive isotope of potassium, ^{40}K, may have induced chiral effects in prebiotic molecular structures.

Heterotrophic versus autotrophic scenarios: An important question concerning the origin of life is the dichotomy between heterotrophic and autotrophic scenarios postulated in studies of life origins [1]. In the heterotrophic scenario, the self-organization processes leading to the origin of life are generated by organic material accumulated on Earth, via Miller-type synthesis, or delivered from space. In the autotrophic scenario, the chemical substrates and intermediates are generated autonomously within self-organized structures. The large number of laboratory experiments of prebiotic chemistry performed in the past seven decades have been able to synthesize most of the basic ingredients of terrestrial life [1,2]. A general conclusion that can be inferred from these experiments is that, in order to be successful, each step of prebiotic chemistry requires its own specific conditions. In other words: life cannot emerge in a single pot with a single recipe. This suggests the following requirements for the emergence of life: (i) the possibility of transporting chemicals between sites with different physico-chemical conditions and/or (ii) the existence of sites that undergo suitable changes of physico-chemical conditions. Based on this and other requirements of abiogenesis, I will point out the potential advantages of planetary surfaces and/or shallow waters for a heterotrophic origin of life. An autothrophic origin in submarine hydrothermal vents faces several problems [3] that I will briefly outline. The implications for the emergence of life in planets or moons of the Solar System, or in different types of exoplanets, will be summarized.

Ionizing radiation and origin of life: Natural radionuclides are often considered as potential actors in the scenario of prebiotic chemistry [4]. Most of the studies driven by this idea have examined the radiochemical impact induced by the unstable isotopes of uranium and thorium. However, the decay products of these heavy isotopes (α particles and unstable nuclei) would severely damage the replicating and/or catalytic molecules that are expected to emerge in the most advanced stages of the transition to the first forms of life. Therefore, while we cannot exclude that radioactive uranium and thorium might have played a role in early prebiotic stages, we should examine alternative sources of radioactivity as potential contributors to the final stages of abiogenesis. In this presentation, I will consider milder sources of radioactivity, namely short-lived radionuclides of astrophysical origin, radiation sources generated by Galactic Cosmic Rays and, in more detail, the unstable isotope of potassium, ^{40}K, which is characterized by decay products (mostly β particles and stable nuclei) that have a moderate radiochemical impact [5].

Radioactive potassium in prebiotic chemistry. Potassium is abundant and widespread in the Earth's crust and oceans, whereas uranium and thorium are rare and concentrated in specific niches. Assuming continuity with extant biology, potassium (including its unstable isotope) was probably incorporated in the earliest, fully developed terrestrial cells. Based on these arguments, ^{40}K was likely to be present in all the prebiotic stages and, with a proper flux of decaying particles, may have influenced the molecular evolution leading to the emergence of life. The fact that the isotopic ratio ^{40}K/K was one order of magnitude higher at the epoch of the origin of terrestrial life than at the present time bolsters this possibility. For plausible values of concentration of potassium compounds, the radiation dose generated by ^{40}K decays in an Archean prebiotic solution could have been two orders of magnitude higher than that generated by the present-day radiation background (Fig. 1). Estimates of the radiochemical impact of the resulting flux of β particles on polymers embedded in prebiotic solutions will be provided for different scenarios of propagation of secondary effects in water. Molecular structures may be af-

fected depending on: (i) the possibility of accumulating radiochemical effects and (ii) the distance range over which hydrogen bonds (expected to be ubiquitous when life emerges [6]) can propagate the effects of β− decays. Finally, the possibility of accumulating radiochemical effects in the primitive Earth or in small bodies of the Solar System will be briefly discussed.

Origin of biomolecular chirality: The origin of the chirality of terrestrial biomolecules is still an open question in studies of the origin of life [1]. In the final part of my presentation I will discuss the possible role of ^{40}K in this context. The potential link between homochirality and ^{40}K is the parity violation of the β− decay [7]. As a result of parity violation, the spin component of the emitted fast electrons is always antiparallel to the direction of motion. By coupling their spin with that of the molecules encountered along their path, the β particles may induce a chiral imprint in the molecular structures [8]. Despite the large number of studies trying to link the origin of homochirality to physical processes, the effects of a persistent injection of β particles in protobiological structures have never been examined. Among other natural sources of β− particles, ^{40}K is the only one that was more abundant at the epoch of the origin of life than today. Its potential chiral impact is discussed in the context of the conditions of the archean earth (stronger UV radiation; flux of Galactic cosmic rays attenuated by enhanced solar activity). The propagation of chiral effects in prebiotic molecules dissolved in formamide, a molecule particularly effective in prebiotic pathways [2], will be briefly discussed. Laboratory experiments will be proposed to test the possible chiral impact of ^{40}K. The possibility that the enantiomeric excesses of L-type amino acids found in Carbonaceous Chondrites [9] could have been triggered by ^{40}K effects accumulated over long periods of time should be explored.

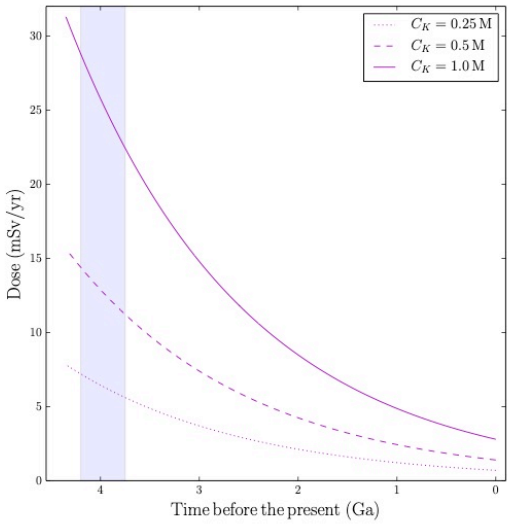

Fig. 1. Dose of β− radiation generated by ^{40}K in aqueous solutions of potassium ions with plausible values of molar concentration, C_K, indicated in the legend. Each curve takes into account the evolution of the ^{40}K/K isotopic ratio from the time of the Earth's formation to the present time. The vertical band indicates a plausible time interval for the emergence of terrestrial life. For comparison, the present-day doses of the Earth radiation background from the ground and cosmic rays are 0.48 and 0.39 mSv/yr, respectively.

References:

[1] Luisi P. L. (2016) *The Emergence of Life: From Chemical Origins to Synthetic Biology, Cambridge Univ. Press*. [2] Saladino R. et al. (2019) *Chemistry-A European Journal*, 25, 3181–3189. [3] Deamer et al. (2019) *Astrobiology* 19, 1523–1537. [4] Altair T. et al. (2020) *Astrobiology* 20, 1489–1497. [5] Vladilo G. (2022) *Life, 12,* 1620. [6] Vladilo G., Hassanali, A. (2018) *Life, 8,* 1. [7] Wu et al. (1954) *Phys. Rev., 105*, 1413. [8] Keszthelyi, L. (1977) *Origins of Life, 8*, 299–340. [9] Pizzarello, S. (2016) *Life*, 6, 18.

DESERT CYANOBACTERIA: LESSON LEARNED FROM ASTROBIOLOGY EXPERIMENTS IN LOW EARTH ORBIT AND IMPLICATIONS FOR FUTURE MISSIONS. D. Billi. University of Rome Tor Vergata. Departmnet of Biology. Via della Ricerca Scientifica snc, 00133 Rome Italy. billi@uniroma2.it

Introduction: The astonishing capability of life to adapt to extreme conditions has provided a new perspective on what 'habitable' means and to detect signatures of past or present life beyond Earth. Desert cyanobacteria of the genus *Chroococcidiopsis* have been exposed to several ground-based simulations of space and planetary (and exoplanetary) conditions as well to real to space and martian conditions simulated in low Earth orbit (LEO).

Results: When exposure conditions did not exceed repair capabilities, insights were gained on the constraints that life can withstand. When the accumulated damage exceeded the survival potential, the scored biomarker persistence contributed to the search for life beyond Earth. Results from the Biology and Mars Experiment (BIOMEX) and (Biofilm Organisms Surfing Space (BOSS) showed that ultraviolet radiation (e.g., doses corresponding to a few hours on the martian surface) is the factor that mostly affects cell survival and biomarkers detectability as reveled by confocal laser scanning microscopy and Raman spectra signals [1,2]. On the contrary, high doses of ionizing radiation (e.g., a dose accumulated in 13 Myr at 2 m depth from the martian surface) did not impair biomarkers detectability both when considering Raman spectra signals [3,4], or fluorescence sandwich microarray immunoassay, the latter tested in the context of the BioSignatures and habitable Niches (BIOSIGN) using the Signs of Life Detector (SOLID)-LDChip system [5]. The capability of desert strains of *Chroococcidiopsi*s to repair the accumulated DNA damage upon rehydration after 1.5-year exposure in LEO provided new insights into the resilience of a putative dormant life in the Martian subsurface [6,7]. Moreover, during the project Life in Space the survival potential of dried *Chroococcidiopsi*s cells exposed to salty-ice conditions simulating the environment of icy worlds was reported [8]. In addition it was reported the capability of a desert strain to modify its photosynthetic apparatus and harvest far-red light (near-infrared) with implications for the possibility of oxygenic photosynthesis on exoplanets and surface biosignatures [9]. In the overall, the gathered knowledge will contribute on how to advance scientific utilization of future space exposure platforms that are either under development or in an advanced planning stage. In addition to the International Space Station, these platforms include CubeSats or platforms like the Lunar Orbital Gateway or the European Large Logistics Lander.

References: [1] Billi D et al. (2019) *Astrobiology, 19(8)*, 1008. [2] Billi D. et al. (2019 *Astrobiology, 19*, 158. [3] Baqué M. et al. (2020) *Life* (Basel) *10*, 83. [4] Baqué M et al. (2022) *Sci. Adv., 8*, 36. [5] Billi D, et al. (2022) *Astrobiology 22*, 1199. [6] Mosca C, et al. (2022) *Int. .J Astrobiol., 1*, 12. [7] Mosca C, et al. (2021). *Astrobiology, 21,* 541. [8] Cosciotti B et al. (2019) *Life* (Basel) *9*, 86. [9] Billi D. al. (2022) *Front. Microbiol., 13*, 933404.

Funding : ASI BIOMEX_Cyano 2013-051-R.0; ASI BOSS_Cyano 2013-053-R.0; ASI BIOSIGN_Cyano 2018-15-U.0; ASI Life in Space 2019-3 U.0 Life in Space.

WORLDWIDE DISTRIBUTION OF ACIDOPHILIC EXTREMOPHILES PROVIDES INSIGHTS INTO FUTURE SPACE BIOLOGY APPLICATIONS

L. Tonietti[1], M. Esposito[2], A. Bastianoni[2], B. Barosa[2], M.T. Muscari Tomajoli[1], S. Fiscale[1], P. Di Donato[1,4], A. Cordone[2], D. Giovannelli[2,5,6,7,8], G. Covone[9], A. Rotundi[1,3]. [1]Department of Science and Technology, Parthenope Univ. of Naples, Italy,. [2]Biology Dept. Univ. Federico II, Naples, Italy, [3]INAF-Istituto di Astrofisica e Planetologia Spaziali, Rome, Italy, [4]CNR-Pozzuoli, Naples, Italy, [5]CNR-IRBIM, Ancona, Italy, [6]Dept of Marine and Coastal Science, Rutgers Univ. New Brunswick, NJ, USA, [7]Marine Chemistry & Geochemistry Dept. WHOI, MA, USA, [8]Earth-Life Science Institute, Tokyo Institute of Technology, Tokyo, Japan, [9]Physics Dept. Univ. Federico II, Naples, Italy.
Corresponding author: L. Tonietti (luca.tonietti001@studenti.uniparthenope.it)

Topic: Astrobiology & Astrochemistry

Introduction: Extremophiles are of paramount importance in human space exploration because of their ability to thrive in extreme environmental conditions. They can be used to build sustainable systems on long-term stations on the Moon and on Mars [1].

Many extremophilic microorganisms, especially acidophilic (i.e..microorganisms that can survive in extremely acidic environments, pH < 2.5) are capable of mobilizing resources e.g., Transition Metals and Rare Earth Elements (REEs) throughout a plethora of reactions with almost the entire periodic table. The ability of these organisms to dissolve, precipitate and mobilize different elements makes them ideal candidates for biotechnological applications, preferably applied directly on-site in space biology, through an approach known as in-situ resource utilization (ISRU) [1,2].

The long-term presence of humans in space is indissolubly linked to our ability to limit the demand for terrestrial materials and resources. ISRU, biomining, and biohydrometallurgy are the only environmentally sustainable approaches for colonizing the Moon and Mars [2]. However, before these approaches, it is imperative to understand the relationship between acidophilic extremophiles and their natural environments, e.g., the type of fluid and the geochemistry of the rock in which they can grow. [3]

It is of fundamental importance to select one or more microorganisms to carry out experiments in future manned space missions (e.g., Artemis missions).

Our mission: Currently, microorganism survival experiments in simulated and natural conditions (as well as on the ISS and in low-Earth orbit) are mainly focused on evaluating the ability of selected groups of microorganisms to cope with severe space conditions. In doing so, the potential of extremophiles to exploit resources in situ has been almost entirely overlooked. [4]. Based on a thorough literature search and a Bibliometric Network Analysis (BNA) (Fig.1) we discovered that *Acidithiobacullus ferrooxidans* is one of the best candidates to perform bioming on Earth.

A. ferrooxidans is an acidophilic organism found in the waters of Acid Mine Drainage (AMD) that has been associated with pyrite oxidation. It is able to utilize Fe(II), S^0, or sulfide minerals as an energy source for metabolic activities and plays an important role in the biogeochemical cycle of iron and sulfur. Because of its well-known ability to dissolve and mobilize metals in extreme environments e.g., AMDs, acidic natural environments, limonite and copper mines, and chalcopyrite-rich ores, it is an excellent candidate to support space exploration. In addition, we found from an analysis of the literature that it is able to mobilize metals from almost all elements of the periodic table (not only from sulfidic iron-nickel-copper ores) (Fig.2) [5].

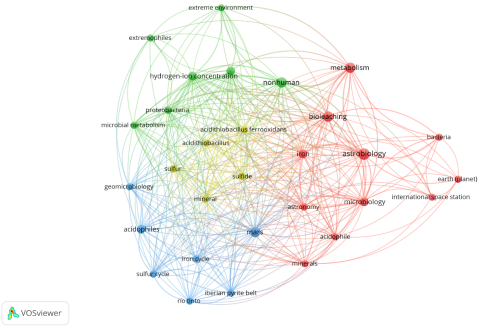

Fig.1. Co-occurrence network map of keywords in the global scientific literature on astrobiology, biomining, and bioleaching. The size of each keyword (node) in the network is directly proportional to the number of occurrences in the documents analyzed. Colors indicate clusters to which keywords are uniquely assigned, based on their reciprocal relatedness.

A. ferrooxidans grows in an acidic environment with an optimal pH between 1.8 and 5.0 and an optimal growth temperature between 30 °C and 40 °C. Knowing the best parameters for *A. ferrooxidans* microbial growth, we checked the sample database (edited with details of coordinates, range of T, pH, etc) of all scientific expeditions conducted from 2017 to 2022 by the GiovannelliLab, at the University of Naples "Federico II". in order to select five different sampling sites and planetary analogs to perform biogeochemical analysis (Tab.1) e.g., metagenomics, geochemistry assays, medium culture, and biomining application.

ExpID	SiteID	Country	SiteName	year	latitude	longitude	altitude	temp	ph
AEO22	AC	Italy	acque_calde	2022	38,417502	14,959262	1	30	3.42
CHL22	IS	Chile	Irruputuncu_Acidic_Spring	2022	-20,7259	-68,5862	4042	38.41	2.38
CR19	LF	Costa Rica	Las Pailas Frias	2019	10,77169	-85,30735	NA	22	2
CR22	HC	Costa Rica	Huacalillo	2022	10,088665	-84,118275	1770	32.2	1.97
FENIX21	PI	Italy	Piccolo Inferno	2021	41,314487	13,894006	61	29.5	2.13
ICE21	HV1	Iceland	Hveragerdi	2021	64,007062	-21,180739	118	25.7	1.82

Tab.1. Distribution and physical-chemical parameters of the chosen sites.

The selected sites are distributed around the world in areas of volcanic activity ranging from the Aeolian Islands and the hydrothermally active areas of the Campania region in Italy (i.e., AEO22 and FENIX21) to the Fire Belt of Chile and Costa Rica (i.e., CHL22, CR19, and CR22) and end in Iceland (i.e., ICE21).

This project aims to harness the natural ability of acidophiles to interact with minerals, rocks, and elements essential to technological development in human settlements for the exploitation of extraterrestrial resources. It is known that numerous minerals found on both the lunar surface and the surface of Mars, e.g., basalts, olivines, and pyroxenes, contain a large number of metals useful for technological development on Earth, e.g. Ni, Cr, Fe, V, Mo, Al, Zn, silicate, and sulfides. All useful and essential elements for both microbial survival and the ISRU approach. [6,7]

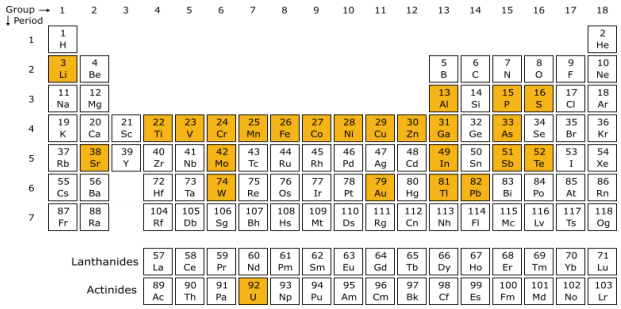

Fig.2. Elements mobilized by *A. ferrooxidans* in biomining and biohydrometallurgy processes.

Results: From BNA analysis, we discovered that acidophilic extremophiles are the best candidates to perform biomining and bioleaching in space long-term stations, as we can see from Fig.1 where we have *A. ferrooxidans* (shown with a yellow bullet) which are closely connected to all the other keywords derived form statistical analysis, e.g., bioleaching, Mars, Astrobiology, acidophiles, minerals, etc. From a deep literature review, we found that acidophilic organisms, and in particular the member of the *Acidithiobacillaceae* family and the experimental candidate *A. ferrooxidans*, are capable of interacting with most metals of biotechnological interest in the periodic table as shown by Fig.2. From metagenomic analysis of some of the selected sites e.g., CR19-Las Pallas Frias modified with CR19-Salitras Lilas, FENIX21-Piccolo Inferno, and ICE21-Hveragerði (Fig.3) the presence of the different families of *Acidithiobacillaceae* is evident. For the other locations e.g., AEO22-Acque Calde, CHL22-Irruputuncu, and CR22-Hucacalillo, further analysis must be carried out.

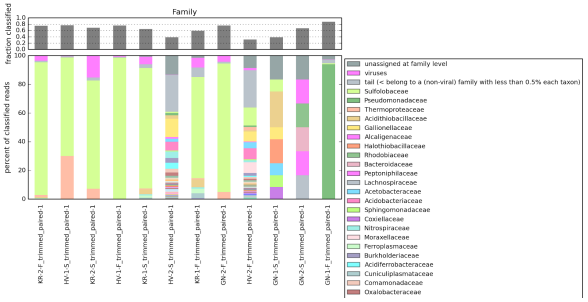

Fig.3. Metagenomic analysis of the ICE21-Hveragerði site. The pink bar represents the presence of *Acidithiobacillaceae* organisms in the soil and liquid samples.

In addition, to test for the presence of *A. ferrooxidans* as a member of the *Acidithiobacillaceae* family, we planned to perform plating experiments in a selective solid medium (9K + agar) already mixed for the biomining liquid experiment, followed by 16S rRNA analysis of the Pure culture after serial dilutions to confirm the species [8,9].

Conclusions: The presence of the family *Acidithiobacillaceae* and the presence of *A. ferrooxidans* are the best evidence for the selection of acidophilic organisms for space biology applications. Through BNA analysis, we found out that acidophilic organisms and *A. ferrooxidans* are the best candidates for space biomining applications. Furthermore, we understood that *A. ferrooxidans* is able to interact with various industrially important elements of the periodic table, e.g., Li, Al, Cr, Fe, Cu, Ni. From metagenomic analysis we found that the distribution of members of the family *Acidithiobacillaceae* in active volcanic areas around the world is the best evidence for the interaction and the co-evolution between minerals and microorganisms capable to perform biomining and bioleaching operations in space environments.

Future Developments: Further analysis, e.g., 16s rRNA characterization (for all samples), metagenomics analysis and geochemical characterization for the 2022 sampling sites, will be performed.

References: [1] Merino N. et al (2019) *Frontiers in Microbiology*, 10:780. [2] Sacksteder K. R. et al (2012) *Aerospace Research Central*, 2007-345. [3] Giovannelli D. (2022) *EarthArXic.* [4] Cockell C. et al (2021) *Frontiers in Microbiology,* 12. [5] Valdes J. (2008) *BMC Genomics* 11;9:597. [6] Covone G and D. Giovannelli (2022) *arXiv* 2207.03748. [7] Wiens R.C. (2022) *Science Advances* 8.34. [8] Chen H. et al (2009) *Microbiological research* 613-623. [9] Fullerton K.M. et al (2021) *Nature Geoscience* 14, 301-306.

EUKARYOTIC ORGANISMS EXPOSED TO SPACE ENVIRONMENT: A FOCUS ON THE PHYSIOLOGICAL ADAPTATIONS OF THE BRINE SHRIMP *A. SALINA* TO ASTROBIOLOGICAL STUDIES

M.T. Muscari Tomajoli[1], A. Rotundi[1,2,3], P. Di Donato[2,4], P. Venditti[5], G. Covone[5,6], V. Della Corte[3], E. Zona[6], L. Tonietti[1], L. Inno[2], G. Fasciolo[5], I. Bertini[2,3], S. Fiscale[1], E. Geremia[2], C. Magliano[5], A.M. Piccirillo[1], G. Napolitano[1,2]

[1] UNESCO Chair "Environment, Resources and Sustainable Development, Department of Science and Technology, Parthenope University of Naples, Italy.
[2] Department of Science and Technology, Parthenope University of Naples, Italy.
[3] INAF-Istituto di Astrofisica e Planetologia Spaziali, Rome, Italy.
[4] Institute of Biomolecular Chemistry, CNR-Pozzuoli, Naples, Italy.
[5] Department of Biology, Univ. Federico II, Naples, Italy.
[6] INAF-Osservatorio Astronomico di Capodimonte, Naples, Italy.

Corresponding author: M.T. Muscari Tomajoli (mariateresa.muscaritomajoli001@studenti.uniparthenope.it)

Topic: Astrobiology & Astrochemistry

Introduction

Space exploration with a view to future animal and human colonization of Solar System bodies poses unique challenges for astrobiological studies. Extraterrestrial environments are the most complex for the biological systems survival. Space travels expose lifeforms to conditions such as microgravity, hypergravity (during launch and propulsion phases) and space radiation [1] that can affect their survival and/or induce mechanisms of adaptation. Moreover, in the absence of proper environmental control, exposure to vacuum and extreme temperatures is also possible. It is reported that the coupled effect of space radiation with vacuum exposure significantly decreased survivability of organisms [1]. Characteristics such as low metabolic rate per unit of mass, cryptobiotic capacity, and high radiation tolerance appear to be critical for the survival of species in space travel [1]. Species exhibiting a low metabolic rate, as compared to other organisms of similar size, will have the possibility to survive for extended periods of time on a spacecraft, where nutrients are scarce. Higher radiotolerance in terms of lower nuclear material content in cells, abilities to regenerate tissue and organs, and ability to repair DNA [2], will allow the organisms to face space conditions. An ideal biological form to be transported alive across large distances in space should undergo cryptobiosis at the beginning of the journey to then be brought out of hibernation at destination. Species with cryptobiotic capability would have higher survival rates during interplanetary travels, as lowered metabolism will confer added protection against the space environment [1].

Recently, the brine shrimp *Artemia salina* (also known as "Sea Monkeys") was proposed to check for its survival in interplanetary space because of its capacity to become anhydrobiotic organism (cyst form) [3]. Dormant gastrulae (cysts) appear particularly useful to study the effects of space environments on biological forms: *Artemia* cysts survived 437 days of space flight [4]. A.*salina* cysts contain only minimal amounts of water and no metabolic activity is performed. During the drying out process (desiccation), the lack of water forces substances to increase their concentration. Adaptations to desiccation are critical for organisms to survive in interplanetary space, considered the "desert" space [3].

Aim and Methods

From the state of the art, our purpose is to study the physiological adaptations of the eukaryotic model brine shrimp *A.salina* to extraterrestrial environmental conditions. We started our investigation analyzing the responses of *A.salina* to low pressure (4-6 mbar) conditions by means of a Mars simulator that we set-up in our laboratory, at the Parthenope University of Naples. The simulator consists in an equipped vacuum chamber in which the samples can be exposed to the following conditions: UV irradiation (254 nm), low pressure (4-6 mbar) and CO_2 environment. It is under development the chamber upgrade that will simulate Martian thermal cycles.

A.salina cysts were exposed to low pressure (4-6 mbar) for one hour and subsequently placed in artificial sea water under controlled temperature (28°C) and aeration conditions. After 72 hours the percentage of hatching was evaluated and the larval forms of *A.salina* (nauplii) were used for the analysis related to physiological adaptations by performing *in vivo* and *in vitro* measures. The *in vivo* experiments were performed on living nauplii of *A.salina* while the *in vitro* experiments was carried out on homogenates of nauplii

populations. Nauplii collected from the artificial seawater were resuspended in ice-cold homogenization medium (HM) (220 mM mannitol, 70 mM sucrose, 1 mM EDTA, 10 mM Tris, pH 7.4) and homogenized using a glass Potter-Elvehjem homogenizer set at a standard velocity (500 rpm) for 1 min. Protein concentration in homogenates was measured by the biuret method [5] and aliquots were used for analytical procedures. The rates of oxygen consumption were polarographically determined at 28°C by using an Hansatech respirometer. The *in vivo* mitochondrial respiration was performed on living nauplii in artificial seawater and the rate of oxygen consumption was normalized for the number of nauplii used for the measure. The *in vitro* mitochondrial respiration was performed on nauplii homogenates by using different substrates like succinate or a mix of pyruvate plus malate, in the absence (State 4 of mitochondrial respiration) and in the presence of ADP (Adenosine Diphosphate) (State 3 of mitochondrial respiration) [6].

Analysis related to the cellular redox state was also performed. The redox homeostasis derives from a delicate balance between the levels of Reactive Oxygen Species (ROS) produced during metabolism, and the antioxidant system that can scavenge ROS [7]. ROS are very unstable molecules able to infer oxidative damage to cellular components, but they are also involved in signaling pathways [8-9], which allow the animals to adapt to new environmental conditions. The investigations related to redox homeostasis are relevant to understand whether *A.salina* can be used as suitable model of eukaryotic organisms to survive in the space environment. In this view, ROS content [10], total antioxidant capacity [11], antioxidant enzymes activity [10], were carried out on nauplii homogenates.

Results:

***In vivo* measures**

1. *Percentage of hatching:* one hour of low-pressure exposure (4-6mbar) significantly increased the percentage of hatching respect to the control group.
2. *Oxygen consumption*: low-pressure exposure significantly increased the *in vivo* oxygen consumption of nauplii hatched after the exposure.

***In vitro* measures**

1. *Oxygen consumption*: one hour of low-pressure exposure significantly reduced the *in* vitro oxygen consumption respect to the control group in both State 4 (in absence of ADP) and 3 (in presence of ADP) of respiration and in presence of Succinate (a substrate linked to the Complex II of the Electron Transport Chain - ETC) and a mixture of Pyruvate plus Malate (substrates linked to the Complex I of ETC).
2. *Reactive Oxygen Species (ROS) content* and *oxidative damage to lipids, Lipids Hydroperoxides (HPs)*: ROS content is significantly decreased after low-pressure exposure respect to the control group. These results parallel the HPs reduction.
3. *Total antioxidant capacity* and *in vitro susceptibility to oxidants*: low-pressure exposure significantly reduced total antioxidant capacity and in parallel increased the *in vitro* susceptibility to oxidants.

Conclusions and future perspectives:

In conclusions, *A.salina* is a suitable model for astrobiological studies. These preliminary results show that nauplii can hatch after a great stress induced by low-pressure, and they show interesting challenges for further experiments.

Nauplii hatched from cysts exposed to low-pressure showed an increased *in vivo* oxygen consumption associated with a reduction of *in vitro* oxygen consumption, probably due to a metabolic shift from aerobic to anaerobic metabolism of animals. Moreover, low-pressure exposure affects the redox homeostasis of samples by reducing ROS content, HPs levels and total antioxidant capacity, while increasing the *in vitro* susceptibility to oxidants.

Further experiments are necessary to clarify the metabolic changes in animals hatched from cysts exposed to one hour of low-pressure, and the mechanisms by which ROS modify redox homeostasis, thus inducing the adaptations of animals.

References:

[1] *Lantin, S. Et al. (2021). arXiv preprint arXiv:2110.13080.* [2] *Harrison, et al. (1996). Taxonomic and Developmental Aspects of Radiosensitivity. UCRL-JC-125920* [3] *Rothschild, L., and Reprinted, A. A. (2002). Part 2. Nasa Ames Research Center.* [4]. *Marthy, H-J. "Developmental biology of animal models under varied Vie et Milieu/Life & Environment (2002): 149-166*. [5] Gornall, *J. Et al.* (1949) *biol. Chem* 177.2: 751-766. [6] *Napolitano, G., et al. JPhysiolBiochem (2022); 78: 415–425.* [7] *Di Meo, S.et al.* (2019) *International Journal of Molecular Sciences* 20.19:4810. [8] *Napolitano, G., Fasciolo and G., Venditti, P. (2021) Antioxidant 10.11: 1824.* [9] Di Meo, S et al. *Oxidative medicine and cellular longevity* 2016 (2016). [10] *Napolitano, G, et al. Journal of Cleaner Production 374 (2022): 133978.* [11] *Erel, O., Clinical biochemistry (2004) 37 (4), pp.277-285.*

Evolution of climate and observational properties of a habitable rocky planet: Earth.

L. Silva[1,2], L. Biasiotti[3,1], E. Bisesi[1,4], S.L. Ivanovski[1], M. Maris[1,2], G. Murante[1,2,4], A. Provenzale[4], P. Simonetti[1] and G. Vladilo[1]. [1]INAF/OATs-Trieste, [2]IFPU-Trieste, [3]Univ. Trieste., [4]CNR/IGG-Pisa

Introduction: The present surface temperatures of rocky planets of the Solar System, as well as of currently detected exoplanets, are just a snapshot within a continuous evolution of properties acting and interacting at all scales – i.e., atmospheric, geological, planetary, stellar, orbital, and even galactic. The evaluation of (exo)planetary and Terrestrial current and past climates is of paramount importance in many research fields: climatology, astrobiology, (exo)planetary habitability and search/interpretation of (atmospheric or in situ) biosignatures.

Investigations of the Earth paleo-climate impact our understanding of the current and future possible climates, by studying the response of surface temperature to different types and amounts of forcings and feedbacks that may have taken place at different geological times (e.g. greenhouse gases, surface ice-land-water coverage, solar luminosity, e.g. [1, 2]). Indications about the surface temperature of the paleo-Earth, as derived by several geological markers, show that, on average, Earth has always been habitable, i.e., liquid water was present on the Earth surface since at least the Archean eon (~ 4 to 2.5 Gyr ago), despite significant differences in insolation and in many other planetary properties (e.g. [3]). It is within these environmental properties that the origin or at least the early evolution of life took place, as witnessed by the most ancient discovered biomarkers on Earth, dating back to the Archean eon.

Earth is currently the only known habitable and inhabited planet, therefore it is the best example to be studied as a reference in the search for habitable exoplanets and for the future detection and interpretation of their spectral features in terms of atmospheric structure, composition and biosignatures (e.g. [4]). During its geological history, Earth climate and its surface, atmospheric and spectral properties have deeply changed, despite remaining inhabited, even during snowball events. Were it observed as an exoplanet, Earth observability and atmospheric spectral features would have been drastically different at different epochs throughout its history, and in particular if compared to the present appearance. In fact, for a long time since Solar System formation, Earth has been characterized by an essentially anoxic atmosphere. Due to the large geological uncertainties, many different but anyway all plausible climate/surface/atmospheric properties may be representative of the early Earth climate, and therefore, for simulating samples of potentially habitable terrestrial-type exoplanets, and their corresponding observable spectra.

The possibility of detecting spectral biosignatures on rocky exoplanets is based on the notion that a widespread surface life may produce metabolic gaseous waste products able to affect the atmospheric composition to detectable levels. This implies that it is important to evaluate not only the current habitability, but also its possible time scale, since long-term habitability is considered as a basic requirement for the development and maintenance of an intense and ubiquitous biological activity. Due to stellar luminosity evolution, any terrestrial-type planet must therefore undergo important atmospheric/climatic evolution to be able to maintain a habitable environment. In addition, the evaluation of the best targets for future spectroscopic surveys, as well as their interpretations, must rely also on simulations of detectable spectral features, possibly accounting for unavoidable observational limitations, such as refraction and clouds.

Here we present preliminary results on the works we are performing aimed at exploring climate, atmospheric properties, habitability and observability of the Archean- and modern-Earth. This work is part of a broader project, aiming to study the climate evolution of other planets such as Venus and, in particular, Mars (see abstract by P. Simonetti). We aim to (i) probe the potential environmental conditions for the origin and early evoution of life; (ii) explore the effects of different climate feedback processes that heavily affect (and/or have affected) Earth habitability and appearance (e.g. ice-albedo and vegetation-albedo feedbacks); (iii) adopt the models of the evolution of Earth climate and appearance as a reference for simulating habitability and detectability of terrestrial-type exoplanets. The simulations are performed with the most recent version of our climate and atmospheric model EOS+ESTM, that is appositely suited to explore a large atmospheric, planetary and orbital parameter space. This model accounts for the full atmospheric radiative transfer, and treats the main climate factors and feedbacks with physically-based formulations.

Climate and atmospheric models: Our climate model ESTM ([5, 6]) is specifically developed to perform multi-parametric explorations of the climate of terrestrial-type rocky planets. Its most recent version is

interfaced with the RT and atmospheric model EOS ([7, 8]), that allows any chemical composition and surface pressure to be explored. We have applied our model to study climate, habitability and observability of rocky exoplanets ([9, 10]); the statistics of the habitability in binary stellar systems ([11]); the statistics of climate bistability induced by the ice-albedo feedback (i.e. the probability of snowball events), and its relation with habitability ([12]).

Modelling the evolution of Earth climate: ESTM has been shown to well reproduce many aspects of the modern Earth (such as temperature and ice distributions, OLR and meridional energy flux, [5, 6]), as well as the possibility of snowball events driven by the ice-albedo feedback ([12]). Recently we have included into ESTM the modelling of the vegetation/albedo feedback and of its effects on Earth's habitability. This feedback can affect, through the so-called Charney mechanism ([13]) the surface temperature and therefore the width of the habitable zone (Bisesi et al. 2023).

We have also recently simulated with EOS+ESTM several atmospheric pressures with anoxic compositions, that might have characterized the early Earth. We are exploring the corresponding expected surface temperatures and habitability, by including in the computations also other available constraints, e.g. the evolution of the solar luminosity, of the rotation period, and of the continent coverage ([8, 14]). We have further connected each simulation to its observability. In fact, the same environmental conditions that determine climate and habitability, rule also the atmospheric (transmission and emission) spectra. In particular, we will present our up-to-date simulations of the effects of refraction in the detectability of spectral features of Earth-analogues observed in transmission (Maris et al. 2023).

References: [1] Cronin T. M. (2010) *Paleoclimates: Understanding Climate Change Past and Present*, Columbia University Press. [2] Krissansen-Totton J., Arney G.N. and Catling D.C. (2018) *PNAS*, 115(16), 4105-4110. [3] Catling D.C. and Zahnle K.J. (2020) *Sci.Adv.* 6(9):eaax1420. [4] Alei E. et al. (2022) *A&A*, 665, 106. [5] Vladilo G. et al. (2015) *ApJ*, 804, 50. [6] Biasiotti L. et al. (2022) *MNRAS*, 514, 5105. [7] Simonetti P. et al. (2022) *ApJ*, 925, 105. [8] Simonetti P. (2022) *PhD Thesis*. [9] Silva L. et al. (2017) *IJAsB*, 16, 244. [10] Silva L. et al. (2017) *MNRAS*, 470, 2270. [11] Simonetti P. et al. (2020) *ApJ*, 903, 141. [12] Murante G. et al. (2020) *MNRAS*, 492, 2638. [13] Charney J. et al. (1975) *Drought in the Sahara: A biogeophysical feedback mechanism*, *Science,* 187, 434. [14] R. Bevilacqua (2022) *Master Thesis*.

Microwave thermal emission from Solar System Planets and CMB calibration. M. Maris[1] and M. Tomasi[2], [1]INAF/Trieste Astronomical Observatory, Via G.B.Tiepolo 11, 34135 Trieste michele.maris@inaf,it, [2]Milano University, Physics Department, Via Celoria 17, Milano, maurizio.tomasi@unimi.it

Introduction:

Microwave thermal emission from Solar System Planets in the frequency range 1 GHz - 1 THz, have been the subject of extensive investigations in the '80 and '90 of last century, producing a legacy of observations and models (as an example: [1-8]).

In the last decades planets, in particular giant planets, have been chosen by ground based and space based CMB observatories as standard calibrators. Planets are considered as reference sources to calibrate the beam pattern of CMB observatories and as secondary reference sources to intercalibrate the different CMB surveys [9-12].

As a by product CMB observatories produced a corpus of observations in microwave bands which covers the last two decades, with higher sensitivity than the legacy observations from the previous decades, and with a more homogeneous calibration based on the observation of the cosmological dipole. With the race to the B modes detection, the next generation of CMB observatories is expected to further improve the sensitivity and to have an even better control over systematics.

However the improved accuracy asks the future CMB observatories to critically review the traditional way in which planets observations are handled and reduced withi the CMB community. As an example tini effects, such as limb darkening, which are neglected in the current pipelines for CMB analysis will have to be accounted for. The beam patterns derived from such observations are convolved with the planet spectrum and has to be deconvolved in order to obtain the effective beam pattern for Galactic emission or CMB. All of this requires appropriate modeling of planets thermal emission.

Most of the models presently available for Gian Planets are Radiative Transfer models derived from codes developed in the '90. In most cases the code for such legacy models are not available, they are not properly documented, or the authors retired, so that information on such models is not readily available. A comparison with new observations shown relarively large deviations of model emission spectra when compared to the error bars in the new data.

There is an evident need for a new generation of Radiative Transfer models which incorporates the new data from CMB missions as WMAP and Planck.

In addition time variability of planets microwave emission will have to be better characterized.

In addition as CMB observations are evolving to give more and more importance to polarization there will is an increasing interest in assessing the level of linear polarization in thermal emission from giant plants. In particular it would be interesting to asses the level of polarization of radiation emitted from Saturn's rings and its variation with the change in Saturn's aspect angle and sub-observer point.

In this talk we move from our experience with the analysis of Planck data [10,12], complemented with results from WMAP [9], and other observatories, and the expectation of planned future experments to review the status of the field.

References:

[1] Klein, M.J., Gulkis, S., 1978, Icarus, **35**, 44

[2] de Pater, I., 1981, A&A, **93**, 370

[3] de Pater, I. 1982, Icarus, **51**, 25

[4] de Pater, I. and Richmond, M., 1989, Icarus, **80**, 1

[5] Greeve, A., et al., 1991, A&A, **286**, 654

[6] Griffin, M., J., Orton, G., S., 1993, Icarus, **105**, 537

[7] Goldin, A.B., et al., 1997, ApJ, **173**, 439

[8] de Pater, I. et al. AJ 2019, **158**, 139

[9] Weiland, J.L., et al., 2011, ApJS, **192**, 19

[10] Planck Collaboration, Akrami, Y., et al., 2017, A&A, **607**, 122

[11] Karim, R., L., DeBoer,, D., de Pater, I., Keating, G. K., 2018, AJ, **155**, 129

[12] Maris, et. al., 2021, A&A, **647**, 104

MINERALOGICAL MAPPING OF CERES AS REVEALED BY THE 1 μm ABSORPTION

F. G. Carrozzzo[1], Maria Cristina De Sanctis[1], Marco Ferrari[1], Andrea Raponi[1], Mauro Ciarniello[1], Eleonora Ammannito[1], F. Tosi[1]
[1]INAF-IAPS (giacomo.carrozzo@inaf.it)

Introduction: Various minerals have been detected on Ceres and their abundance and spatial distribution has been mapped in the near infrared spectral domain [i.e. 1, 2]. In this work we study the 1 μm absorption to map Ceres mineralogy at a global scale. It is based on the determination of the whole 1 μm absorption from VIR spectra. VIR is the imaging spectrometer on board the NASA mission Dawn in orbit around Ceres and still operating. VIR is composed of two channels: the VIS channel working in the visible wavelengths between 0.26-1.07 μm and the NIR channel operating in the near infrared between 1.02-5.1 μm. The 1 μm absorption is, indeed, in between the instrument channels.

Method: To study the 1 μm spectral range, an automatic method to co-register the VIR and NIR channels, where they overlap, has been implemented, thus allowing the study of this band. After the spatial co-registration, a residual difference in the I/F at 1 μm between the two channels can still remain due to the difference in the PSF's. To avoid this problem, each VIS spectrum is rescaled to the value of the I/F at ~1 μm of the corresponding NIR spectrum. The exact wavelength at which the two VIR channels are matched, inside the overlapping range between 0.92–1.8 μm, is selected for each spectrum on the basis of the best match. The difference between the VIS and NIR reflectance at ~1 μm (ΔR) is usually 1-2% and only about 1% of data show a ΔR>10%. The spectra with the largest mismatch between the two channels are located along the walls of the craters and valleys where the influence of PSF differences is expected to be larger. In this study the data with ΔR>10% are discarded. The maps have global longitudinal coverage, latitudinal coverage from 66°S to 66°N, and a spatial resolution of ~1.86 km/pixel at the equator.

Each spectrum of the surface is the result of areal or intimate mixing of different minerals, and the resulting spectral reflectance properties are a complex combination of the spectra of each mineral end-member. Several studies have shown that it is possible to explore Ceres mineralogical diversity utilizing specific spectral parameters [1,2].

In order to extract compositional information from the spectra, we have introduced some spectral indices and studied the correlations between them all over the VIR data set. Global maps of the 1 μm signature on Ceres have been derived from various spectral indices, such as band centers, depths, integrated areas, etc.

Results: A better understanding of the spatial distribution and the content of the different mineral phases can thus be obtained by investigating the spectral characteristics of the 1 μm band.

In general, the VIR spectrum of Ceres is dominated by a broad absorption at about 1.2 μm. It is mostly uniform across the surface, but some differences can be seen in the map of the band parameters, like the band depth. Variation in the band depth could be due to various factors, such as relative abundance and grain size of the present minerals.

However, the spectral properties of the 1 μm band have been related to other spectral parameters in the NIR domain where mineralogy is known. For example, the attribution of the 3.1 μm band to ammonia-bearing species [1] show that this mineral phase dominant where we see for low values of 1 micron band. In fact, the spatial variability in the 1.0 μm band intensity is anticorrelated respect to the 3.1 μm band.

Some terrains show a different behavior of the 1 μm band respect to 3.1 band. This suggests the presence of a distinctive mineralogy.

This work, together with the results of other authors [1,2], completes the global mapping of the Ceres mineralogy.

Acknowledgments: We thank the Italian Space Agency (ASI). The Visible and Infrared Mapping Spectrometer (VIR) was funded and coordinated by the Italian Space Agency, with the scientific leadership of the Institute for Space Astrophysics and Planetology, Italian National Institute for Astrophysics, Italy.

References: [1] E. Ammannito et al. (2016) *Science, 353*, issue 6303. [2] Carrozzo et al. (2018), *Science Advances*, vol. 4, 3, e1701645.

VOLATILE EMISSION FROM A FRACTURE ON A PLANETARY SURFACE: A SMOOTHED-PARTICLE-HYDRODYNAMICS APPROACH

M. Teodori[1*], G. Magni[1], M. Formisano[1], M. C. De Sanctis[1] and F. Altieri[1], [1]INAF-IAPS, Via del Fosso del Cavaliere 100, Rome, Italy; *matteo.teodori@inaf.it.

Introduction: The study of volatiles emission form planetary surfaces is fundamental since it can provide important information concerning formation and evolution of the planetary bodies as well as their internal structure.

Some icy satellites (e.g. Europa and Enceladus) are characterized by the presence of plumes, mainly composed of water vapor and ice particles [1-10].

In this work we investigate the plume emission on Enceladus south polar region, by applying a smoothed-particle-hydrodynamics based code, providing some preliminary results about the water vapor emission from a fracture on the surface.

Numerical approach: We present our work concerning the study of hydrodynamical simulations for volatiles emission from a cavity using PySPH [11], a Python based framework code for Smoothed Particle Hydrodynamics (SPH) [12]. SPH simulations allow to study the evolution of a fluid (with single or multiple component) following the variation of its physical quantities and water phase transitions (condensation and sublimation), even when they rapidly change, in the Lagrangian approach.

Numerical tests: We initially tested the code in very simple situations, in order to quantify its reliability in reproducing a known physical behavior. We would like to understand its strength and weakness in SPH context by modeling the emission of gas and dust from a solid fracture.

Closed fracture: We performed a set of preliminary tests, mainly focusing on the stationary state of the gas inside a closed fracture, quantifying the capability of the code of preserving the energy of the system in absence of any dissipation, finding a good conservation, supporting the strength of the code in reproducing the thermal and dynamical behavior of a stationary fluid. These tests were needed also for randomizing particles positions, since the code suffers random initial positions, due to the available neighbors searching algorithm. The closed fracture phase lead to a stabilization time, which tells us when we have reached the initial conditions we want, in order to open the fracture and let the fluid free to evolve.

Interaction with solid boundaries: We studied and tested different ways of treating the interaction with a solid boundary, first by assuming the mirroring of particles that cross the boundary surfaces, mimicking an elastic/inelastic bounce that, otherwise, would be time consuming (the timescale for interaction between fluid and solid is several order magnitude less than the typical dynamical timescale for the fluid). SPH allows to describe the solid with SPH-pseudoparticles, leading to our second treatment. Finally, due to the discontinuity and numerical problems that each of this treatment can bring, we find a good compromise by using both approaches: particles are mirrored when they cross the boundary, but solid particles prevent discontinuity since are similar to fluid particles in their physical properties. We are then able to simulate the emission of the fluid from a cavity, that can mimic a fracture in the planetary surface and the loss of particles from the subsurface, following the fluid behavior during its evolution in time. The treatment of the boundary is also used to take into account the possible interaction with the planetary surface after the emission.

Initial conditions: In the framework of the scientific case initially considered, that are the Enceladus Plumes [5-10], we assumed an initial density constrained from the observations concerning mass loss, outflow velocity and considering a single emitting region. We also assumed a saturated water vapor, leading to temperatures of ~160 K. We compared simulations with different number of particles (from 25000 to 100000) and geometries of the fracture (rectangular, cubic and cylindrical), without finding any strong unexpected dependence on them. In these tests, we are considering a fix amount of gas, i.e. we do not refill the fracture, leading us to an initial strong mass loss after the opening time (with the same order of magnitude of the observed one), rapidly decreasing in time.

Results: Our preliminary simulations of pure water vapor show a non negligible fraction of the particles interacting with the surface after the emission (up to ~2% at t = 1700 s). This can lead to interesting insight when considering icy grains and dust.

The most of the particles present supersonic velocities (also greater than the escape velocity), while the average density and temperature rapidly decrease as expected from a free expansion of the gas. We find that the time for evacuating 95% of the reservoir is ~ 400 s and the mass loss reaches ~ 120 kg/s immediately after the opening of the fracture.

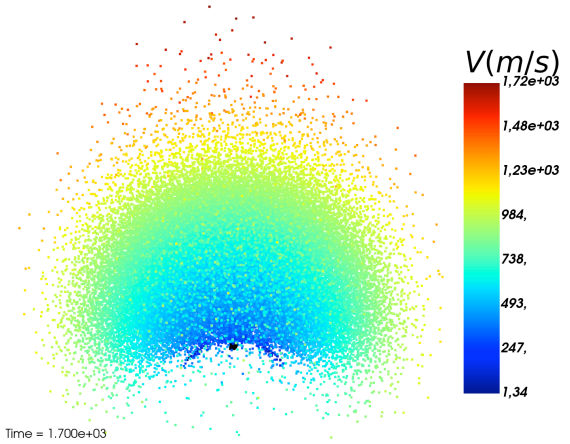

Fig. 1 Plume velocity distribution after 700 s from the opening of the fracture.

Fig. 1 shows the velocity distribution after 700 s from the opening of the fracture, fixed at t_{open} = 1000 s.

Conclusions and future work: Our plan is to use the PySPH framework to provide a flexible python code for SPH simulations, that can be able to model several aspects of volatiles emission from planetary surface and subsurface, to treat the interaction with solid bodies and boundaries and work together with other codes capable of surface and subsurface modeling [4]. We think that a connection between Eulerian and Lagrangian codes can be a strong tool, useful in a wide range of planetary science problems that consider several and different kind of phenomena.

We plan to improve our model gradually upgrading the code, taking into account several additional physical processes. Among them, we have the evaporation/condensation of water vapor (so we will also have an icy component), energy transfer with the fracture boundaries, the Sun heating after the emission, the coupling with the dust for both ice and gas, the possibility of tidal forces of another body (such as the Earth for the Moon or Saturn for Enceladus etc) leading to treat transient atmospheres.

References:

[1] Sparks W. B. (2016) ApJ, 829, 2.

[2] Arnold A. et al. (2019) Geophys. Res. L., 46, 1149.

[3] Huybrighs H. L. F. et al. (2020) Geophys. Res. L., 47, e2020GL087806.

[4] Vorburger A. and Worx P. (2022) 44th COSPAR Scientific Assembly, 44, 506.

[5] Dong Y. et al. (2011) J. Geophys. Res., 116, A10204.

[6] Thomas P. C. et al. (2016) Icarus, 264, 37.

[7] Yeoh S. K. et al. (2016) Icarus, 281, 357.

[8] Choblet G. et al. (2017) Nat. Astron., 1, 841.

[9] Postberg F. et al. (2018) Nature, 558, 564.

[10] Cazaux S. et al. (2022) European Science Congress 2022, EPSC2022-686.

[11] Ramachandran P. et al. (2021) ACM Trans. Math. Softw., 34, 38.

[12] Monaghan J. J. (2005) Rep. Prog. Phys. 68, 1703–1759.

[13] Formisano M. et al. (2018) J. Geophys. Res., 123, 2445.

Acknowledgments: This work was supported by a grant funded by INAF-IAPS within the projects “ExoMars”, “Dawn” and “TRIS”.

ROUGHNESS OF PLANETARY SURFACES: HAPKE THEORY AND STATISTICAL MULTI-FACET ALGORITHM. PRELIMINARY ANALYSIS OF DWARF PLANET CERES.

A. Raponi, M. Ciarniello, M. Formisano, M.C. De Sanctis, G. Filacchione, F. Capaccioni, A. Frigeri, F. Tosi.
Istituto di Astrofisica e Planetologia Spaziali (IAPS), Istituto Nazionale di Astrofisica (INAF), Rome, Italy.
(andrea.raponi@inaf.it).

Introduction: The analysis of surface roughness is mandatory to constrain spectrophotometric and thermophysical model of planetary surfaces (e.g. [1] and [2]). Moreover, the information on the roughness can be important by itself for interpretation of the geological and physical processes in place, or for engineering use in a case of a landing site selection.

Most of the space missions targeting planetary bodies provided large amount of spatially resolved images of the surfaces, allowing the analysis of the roughness down to a certain spatial scale, equivalent to the resolution of the instrument. However, most of the photometric and thermal effect act to a spatial scale which is often smaller.

To constrain the roughness at non-spatially-resolved scales several methods have been proposed. Among the interpretative physically-based models describing the reflection of the light from surfaces, Hapke [3] theory is among the most used in literature, thanks to its completeness in the description of the surface, and the practicality of use, being an analytical model. According to Hapke, a rough surface can be described as a collection of facets, each with a certain slope (θ), in such a way that the distribution of slopes is completely identified by a unique parameter (the mean slope $\boldsymbol{\theta}$).

Constraining the roughness parameter with a novel method: According to Hapke theory, several photometric parameters affect the surface reflectance as a function of the viewing geometry, so that a full characterization of them should be performed simultaneously, taking advantage of the largest possible statistic from acquired data (see e.g [1]). In this way it is generally possible to assign a global value for the mean slope parameter, thus representing an effective average roughness. Here we show that within the Hapke theory, in particular conditions, the ratio of reflectances coming from two different portions of the terrain can be modeled as a function of only the viewing geometries (usually known from shape model and spacecraft attitude) and the non-resolved roughness alone, disregarding all other photometric parameters. Such conditions consist of the two terrain having: i) the same photometric properties, including roughness (reasonable assumption when they are spatially close); ii) a dark albedo (geometric albedo below 0.10-0.15) ; iii) the respective reflectances acquired at similar phase angles (with difference not larger than a few degrees).

All high-spatial-resolution images and hyperspectral images obtained by recent space missions ESA/Rosetta to comet 67P and NASA/Dawn to dwarf planet Ceres comply with these requirements. Upcoming ESA/Bepi-Colombo data from planet Mercury are also suitable for these conditions, along with past and future data from dark asteroids and moons of the solar system (including Earth's Moon).

Numerical algorithm: Reflectance ratios can be modeled according to Hapke's analytical formulation. However, in place of that, we proposed a statistical multi-facet algorithm (SMFA) [4], which allows: i) a better accuracy than the analytical model which requires mathemathical approximations; ii) the possibility to obtain the full distribution of slopes and facet orientations, which is an information needed to perform thermal modeling; iii) the possibility of complicating the roughness model by mixing different populations of slopes ($\boldsymbol{\theta_{1,2,..}}$), to obtain better fits with data. In particular we can model two or more spatially separated populations of slopes (areal mixing) or not spatially separated (intimate mixing). Another possibility is to model a population of facets distributed according to $\boldsymbol{\theta_1}$, each facet having in turn a certain roughness characterized by $\boldsymbol{\theta_2}$ (intrafacet mixing).

Preliminary analysis on Ceres surface: We have taken into account an acquisition of the VIR-VIS imaging spectrometer [5] onboard Dawn space mission to Ceres, targeting the floor of a crater named Ezinu (110.5 km in diameter with center coordinates 42.97 °N, 195.83 °E) with a resolution of ~100 m/px (see Fig. 1).

For each spatial pixel we take the spectral average of 150 spectels in the range 0.7-0.9 μm. A simple way to deal with the many possible reflectance ratios obtainable from the observations is collecting and averaging reflectances over corresponding bins of incidence and emission angles (+/- 1°), parametrizing the latter with the former angles, in a way to obtain a one-dimensional profile of the reflectance ratios as a function of the viewing geometry (see Fig. 2). We take into account all bins which include more than 100 spatial pixels to minimize statistical errors. We divided all average reflectances by the one corresponding to the lowest incidence angle. The so obtained reflectance ratio profile can be compared to modeled reflectance ratios in order to constrain the roughness parameter. We found that with a single population of slopes we

obtain unsatisfactory models. An intimate mixture of two slope populations marginally improves the fit. The best fit is obtained with an intrafacet mixture with θ_1 = 25° and θ_2 = 65°. The corresponding histograms of slopes are shown in Fig. 3.

Conclusions: We performed a preliminary implementation of a new method to retrieve the roughness of planetary surfaces. We used the numerical algorithm (SMFA) which replaces the analytical formulation by Hapke, allowing us to build up simulated terrains with more complex roughness configurations. In principle, the slopes' histrogram corresponding to the best fit could be obtained by other types of terrain (rather than multi-fractal), e.g highly craterized of boulder-rich terrains. This will be matter of future investigations.

Here we have chosen an observation at higher incidence angles, which is a condition where roughness can be retrieved with more accuracy. Further testing is needed to explore the space of viewing geometries where the method can retrieve reliable results.

References: [1] Ciarniello M. et al. (2017) *A&A, 598,* A130. [2] Davidsson B. J. R. et al. (2009) *Icarus, 201,* 335-357. [3] Hapke B. (1993) *Theory of Reflectance and Emittance Spectroscopy*. [4] Raponi A. et al., (2020) *14th EPSC 2020*, abstract 761. [5] De Sanctis M. C. (2002) *SSR, 163,* 329-369.

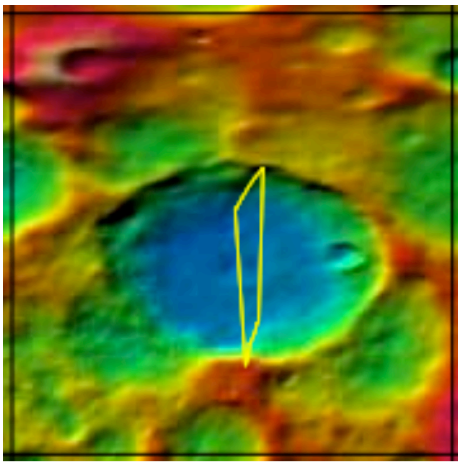

Figure 1: The portion of Ceres surface (180-210° E, 30-60° N) including Ezinu crater. The area limited by the yellow line corresponds to the footprint of the VIR-VIS acquisition (id. 518859135, 256x50 spatial pixels) taken into account in this work, overimposed on Ceres' color-coded topographic map (blue: lower elevation, red: higher elevation).

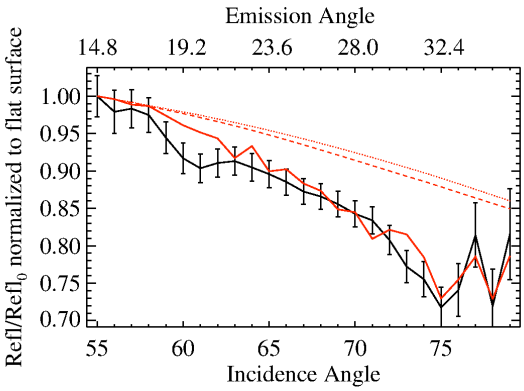

Figure 2: Reflectance Ratio profile as a function of the viewing geometry (black line with error bars). Phase angle varies in the range 43.0° – 43.5° along the profile. The ratios have been further divided by the respective ratios in the theoretical case of a flat surface. Red dotted line: best fit with a single slope population (θ = 35°). Red dashed line: best fit with intimate mixture of two population of slopes (θ_1 = 25°, θ_2 = 85°, having as weights respectively 0.8 and 0.2). Red solid line: best fit with intrafacet mixture (θ_1 = 25°, θ_2 = 65°). All models have been retrieved varying θ with steps of 5°.

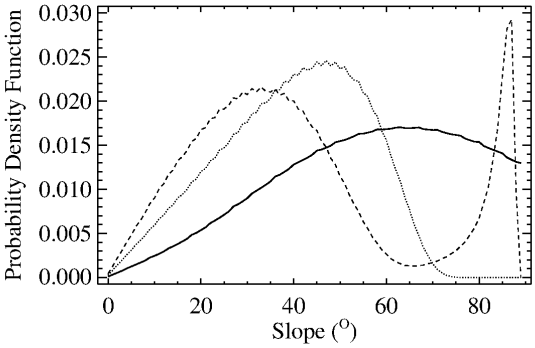

Figure 3. Histograms of slopes produced by the SMFA corresponding to the models in Fig. 2: single population with θ = 35° (dotted); two populations intimately mixed θ_1 = 25°, θ_2 = 85° with weights 0.8 and 0.2 (dashed); intrafacet mixture with θ_1 = 25° and θ_2 = 65° (solid bold line).

SEARCH FOR AND OCCURRENCE RATE OF JUPITER ANALOGS IN PLANETARY SYSTEMS WITH SHORT-PERIOD SUB-NEPTUNES

A. S. Bonomo[1], A. Massa[2], M. Damasso[1], M. Pinamonti[1] and A. Sozzetti[1]
[1]INAF-Osservatorio Astrofisico di Torino (e-mail: aldo.bonomo@inaf.it); [2]Università degli Studi di Torino.

Abstract: The study of exoplanets has led to the finding that the most common planets in the universe are sub-Neptunes, i.e. planets smaller than Neptune ($1<R_p<4$ Re, Earth radii), such as rocky super-Earths and (non-rocky) volatile-rich mini-Neptunes, with relatively short orbital periods (P<100d) [1]. However, these planets are missing in our Solar System, and the reason for that is not yet clear.

Two possible scenarios attribute the absence of sub-Neptunes in the Solar System to Jupiter. The first scenario predicts that Jupiter may have acted as a dynamical barrier to more distant sub-Neptunes and prevented the rocky cores of Saturn, Uranus and Neptune from migrating towards the Sun and thus becoming a compact system of sub-Neptunes [2], like those found by the Kepler, K2 and TESS space missions (e.g., [3]). Alternatively, Jupiter may have reduced the inward drift of material (pebbles) needed to form sub-Neptunes within the water snowline, by opening a gap in the protosolar disk [4]. Both scenarios predict an anti-correlation between the presence of short-period sub-Neptunes and that of cold Jupiters (i.e., Jupiter-like planets), which can be investigated observationally.

By analyzing homogeneously more than 3600 high-precision radial velocities of 38 Kepler and K2 sub-Neptune transiting systems, gathered over almost 10 years with the HARPS-N@TNG spectrograph and other spectrographs, we searched for cold Jupiters and found five of them in three systems. By accounting for the survey sensitivity, we derived an occurrence rate of cold Jupiters f_{CJ}=9.3 +7.7 -□2.9% in our sample. Our f_{CJ} is four times lower than that found by [5], who claimed instead an excess of Jupiter analogs in sub-Neptune systems. It is also lower than frequency of cold Jupiters in field stars [6], though compatible with it at 1.3σ given the large uncertainties. This might support the theoretically predicted anti-correlation between inner sub-Neptunes and outer Jovian planets, but a considerably larger sample is needed to draw a firm conclusion as well as to unveil possible intriguing differences in f_{CJ} as a function of planet multiplicity and composition, which might in principle allow us to pinpoint the dominant mechanism of sub-Neptune formation.

References: [1] Fulton B. J. et al. (2017) *AJ*, *154,* 109; [2] Izidoro A. et al. (2015), *ApJL, 800*, L22; [3] Winn J. N. and Fabricky D. C. (2015) *ARA&A, 53*, 409; [4] Lambrecths M. et al. (2019) *A&A, 627*, A83; [5] Bryan M. L. et al. (2019) *AJ, 157*, 52; [6] Wittenmyer R. A. et al. (2020) *MNRAS, 492*, 377.

COLD JUPITERS SHAPING THE FORMATION OF SUPER-EARTHS AROUND M-DWARFS

M. Pinamonti[1], D. Barbato[1,2], A. Sozzetti[1], and GAPS collaboration
[1]INAF-Osservatorio Astrofisico di Torino (matteo.pinamonti@inaf.it), [2]Observatoire de Genève.

Introduction: The relationships between inner and outer planets plays a key role in unveiling the mechanisms that govern formation and evolution models. For this reason, it is important to probe the inner region of systems hosting long-period giants, in search for undetected lower-mass planetary companions: some models suggest that Jupiter-like planets produce dynamical barriers preventing the formation of inner super Earths [1], while others make the opposite prediction of a direct correlation between the two populations of planets [2]. Moreover, to properly characterize such systems and their evolution, it is important to measure with great accuracy the orbital parameters of the Cold-Jupiter planets.

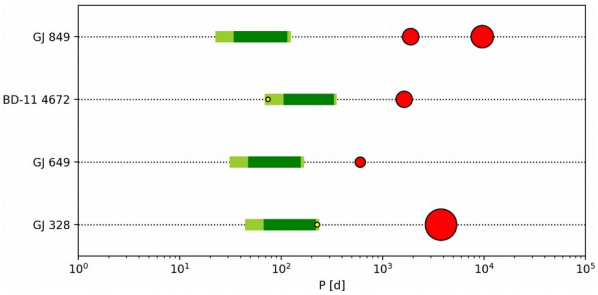

Figure 1: Orbital architecture of the observed systems. The conservative and optimistic limits of the habitable zone of each system are shown as thick dark green and light green bands, respectively

In this framework, taking advantage of high-resolution echelle spectrographs such as HARPS-N@TNG, we present the high-cadence and high-precision Radial Velocity (RV) monitoring of low-mass stellar hosts to long-period giants with well-measured orbits, in order to search for short-period low-mass planets. Additionally, we take advantage of Gaia DR3 astrometric data to constrain the orbital parameters of the Cold Jupiters. We present the results of the monitoring with the high-precision HARPS-N spectrograph of 4 M-dwarf systems with Jupiter-like planets (Fig. 1), and the detection of two close-in low-mass planets.

Analyses: The four observed targets are all known low-mass planet-hosting stars: BD-11 4672 [3], GJ328 [4], GJ649 [5], and GJ849 [6,7]. High-cadence high-precision RV measurements of the targets were collected with HARPS-N spectrograph at TNG from April 2018 to May 2021. This intensive monitoring allowed for the discovery of a Neptune-mass planet close to the habitable zone of BD-11 4672 [8], and of another small-mass planet around GJ 328 [9].

We then derived an accurate estimate of the detection probability function of the survey (shown in Fig. 2), taking advantage of Bayesian statistics [10].

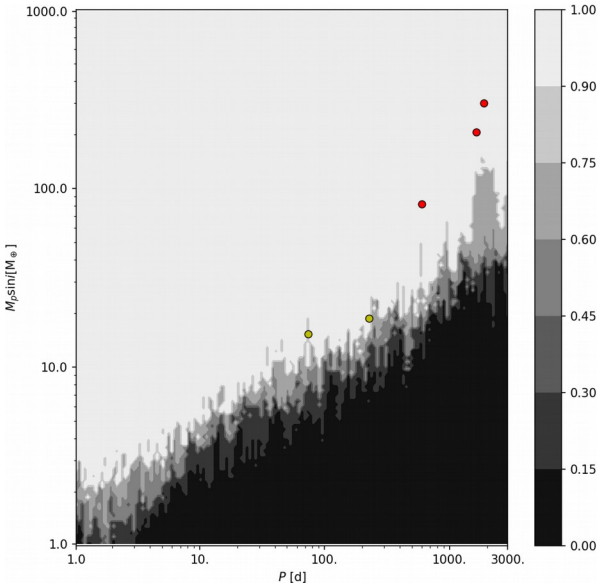

Figure 2: Survey detection map. The color scale expresses the detection probability. The red and yellow circles show the positions of the planets orbiting the observed systems.

From this, we calculated the occurrence rate of small-mass planets in M-dwarf systems hosting Cold-Jupiters, which we can compare with the occurrence rate for field early-M dwarfs [10]: we measure a significantly higher (>2σ) frequency of high-mass Super-Earth (10-30 $M_\oplus$) in the observed Cold-Jupiter sample, with respect to the observed frequencies for field M dwarfs, while the frequency of low-mass (<10 $M_\oplus$) planets appears to be lower (≈1σ).

Moreover, to overcome the limitations of RV-detected planets, for which only the minimum-mass is known, it is possible to combine RV information with the absolute astrometry from Gaia and Hipparcos [11], fitting together the planets' orbital signals in the RVs and the targets' Proper Motion anomalies. This allows to constrain the orbital parameters of long-period planets, in particular the inclination, from which the real mass can be derived.

Summary: The results of this survey provide an important advancement in discriminating between proposed outcomes of different processes for the influence of Cold Jupiters on the formation of super Earths, and the dependence of these phenomena on the mass of the stellar host. The combination of high-cadence RV monitoring and high-precision astrometric data allows for a complete characterization of both the outer and inner regions of planetary systems.

References: [1] Izidoro, A.et al. (2015), ApJ, 800, L22. [2] Chiang, E., Laughlin, G. (2013), MNRAS, 431, 3444. [3] Moutou, C., et al. (2011), A&A, 527, A63. [4] Robertson, P. et al. (2013), ApJ, 774, 147. [5] Johnson, J. A. et al. (2010), PASP, 122, 14. [6] Butler, R. P. et al. (2006), PASP, 118, 1685. [7] Feng, Y. K. et al. (2015), ApJ, 800, 22. [8] Barbato, D. et al. (2020), A&A, 641, A68. [9] Pinamonti, M. et al. (to be submitted). [10] Pinamonti, M. et al. 2022, A&A, 664, A65. [11] Damasso, M. et al. 2020, A&A, 642, A31.

RESPONSES OF EUKARYOTIC PHOTOSYNTHETIC ORGANISMS FROM DIFFERENT SYSTEMATIC GROUPS TO A SIMULATED M-DWARF STAR LIGHT. M. Battistuzzi[1], L. Cocola[2], E. Liistro[1], R. Claudi[3], L. Poletto[2] and N. La Rocca[1], [1]Dept. Biology, Padova Univ., Via U. Bassi 58/b, 35131, Padova, E-*mail: mariano.battistuzzi@unipd.it*, E-*mail: nicoletta.larocca@unipd.it,* [2]CNR-IFN, Via Trasea 7, 35131, Padova, [3]INAF – Astronomical Observatory, Vicolo Osservatorio 5, 35122, Padova.

In the last couple of decades, more and more Earth-like exoplanets were discovered orbiting the Habitable Zone (HZ) of M-dwarf stars, the most abundant and long-lived stars known in the Milky Way. Such stars have different spectral characteristics with respect to the Sun, being far less luminous and generating a light spectrum with a major component in far-red and infrared (700 – 1000 nm) while emitting very low in the visible (400 – 700 nm). Visible light however is the region of the electromagnetic spectrum mostly utilized by Oxygenic Photosynthetic Organisms (OPOs), which on Earth drive the primary production of sugars and molecular oxygen (O_2), fundamental molecules that are then made available to all other organisms. In addition, these organisms are capable of producing different kinds of biosignatures, which make them ideal targets to investigate the possibility of life beyond Earth. The possibility of oxygenic photosynthesis in the HZ of M-dwarfs has been discussed so far through models and a theoretical approach (among others, [1,2,3]) but experimental research, testing OPOs under a simulated light spectrum similar to that of an M-dwarf, lags behind. We developed and built an experimental setup that allows to grow photosynthetic organisms under selected non-terrestrial conditions [4]. This setup includes a Star Light Simulator, able to generate different light intensities and spectra, which was used to simulate the lighting of an M-dwarf in the range of 365 – 850 nm. We initially focused on prokaryotic microorganisms (cyanobacteria) as targets of our research, due to their extraordinary capacities to withstand every kind of environment on the Earth as well as their ability to acclimate to Far-Red light [5]. Here we present instead the responses of eukaryotic OPOs. We selected several microalgae from different systematic groups (*Dixoniella giordanoi, Microchloropsis gaditana, Chromera velia, Chlorella vulgaris*), a moss (*Physcomitrium patens*) and a higher plant (*Arabidopsis thaliana*), to have the most accurate picture on the possibility of OPOs to acclimate to the M-dwarf light spectrum. For these organisms, we tested the survival, growth and photosynthetic activity under the M-dwarf simulated spectrum, comparing the results to samples grown under solar and far-red light spectra. The possible contribution of eukaryotic OPOs to the production of biomass and O_2 on planets orbiting the HZ of M-dwarfs will be discussed.

References: [1] Kiang N. Y. et al. (2007) *Astrobiology*, 7(1):252-74. [2] Wandel A. and Gale J (2020) *Int. Jou. Ast.*, 19(2), 126-135. [3] Covone G. et al. (2021) *Mon. Not. R. Astron. Soc.*, 505(3), 3329-3335. [4] Battistuzzi M. et al. (2020) *Front. Plant Sci.*, 11:182. [5] Claudi R. et al. (2021) *Life*, 11,10.

The GAPS Program at TNG: That strange case of the young planetary system V1298 Tau. R. Claudi[1,2] and GAPS collaboration, [1]INAF- Astronomical Observatory of Padova (vicolo Osservatorio, 5, 35122 Padova riccardo.claudi@inaf.it), [2]Mathematichs and Physic Department, Università Roma Tre (via della Vasca Navale, 84,00146 Roma).

Introduction: Young planets offer us the unique opportunity to study the unaltered products of planet formation, before secular evolution and the interaction with the host stars modify or cancel their orginal characteristics. Current theories of planetary evolution predict that infant giant planets have large radii and very low densities before they slowly contract to reach their final size after about several hundred million years[1,2]. These theoretical expectations remain untested so far as the detection and characterization of very young planets is extremely challenging due to the intense stellar activity of their host stars[3,4]. Only the recent discoveries of young planetary transiting systems allow initial constraints to be placed on evolutionary models[5-7]. Since the October 2017, the Young Objects (YO) sub-program of GAPS (Global Architecture of Planetary System)[8] searches for planets by surveying young stars spanning from the ~2 Myr of the Taurus star forming region to the 400-600 Myr age of members of open clusters such as Coma Ber and moving groups such as Ursa Major. The YO sub-program has the aim to confirm or disprove the significantly higher frequency of hot Jupiters (HJ) at very young ages[9], and to distinguish among the timescales of the HJs migration, by comparing the frequencies and properties of planets at the age of few Myr to those at a few hundreds Myr and to those orbiting old stars. Furthermore, GAPS-YO program is also aimed to understand how the planetary photoevaporation due to the high irradiation from the host star, impacts on the evolution of these young systems.

One of the most puzzling young systems discovered by *Kepler* and followed up by GAPS-YO is the V1298 Tau system.

V1298 Tau System: With an estimated age of 20 million years, V1298 Tau is one of the youngest solar-type stars known to host transiting planets. V1298 Tau is a K1 pre-main-sequence dwarf (T_{eff}=5050 K) with a mass of 1.17 $M_{\odot}$, belonging to the Group 29 stellar association[10], whose members are 10–30 Myr old. Analyzing its *Kepler* light curve (K2 Mission[11]), David et al. (2019)[12] discovered the first Jupiter-size planet (V1298 Tau b) to which David et al. (2019)[13] soon added other three planets after a forward analysis of the K2 Campaign 4 photometry. V1298 Tau has later been observed, in collaboration with other groups, in the GAPS framework, with an intensive spectroscopic campaign, obtaining radial velocity (RV) measurements using several high-resolution spectrographs (HARPS- N, CARMENES, SES and HERMES), to characterize the masses of its four planets (see Table 1). We find[14] that the two outermost giant planets, have the following masses: V1298 Tau b (0.64 ± 0.19) M_J and V1298tau e (1.16 ± 0.30) M_J.

Table 1: *Main planetary parameters of V1298 Tau*

	a	**P**	**M_P**	**R_P**
	(au)	*(d)*	*(M_J)*	*(R_J)*
Planet b	0.1719	24.1315	0.64	0.84
Planet c	0.0841	8.2438	<0.24	0.45
Planet d	0.1103	12.396	<0.31	0.54
Planet e	0.2409	44.1699	1.16	0.88

The density values of planets b and e are 1.2±0.45 and 3.6±1.6 g cm−3, respectively, and are larger than those predicted by formation theories for such young planets. Two possible explanations are: the more rapid contraction of these young planets than predicted by interior evolution models, or their extreme enrichment in heavy elements[14].

Planetary Evaporation: We investigated[15] the predicted evolution of planetary atmospheres induced by the stellar high energy radiation. To do this, we observed V 1298 Tau with XMM-Newton on 2021 February 24, for about 30ks of exposure time, with all the CCD-based EPIC cameras and with the high- resolution RGS spectrometers. The light curves are shown in Figure 1.

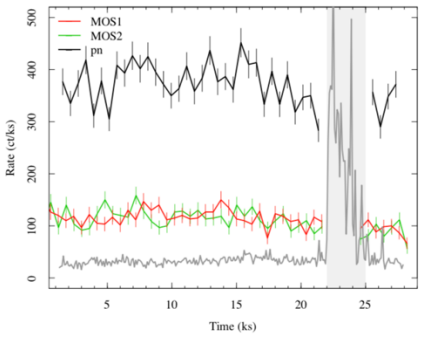

Figure 1: *pn and MOS light curves with bin size of 600s. The gray area marks the region of high background (gray curve), filtered out for the spectral analysis.*

Proceeding similarly as in Georgieva et al. (2021)[16] and in Benatti et al. (2021)[17], we evaluated the mass loss rate of the planetary atmosphere using the hydrodynamic-based approximation developed by Kubyshkina et al. (2018a)[18] for planetary masses lower than 40 $M_{\oplus}$, or the energy limited approximation[19] for higher values. Then

we computed the change in atmospheric mass fraction, planetary mass and radius, from the present age to 5 Gyr, in steps of 1 Myr, assuming a fixed circular planetary orbit. Contrary to previous expectations, we find that the two outer Jupiter-size planets (planet b and e) will not be affected by any evaporation on Gyr time scales, and the same occurs for the two smaller inner planets (planet c and d), unless their true masses are lower than ~ 40 $M_{\oplus}$. These results reveal that relatively massive planets can reach their final position in the mass-radius diagram very early in their evolutionary history.

Stability of the V1298 Tau system: We investigate[20] also the formation of the two outermost giant planets, V1298 Tau b and e, and the present dynamical state of V1298 Tau's global architecture with detailed n–body simulations to explore the link between the densities of V1298 Tau b and e and their migration and accretion of planetesimals within the native circumstellar disk[20]. We combine n-body simulations and stability metrics to characterize V1298 Tau's dynamical state and connect it to the formation history of the system. The results show that because the high densities of V1298 Tau b and e, these planets formed quite distant from their host star, likely beyond the CO_2 snowline. The higher nominal density of V1298 Tau e suggests it formed farther out than V1298 Tau b. The current architecture of V1298 Tau is not characterized by resonant chains and is unstable. Planet-planet scattering with an outer planet is the most likely cause for the instability.

Conclusions: The V1298 Tau system seems to contradict our knowledge of early-stages planetary evolution. According to models, they should reach their mass–radius combination only hundreds of millions of years after formation. This result suggests that giant planets can contract much more quickly than usually assumed. Furthermore, the most plausible scenario for V1298 Tau's formation is that the system is formed by convergent migration and resonant trapping of planets born in a massive yet compact disk.

References:

[1] Mordasini, C. et al. (2012) *A&A,* **547**, A112.
[2] D'Angelo, G., et al. (2021), *Icarus* **355**, 114087.
[3] Donati J,F., et al., (2016), *Nature*, 534, 662.
[4] Damasso M., et al., (2020), *A&A.,*642, A133
[5] David T.J., et al., (2016), *Ap.J*, 816, 21
[6] Plavchan P., et al., (2020), *Nature*, 582, 497
[7] Klein B., et al., (2021), *MNRAS*, 502, 188
[8] Covino et al., (2013), *A&A*, 554,A28
[9] Yu et al., (2017), *MNRAS*, 467,1342
[10] Oh S., et al. (2017), *AJ*, 153,257
[11] Howell S.B., et al. (2014), *PASP*, 126,398
[12] David T.J., et al., (2019), *AJ*, 158,79
[13] David T.J., et al. (2019), *ApJ*, 885,L12
[14] Suárez Mascareño A., et al., (2021), *Nature Astronomy*, 6, 232.
[15] Maggio A., et al., (2022), *ApJ*, 925,172
[16] Georgieva I.Y., et al. (2021), *MNRAS*, 505, 4684
[17] Benatti S., et al., (2021), *A&A*, 650, A66
[18] Kubyshkina D., et al. (2018), *A&A*, 619, A151.
[19] Erkaev N.V., et al. (2007), A&A, 472, 329.
[20] Turrini D., et al, (2022), Submitted

An Exoplanet Atmosphere as Never Seen Before.

L. Mancini[1]
[1]University of Rome "Tor Vergata", Via della Ricerca Scientifica 1, I-00133 Roma, Italy
E-mail: lmancini@roma2.infn.it

The successful launch of JWST ushers in a new era of astrophysics by bringing forth the ability to measure the compositions of planet atmospheres beyond our own Solar System with exquisite precision. Tracers for formation and migration are predicted to be encoded in the composition and elemental ratios of a planet's atmosphere.

The JWST Transiting Exoplanet Community Director's Discretionary Early Release Science (JTEC ERS) program has observed a single exoplanet's transmission spectrum with different instrument configurations to test their capabilities and provide lessons learned for the community. The target, WASP-39b, is a hot (T_{eq} = 1120 K) giant planet at 215 pc from Earth, with a mass similar to Saturn (M_p = 0.28 M_{Jup}) but a radius in excess of Jupiter (R_p = 1.27 R_{Jup}) likely due to the high atmospheric and interior temperatures, resulting in an extended atmosphere. The host, WASP-39, is a G8 V type star, with T_{eff} = 5400 K, little stellar activity, and has elemental abundance patterns that are nearly solar. Its quiet host and extended atmosphere make WASP-39b an ideal exoplanet for transmission spectroscopy observations.

Using three of its instruments, the JWST observed WASP-39 for more than 40 hours in July 2022 at IR wavelenghts that were hitherto inaccessible.

As a member of the JTEC ERS program, I will report on these observations that lead to unprecedented discoveries, such as the first detection in the atmosphere of an exoplanet of carbon dioxide (CO_2) and sulfur dioxide (SO_2), the latter produced by chemical reactions triggered by highly energetic radiation from the parent star of the planet (see Fig. 1).

Other atmospheric constituents detected by the JWST include sodium (Na) potassium (K), water vapour (H_2O) and carbon monoxide (CO), confirming previous observations from space and ground-based telescopes [1, 2, 3, 4, 5].

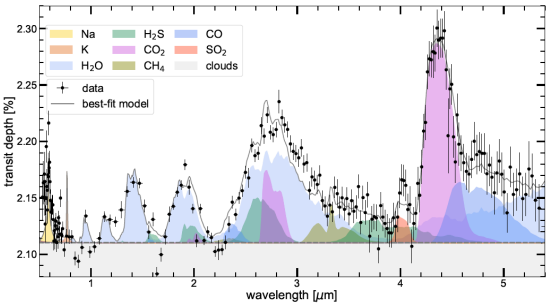

Fig.1. The JWST-PRISM transmission spectrum of WASP-39b with key contributions to the atmospheric spectrum.

References

[1] Ahrer et al., 2022, arXiv:2208.11692
[2] Rustamkulov et al., 2022, arXiv:2211.10487
[3] Alderson et al., 2022, arXiv:2211.10488
[4] Ahrer et al., 2022, arXiv:2211.10489
[5] Feinstein et al., arXiv:2211.10493

The HADES Program with HARPS-N@TNG
HADES: THE HArps-n red Dwarf Exoplanet Survey

L. Affer[1] and HADES Team,
[1] INAF – Osservatorio Astronomico di Palermo, Piazza del Parlamento 1, 90134 Palermo, Italy - laura.affer@inaf.it

Many efforts to detect Earth-like planets around low-mass stars are currently devoted to almost every extra-solar planet search. M dwarfs stand as ideal targets for Doppler radial velocity searches as their low masses and luminosities make low-mass planets orbiting within their habitable zones more easily detectable than those around higher-mass stars. Nonetheless, the statistics of the frequency of this kind of planet hosted by low-mass stars remains poorly constrained.

Our M-dwarf radial velocity monitoring with HARPS-N within the HARPS-N Red Dwarf Exoplanet Survey Radial Velocity (HADES) project started in 2012 and is contributing to the widening of the current statistics through the in-depth analysis of accurate radial velocity observations in a narrow range of spectral subtypes from M0 to M3, to investigate the planetary population around a well-defined class of host stars.

The HADES project is the result of a collaborative effort between the Italian Global Architecture of Planetary Systems (GAPS) Consortium, the Institut de Ciències de l'Espai de Catalunya (ICE), and the Instituto de Astrofísica de Canarias (IAC).

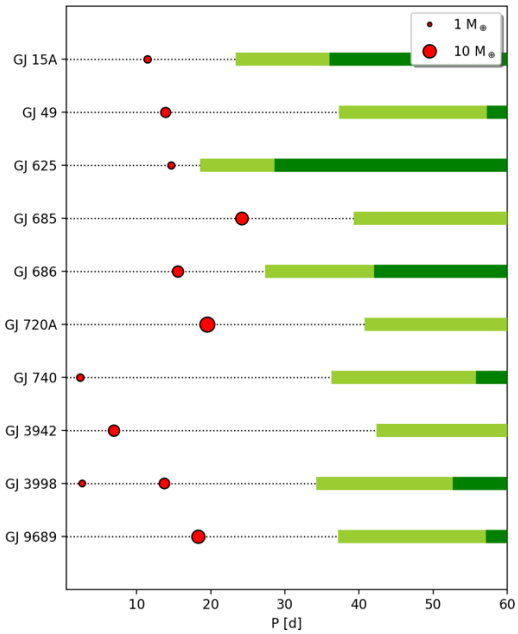

Figure 1: Overview of the HADES detected planetary systems.The sample's published planets are shown as red circles: the symbol size is proportional to the minimum planetary mass. Each system's Habitable Zone conservative and optimistic limits, are shown as thick dark green and light green bands, respectively (from [3]).

Two photometric programs regularly and almost simultaneously follow up the sample of M stars to characterize the stellar activity, to highlight periods that are due to chromospheric inhomogeneities modulated by stellar rotation and differential rotation, and thus to distinguish from the periodic signals those due to activity and to the presence of planetary companions.

We present the complete analysis of the HADES survey and the results obtained concerning the statistical ([1], [2], [3]), activity ([4], [5], [6]), and characterization ([7], [8]) part as well as the planet revealing part ([9] to [18]), around M dwarfs.

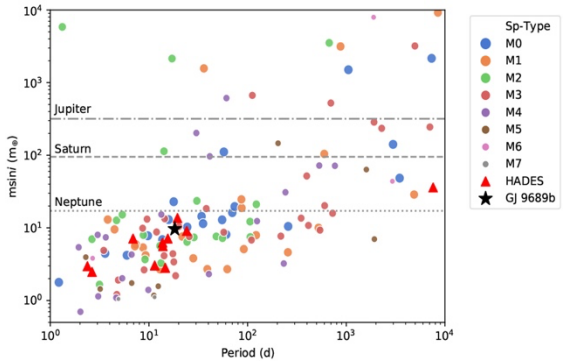

Figure 1: Known radial velocity planets (planetary mass vs. orbital period diagram) around M dwarfs (as listed at http://exoplanet.eu/ in December 2020. Planets discovered by the HADES survey are shown as red triangles (from [18], the planet GJ 9689 is shown as a black star).

References:

[1] M. Perger et al. (2017) *A&A*, Volume 598, id.A26. [2] E. González-Álvarez et al. (2019) *A&A*, Volume 624, id.A27. [3] M. Pinamonti. et al. (2022) *A&A,* Volume 664, id.A65. [4] J. Maldonado et al. (2017) *A&A*, Volume 598, id.A27. [5] G. Scandariato et al. (2017 *A&A*, Volume 598, id.A28. [6] A. Suárez Mascareño et al. (2018) *A&A*, Volume 612, id.A89. [7] J. Maldonado et al. (2015) A&A, Volume 577, id.A132. [8] J. Maldonado et al. (2020) *A&A*, Volume 644, id.A68. [9] L. Affer et al. (2016) *A&A*, Volume 593, id.A117. [10] A. Suárez Mascareño et al. (2017) *A&A*, Volume 605, id.A92. [11] M. Perger et al. (2017) *A&A*, Volume 608, id.A63. [12] M. Pinamonti et al. (2018) *A&A*, Volume 617, id.A104 [13] L. Affer et al. (2019) *A&A*, Volume 622, id.A193. [14] M. Perger et al. (2019) *A&A*, Volume 624, id.A123. [15] M. Pinamonti et al. (2019) *A&A*, Volume 625, id.A126. [16] B. Toledo-Padrón et al. (2021) *A&A*, Volume 648, id.A20. [17] E. González-Álvarez et al. (2019) *A&A*, Volume 649, id.A157. [18] J. Maldonado et al. (2021) *A&A,* Volume 651, id.A93.

BEPICOLOMBO FIRST RESULTS OF THE CRUISE AND FLYBYS. A. Milillo[1] J. Benkhoff[2] , G. Murakami[3], J. Zender[2] and BC ESA science and Environment Instrument teams* [1] INAF/IAPS, (via del Fosso del Cavaliere, 00133, Rome, Italy, anna.milillo@inaf.it); [2] ESA/ESTEC, The Netherlands; [3] JAXA/ISAS, Japan

Introduction: The ESA-JAXA BepiColombo satellite suite [1] was lauched in 2018 and is travelling to reach its final target Mercury at the end of 2025. Despite science observations during cruise were not originally among the mission goals, some of the instruments are able to perform science observations in the stacked configuration. In particular, both BepiColombo spacecraft, i.e. MPO and MMO, are able to observe particles at different energy ranges and to measure magnetic field [2]. In fact, some interesting observations have been obtained during interplanetary cruise as well as during the Venus' and Mercury's flybys.
In this paper, few highlights of the most interesting results obtained so far during cruise and flybys will be presented.

Observations:
Highlights of interplanetary cruise science include BepiColombo magnetic field observations coupled with other observations from Parker Solar Probe for investigating the solar wind propagation and evolving plasma regimes from the inner to the outer Solar System.
Highlight of Venus Flyby include the pass at the subsolar stagnation region close to the inner induced magnetopause never observed before [3]. The Solar Orbiter measurements are used as monitor of the external conditions.
The first two Mercury's flybys revealed a magnetosphere completely different from each other. This is the signature of a really dynamic and totally reconfigured magnetosphere as response to different external conditions. The observations include a) magnetic fields, b) solar wind and magnetospheric ions observed by different instruments, c) electron in different energy ranges, d) plasma waves able to provide information on the electron density, e) energetic particles and f) exosphere components [4].

This paper will present a general overview of the observations, just as a first taste of the great results expected from this mission [5].

References:

[1] Benkhoff J. et al. (2021) *Space Science Reviews* 217 90. [2] Mangano et al. (2021) *Space Science Reviews* 217 23. [3] Persson et al. *Nature Communication* (2022) [4] Orsini et al. *Nature Communication* (2022) [5] Milillo A. et al. (2020) *Space Science Reviews* 216 93.

Theme:
Pianeti e Satelliti
- Analisi dati, Analisi di superfici, atmosfere, esosfere, modellistica

*** BC ESA science** (represented by WG coordinators) **and Environment Instrument teams** (represented by PIs and Co-PIs)

N. André4, S. Barabash5, W. Baumjohann6, E.J. Bunce7, C.M. Carr8, D. Delcourt9, C-H. Glassmeier10, M. Grande11, D. Heyner10, M. Hirahara12, J. Huovelin13, K. Issautier14, T. Karlsson15, R. Y. Kasaba16, M. Kobayashi17, O. Korablev18, H. Kojima19, H. Lichtenegger6, S. Livi20, A. Matsuoka5, Moissl2, M. Moncuquet14, K. Muinonen13, S. Orsini1, E. Quèmerais21, Y. Saito3, R. Vainio22, A. Varsani6, S. Yagitani23, I. Yoshikawa24, J.-E. Wahlund5,

S. Aizawa25, L. Hadid9, V. Mangano1, B. Sanchez-Cano7

4. IRAP, France, 5. IRF, Sweden; 6. IWF, Austria; 7. University of Leicester, UK; 8. Imperial College London, UK; 9. Orleans University, France; 10. University of Braunschweig, Germany; 11. University of Wales, UK; 12. Nagoya University, Japan; 13. Helsinki University, Finland; 14. LESIA, Sorbonne Université, France; 15. KTH Royal Institute of Technology, Sweden;16. Tohoku University, Japan; 17. Chiba Institute of Technology, Japan; 18. IKI, Russia;19. Kyoto University, Japan; 20. SWRI, TX, USA; 21 LATMOS, Université Versailles Saint-Quentin, France; 22. Turku University, Finland; 23. Kanazawa University, Japan; 24. Tokyo University, Japan; 25. Pisa University, Italy

Ca and CaO Mercury exosphere as product of micro-meteoroids and comet stream particles impact

M. Moroni[1], A. Mura[1], A. Milillo[1], C. Plainaki[2-1], V. Mangano[1], T. Alberti[1], N. Andre'[3], A. Aronica[1], E. De Angelis[1], D. Del Moro[4], A. Kazakov[1], S. Massetti[1], S. Orsini[1], R. Rispoli[1], R. Sordini[1]

[1]Istituto Nazionale di Astrofisica – Istituto di Astrofisica e Planetologia Spaziali (INAF – IAPS), Rome, Italy; martina.moroni@inaf.it
[2]Agenzia Spaziale Italiana (ASI), Rome, Italy
[3]Research Institute in Astrophysics and Planetology (IRAP), Toulose, France
[4]Department of Physics, University of Rome Tor Vergata, Italy

Introduction The study of the micro-meteoroid environment is relevant to planetary science, upper atmospheric chemistry, and space weathering of airless bodies, as Mercury. In that case, the meteoroids hit directly the surfaces producing impact debris and vapor, thus contributing to shape thin exosphere of the planet. The present work is focused on the study and modelling of the Mercury's exosphere formation through the process of Micro-Meteoroids Impact Vaporization (MMIV). The MESSENGER/NASA mission provided measurements of Mercury's Ca exosphere, allowing the study of its configuration and its seasonal variations [2]. The observed Ca exhibited very high energies, with a scale height consistent with a temperature > 50,000 K, measured mainly on the dawn-side of the planet [1]. It was suggested that the originating process is due to MMIV, but previous estimations were not able to justify the observed intensity and energy. We investigate the possible pathways to produce the high energy observed in the Ca exosphere and discuss about the generating mechanism that produces the required abundance of this element. The most likely origin may be a combination of different processes involving the release of atomic and molecular surface particles [5]. We use the exospheric Monte Carlo model by *Mura et al. (2007)* [4] in order to simulate the 3-D spatial distribution of the CaO and Ca exospheres generated through the MMIV process, including specific events like comet stream crossing, and we show that their morphology and intensity are consistent with the available MESSENGER observations.

Methods
In this paper we work on models of Mercury's impactors: using as an input the information on the arrival geometry of the Mercury-intercepting particles [7], we modify the exosphere generation model by *Mura et al. 2007* [4]. In order to provide a detailed Ca-source extraction model, we simulate the expected 3-D CaO and Ca density distribution in Mercury's exosphere due to the MIV mechanism.
A low energy Ca component derives from the photodissociation of the initially released CaO molecules released by MMIV, while energetic Ca component is generated from the dissociative ionization and neutralization processes. We reproduce the different contributions of Ca exosphere due to each process, including specific events like comet stream crossing: we showed a persistent Ca enhancement located in the dawn equatorial region, peaking at ~20° True Anomaly Angle (TAA), that was attributed [3][6] to the vaporization of surface material induced by the comet Encke's stream particles.
We compare the results to the MESSENGER observations.

Results
Our results show that the 3-D morphology of the MIV-generated Ca exosphere, low and high energy component, is consistent with the UVVS observations. These support the idea that the Ca source peaks near the dawn region. The CaO exosphere is denser above the dawn hemisphere where the molecules are preferentially ejected into the exosphere by MIV process; Ca is preferentially seen in the midnight-to-dawn quadrant where CaO molecules are released by micrometeroid impacts and dissociated by the sunlight. The energetic Ca component is expected to be more intense than the other one, especially at high altitudes, but in the post-dawn low altitudes it is not excluded a possible substantial contribution of the low energy component to the global Ca exospheric content.

Conclusions
The results presented in this work will be useful for the exosphere observations planning and for the data interpretation in the frame of the ESA/JAXA BepiColombo mission, that will start its nominal mission phase in 2026. In particular, the resulting molecular distribu-

tions will be compared to the measurements of the MPO/SERENA-STROFIO mass spectrometer that will be the only instrument able to identify the molecular components, as CaO, and will permit to obtain simultaneous observations of different molecular and atomic components of the exosphere. These measurements coupled with the dust measurements by Mio/MDM instrument will allow for the first time a full investigation of the effect of MMIV at a planet.

Acknowledgments: the study is supported by ASI-SERENA contract no. 2018-8-HH.O
Partecipazione scientifica alla missione BEPICOLOMBO SERENA Fase E1 and Addendum no. 2018-8-HH.1-2022
The Sun Planet Interactions Digital Environment on Request (SPIDER) Virtual Activity of the Europlanet H2024 Research Infrastucture is funded by the European Union's Horizon 2020 research and innovation programme under grant agreement No 871149 (https://www.europlanet-society.org/europlanet-2024-ri/spider/)

References:

[1] Burger, M.H. et al., "Modeling MESSENGER observations of calcium in Mercury's exosphere", J. Geophys. Res. 117, E00L11, (2012)

[2] Burger, M.H. et al., "Seasonal variations in Mercury's dayside calcium exosphere", Icarus 238 (2014) 51–58 , (2014)

[3] Christou, A. A., R. M. Killen, and M. H. Burger (2015), The meteoroid stream of comet Encke at Mercury: Implications for MErcury Surface, Space ENvironment, GEochemistry, and Ranging observations of the exosphere, Geophys. Res. Lett., 42, 7311–7318

[4] Mura, A., Milillo, A., Orsini, S., Massetti, S., 2007. Numerical and analytical model of Mercury's exosphere: dependence on surface and external conditions. Planet. Space Sci. 55, 1569–1583

[5] Killen, R. M., 2016. Pathways for energization of Ca in Mercury's exosphere, Icarus, 268, 32–36

[6] Plainaki C., A. Mura, A. Milillo, S. Orsini, S. Livi, V. Mangano, S. Massetti, R. Rispoli, E. De Angelis, "Investigation of the possible effects of comet Encke's meteoroid stream on the Ca exosphere of Mercury", J. Geophys. Res., Planets 122, 1217–1226 (2017)

[7] Pokorný P., M. Sarantos, D. Janches, "A comprehensive model of the meteoroid environment around Mercury". Astrophys. J. 863(1), 31 (2018)

REMOTE SENSING OF MERCURY SODIUM EMISSION AND RELATIONSHIPS WITH MAGNETOSPHERIC ACTIVITY. S. Orsini[1], V. Mangano[1], A. Milillo[1], A. Mura[1], T. Alberti[2], [1]INAF-IAPS, via del Fosso del Cavaliere 100, 00133 ROMA, stefano.orsini@inaf.it; [2]INGV, Via di Vigna Murata, 605, 00143 Roma .

Introduction: The THEMIS ground-based solar telescope performed several Mercury Na emission remote sensing campaigns during times when the MESSENGER spacecraft was orbiting around the planet, in between 2011-2013. By taking profit from local magnetic field measurements as taken by MESSENGER, the typical two-peaks sodium emission detected by means of one-hour scans images of the day-side planet, as performed by THEMIS, have been statistically related to the local IMF intensity and direction. In this presentation, we show how the Mercury magnetosphere structure reacts to the IMF features, in terms of reconnection and ion precipitation rates. At the Earth, magnetic field reconnection and consequent particle precipitation is strongly related to the orientation of the IMF Z component, so that when this component is positive the magnetosphere is basically colosed in the front side, whereas when it is negative the magnetosphere is open to the penetration of solar wind particle in the front side, where they precipitate into the atmosphere along the cusp regions. At Mercury such an effect is not so evident, especially because the IMF magnitude is very strong respect to the weak magnetic field of this planet. We notice that the Mercury's magnetosphere is sensitive to the orientation of the IMF Z component only whe IMF is relatively weak, up to about 25 nT. Following a paper by Orsini et al. [1], we show by a statistical approach that the sodium polar emission can be interpreted as a perfect tracer of such dynamics, so that in this way, ground-based remote sensing may use Mercury as a permanent monitor of the solar activity in the inner heliosphere.

References:

[1] Orsini, S., V. Mangano, A. Milillo, C. Plainaki, A. Mura ,J. M. Raines, E. De Angelis, R. Rispoli, F. Lazzarotto, A. Aronica, 'Mercury sodium exospheric emission as a proxy for solar perturbations transit', Scientific Reports 8:928 DOI:10.1038/s41598-018-19163-x (2018).

PERMANENT SHADOWED REGIONS OF MERCURY: NEW HYPOTHESIS ABOUT WATER ICE ORIGIN.

Bertoli S.[1,2], Cremonese G.[2], Pajola M.[2], Lucchetti A.[2], Cambianica P.[2], Simioni E.[2], Martellato E.[2], Massironi M.[3], Borin P.[2 1] Center of Studies and Activities for Space "G. Colombo" (CISAS), Padova, (silvia.bertoli.3@phd.unipd.it)
[2] INAF, Padova Astronomical Observatory, Padova, Italy,
[3] Department of Geological Sciences, University of Padova, Padova, Italy.

Introduction: Earth-based radar observations performed in 1991 by the Goldstone Very Large Array (VLA) 70 m dish revealed areas with high radar backscatter within Mercury's north polar region [1]. These radar-bright materials have been interpreted as water ice deposits located within the Permanently Shadowed Regions (PSRs) of polar craters due to the similar radar characteristics between them and those observed on Martian polar ice caps. The thermal models constructed by [2] and the multiple data sets from the MErcury Surface, Space ENvironment, GEochemistry, and Ranging (MESSENGER, [3]) mission also supported this hypothesis.

There are two main mechanisms that can be responsible for the origin of the ice deposits on Mercury. The first is the steady state accumulation of ice delivered constantly by ice-bearing micrometeorites [4, 5]. However, [6] discussed that the mixing rate of micrometeorites is huge compared to the accumulation one, suggesting that the volatiles delivered by micrometeorites are not sufficient to explain the presence of the observed pure ice. The other accepted mechanism for the delivery of a large amount of ice, could be comets or asteroids impact. A candidate impact for this huge delivery is Hokusai crater [7], an extremely young structure, with asymmetrical rays and ejecta that indicate an oblique impact. An advancement in such debate can be given by the detailed chronological analysis of the craters with PSRs, because it can provide new insights into the origin and behaviour of water ice deposits. Therefore, we performed crater counting and age determination of 14 craters located over 80°N, with the goal to unravel two main issues: i) understanding the relationship between radar bright deposits and crater ages, and ii) establishing the origin of water ice deposits on the Mercury north pole.

The outcome of this work is key not only for understanding of the evolution of Mercury, but also in view of target definition of the Spectrometer and Imagers for MPO BepiColombo Integrated Observatory SYStem (SIMBIO-SYS) [8], the camera onboard the ESA BepiColombo mission [8BIS]. The investigation of the PSRs have been indeed identified with high priority and have been selected as one of the features to be observed at the beginning of the nominal mission of BepiColombo.

Methods: We performed crater counting on the floors and ejecta of 14 craters (Figure 1) located 80°N.

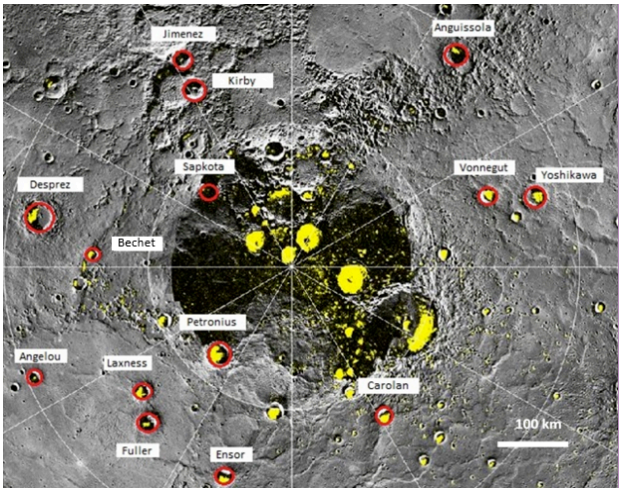

Figure 1 – Picture of the craters of this study. The yellow spots indicate the radar bright deposit (Credits: NASA/Johns Hopkins University Applied Physics Laboratory/Carnegie Institution of Washington).

In *QGIS 3.16* we mapped the ejecta and floor units. Then we identified the small impact craters rim, and we calculated their diameters using the Field Calculator. We used CraterStats II software [9] to plot the data on a cumulative distribution, i.e., the crater size-frequency distribution (SFD) as a function of the crater diameter. These plots are made for each unit. In order to estimate the age of each terrain we fitted the distributions by means of the chronology curves of [10] for Mercury.

Results: In this work, we aim to infer the relative chronology between these craters and their geological units, and the relationship between the inferred age of the different terrains and the presence and extent of the radar bright features within them. Comparing ejecta ages with the chronological system of Mercury we found that one crater formed during the Mansurian Period, six craters during the Calorian Period and the others in the beginning of Tolstojan Period (Figure 2).

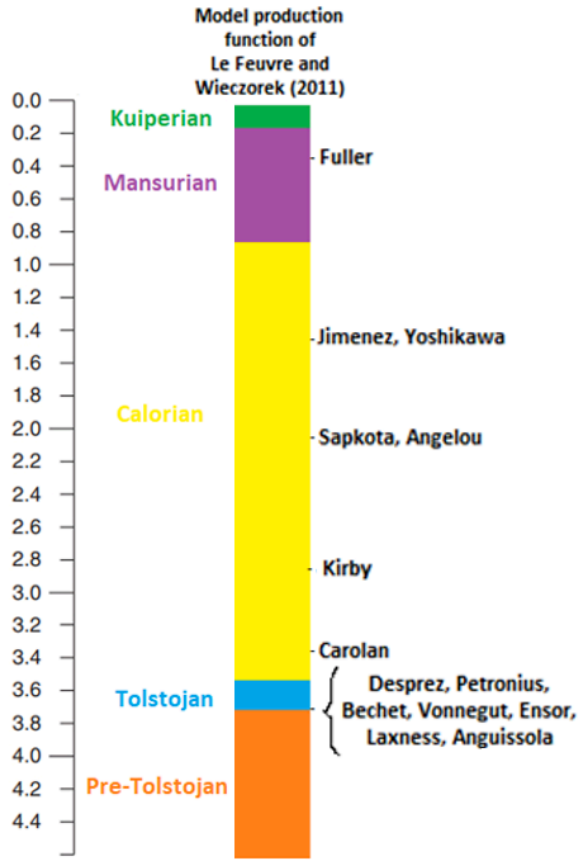

Figure 2 – Mercury's time-stratigraphic system, with the absolute ages (given in Ga) as derived from the crater production model by [10]. Along the chronological timeline, the craters of this work are here aligned according to the age of their ejecta.

The preliminary results also highlight a general rejuvenation of the floor compared to the ejecta, particularly for the part of the floor covered by radar deposits. Indeed, except two cases dated in the Calorian period, all the radar-deposits in the floor are <700 Ma old.

On one hand, the youngest radar bright deposit ages seem to be in line with the hypothesis of Hokusai impact [7] (which is Kuiperian). However, older ages would indicate that there were other cometary impacts in the past anyway, and probably the Hokusai impact did not provide ice to all the craters. On the other hand, if we compare the absolute ages of craters with the radar bright deposit percentile of their PSRs, we could observe an interesting correlation. Indeed, it seems that the older the craters are, the more they have bright radar deposits accumulated in the PSRs. This correlation would be more in line with the hypothesis of a steady state accumulation over time by micrometeorite impacts. This trend has two outliers, which have a large amount of bright deposits notwithstanding their young age. This may suggest that they could be the results of a cometary impact (which is connected to the second hypothesis).

Thus, considering this evidence, we propose that both processes could have acted in the formation of ice deposit in the PSRs. The next step will be to i) carefully test whether the micrometeorite fluxes can sustain such an accumulation with respect to mixing rates, and ii) verify the possibility that the two outliers may be formed by a cometary projectile.

Acknowledgement: This activity has been realized under the BepiColombo ASI-INAF contract no 2017-47-H.0

References: [1] Butler et al., (1993) *JGR, 98,* 15003–15023. [2] Paige et al., (2013) *Science, 339, 300-303*. [3] Solomon et al., (2007) *Space Sci. Rev., 131, 3-39*. [4] Moses et al., (1999) *Icarus, 137, 197-221*. [5] Syal et al., (2015) *Nature Geoscience, 8, 352.* [6] Rubanenko et al., (2018) *JGR: Planets, 123, 2178-2191*. [7] Ernst et al., (2018) *JGR: Planets, 123, 2628-2646.* [8] Cremonese et al., (2020) *Space Sci. Rev., 216, 75.* [8BIS] Benkhoff J. et al. (2021) *Space Sci. Rev., 217*, 90, [9] Michael G. G. and Neukum G. (2010) *Earth and Planetary Science Letters, 294 (3-4), 223-229.* [10] Le Feuvre M. and Wieczorek MA (2011), *Icarus, 214, 1-20*

SPECTRAL DETECTION OF WATER ICE, S-BEARING AND ORGANIC SPECIES IN MERCURY'S PSRs BY SIMBIOSYS-VIHI ON BEPICOLOMBO MISSION. G. Filacchione[1], A. Raponi[1], A. Frigeri[1], M. Ciarniello[1], F. Capaccioni[1], A. Galiano[1], M.C. De Sanctis[1], M. Formisano[1], V. Galluzzi[1], G. Cremonese[2]. [1]INAF-IAPS, via del Fosso del Cavaliere, 100, 00133, Rome, IT (gianrico.filacchione@inaf.it), [2]INAF-Padua Observatory, Vicolo dell'Osservatorio, 5, 35122, Padua, IT.

Introduction: The exploration of Mercury's polar regions [1] is among the main scientific objectives of the SIMBIO-SYS instrument [2] aboard ESA's Bepi-Colombo mission. Polar regions host many Permanent Shadowed Regions (PSRs) which can be found within deep craters and rough terrains inaccessible to direct solar illumination. The surface area occupied by PSRs is estimated in about 25.000 and 12.000 km^2 respectively across the South [3] and North polar regions [4]. The illumination conditions occurring near the PSRs are largely variable [5] during the hermean year due to the planet's 3:2 orbital resonance and rough local morphology. Thanks to these conditions, Mercury's PSRs experience cryogenic temperatures across geological timescales regardless of the orbital vicinity of the planet to the Sun. By acting like cold traps, the condensation and accumulation of volatile species in the PSR is favored [6]. These volatile species, and their alteration byproducts, could be of exogeneous or endogenous origin. To the former class belong volatiles released from asteroidal and cometary impacts: condensed volatiles can be further processed in CHONS and organic matter by radiation processing. The latter class includes the bombardment of magnetospheric particles occurring preferentially above the polar regions able to induce dissociation, ion implantation and hot atom chemistry [7].

In a previous work [5] we have discussed how the light scattered by the illuminated part of a PSR crater's rim can be exploited to detect ice deposits located in the crater's floor within the shadowed areas. Moreover, the extended apparent dimension of the Sun (between 1.15° and 1.75° at aphelion and perihelion, respectively) causes the occurrence of blurred shadow lines (e.g. penumbras) favoring a further faded illumination towards otherwise shadowed areas [5].

In this work, we report about comprehensive spectral simulations in the SIMBIOSYS-VIHI [2,8] 0.4-2.0 μm spectral range aiming to asses the instrument capabilities to detect binary mixtures made of water, S-bearing species (SO_2, H_2S), and organic matter from orbit. Apart assessing the detection of icy species from orbit our work is necessary to optimize the future VIHI observations above the PSRs [9].

Our spectral simulations are performed for several binary mixtures made of water ice and non-icy materials (S-bearing species and organic matter) by adopting the method described in [10], and including the mixing cases (areal or intimate) as modeled in [11]. This approach allows to simulate different volatile species abundances (at steps of 20% between 0% and 100%) and grain size populations (between 10 μm and 1 mm).

The simulated I/F for intimate mixtures made of water ice and H_2S (shown in Fig. 1), water ice and SO_2 (Fig. 2) and water ice and Wurtzilite (as an example of aromatic organic matter, Fig. 3) for a monodisperse grain size distribution of 100 μm are derived for the exposed ice deposit placed on the floor of the Prokofiev crater (lat=86°N, lon=296.3W) for typical grazing solar geometry and nadir-pointing observations of the VIHI imaging spectrometer.

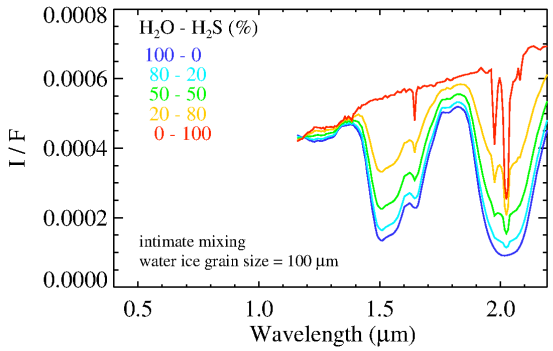

Fig.1: I/F Spectral simulation of H_2O-H_2S intimate mixture made of 100 μm grains for the exposed ice deposit located within Prokofiev crater PSR under indirect illumination conditions. The five curves correspond to running abundances of the two components between 0% and 100% at incremental/decremental steps of 20%.

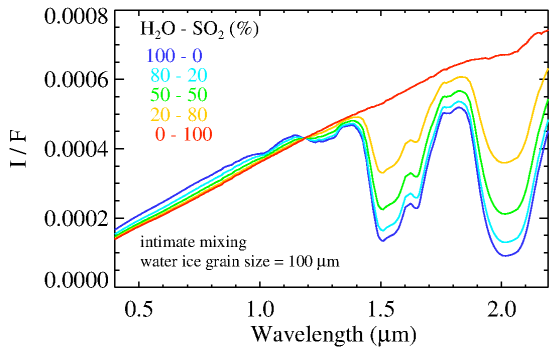

Fig. 2: The same as Fig. 1 but for a H_2O-SO_2 intimate mixture.

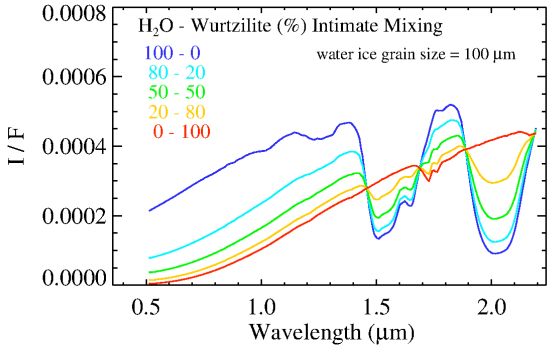

Fig. 3: The same as Fig. 1 but for a H_2O-Wurtzilite intimate mixture.

These results are currently used to compute the VIHI signal-to-noise ratio, as derived from the instrumental radiometric model [12], for different PSRs locations under varying illumination conditions. By coupling spectral simulations with instrumental performances, it is possible to estimate the detection threshold for distinct ice deposits located within the PSRs given a set of instrumental operative parameters, like integration time and spatial/spectral binning, during the different orbital phases of the BepiColombo mission.

References:

[1] Rothery, D. A., et al., *Space Sci. Rev.*, 216, 66, 2020. [2] Cremonese G. et al., *Space Sci. Rev.*, 216, 75, 2020. [3] Chabot N. L. et al., *J. Geophys. Res.*, 123, 666, 2018. [4] Deutsch A. N. et al., *Icarus*, 280, 158, 2016. [5] Filacchione G. et al., *MNRAS*, 498, 1308-1318, 2020. [6] Paige D. A. et al., *Science*, 339, 300, 2013. [7] Delitsky et al., *Icarus*, 281, 19-31, 2017. [8] Capaccioni F. et al., *IEEE Trans. Geosci. Remote Sens.*, 48, 3932, 2010. [9] Filacchione et al., IEEE TGRS, submitted. [10] Raponi A. et al., *Sci. Adv.*, 4, eaao3757, 2018. [11] Ciarniello. M. et al., *Icarus,* 214, 541, 2011. [12] Filacchione G. et al., *Rev. Sci. Instrum.*, 88, 094502, 2017.

LICIACube: THE LIGHT ITALIAN CUBESAT FOR IMAGING OF ASTEROIDS IN SUPPORT TO THE NASA MISSION DART

E. Dotto[1], M. Amoroso[2], I. Bertini[3,4], J.R. Brucato[5], A. Capannolo[6], S. Caporali[5], M. Ceresoli[6], G. Cremonese[7], M. Dall'Ora[8], V. Della Corte[4], J.D.P. Deshapriya[1], I. Gai[9], L. Gomez Casajus[9], E. Gramigna[9], P. Hasselmann[1], S. Ieva[1], G. Impresario[2], S.L. Ivanovski[10], R. Lasagni Manghi[9], M. Lavagna[6], M. Lombardo[9], A. Lucchetti[7], E. Mazzotta Epifani[1], D. Modenini[9], M. Pajola[7], P. Palumbo[4,3], D. Perna[1], S. Pirrotta[2], G. Poggiali[5], A. Rossi[11], P. Tortora[9], F. Tusberti[7], M. Zannoni[9], G. Zanotti[6], A. Zinzi[12,2], N.L. Chabot[13], A.F. Cheng[13], A.S. Rivkin[13], [1]INAF Osservatorio Astronomico di Roma, via Frascati 33, 00078 Monte Porzio Catone (Roma), Italy, elisabetta.dotto@ inaf.it , [2]Agenzia Spaziale Italiana, Roma, Italy, [3]Università degli Studi di Napoli "Parthenope", Napoli, Italy, [4]INAF Istituto di Astrofisica e Planetologia Spaziali, Roma, Italy, [5]INAF Osservatorio Astrofisico di Arcetri, Firenze, Italy, [6]Politecnico di Milano, Italy, [7]INAF Osservatorio Astronomico di Padova, Italy, [8]INAF Osservatorio Astronomico di Capodimonte, Napoli, Italy, [9]Università di Bologna, Bologna, Italy, [10]INAF Osservatorio Astronomico di Trieste, Italy, [11]CNR Istituto di Fisica Applicata "Nello Carrara", Sesto Fiorentino (Firenze), Italy, [12]Space Science Data Center-ASI, Roma, Italy, [13]Johns Hopkins Applied Physics Lab, Laurel, MD, USA

Introduction: LICIACube, the Light Italian Cubesat for Imaging of Asteroids [1,2] is an ASI cubesat that witnessed the impact of DART [3] on Dimorphos, the moonlet of the binary asteroid Didymos. LICIACube was launched with DART on November 2021 and travelled for 9.5 months, as a piggyback. Fifteen days before the DART impact, LICIACube was deployed and started its approaching phase towards the target, performing several communications session with the DSN antennas, that allowed to download satellite telemetries and data and to upload commands for the spacecraft. In the terminal phase of the closest approach, no guidance was possible from the Earth, thus the last pointing was automatically decided and executed by the Artificial Intelligence on board of the small satellite. During this phase, also stars and planets observations were performed for calibration (Fig.1).

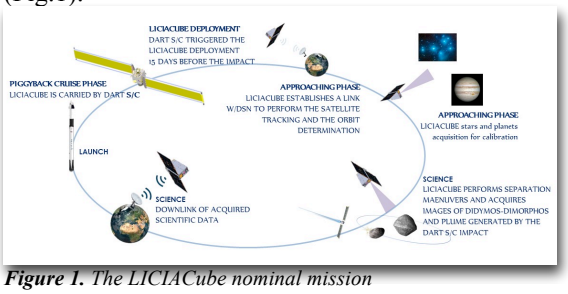

Figure 1. *The LICIACube nominal mission*

The scientific phase: The LICIACube scientific phase started 71 seconds before the nominal DART impact time, when LICIACube was 1466 km from Dimorphos. Three minutes after the DART impact nominal time, LICIACube passed at the minimum distance of about 58 km from Dimorphos (closest approach, CA) flying at a velocity of 6.1 km/s. During its science phase, LICIACube acquired a total of 426 scientific images, obtaining a unique view of the event with a phase angle ranging from 43° to 118°.

First results: LICIACube was equipped with two different cameras: LEIA (Liciacube Explorer Imaging for Asteroid) with dual functionality of managing the cubesat operations/pointing and obtaining scientific images, and LUKE (Liciacube Unit Key Explorer) able to acquire images in three different colors (red, green and blue) [1]. In the LEIA images the DART impact was testified by an increase in the luminosity of the target. LUKE acquired images beginning 29 seconds after the impact and both the instruments followed the target and the evolution of the impact effects up to 320 seconds after the nominal impact time. In the LICIACube viewing geometry the effects produced by the DART impact were clearly seen in both pre-CA and post-CA LUKE images. The LICIACube images show that the DART impact on Dimorphos generated a cone of ejected surface material with a large aperture angle. This plume has a complex and inhomogeneous structure, characterised by non-radial filaments, dust grains, and single and clustered boulders (Fig. 2) that allows us to deeply investigate the nature of the ejecta and the structure of Dimorphos.

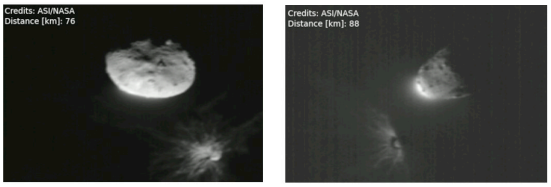

Figure 2. *Images obtained by LUKE pre-CA and post-CA.*

Measurements from the LICIACube flyby constrain the shape of the target, and quantitatively characterise the ejecta and their early evolution velocities, providing also pivotal input for measuring the momentum transferred to Dimorphos [4].

Acknowledgments: Acknowledgements: The LICIACube team acknowledges financial support from Agenzia Spaziale Italiana (ASI, contract No. 2019-31-HH.0 CUP F84I190012600).

References: [1] Dotto E., et al. (2021) PSS 199, id. 105185. [2] Dotto E. et al. (2023) Nature, in preparation. [3] Rivkin A.S. et al. (2021) PSJ 2(5), id.173. [4] Cheng A.F. et al. (2023) Nature, in press.

MODELLING OF THE EJECTA PLUME AFTER THE DART IMPACT. Rossi A.[1], Marzari F.[2], Zanotti G.[3], Deshapriya J.D.P.[4], Hasselmann, P.[4], Dotto, E.[4], Amoroso, M.[5], Bertini, I.[6,7], Brucato, J.R.[8], Capannolo, A.[3], Caporali, S.[8], Ceresoli, M.[3], Cremonese, G.[9], Dall'Ora, M.[10], Della Corte, V.[7], Gai, I.[11], Gomez Casajus L. [11], Gramigna E. [11], Ieva, S.[4], Impresario G.[5], Ivanovski, S.L.[12], Langner K.[1,2] ,Lasagni Manghi R. [11], Lavagna, M.[3], Lombardo M.[11], Lucchetti, A.[9], Mazzotta Epifani, E.[4], Modenini, D.[10], Pajola, M.[9], Palumbo, P.[7,6], Perna, D.[4], Pirrotta, S.[5], Poggiali, G.[8], Tortora, P.[11], Tusberti, F.[9], Zannoni, M.[11], Zinzi A.[13], Barbee B.W.[14] , Campo Bagatin A.[15], Chabot, N. L.[16], Chang, A.[16], Fahnestock G.[17], Farnham T.L.[18] ,Ferrari F.[3], Hirabayashi M.[19], Jutzi M.[20], Li Jian-Yang.[21], Luther R.[22], Moreno F.[23], Nakano R.[19], Pérez-Molina M.[15], Raducan S.[20], Rivkin A.[16] , Scheeres D.J.[24], Soldini S.[25], Trógolo N.[15,26], [1]CNR Istituto di Fisica Applicata "Nello Carrara", Sesto Fiorentino (Firenze), Italy, a.rossi@ifac.cnr.it, [2]Department of Physics and Astronomy, University of Padova, Italy, [3]Department of Aerospace Science and Technology, Politecnico di Milano, Italy, [4]INAF Osservatorio Astronomico di Roma, Italy,[5]Agenzia Spaziale Italiana, Roma, Italy,[6]Università degli Studi di Napoli "Parthenope", Napoli, Italy, [7]INAF Istituto di Astrofisica e Planetologia Spaziali, Roma, Italy, [8]INAF Osservatorio Astrofisico di Arcetri, Firenze, Italy, [9]INAF Osservatorio Astronomico di Padova, Italy, [10]INAF Osservatorio Astronomico di Capodimonte, Napoli, Italy, [11]Università di Bologna, Bologna, Italy, [12]INAF Osservatorio Astronomico di Trieste, Italy, [13]Space Science Data Center-ASI, Roma, Italy, [14]NASA Goddard Space Flight Center, Greenbelt, MD 20771, USA, [15]IUFACyT—DFISTS, Universidad de Alicante, Alicante, Spain, [16]Johns Hopkins Applied Physics Lab, Laurel, MD, USA, [17]Jet Propulsion Laboratory, California Institute of Technology, Pasadena, CA, USA, [18]University of Maryland, College Park, MD, USA, [19]Department of Aerospace Engineering/Geosciences, Auburn University, Auburn, AL 36849, USA, [20]Space Research and Planetary Sciences, University of Bern, Switzerland, [21]Planetary Science Institute, Tucson, AZ, USA, [22]Museum für Naturkunde - Leibniz Institute for Evolution and Biodiversity Science, Berlin, Germany, [23]Instituto de Astrofísica de Andalucía, CSIC, E-18008 Granada, Spain, [24]Smead Department of Aerospace Engineering Sciences, University of Colorado Boulder, CO 80303, USA, [25]University of Liverpool, UK, [26]Observatorio Astronómico, Universidad Nacional de Córdoba, Argentina.

Introduction: In the first real scale test of the kinetic impactor technique, on September 26, the NASA DART mission impacted the asteroid Dimorphos, the small satellite of the binary asteroid Didymos [1].

The impact generated a large ejecta plume which was imaged by the Italian Space Agency probe LICIACube (Light Italian Cubesat for Imaging of Asteroids) which was carried as a piggy back payload by the NASA/APL DART spacecraft [2][3]. Beside LICIACube many ground and space based observatories (e.g., HST, JWST) carried out extensive observation campaigns to characterize the event [4].

The LICIACube images revealed complex structures with the plume including filaments, clumps and nodules possibly related to the presence of large boulders and to other superficial features in the impact area. The ground and space telescopes images also showed the formation of a long tail which, for a limited time also had a double structure.

Methods and models: Will all the information coming from the available images and, in particular, the observed ejecta geometries, we aim at reconstructing the plume generation and evolution by means of the comprehensive LICEI model [5], considering all the relevant gravitational and non-gravitational perturbations.

Analysis and results: A range of initial conditions, both in terms of ejection speed and direction are integrated, considering different size ranges to explore the formation of the observed features. Especially in the first phases of the plume generation the evolution of the ejecta are critically dependent on the initial ejection velocity, hence we test different plausible velocity field to try and find a best match with the observed behavior. To study the brightness profile of the plume and compare to the LICIACube observations, from LICEI output we produce synthetic images relying on Mie-scattering radiative transfer and ray optics to cover radiances from micrometer to millimeter size range [6][7]. This way, we will understand iteratively how the inputs can be improved to better describe the LICIAcube observations.

The dynamical evolutions are performed over different time spans in an effort to characterize the event and its possible consequences on the binary system environment also in the view of the upcoming Hera mission.

In particular, specific attention is devoted to the medium to long term evolution of the boulders observed by LICIACube which might be prone to attain stable orbits surviving up to the Hera arrival. Re-impacting of larger ejecta on the surface of either

asteroid and the consequences of these events of the circum-binary environment are the subject of specific analysis as well.

The implications of the ejecta evolution for the evaluation of the collision enhancement factor, the so-called β, of paramount importance for the planetary defense test, will be discussed too.

References: [1] Rivkin, A.S. et al. (2021) *PSJ*, 2, 24pp. [2] Dotto, E. et al. (2021) *Planet. Space Sci.* 199, 105185. [3] Dotto, E., et al. (2023), *in preparation*. [4] Li et al. (2023) *submitted*. [5] Rossi A. et al. (2022) *PSJ*, 3:118. [6] Hasselmann et al., 2022, Vol. 16, EPSC2022-615. [7] Hasselmann et al., 2023, *in prep*.

Acknowledgements: The LICIACube team acknowledges financial support from Agenzia Spaziale Italiana (ASI, contract No. 2019-31-HH.0 CUP F84I190012600).

COLOR ANALYSIS OF DIMORPHOS PLUME PRODUCED BY DART IMPACT USING LICIACUBE-LUKE DATA Poggiali G.(1)(2), Brucato J.R.(1), Caporali S.(1), Deshapriya J.D.P.(3), Hasselmann, P.(3), Ieva S.(3), Bertini I.(4), Dotto E.(3), Ivanovski, S.L.(5), Rossi A.(6), Della Corte, V.(4), Zinzi A.(7,8), Mazzotta Epifani E.(3), Dall'Ora M.(9), Pajola M.(10), Lucchetti A.(10), Amororso M.(7), Capannolo, A.(11), Ceresoli, M.(11), Cremonese, G.(10), Gai, I.(12), Gomez Casajus L.(12), Gramigna E.(12), Impresario G.(7), Lasagni Manghi R.(12), Lavagna, M.(11), Lombardo M.(12), Modenini, D.(9), Palumbo, P.(4,13), Perna, D.(3), Pirrotta, S.(7), Tortora, P.(12), Tusberti F.(11), Zannoni, M.(12), Zanotti, G.(11) (1)INAF-Astrophysical Observatory of Arcetri, l.rgo E. Fermi n.5, 50125 Firenze, Italy giovanni.poggiali@inaf.it (2)LESIA-Observatoire de Paris, Université PSL, CNRS, Sorbonne Université, Université de Paris, 5 place Jules Janssen, 92190 Meudon, France (3)INAF-Osservatorio Astronomico di Roma, Monte Porzio Catone (Roma), Italy (4)INAF-IAPS Istituto di Astrofisica e Planetologia Spaziali, Roma, Italy (5)INAF-Osservatorio Astronomico di Trieste, Trieste, Italy (6)CNR Istituto di Fisica Applicata "Nello Carrara", Sesto Fiorentino (Firenze), Italy (7)Agenzia Spaziale Italiana, Roma, Italy (8)Space Science Data Center-ASI, Roma, Italy (9)INAF-Osservatorio Astronomico di Capodimonte, Napoli, Italy (10) INAF-Osservatorio Astronomico di Padova, Padova, Italy (11)Politecnico di Milano, Milano, Italy (12)Università di Bologna, Bologna, Italy (13) Università degli Studi di Napoli "Parthenope", Napoli, Italy

Introduction: NASA Double Asteroid Redirection Test (DART) mission [1] impacted the surface of Dimorphos, the secondary asteroid of Didymos binary system on 26 September 2022. The Light Italian Cubesat for Imaging of Asteroids (LICIACube) [2], provided by the Italian Space Agency (ASI) was released 15 days before the impact to acquire high-resolution images of its effects. During the LICIACube flyby of Dimorphos (minimum distance of 57.78 km), LEIA and LUKE the two cameras on board the cubesat acquired more than 400 images.

LUKE (LICIACube Unit Key Explorer) is a wide-field camera (5°x10° field-of-view), with an RGB Bayer pattern filter to acquire simultaneously color data to recompose the three final 24-bit colour images. Its main aim was to study the colours of surfaces and plume and acquire information about the plume evolution [3]. Color analyses are fundamental to investigate the physical properties of the plume, such as the grain size [4] or the degree of alteration of the surface from space weathering of Dimorphos [5].

Methods: We evaluated the relationship between different RGB filters of LUKE to investigate possible color differences. The ratio of red to blue filter shows that the center of the plume has a prominence of blue likely related to the presence of small grains and material less altered by the space weathering excavated by the Dimorphos subsurface. Intensity profiles on the various channels along the streams of the plume reveal its inhomogeneity and allow us to assess color differences within the dust filament of the ejecta by tying these results to patterns of plume evolution.

Results: Several color variation were observed within Dimorphos plume [6]. The inner part of the plume is characterized by a stronger blue colour while as the distance from the asteroid is increasing, the plume colour is progressively shifted towards the red within increasing distance from Dimorphos. This could be related to abundant micrometer, or even smaller, submicron dust grains <1 μm and a possible contribution from excavated material from the fresh subsurface of Dimorphos therefore less altered material with a bluer slope as shown by laboratory experiments. Profile of RGB color intensity within the single filaments visible in the plume reveal dishomogenity likely related to the complex structure of the plume.

References: [1] Rivkin, A.S. et al. (2021) PSJ, 2, 24 [2] Dotto, E. et al. PSS, 199, 105185 [3] Poggiali, G. et al (2022) PSJ, 3, 161 [4] Meech, K.J. et al. (2005) Science, 310, 265 [5] Clark, B. E. (2002) Asteroid III, p.585-599 [6] Dotto, E. et al. Nature (submitted)

Acknowledgments: This research was supported by the Italian Space Agency (ASI) within the LICIACube project (ASI-INAF agreement AC n.2019-31-HH.0) and the DART mission, NASA Contract No. NNN06AA01C to JHU/APL..

TOWARDS RECONSTRUCTING THE DIMORPHOS EJECTA PLUME BY MEANS OF NON-SPHERICAL DUST SIMULATIONS AND DART/LICIACUBE DATA.

S. L. Ivanovski [(1)], G. Zanotti [(2)], I. Bertini[(3,4)], P. Hasselmann[(5)], J.D.P. Deshapriya[(5)], A. Lucchetti[(6)], M. Pajola[(6)], D. Perna[(5)], G. Poggiali[(7,8)], E. Dotto[(5)], M. I. Herreros[(9)], J. Ormo [(9)], J.-Y. Li[(10)], M. Amoroso[(11)], J.R. Brucato[(7)], A. Capannolo[(2)], S. Caporali[(6)], M. Ceresoli [(2)], G. Cremonese[(6)], M. Dall'Ora[(12)], V. Della Corte[(4)], I. Gai [(13)], L. Gomez Casajus[(13)], E. Gramigna[(13)], S. Ieva[(5)], G. Impresario[(11)], R. Lasagni Manghi[(13)], M. Lavagna[(2)], M. Lombardo[(13)], F. Marzari[(14)], E. Mazzotta Epifani[(5)], D. Modenini[(13)], P. Palumbo[(3,4)], S. Pirrotta[(11)], A. Rossi[(15)], P. Tortora[(13)], F. Tusberti[(6)], M. Zannoni[(13)], A. Zinzi[(11)], E. G. Fahnestock[(16)], T. L. Farnham[(17)], M. Hirabayashi[(18)], S.D. Raducan[(19)], F. Ferarri[(2)], S. Soldini[(20)], and R. Luther[(21)]

(1) INAF Osservatorio Astronomico di Trieste, Italy stavro.ivanovski@inaf.it; (2) Politecnico di Milano, Italy; (3) Università degli Studi di Napoli "Parthenope", Napoli, Italy; (4) INAF Istituto di Astrofisica e Planetologia Spaziali, Roma, Italy; (5) INAF Osservatorio Astronomico di Roma, Italy; (6) INAF Osservatorio Astronomico di Padova, Italy; (7) INAF Osservatorio Astrofisico di Arcetri, Firenze, Italy; (8) Observatory of Paris, France; (9) Centro de Astrobiología (CAB), CSIC-INTA; (10) Planetary Science Institute, Tucson, AZ, USA; (11) Agenzia Spaziale Italiana, Roma, Italy; (12) INAF Osservatorio Astronomico di Capodimonte, Napoli, Italy; (13) Università di Bologna, Bologna, Italy; (14) Università di Padova, Italy; (15) CNR Istituto di Fisica Applicata "Nello Carrara"; (16) Jet Propulsion Laboratory, California Institute of Technology, USA; (17) University of Maryland, College Park, Maryland, USA and (18) Auburn University, Auburn, AL, USA.

Abstract: On the 26th of September 2022, NASA's Double Asteroid Redirection Test (DART) mission [1] was the first space mission demonstrating the kinetic impactor method for planetary defence. ASI's Light Italian Cubesat for Imaging of Asteroids (LICIACube) [2] was the first to image it.

To reconstruct the ejecta plume, we apply a 3D+t model – LIMARDE [3, 4] - constrained with laboratory observations [5], impact simulations and near- and far- field observations such the LICIACube [6] images and HST [7] dust observations, respectively. The main tasks that have been pursuing are the following: to compute the dust velocity distribution based on the physical properties (size, mass and shape) derived from the LICIACube observations; to reconstruct the dust distribution of the plume with its filaments, spikes and large aperture; to determine the contribution of the rotation of the dust in the optical thickness of the plume; to check what is the role of the fragmentation of the particles; to constrain the dust density and shape based on the dynamical properties of the ejected dust in the near- mid- and far- environment.

LIMARDE can compute single trajectories and obtain time dependently the rotational frequency and velocity as well as the particle orientation at any time and distance. The latter will be used not only to calculate the deviation of different shapes in the ejecta evolution but also to provide insights on the optical thickness of the plume and the collision enhancement factor β. This can be addressed by estimating how much momentum the ejected particles had to form the observed filamentary-like ejecta.

References: [1] Rivkin A. et al. (2021), PSJ. [2] Dotto E. et al. (2021), PSS. [3] Ivanovski S. et al. (2023), PSJ. [4] Fahnestock E. et al. (2022), PSJ. [5] Ormo J. et al. (2022), *E&PSL* [6] Dotto E. et al. submitted [7] Li J-Y. et al. (2023), Nature.

Acknowledgements: The LICIACube team acknowledges financial support from Agenzia Spaziale Italiana (ASI, contract No. 2019-31-HH.0 CUP F84I190012600.

THE SHAPE OF DIMORPHOS AS SEEN BY LICIACUBE LUKE IMAGES. A. Zinzi[1,2], V. Della Corte[3], O. Barnouin[4], T. Daly[4], E. Dotto[5], M. Amoroso[1], I. Bertini[6,3], J.R. Brucato[7], A. Capannolo[8], S. Caporali[7], M. Ceresoli[8], G. Cremonese[9], M. Dall'Ora[10], J.D.P. Deshapriya[5], I. Gai[11], L. Gomez Casajus[11], E. Gramigna[11], P. Hasselmann[5], S. Ieva[5], G. Impresario[1], S.L. Ivanovski[12], R. Lasagni Manghi[11], M. Lavagna[8], M. Lombardo[11], A. Lucchetti[9], E. Mazzotta Epifani[5], D. Modenini[10], M. Pajola[9], P. Palumbo[3,6], D. Perna[5], S. Pirrotta[1], G. Poggiali[7], A. Rossi[13], P. Tortora[11], F. Tusberti[9], M. Zannoni[11], G. Zanotti[8].

[1]Agenzia Spaziale Italiana, Roma, Italy (angelo.zinzi@ssdc.asi.it), [2]Space Science Data Center-ASI, Roma, Italy, [3]INAF Istituto di Astrofisica e Planetologia Spaziali, Roma, Italy, [4]Johns Hopkins Applied Physics Lab, Laurel, MD, USA, [5]INAF Osservatorio Astronomico di Roma, Monte Porzio Catone (Roma), Italy, [6]Università degli Studi di Napoli "Parthenope", Napoli, Italy, [7]INAF Osservatorio Astrofisico di Arcetri, Firenze, Italy, [8]Politecnico di Milano, Italy, [9]INAF Osservatorio Astronomico di Padova, Italy, [10]INAF Osservatorio Astronomico di Capodimonte, Napoli, Italy, [11]Università di Bologna, Bologna, Italy, [12]INAF Osservatorio Astronomico di Trieste, Italy, [13]CNR Istituto di Fisica Applicata "Nello Carrara", Sesto Fiorentino (Firenze), Italy

Introduction: The LICIACube ASI mission has been designed to acquire images of the Didymos-Dimorphos binary asteroidal system and of the plume generated by the DART-Dimorphos impact soon before and soon after this impact, happened on 26th September 2022.

In order to better witness this event, LUKE camera, onboard LICIACube, has been commanded to acquire images in a peculiar way, i.e., triplets of images at different exposure times is shoot in a very short time range and they were separated from each other from 1 to 6 seconds, depending on the distance from the target.

In this way it has been possible to accurately capture details of both asteroid surfaces and plume dynamics and, differently from what the DRACO camera onboard DART, LICIACube has been allowed to take images of both hemisphere of Dimorphos [1].

Dimorphos shape detection: In some triplets, located soon before and soon after the flyby's closest approach, it has therefore been possible to detect the whole projected portion of Dimorphos, using images in the same triplets at different exposure times: in the short-exposure images only the illuminated hemisphere is visible, whereas in the long-exposure images, where the plume and the illuminated hemisphere are saturated, the shadowed (i.e., non illuminated) hemisphere of Dimorphos becomes visibile in contrast to the bright plume.

Exploiting some standard Computer Vision algorithms we developed an automated pipeline able to detect objects inside LUKE images, based on the expected size of Dimorphos, as seen at the known distances between LICIACube and the target.

In this way we succeded to isolate from the whole image only the Dimorphos hemisphere of interest (e.g., the illuminated one in short-exposure images and the shodowed one in the long-exposure images – Fig. 1).

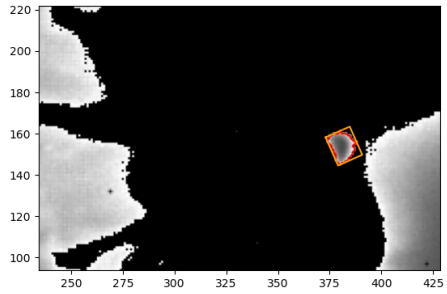

Fig. 1: An example of hemisphere detection

In particular, in two cases we have been able to use couples of images (short- and long-exposure ones), making it possible to compare the results.

Preliminary results: As can be seen in Table 1, the size of the Dimorphos shadowed hemisphere is comparable between all the long-exposure images processed and it can be considered compliant to what found by DART [2].

Timestamp	Exposure Time [s]	Hemisphere area [m^2]	Shadowed [Y/N]
1664234241	0.035	5325	Y
1664234241	0.0007	3133	N
1664234242	0.05	5156	Y
1664234242	0.0003	2150	N
1664234244	0.035	5316	Y
1664234244	0.0007	2165	N

Table 1: Size of the hemisphere as computed with the CV algorithm

On the contrary, the illuminated hemisphere detected by this algorithm shows a size smaller than the shadowed one and not in line to what expected by taking into account DART measurements.

However, by looking at the short-exposure images, a dark annulus can be seen dividing the illuminated hemisphere and the plume. It is likely that, by adding at least a portion of this annulus to the size of the illuminated hemisphere, its size will become compliant to what expected.

Conclusions and future works: Therefore we hypothesize that not all the illuminated hemisphere is really visible in the short-exposure images, as part of it is located in the shadow of the plume.

In the future we plan to improve our automatic Computer Vision algorithm, coupling it with simulated images and to process other image series, so that more robust results could be accomplished, in ordet to better determine the shape of Dimorphos and thus helping reaching all the scientific objectives of the DART-LICIACube mission.

References: [1] Dotto E. et al. (2023) *Nature, In preparation*. [2] Daly T. et al. (2023) *Nature, Submitted*.

BOUNCING BOULDERS: A "SECONDARY PLUME" FROM DIDYMOS SURFACE OBSERVED BY LICIACUBE LUKE CAMERA AFTER DART IMPACT ON DIMORPHOS' SURFACE

E. Mazzotta Epifani[1], M. Dall'Ora[2], E. Dotto[1], V. Della Corte[3], S. Ieva[1], G. Cremonese[4], A. Lucchetti[4], M. Pajola[4], G. Poggiali[5,6], J.R. Brucato[5], A. Rossi[7], P. Palumbo[8,3], D. Perna[1], I. Bertini[8], J.D.P. Deshapriya[1], P.H.A. Hasselmann[1], S. Caporali[5], F. Tusberti[4], S.L.Ivanovski[9], M. Zannoni[10], D. Modenini[10], I. Gai[10], P. Tortora[10], M. Lavagna[11], A. Capannolo[11], G. Zanotti[11], M. Ceresoli[11], E. Gramigna[10], M. Lombardo[10], R. Lasagni Manghi[10], L. Gomez Casajus[10], M. Amoroso[11], S. Pirrotta[11], G. Impresario[11], A. Zinzi[11]

[1]INAF-Osservatorio Astronomico di Roma, Via Frascati 33, 00040 Monte Porzio Catone (Roma), Italy, elena.mazzottaepifani@inaf.it; [2]INAF-Osservatorio Astronomico di Capodimonte, Napoli, Italy; [3]INAF-Istituto di Astrofisic e Planetologia Spaziali, Roma, Italy; [4]INAF-Osservatorio Astronomico di Padova, Italy; [5]INAF-Osservatorio Astrofisico di Arcetri, Firenze, Italy; [6]ALESIA-Observatoire de Paris, PSL, Paris, France; [7]AIFAC-CNR, Sesto Fiorentino (Firenze), Italy; [8]Università degli Studi di Napoli "Parthenope", DIST, Napoli, Italy; [9]INAF-Osservatorio Astronomico di Trieste; [10]Università di Bologna, Bologna, Italy; [11]Politecnico di Milano, Milano, Italy; [11]ASI-Agenzia Spaziale Italiana, Roma, Italy

Introduction: On 26 September 2022, at 23:14 UT, the first demonstration test in real (space) scale of the "kinetic impactor" technique to deal with the "asteroid hazard mitigation" issue took place.

The NASA DART (Double Asteroid Redirection Test) [1] spacecraft impacted the asteroid Dimorphos, the smallest member of the binary system (65803) Didymos, and modified its orbital period around the primary member by ~ 30 minutes [2]. Hosted as piggyback on DART during the 10-months travel in space, the small Italian satellite LICIACube [3] was released 15 days before the impact and, few minutes after it, fly-byed the impacted asteroid at 57.8 km from its surface, to take images of the impact effects.

The primary instrument LEIA (LICIACube Explorer Imaging of Asteroid) and the color camera LUKE (LICIACube Unite Key Explorer) onboard the cubesat obtained more than 400 images of the two bodies in the binary system and of the huge and spectacular debris plume lifted up from Dimorphos' surface by the impact itself. In particular, LUKE camera, equipped with a RGB Bayer pattern filter to acquire simultaneously color data, allowed a deep analysis (dynamic, structure, colors) of what could be called the "primary plume" (see abstracts by G. Poggiali, A. Rossi).

Methods: LUKE images were obtained with a wide range of exposure time, from tenths of ms to tenths of s. "Triplets" of images (very short, medium, long exposure time) were obtained for each position of LICIACube along its fly-by trajectory, in order to ensure a high dynamics of the signal, from the very faint debris plume to the highly illuminated surfaces of the two larger bodies.

The object of the analysis presented in this work is a subset of the whole LUKE images obtained before and after the LICIACube flyby, in the timeframe [23:16:44 – 23:18:27 UT] around the closest approach (CA, occurred at 23:17:11.5 UT), obtained with very short exposure time (≤ 0.7 ms).

Each single image was "decomposed" in three frames, one for each of the R, G, and B Bayer pattern filter, and the resulting monochromatic images were injected in a "debayerising" pipeline specifically designed for LUKE images, in order to correctly reconstruct a full color image from the incomplete color samples output through interpolation (color reconstruction).

Thanks to in-flight calibration with well-known stars coupled with RGB performances investigated on-ground, each color image was then photometrically calibrated. This allowed to obtain pixel fluxes in physical quantities.

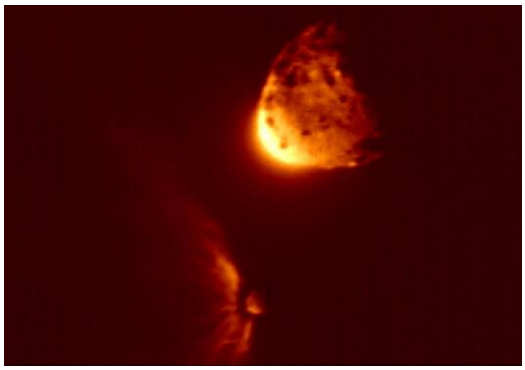

Figure 1 – Calibrated LUKE image in the R plane of the binary system (Didymos, Dimorphos and the impact plume) obtained 174 sec after DART impact, 3 sec after LICIACube CA, with LICIACube at 97 km from Dimorphos' surface.

Results: The visual inspection of the image subsample described above lead to the discovery of a fea-

ture (somehow unexpected in this extent) close to the surface of the main body Didymos. In these images, where the asteroid's surface appears not saturated, a bright feature compatible with a plume expanding from the Didymos' surface itself is clearly visible, as shown in Figure 1.

This feature has been called "secondary plume", since it appears as being produced by a secondary impact on the main body occurred after the DART impact on the moonlet, likely due to a (large?) boulder or a debris stream that hit Didymos and lifted off surface material. The possibility of reimpact against the main component of the binary system was foreseen and studied in model simulating the evolution of the ejecta particles [4].

In the present work, we will describe the first preliminary results obtained with the analysis of the glare, which is present in all the color images even if with different extent and luminosity distribution, and appears to expand with time, anisotropically towards open space.

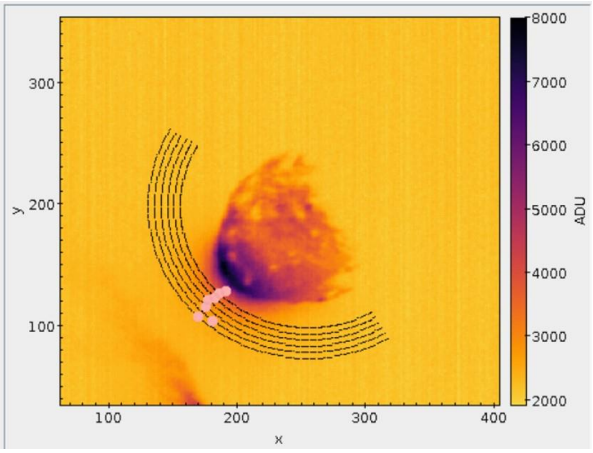

Figure 2 – Sketch of the partial, curved profiles (black continuous lines), superimposed to Didymos image, to be designed, extracted and analysed in the vicinity of the asperoid, for each of the images in which the secondary plume is detected.

Several issues have been assessed for the analysis:

Exclusion of possible instrumental effects. This issue has been tackled and excluded thanks to coupled investigation of LEIA and LUKE images, and of saturated and non-saturated LUKE images at different exposure time.

Geometrical reconstruction. As LICIACube moved along its trajectory towards the CA and beyond, the pointing geometry changed, since Dimorphos was continuously recognized as the target of the cubesat autonomous navigation. Therefore, multiple sets of images with similar observing geometry have been selected to investigate the actual behaviour of the secondary plume.

Profile extraction. A specific extraction tool has been designed and built in order to extract *partial, curved* profiles around Didymos (see Figure 2).

The preliminary results of the analysis will be discussed and presented.

References: [1] Rivkin A.S. et al. (2021) *PSJ*, 2, 24pp. [2] Thomas C.A. et al. (2022), *submitted to Nature* [3] Dotto E. et al. (2021), Planet. Space Sci. 199, 105185 [4] Rossi A. et al. (2022), Planet. Sci. J. 3, 118

Aknowledgements: This research was supported by the Italian Space Agency (ASI) within the LICIACube project (ASI-INAF agreement AC n.2019-31-HH.0)

AFTER DART: THE DIDYMOS SYSTEM IN THE AFTERMATH OF THE DART EVENT.

S. Ieva[1], E. Mazzotta Epifani[1], V. Petropoulou[1], J. D. P. Deshapriya[1], P. H. Hasselmann[1], D. Perna[1], M. Dall'Ora[2], G. Poggiali[3,4], J.R. Brucato[3], M. Pajola[5], A. Lucchetti[5], S. Ivanovski[6], A. Rossi[7], P. Palumbo[8,9], V. Della Corte[9], A. Zinzi[10,11], C. Thomas[12], J. de Leon[13,14], A.S. Rivkin[15], E. Dotto[1], M. Amoroso[10], I. Bertini[8,9], A. Capannolo[16], S. Caporali[3], M. Ceresoli[16], G. Cremonese[5], I. Gai[17], L. Gomez Casajus[17], E. Gramigna[17], G. Impresario[10], R. Lasagni Manghi[17], M. Lavagna[16], M. Lombardo[17], D. Modenini[17], S. Pirrotta[10], P. Tortora[17], F. Tusberti[5], M. Zannoni[17], G. Zanotti[16].

[1]INAF - Osservatorio Astronomico di Roma, Via Frascati 33, 00040 Monte Porzio Catone (Roma), Italy, +39-0694286431, simone.ieva@inaf.it, [2]INAF - Osservatorio Astrofisico di Capodimonte, Napoli, Italy, [3]INAF - Osservatorio Astrofisico di Arcetri, Firenze, I, [4]LESIA - Observatoire de Paris, Paris, F, [5]INAF - Osservatorio Astronomico di Padova, Padova, I, [6]INAF Osservatorio Astronomico di Trieste, Trieste, I, [7]CNR Istituto di Fisica Applicata "Nello Carrara", Sesto Fiorentino (Fi), I, [8]Università degli Studi di Napoli "Parthenope", Napoli, I, [9]INAF - Istituto di Astrofisica e Planetologia Spaziali, Roma, I, [10]Agenzia Spaziale Italiana, Rome, I, [11]Space Science Data Center - ASI, Rome, I, [12]Northern Arizona University, Flagstaff, USA, [13]Instituto de Astrofisica de Canaria, Santa Cruz de Tenerife, E, [14]Universidad de La Laguna, La Laguna, E, [15]JHU-APL, Laurel, USA, [16]Politecnico di Milano, Milano, I, [17]Università di Bologna, Bologna, I.

Introduction: Near-Earth objects (NEOs), due to their proximity to our planet, represent one of the most accessible bodies in the whole Solar System. Their investigation, other than providing vital information to planetary formation and water delivery, is compelling due to the hazard these bodies pose to human civilization.

The DART/LICIACube mission: To this purpose, the NASA Double Asteroid Redirection Test (DART) has been approved to be the first demonstration of kinetic impactor as an asteroid hazard mitigation [1]. The DART spacecraft successfully crashed onto the secondary member of the Didymos system (Dimorphos) on September 26th 2022 at 23:14 UTC. Hosted as a piggyback and released fifteen days before the DART impact there was also the Light Italian Cubesat for Imaging of Asteroids (LICIACube, 2), a 6U cubesat space mission financed by the Italian Space Agency (ASI). LICIACube with its two scientific cameras (LUKE & LEIA) has testified the impact and characterized the system and the ejecta plume in the aftermath of DART event with an incredible level of detail. In addition, the ESA Hera mission, to be launched in 2024, will continue the characterization of the binary system.

New NIR spectra for Didymos: Taking advantage of the unprecedented brightness of Didymos near the DART collision and close approach in 2022 (Vmag=14.7) we decided to characterize the system with spectroscopic ground-based observations at different rotational phases, in analogy to what we performed in the visible in 2021 [3]. New data were particularly needed in the near-infrared, where the only spectrum available in literature showed an unusual shallower spectrum compared to a typical silicate asteroid [4]. In the framework of a large worldwide campaign of characterization we obtained a series of NIR spectra from Telescopio Nazionale Galileo (TNG) with NICS, and a series of complete UVNIR spectra taken at VLT, with X-Shooter.

Remote characterization of the system is crucial to assess the heterogeneity of the surface composition, waiting for the Hera arrival in 2027. We will present these new data, the first obtained almost twenty years after the last one retrieved by [4], and compared with what scarcely is known from literature data. We will compare spectra taken before and after the impact in search of potential changes induced by the DART event, and also look for long-term variability. Finally, we will put ground-based observations in the context of laboratory measurements, providing comparison with meteorites and analogue minerals and connections with color-data acquired by the LICIACube cameras.

Acknowledgments: This research was supported by the Italian Space Agency (ASI) within the LICIACube project (ASI-INAF agreement AC n. 2019-31-HH.0).

References: [1] Rivkin, A.S. et al. (2021) PSJ, 2, 24 [2] Dotto, E. et al. PSS, 199, 105185 [3] Ieva, S. et al (2022) PSJ, 3, 183. [4] De Leon, J. et al. (2006) AdSpR, 37, 178.

A FIRST ASSESSMENT ON THE ORIGIN OF DIDYMOS AND DIMORPHOS, NASA's DART MISSION TARGETS.

F. Ferrari[1], H. F. Agrusa[2,3], Y. Zhang[2], O. S. Barnouin[4], R. T. Daly[4], A. F. Cheng[4], C. M. Ernst[4], M. Hirabayashi[5], S. A. Jacobson[6], M. Jutzi[7], A. Lucchetti[8], P. Michel[3], N. Murdoch[9], R. Nakano[5], M. Pajola[8], E. E. Palmer[10], S. D. Raducan[7], D. C. Richardson[2], C. Robin[9], S. Soldini[11], F. Tusberti[8], R.-L. Ballouz[4], B. W. Barbee[12], A. Campo Bagatin[13], I. Gkolias[14], J. Lyzhoft[12], J. McMahon[15], A. J. Meyer[15], P. Sánchez[15], D. J. Scheeres[15], P. Tanga[3], K. Tsiganis[14], S. Ivanovski[16], S. R. Schwartz[10], A. S. Rivkin[4], N. L. Chabot[4] and the DART Investigation Team.

[1]*Department of Aerospace Science and Technology, Politecnico di Milano, Italy.* [2]*University of Maryland, College Park, MD, USA.* [3]*Université Côte d'Azur, Observatoire de la Côte d'Azur, CNRS, Nice, France.* [4]*Johns Hopkins University Applied Physics Laboratory, USA.* [5]*Auburn University, Auburn, AL, USA.* [6]*Michigan State University, East Lansing, MI, USA.* [7]*Space Research and Planetary Sciences, University of Bern, Switzerland.* [8]*INAF-Osservatorio Astronomico di Padova, Italy.* [9]*Institut Supérieur de l'Aéronautique et de l'Espace (ISAE-SUPAERO), Université de Toulouse, Toulouse, France.* [10]*Planetary Science Institute, Tucson, AZ, USA.* [11]*University of Liverpool, UK.* [12]*NASA/Goddard Space Flight Center.* [13]*IUFACyT-DFISTS, Universidad de Alicante, Spain.* [14]*Aristotle University of Thessaloniki, Greece.* [15]*University of Colorado Boulder, CO, USA.* [16]*INAF - Osservatorio Astronomico di Trieste.*

Introduction: On September 26th, 2022, NASA's Double Asteroid Redirection Test (DART) performed the first full-scale demonstration of kinetic impact for planetary defense purposes, by impacting at high speed the asteroid Dimorphos, the secondary component of (65803) Didymos binary system. Before impact, DART provided exceptional close-up images of both Didymos and Dimorphos, revealing that both asteroids have oblate shapes and rocky surfaces [1].

We perform here a first assessment of formation and evolutionary paths that may have led to the observed, pre-impact state of the Didymos system. We account for asteroids' internal structures that are consistent with their observed asteroid shapes and the geomorphological features appearing on their surfaces. Key parameters to this analysis are the bulk densities of the two asteroids, which have a high uncertainty and currently estimated in the range 2100–2700 kg/m^3 (one sigma) [1], and their spin rate, which is directly constrained for the Didymos primary only (2.260 h) [2], and has not been measured for Dimorphos, for which is typically assumed to equal its orbit period (11.92 h).

Methodology: We use N-body discrete-element codes to reproduce the dynamical evolution of Didymos and Dimorphos, which are modelled as loosely consolidated self-gravitating (rubble-pile) aggregates [3]. We investigate evolutionary processes that may have led to the formation of Dimorphos, such as major fission events, mass shedding or transport within the binary system, and their possible causes, such as slow reshaping due to YORP-driven spin change, or abrupt reshaping due to meteoritic impacts [4,5,6].

Preliminary results: Results based on preliminary models suggest that both Didymos and Dimorphos may have a rubble-pile inner structure, as this appears consistent with both dynamical simulations and preliminary geological assessments of their surfaces.

In particular, a rubble-pile Didymos is structurally stable when assuming a bulk density of 2700 kg/m^3 (the higher-end of pre-impact density estimates), or for a smaller density, in the presence of some structural coherence in the inner part of the asteroid [7,8]. Such coherence might be provided by grain interlocking and/or a small cohesion level (few Pa) between rubble-pile constituents, or by a small (30–50% volume) inner rigid core. Also, numerical simulations show that reshaping processes on Didymos imply mass movements from mid-latitudes to the equator, where particles would be only tenuously bound to Didymos [9]. This appears consistent with the equatorial region of Didymos, which, compared to the mid-latitude region, appears smoother and less boulder-rich, suggesting materials might have been shed from the equator due to Didymos's high spin rate [10].

Under the assumption of tidally locked behavior, Dimorphos has a sensibly lower spin rate compared to Didymos, and this makes Dimorphos's shape stable at any density value within the estimated one-sigma uncertainty range. From a dynamical perspective, Dimorphos's shape would be stable even with a fully-fragmented interior and in the absence of cohesion/interlocking. A major source of dynamical perturbation is provided by the presence of Didymos, which makes Dimorphos's shape unstable at distances smaller than 900–1000 m (depending on the bulk density, and in absence of internal strength). A preliminary assessment shows that Dimorphos would disrupt under Didymos-induced tides at distances closer than 500–600 m, and would have a more elongated shape in the range 600–900 m. The ESA Hera mission will provide

detailed measurements of key properties, including internal ones, during its rendezvous with Didymos through close proximity operations of the spacecraft and its two Cubesats Milani and Juventas in 2027, allowing us to check our predictions [11]..

References: [1] Daly et al., 2022 (submitted). [2] Thomas et al., 2022 (submitted). [3] Agrusa et al., 2022, PSJ. [4] Richardson et al., 2022, PSJ. [5] Nakano et al., 2022, PSJ. [6] Hirabayashi et al., 2022, PSJ. [7] Ferrari & Tanga 2022, Icarus. [8] Hirabayashi et al, 2015, ApJ. [9] Sánchez, Scheeres, 2018, Icarus. [10] Tardivel et al, 2018, Icarus. [11] Michel et al., 2022, PSJ.

The boulder size-frequency distribution derived from DART/DRACO images of Dimorphos: Preliminary results

M. Pajola[1], F. Tusberti[1], A. Lucchetti[1], O. Barnouin[2], C.M. Ernst[2], E. Dotto[3], R.T. Daly[2], G. Poggiali[4,5], M. Hirabayashi[6], E. Mazzotta Epifani[3], N. L. Chabot[2], V. Della Corte[7], H. Agrusa[8,22], R.-L. Ballouz[2], N. Murdoch[9], C. Robin[9], A. Rossi[10], S.R. Schwartz[11], S. Ieva[3], S. Ivanovski[12], A. Campo-Bagatin[13], L. Parro[13,18], P. Benavidez[13], J.B. Vincent[14], F. Ferrari[15], G. Tancredi[16], J.M. Trigo-Rodriguez[17], J. Sunshine[8], T. Farnham[8], E. Asphaug[18], A. Rivkin[2], J.D.P. Deshapriya[3], P.H.A. Hasselmann[3], J.R. Brucato[3], A. Zinzi[19,20], M. Amoroso[19], S. Pirrotta[19], G. Impresario[19], S. Cambioni[21], P. Michel[22], A. Cheng[2], I. Bertini[23], A. Capannolo[9], S. Caporali[3], M. Ceresoli[15], B. Cotugno[24], G. Cremonese[1], M. Dall'Ora[25], V. Di Tana[24], I. Gai[26], M. Lavagna[15], F. Miglioretti[24], D. Modenini[26], P. Palumbo[23], D. Perna[3], S. Simonetti[24], P. Tortora[26], M. Zannoni[26], G. Zanotti[15].

[1]INAF-Astronomical Observatory of Padova, Vic. Osservatorio 5, 35122 Padova, Italy (maurizio.pajola@inaf.it); [2]Johns Hopkins University Applied Physics Laboratory, Laurel, MD-USA; [3]INAF-Osservatorio Astronomico di Roma, Monte Porzio Catone, Roma, Italy; [4]INAF-Osservatorio Astrofisico di Arcetri, Firenze, Italy; [5]LESIA-Observatorie de Paris PSL, Paris, France; [6]Auburn University, AL-USA; [7]INAF-Istituto di Astrofisica e Planetologia Spaziali, Roma, Italy; [8]University of Maryland, Department of Astronomy, MD-USA; [9]Institut Supérieur de l'Aéronautique et de l'Espace (ISAE-SUPAERO), Université de Toulouse, France; [10]IFAC-CNR, Sesto Fiorentino, Firenze, Italy; [11]Planetary Science Institute; University of Arizona, AZ-USA; [12]INAF-Osservatorio Astronomico di Trieste, Trieste, Italy; [13]Universidad de Alicante, Spain; [14]DLR Berlin, Germany; [15]Politecnico di Milano - Bovisa Campus, Dipartimento di Scienze e Tecnologie Aerospaziali, Milano, Italy; [16]Dpto. Astronomia, Facultad Ciencias Igua 4225, Montevideo, Uruguay; [17]Institute of Space Sciences (ICE, CSIC) and Institut d'Estudis Espacials de Catalunya (IEEC), Spain; [18]University of Arizona, AZ-USA; [19]Agenzia Spaziale Italiana, Roma, Italy; [20]Space Science Data Center – ASI, Roma Italy; [21]Dept. of Earth, Atmospheric and Planetary Sciences, Massachussets Institute of Technology, Cambridge, MA-USA; [22]Université Côte d'Azur, Observatoire de la Côte d'Azur, CNRS, Laboratoire Lagrange, Nice, France; [23]Università degli Studi di Napoli "Parthenope", Dipartimento di Scienze & Tecnologie, Centro Direzionale, Napoli, Italy; [24]Argotec, Torino, Italy; [25]INAF-Osservatorio Astronomico di Capodimonte, Napoli, Italy; [26]Alma Mater Studiorum - Università di Bologna, Dipartimento di Ingegneria Industriale, Forlì, Italy; Alma Mater Studiorum - Università di Bologna, Centro Interdipartimentale di Ricerca Industriale Aerospaziale, Forlì, Italy.

Context: On 26 September 2022, the Double Asteroid Redirection Test (DART) spacecraft impacted the surface of Dimorphos, the ~150 m size satellite of the near-Earth binary asteroid (NEA) (65803) Didymos (~780 m-size, [1]). Numerical models of asteroid disruption, the analyses of asteroids' shapes, and in situ observations, support the interpretation that small asteroids (0.2-10 km size range) are reaccumulated remnants from disrupted parent bodies, also called rubble-piles (e.g. [2, 3]). Surface boulders, therefore, represent directly the fragments of those parent-body disruptions followed by some evolutionary process such as cratering and thermal breakdown, followed by the size-sorting and migration of granular materials when an asteroid's regolith is mobilized. Hence, the observed size-frequency distribution (SFD) of boulders on the surface of a NEA and the corresponding fitting indices is a powerful tool for understanding the initial formation of boulders and their subsequent evolution. The boulder SFD is also important in understanding the conditions of the surface for any kinetic deflection experiment such as DART.

Dataset: During the last minutes of the DART mission, the DRACO scientific camera [4] imaged the surface of Dimorphos at increasingly fine spatial scales, ranging from few meters to a maximum resolution of 5.5 cm. In order to identify and manually count all boulders located in the illuminated surface of the asteroid, we decided to use two DRACO images with a phase angle of 59.4°, taken from target distances of 52.56 km and 40.73 km. The resulting illuminated surface has a spatial scale of 0.26 m and 0.20 m, hence all features larger than 0.6-0.8 m in size can be identified (Fig. 1).

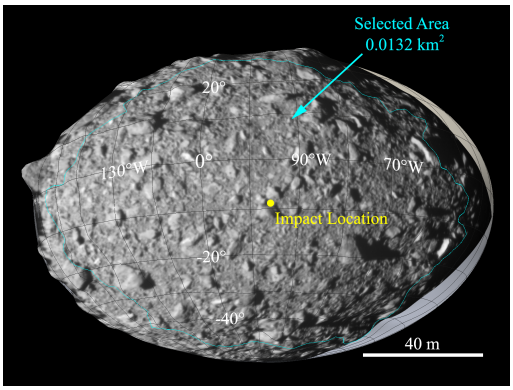

Figure 1. The DRACO images projected onto the Dimorphos shape model. The study area is within the light-blue polygon. The DART impact location is indicated with a yellow dot.

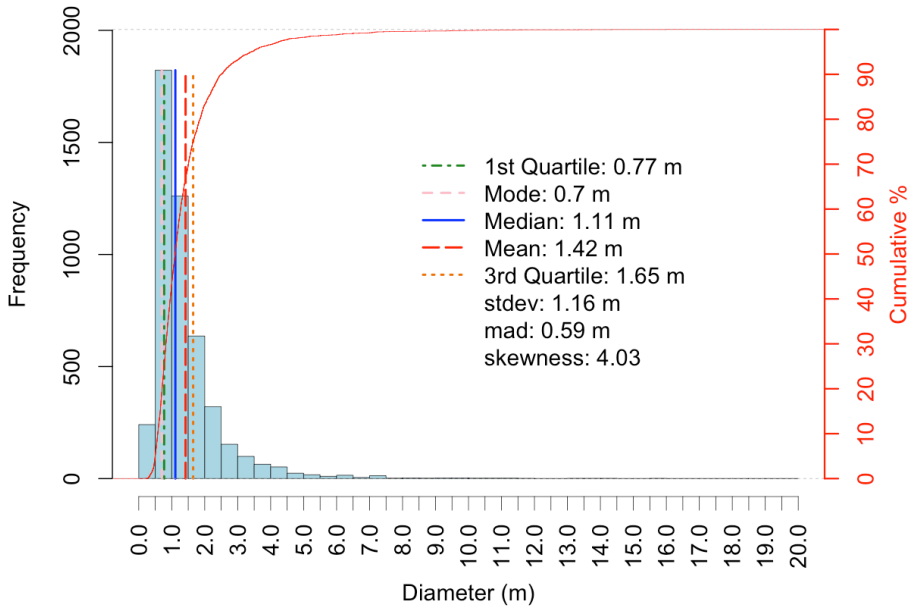

Figure 2. Frequency histogram of the Dimorphos identified boulders.

By using the Small Body Mapping Tool (SBMT, [5]) we directly projected the DRACO images onto the Dimorphos shape model [6] and then counted boulders as ellipses from an area that is 0.0132 km^2 wide (this area is the largest one identifiable where distorted features are not present, Fig. 1). The value of an ellipse's major axis is then used as the maximum size of the boulder. The total number of boulders identified is 4757, with a maximum size of 16 m. The frequency histogram of the counts is in Fig. 2.

SFD fitting curves: To evaluate whether or not the resulting SFD is fitted by a power-law or not we made use of the Clauset et al. [7] method to validate the existence of the power-law fitting model. This method allows the identification of the completeness limit, x_{min}, which is the threshold value above which the power-law exists. The estimation of x_{min} is done through the Kolmogorov-Smirnoff (KS) statistic and allows to find the value minimizing it. Afterwards, the power-law index (α) of the fitting curve is determined through the maximum likelihood estimator (MLE). The uncertainty for both α and x_{min} is then derived through a non-parametric bootstrap procedure that generates a large number of synthetic datasets from a power-law random generator and performs a number of KS tests to verify if the generated and observed data come from the same distribution. This technique returns a p-value that can be used to quantify the plausibility of the hypothesis.

The above methodology applied on our data return an α value of -2.45 $\pm$ 0.2 and an x_{min} of 2.0 $\pm$ 0.5 m. Nevertheless, considering the significance level of 0.10, our preliminary p-value of 0.06 (computed from 2500 KS statistic tests) suggests that the Dimorphos boulder SFD does not come from a power law distribution, but instead, from a different one.

Due to the 0.20-m spatial scale of the images used, all boulders larger than 0.60 m, i.e., 3 pixels, can be positively identified. To be conservative, we then decided to use a lower limit of 1.0 m to compute the exponential-law and Weibull parameters.

Through this preliminary work, we have identified that the Weibull fitting curve better represents the boulder SFD on Dimorphos in the 1.0-16.0 m size range. While a power-law SFD would indicate a single-event fragmentation (for example during impact cratering) that leads to a branching tree of cracks that have a fractal character [8, 9], the Weibull distribution is thought to result from sequential fragmentation [10] and is often used to describe the particle distribution resulting from grinding experiments [11]. This suggests that the boulders SFD on Dimorphos might have originated from impacts, but it was later modified by other processes that are still being debated and that will be presented at the time of the conference.

Acknowledgments: This research was supported by the Italian Space Agency (ASI) within the LICIACube project (ASI-INAF agreement AC n. 2019-31-HH.0) and the DART mission, NASA Contract No. NNN06AA01C to JHU/APL. This project has received funding from the European Union's Horizon 2020 research and innovation programme under grant agreement No 870377 (project NEO-MAPP) and CNES.

References: [1] Rivkin, A.S., et al. 2021. PSJ, 2, 173. [2] Watanabe, S., et al. 2019. Science, 364, 268. [3] Lauretta, D.S., et al. 2019. Nature, 568, 55. [4] Fletcher, Z. J., et al. 2018. SPIE 10698. [5] Ernst, C.M. et al. (2018), *LPSC #49, 2018, ab. 2083.* [6] Daly, R.T., et al. (2022), PSJ, 3:207. [7] Clauset, A., et al., (2009) SIAM Rev. 2009, 51, 661–703. [8] Turcotte, D.L., 1997. Cambridge University Press. [9] Pajola, M., et al. (2022), Icarus, 375, 114850. [10] Brown, W.K., Wohletz, K.H. (1995). J. Appl. Phys. 78, 2758. [11] Rosin, P., Rammler, E. (1933). J. Inst. Fuel 7, 29.

ON THE SYNERGY BETWEEN PLANETARY SCIENCE AND SPACE ENGINEERING IN THE STUDY AND EXPLOITATION OF NATURAL ROUTES. E. M. Alessi[1], [1]Istituto di Matematica Applicata e Tecnologie Informatiche "E. Magenes", Consiglio Nazionale delle Ricerche, via Alfonso Corti 12, 20133 Milano, Italy, em.alessi@mi.imati.cnr.it

Introduction: Giorgio Parisi, one of the recipients of the 2021 Nobel Prize in Physics, in his lectio magistralis at the University of Rome, remarked that "science is an enormous puzzle and each piece that is put in the right place opens the possibility to put others".

This statement fits perfectly with the field of orbital dynamics, where the understanding of the behavior of natural objects and the development of advanced concepts in mission design cannot stand one without the other. I like to see the interaction between planetary science and space engineering as a synergy, not only for the conceivement and development of ambitous missions, but especially because we can aim at following at low cost the routes that natural bodies indicate and, on the other hand, advanced trajectory design and related studies can shed light on the fundamental mechanisms that drive natural bodies.

In this talk, I will show three illustrative cases of this synergy, in particular of cases not yet fully exploited.

Deorbiting corridors: The first example belongs to the field of space debris, in particular, to the mitigation strategies that can be adopted at the end of life of a satellite orbiting the Earth. Recent works, e.g., [1], have proved the existence of natural highways, that can bring the spacecraft back to the Earth. For the LEO region, the main responsible is the solar radiation pressure coupled with the oblateness of the Earth [2]. For the MEO region, the lunisolar perturbations can trigger a similar natural eccentricity growth, e.g., [3]. In both cases, orbital resonances concerning the orientation of the satellite towards Sun or Moon are key to "destabilize " the orbit and achieve reentry, similar to what happens in the Main Asteroids Belt.

Co-orbital dynamics: The second example is the co-orbital motion, that is a particular type of dynamics that occurs in the Three-Body Problem, such that two bodies (e.g., an asteroid and a planet) orbit the same main body (e.g., Sun) in the same period (1:1 mean motion resonance), e.g., [4].

Many objects susceptible to be at least temporary co-orbitals have been observed in the solar system, e.g., [5], [6], [7], [8]. In the prograde case, the three fundamental configurations are tadpole motion, horseshoe trajectories and quasi-satellite orbits.

This kind of trajectories, their possible mutual transitions together with escaping/trapping mechanisms are not only evident in the natural dynamics observed in the solar system, but also they have assumed an important role for space exploration missions (e.g., to monitor the solar activity, or to visiting the near-Earth asteroid Kamo'oalewa).

Temporary capture: The last example is the temporary capture, that is a special configuration in the Restricted Three-Body Problem, that can allow to orbit temporary a given target (e.g., a moon) without being inserted around it with a proper maneuver. Given the benefits in terms of propellant, this kind of design is being considered more and more for actual missions, e.g., [9], [10], but an analytical explanation has not been unveiled yet. Recently, small asteroids of the order of few meters have been discovered to orbit the Earth for a few months in the same way, but their number is still too low compared to statistical numerical studies that foresee their existence [11].

References:

[1] Rossi A. et al. (2018) *Aerospace*, 5, 64. [2] Alessi E. M. (2018) *Mon. Not. R. Astron. Soc., 473*, 2407-2414. [3] Daquin J. et al. (2022) *Celestial Mech. Dyn. Astron., 134,* 6. [4] Pousse A. and Alessi E. M. (2022) *Nonlinear Dynamics*, 108, 959-985. [5] Mikkola S. et al. (2004) *Mon. Not. R. Astron. Soc., 351*, L63-L65. [6] Brasser R. et al. (2004) *Icarus, 171,* 102-109. [7] Wajer P. (2020) *Icarus, 209,* 488-493. [8] Di Ruzza S. et al. (2023) *Icarus, 390,* 115330. [9] Dei Tos D. A. et al. (2018) *JGCD, 41,* 1227-1242. [10] Benkhoff J. et al. (2021) *Space Science Reviews, 217*, 90. [11] Jedicke R. et al. (2018) *Front. Astron. Space Sci.*, 5:13.

THE LICIACUBE EXTENDED MISSION AS AN IMMINENT IMPACTOR SENTINEL. M. Ceccaroni[1] and E. Perozzi[2], [1]Cranfield University, UK, m.ceccaroni@cranfield.ac.uk, [2]ASI- Agenzia Spaziale Italiana, ettore.perozzi@asi.it.

Introduction: On 27 Novembre 2022, LICIAcube (Light Italian Cubesat fort Imaging Asteroids) has successfully carried out its primary mission by imaging the plume generated by the impact of the US DART spacecraft on asteroid Dimorphos. After the flyby, a 6-month mission extension was envisaged and possible scenarios were therefore proposed.

LICIAcube and DRO: The post-encounter orbital path of the Cubesat is here shown to be remarkably close to a DRO (Distant Retrograde Orbit) configuration, an orbit well known to have potential Planetary Defence applications in detecting NEOs coming nearly from the direction of the Sun [1].

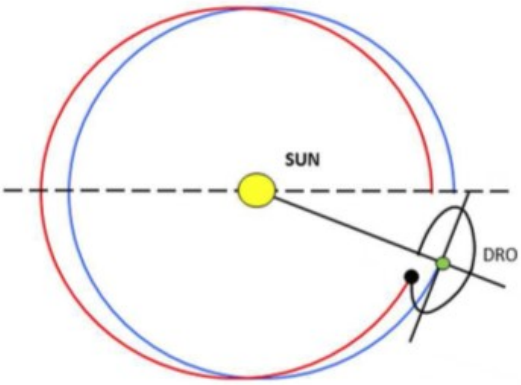

Fig. 1 - An Earth DRO results from the motion of a body with negligible mass in an heliocentric orbit having the same semimajor axis as the Earth and a higher eccentricity. When properly phased, the former appears to move in a retrograde orbit around the Earth.

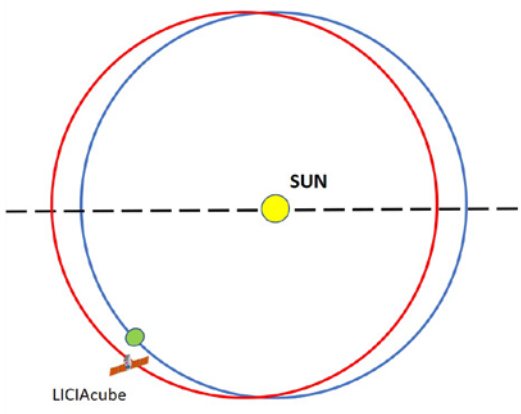

Fig. 2 - The positions and the osculating orbits of the Earth and of LICIAcube at the DART impact epoch.

A spacecraft placed in a DRO and pointing in the anti-solar direction could be observing at favorable phase angles when transiting the trajectory branch between the orbit of the Earth and the Sun. This could be extremely helpful in detecting the so-called "imminent impactors" (objects in the 10-40 m range in route of collision with the Earth that are likely to represent, in the short run, the most probable asteroid threat) ensuring a significant warning time [2]. Because of the small size and unfavorable geometry their observation is challenging and needs to be specifically addressed both, from the ground (e.g. ESA Flyeye telescope) and from space (e.g. NASA NEO Surveyor). By comparing the plots of Fig. 1 and Fig. 2 it is appears that the dynamical configuration of the Earth and LICIAcube at the time of the DART impact epoch could lead to DRO-like configurations.

Mission design: Further analysis has shown that without any manoeuvring LICIAcube would travel the inner branch of a DRO-like trajectory having an altitude of about 0.06au, which has been indicated in [2] as the best compromise between accessibility and warning time. The possibility of using LICIAcube as a precursor for an in-flight test of the feasibility and the performances of a DRO imminent impactor sentinel turned out to be appealing.

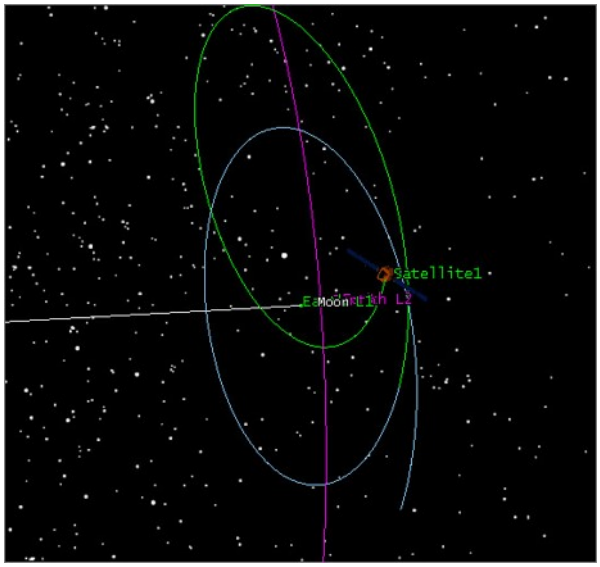

Fig. 3 - The LICIAcube (Satellite 1) trajectory in an Earth rotating frame (Sun is on the left side); every loop lasts one year, thus travelling the inner branch satisfies the 6-month mission extension requirement.

A preliminary mission analysis, taking into account onboard propulsion, imaging and telecommunication systems, has been therefore carried out, showimg promising results. Although LICIAcube lost contact a few weeks after the DART impact, the advantages and drawbacks of the proposed mission extension can be discussed in the wider context of the near-future low-cost Cubesat access to interplanetary space.

References:

[1] Perozzi E., Ceccaroni M., Valsecchi G.B., Rossi A., (2017). Distant retrograde orbits and the asteroid hazard, *European Physical Journal Plus, 132 (8) Article No. 367.*

[2] Martinez Mata A., Perozzi E., Ceccaroni M., (2022). Addressing the imminent impactors threat from distant retrograde orbits (DRO). *IAC-22-D9.2.8,*

THE NEOROCKS "RAPID-RESPONSE EXPERIMENT".

Davide Perna[1], Ettore Perozzi[2], Anabel Mediavilla[3], Fabrizio Bernardi[4], Elisabetta Dotto[1], Mirel Birlan[5], Julia de Léon[6], Marcel Popescu[7], Tetiana Hromakina[8], Simone Ieva[1], Monica Lazzarin[9], Alessandro Nastasi[10], Vasiliki Petropoulou[1], Petr Pravec[11], Claudiu Teodorescu[12], Marek Banaszkiewicz[13], Sara Banchi[14], Maria Antonietta Barucci[8], Benoit Carry[15], Alberto Cellino[16], Elena Mazzotta Epifani[1], Jaime Nomen Torres[17], Colin Snodgrass[18], and the NEOROCKS team*

[1]INAF-Osservatorio Astronomico di Roma, , Via Frascati 33, 00040 Monte Porzio Catone (Roma), Italy, +39-0694286431, davide.perna@inaf.it, [2]ASI-Agenzia Spaziale Italiana, I, [3]DEIMOS Space, S, [4]Space Dynamics Services s.r.l., I, [5]IMCCE – Observatoire de Paris, F, [6]Instituto de Astrofisica de Canarias, S, [7]Astronomical Institute of the Romanian Academy, RO [8]LESIA – Observatoire de Paris, F, [9]Università di Padova, I, [10]Gal Hassin Center, Isnello (PA), I, [11]Astronomicky Ustav AV CR, CZ, [12]DEIMOS Space s.r.l., RO, [13]NEOSPACE sp. z o.o., PL, [14]Resolvo s.r.l., I, [15]Observatoire de la Côte d'Azur, F, [16]INAF – Osservatorio Astrofisico di Torino, I, [17]DEIMOS Castilla La Mancha sl, S, [18]University of Edinburgh, UK

Context: The "NEO Rapid Observation, Characterization and Key Simulations" (NEOROCKS) project is funded by the EU H2020 programme with the aim to improve our knowledge on the characterization of the Near Earth Object (NEO) population. The project connects expertise in performing observations of solar system small bodies and the related modeling needed to derive their dynamical and physical properties, to the pragmatic planetary defense approach. A specific challenge for NEOROCKS is to keep the physical characterization up with the increasing NEO discoveries dominated by small-size objects, yet capable of producing damage in case of impact. Among them are the so-called "imminent impactors" characterized by short warning times before impact.

Outline: One of the ambitions of NEOROCKS is the organization of a "rapid response experiment", in order to put to test our ability to face the imminent impactor threat by resorting to existing assets. This implies to be able to react promptly when a potential object of this kind appears on the MPC NEO Confirmation Page, tasking astrometric follow-up for improving orbit determination and triggering the Consortium telescope network for physical characterization. Particular care has been taken to reduce as much as possible human intervention by resorting to remote telescope tasking procedures and fast data dissemination techniques.

In Spring 2022 the "detect-and-characterize" chain described above has been successfully implemented thanks to the experience of the NEOROCKS Consortium Partners in NEO and Space Debris monitoring as well as in accessing upon short notice large-aperture telescopes equipped with state-of-the-art instrumentation. In particular, we obtained light-curve and spectrophotometric data of several imminent impactor candidates using the 3.6-m INAF-TNG (Telescopio Nazionale Galileo, Canary Islands) and other facilities, thus demonstrating the feasibility of our approach. The details and results of such experiment will be presented and discussed in the wider context of the actions needed to set-up an operational rapid response system for civil protection purposes.

Acknowledgements: This project has received funding from the European Union's Horizon 2020 research and innovation programme under grant agreement No 870403 (project NEOROCKS).

** The NEOROCKS Team is composed also by:*
S. Anghel, A. Bertolucci, F. Calderini, F. Colas, A. Del Vigna, A. Dell'Oro, A. Di Cecco, L. Dimare, I. Di Pietro, P. Fatka, S. Fornasier, E. Frattin, P. Frosini, M. Fulchignoni, R. Gabryszewski, M. Giardino, A. Giunta, J. Huntingford, J.P. Kotlarz, F. La Forgia, J. Licandro, H. Medeiros, F. Merlin, F. Pina, G. Polenta, A. Rozek, P. Scheirich, A. Sergeyev, A. Sonka, G.B. Valsecchi, P. Wajer, A. Zinzi.

NEOROCKS: INVESTIGATING THE PHYSICAL NATURE OF THE SMALL ASTEROID POPULATION.

V. Petropoulou[1], D. Perna[1], S.Ieva[1], E. Dotto[1], M. Banaszkiewicz [2], S. Banchi [3], M. A. Barucci [4], F. Bernardi [5], M. Birlan [6], B. Carry [7], A. Cellino [8], J. De Léon [9], M. Lazzarin [10], E. Mazzotta Epifani [1], A. Mediavilla Garay [11], J. Nomen Torres [12], E. Perozzi [13], P. Pravec [14], C. Snodgrass [15], C. Teodorescu [16], and the NEOROCKS team*, [1]INAF-OAR (via Frascati 33, Monte Porzio Catone 00078, IT, vasiliki.petropoulou@inaf.it); [2]NEOSPACE sp. z o.o., PL, [3]Resolvo s.r.l., I; [4]LESIA – Observatoire de Paris, F; [5]Space Dynamics Services s.r.l., I; [6]IMCCE – Observatoire de Paris, F; [7]Observatoire de la Côte d'Azur, F; [8]INAF – Osservatorio Astrofisico di Torino, I; [9]Instituto de Astrofisica de Canarias, S; [10]Università di Padova, I; [11]DEIMOS Space, S; [12]DEIMOS Castilla La Mancha sl, S; [13]ASI-Agenzia Spaziale Italiana, I; [14]Astronomicky Ustav AV CR, CZ; [15]University of Edinburgh, UK; [16]DEIMOS Space s.r.l., RO

Introduction: The "NEO Rapid Observation, Characterization and Key Simulations" (NEOROCKS) project has been financed since Jan. 2020 through the H2020 European Commission programme to improve knowledge on NEOs by connecting expertise in performing small body astronomical observations and the related modelling needed to derive their dynamical and physical properties, and profiting from international collaboration devoted to the asteroid hazard. A specific challenge for NEOROCKS is to keep the physical characterization up with the increasing NEO discoveries dominated by small-size objects.

In the framework of NEOROCKS we executed early-response (within a month of discovery) spectroscopic observations of newly-discovered small – meteres to hectometeres– NEOs in order to investigate the physical nature of this population. Our sample is composed by "high-priority" NEOs, identified due to small size and/or planetary protection considerations, which could be lost if not characterized with early-response observations, usually becoming too faint for characterization within 2-8 weeks from discovery, whereupon becoming unobservable for years or even decades.

The small NEOs population: The investigation of such small-sized NEOs is particularly important to constrain the asteroidal contribution to the delivery of prebiotic material (water and organics) to our planet [1]. More in general, the proximity of NEOs allows us to study asteroids about two to three orders of magnitude smaller than those observable in the main belt (i.e., down to metre-sized objects), hence to open new frontiers in asteroid science. Indeed, investigating the physical properties of small asteroids allows us to shed light on planetary accretion mechanisms that took place in the primordial solar system under the same low-gravity environments [2]. Recent results already suggested that small asteroids behave differently than the larger bodies in terms of regolith generation [3] and spectral properties [4,5].

Planetary defense: In terms of the current impact risk, the small objects deserve our particular attention, as they have the highest statistical likelihood of impact, and can still produce a catastrophe at a regional/national scale [6]. Moreover, to confirm or reject collision scenarios to a high confidence level with small asteroids (smaller than ∼300 m) it is crucial to reduce the uncertainty regarding their dynamical evolution on a timespan of decades/centuries. We can reduce this uncertainty by determining, with good confidence, physical properties such as surface composition and surface scattering properties, to constrain the object's response to the Yarkovsky effect due to radiative recoil of anisotropic thermal emission [7].

Spectroscopic survey: We acquired TNG-3.5m/ DOLORES low-resolution visible spectra of "high-priority" targets during three observing semesters, from spring 2021 to fall 2022 and our programme is currently ongoing at NOT-2.56m with ALFOSC and NOTCam programmed observations. Visible-range low-resolution asteroid spectra allow to properly identify a number of broad absorption features (e.g., at 0.5, 0.55, 0.60-0.65, 0.7, 0.8-0.9 μm) related to the presence of different types of anhydrous and/or hydrated minerals, hence carrying information on the asteroid composition (e.g., silicaceous, carbonaceous, metallic, etc.) and thermal history. Such highly diagnostic spectral signatures correspond to different well-determined taxonomic compositional classes [8]. Besides composition, low-resolution visible spectra are used to obtain a rough but yet reasonable estimation of further properties (e.g., compaction state, surface scattering properties, etc.) of the material making up the asteroids, mainly through the comparison with laboratory spectra of meteorite samples available in the literature.

NEOROCKS product: Physical characterization (i.e. taxonomic classification, matching with meteorites laboratory spectra etc) of a large sample of small-sized NEOs sheds light on the poorly known physical properties of this asteroid population and constitutes a fundamental input for an accurate planning of eventual impact risk mitigation measures. All our data finally flow into the NEOROCKS technical web portal, a unique dynamical and physical properties database which ensures an efficient data products

dissemination, short/long-term data storage and data availability.

References: [1] O'Brien et al. 2014, Icarus 239, 74. [2] Chambers 2016, ApJ 825, 63. [3] Delbo et al. 2014, Nature 508, 233. [4] Perna et al. 2018, P&SS 157, 82. [5] Devogèle et al. 2019, AJ 158, 196. [6] Perna et al. 2015, P&SS 118, 311. [7] Farnocchia et al. 2013, Icarus 224,1. [8] Bus and Binzel 2002, Icarus 158, 146.

Acknowledgement: This project has received funding from the European Union's Horizon 2020 research and innovation programme under grant agreement No 870403 (project NEOROCKS).

* The NEOROCKS Team is composed also by: S. Anghel, N. Ariani, A. Bertolucci, F. Colas, A. Del Vigna, A. Dell'Oro, A. Di Cecco, L. Dimare, I. Di Pietro, P. Fatka, S. Fornasier, E. Frattin, P. Frosini, M. Fulchignoni, R. Gabryszewski, M. Giardino, A. Giunta, T. Hromakina, J. Huntingford, S. Ieva, J.P. Kotlarz, F. La Forgia, J. Licandro, H. Medeiros, J.A. Gonzalez Abeytua, G. Polenta, M. Popescu, A. Rozek, P. Scheirich, A. Sergeyev, A. Sonka, G.B. Valsecchi, P. Wajer, A. Zinzi

ANALYSIS OF SPECTRAL VARIABILITY OF ASTEROID 3200 PHAEHTON IN PREPARATION TO DESTINY+ SPACE MISSION. M. Angrisani[1-2] , E. Palomba[1], G. Pratesi[3] , F. Dirri[1] , A. Longobardo[1] , L. Chelazzi[3], B. Cortigiani[3], C. Gisellu[1], T. Catelani[3], G. Massa[1]; [1]INAF-IAPS Rome, Via Fosso del Cavaliere ,100 Rome, [2] Sapienza Università di Roma, [3] Università degli studi di Firenze.

Introduction to DESTINY+ mission: 'DESTINY+' (Demonstration and Experiment of Space Technology for INterplanetary voYage, Phaethon fLyby and dUst Science) is a joint mission of technology demonstration and science observation, which was selected for JAXA/ISAS small-class space program. The spacecraft will be launched in 2024 and (3200) Phaethon asteroid will be the flyby target [1].

The science observation includes high-speed flyby imaging of Phaethon, and direct measurement of physical and chemical properties of dust particles in the interplanetary space, dust trail and nearby Phaethon. The flyby imaging is performed with a panchromatic telescopic camera (TCAP) with a tracking mirror and a VIS-NIR multiband camera (MCAP) with four bands (425, 550, 700, 850 nm) [2]. In-situ dust analyses with a dust analyser (DDA) which is a combination of impact-ionization dust detector and time-of-flight mass spectrometer enables to analyse mass, arrival direction speed and element composition for dust particle.

Asteroid (3200) Phaethon: 3200 Phaethon is the parent of Geminids meteor shower [3]. It is an active asteroid, recurrently ejecting dust during the perihelion passage at 0.14 au and dynamically related to kilometer-sized asteroids 2005 UD [4]. The top-shaped Phaethon has an effective diameter estimated to be in the range of 5–6 km with a rotation period of ≈ 3.6 h [5,6]. The ejection of micrometer-sized dust particles from Phaethon near its perihelion has been observed by [7,8,9]. However, the non-detection of a 3-micron hydration feature [10] rules out the possibility that Phaethon's has hydrated minerals and so that it is a comet. Morever, [11] shows that water ice cannot have survived on Phaethon longer than 5 Myr down to 200 m below the surface and nowhere in Phaethon can water ice survive past 50 Myr.

Different studies revealed that at the perihelion Phaethon can have a temperature sufficient for surface dehydration and decomposition, due to solar radiation. [12] calculated its surface temperature caused by solar radiation using the pole solution of [13] and they found that Phaethon's subsolar temperatures is approximately 800–1100K at the perihelion, with a latitude-dependent solar-radiation heating, in which the northern hemisphere would selectively be more heated than the southern hemisphere. Instead, [11] showed that the maximum global temperatures (≈ 1050 K) can be found at equatorial latitudes, due to its location of the subsolar point at perihelion. [14], using the pole orientation of [15], calculated Phaethon surface temperature using the energy balance equation on the asteroid's surface, and their result confirmed that the solar-radiation heating appears similar at every latitude, implying a latitudinally uniform surface for this asteroid.

Phaethon is actually classified as a B-type asteroid [16]. B-type asteroids are commonly linked to dehydrated CI/CM chondrites. The spectral features of CI/CM chondrites are chemically altered from hydrated C-type to B-type by thermal metamorphism [17]. In other words, B-type asteroids are considered to have undergone surface alteration by thermal metamorphism.

Study of Phaethon spectral observations: The objective of our work is to understand if the spectral variability detected on the 3200 Phaethon ground-based observations can be associated to real asteroid surface heterogeneities. We have created a complete Phaethon spectral (VIS-NIR range) database thanks to all telescopic observations obtained from several observers in different times, telescope and years (Table 1). For every observation, geometry, i.e., the observed asteroid portion, has been extracted by using the Phaethon shape model of [6] (Fig.1). The geometric parameters are summarized in Table 1. We have also located on Phaethon shape model the surface features (boulder, concavity, linear facet and polar dark spot) observed by means of radar observations of [5] (Fig. 1, black square).

Thorough a re-analysis of all the VIS observations, Phaethon shows a slight difference in slope maybe reflecting a heterogeneity of its surface, probably due to different heating or different grain size. The spectral phase reddening covering a phase angle range of 20°-80° was analyzed. The spectral slope increases with a coefficient of $(4.0\pm0.6)\times10^{-3}$ μm^{-1} deg^{-1} in the ~0.55-0.7 μm range. The slope around ~0.4-0.45 μm shows a reddening as a function of sub-earth longitude and latitude, the slope around 0.45-0.55 μm is slight blueing on the longitudinal variations while it is reddening with the latitude, whereas the slope ~0.55-0.7 μm does not show any variations due to its sub-earth point coordinates.

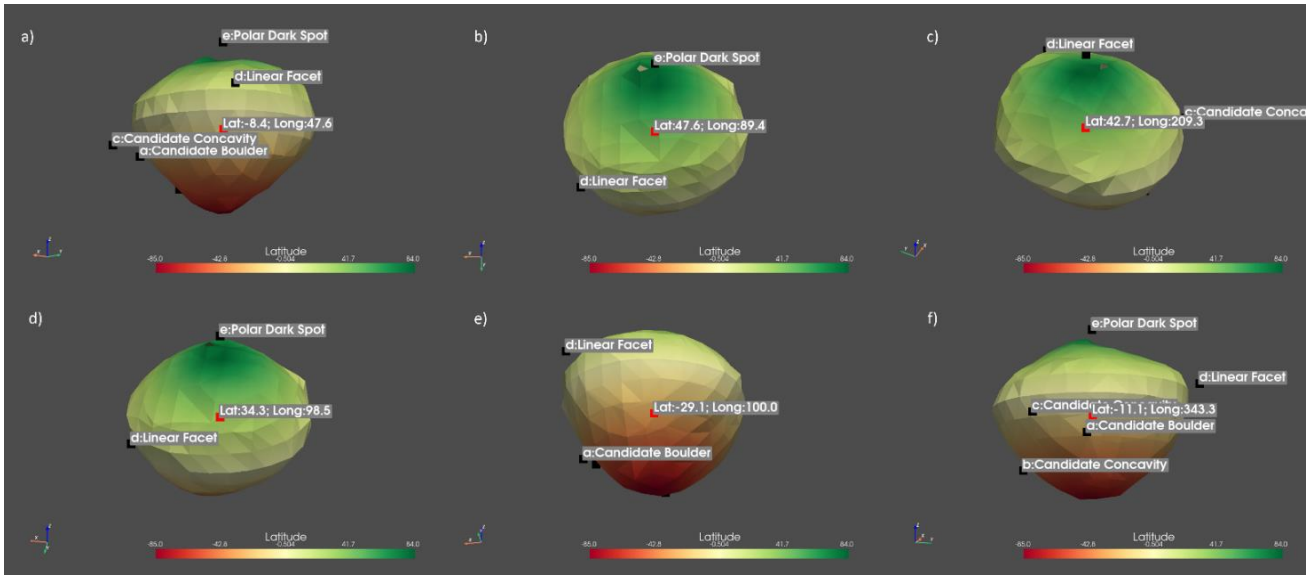

Figure 1: Spectral observations of Phaethon. The red square is the sub-earth latitude-longitude coordinate. The black square shows the position of the surface feature found with radar observation by Taylor et al.,2019. a) Licandro et al., 2007; b) Kareta et al.,2018 (VIS-range); c) Lee et al., 2019; d) Kareta et al., 2018 (NIR-range); e) Palomba et al. 2018 ; f) Lazzarin et al., 2019.

References	Date of observation	Telescope	Spectral range	Phase angle	Sub-Earth Latitude	Sub-Earth Longitude
Licandro et al., 2007	2003, Nov.14	WHT	0.35-0.95 um	57.1	-8.4	47.6
Kareta et al.,2018	2007, Nov. 5	Tillinghast	0.4-0.74 um	(40.8-40.9)	(47.5-47.6)	(123.7-6.2; 356.2-147.8)
Lee et al., 2019	2017, Dec. 7	BOAO	0.4-0.7 um	20.6	(42.8-42.7)	(345.1-209.3)
Kareta et al., 2018	2017, Dec. 12	IRTF	0.7-2.5 um	(21.5-21.9)	(34.4-33.8)	(98.5-123.0)
Palomba et al. 2018	2017, Dec. 16	TNG	0.4-2.5um	101.5	-29.1	(119.2; 108.9; 100.0)
Lazzarin et al., 2019	2017, Dec. 16-17	Galileo	0.32-0.78 um	(62.8; 63.4; 76.6)	(-0.4; -0.9; -11.1)	(79.0; 339.4; 343.3)

Table 1:Telescopic observations and the range of phase angle and of the sub-Earth point coordinates on the asteroid surface for each observer extracted by using the Phaethon shape model of [6].

Future steps: experimental activity To better understand if thermal processing induced some sort of compositional transformation on the asteroid surface material we are preparing dedicated laboratory experiments. To simulate 3200 Phaethon surface, carbonaceous chondrite meteorites will be used as analogues. Then, the thermal processes experienced by Phaethon at perihelion passages will be reproduced in laboratory by well calibrated heating cycle.

References: [1] Arai et al. (2021) 52nd LPSC, No. 2548;[2] Ishibashi K. et al. (2021) 52nd LPSC No. 2548;[3] Whipple, 1983 IAU Circ., No. 3881;[4] Ohtsuka et al. (2006) A&A, Vol.450, Issue 3, pp.L25-L28;[5] Taylor et al., (2019) Planetary and Space Science, Vol. 167, p. 1-8.;[6] Hanuš et al. (2018) A&A, Vol. 620, id.L8;[7] Li and Jewitt, (2013) AJ, Vol. 145, Issue 6, article id. 154, 9 pp.;[8] Jewitt et al. (2013), AJ, Vol.771, Issue 2, article id. L36, 5 pp. ;[9] Hui and Li, (2017) AJ, Vol. 153, Issue 1, article id. 23, 7 pp.;[10] Takir et al. (2020) Nat. C., Vol. 11, article id. 2050; [11] MacLennan et al. (2021) Icarus, Vol. 366, article id. 114535;[12] Ohtsuka et al. (2009) Astronomical Society of Japan, Vol.61, No.6, pp.1375-1387;[13] Krugly et al., (2002) Icarus, Vol. 158, Issue 2, p. 294-304;[14] Lee et al. (2019) Planet. Space Sci, Vol. 165, p. 296-302; [15] Kim et al. (2018) A&A, Vol. 619, id.A123, 8 pp;[16] De Meo et al. (2009), Icarus 202 ,160–180;[17] Hiroi et al. (1996) Meteorit. Planet. Sci., Vol. 31, Issue 3, pp. 321-327;[18] Licandro et al.,(2017), A&A, Vol 461, Issue 2, pp.751-757; [19] Kareta et al.,(2018) , AJ, 156:287 (9pp); [20] Lee et al., (2019), P&SS 165 , 296–302;[21] Palomba et al.,(2018) 42nd COSPAR id. B1.1-44-18;[22] Lazzarin et al.,(2019) , P&SS, Vol 165, p. 115-123.

Acknowledgements: This research is supported by PRIN-INAF-2019, 'PACMAN' (3200 Phaethon Asteroid Composition by Multiple Analysis) project, objective function 1.05.01.85.06. The team thanks Monica Lazzarin, Teddy Kareta, Myung-Jin Kim and Javier Licandro to share with us Phaethon telescopic observations.

WATER REACTIVITY ON SCHREIBERSITE: FROM PHOSPHITES TO PHOSPHATES

S. Pantaleone,[1,2] M. Corno,[1] A. Rimola,[3] N. Balucani,[2,4,5] and P. Ugliengo[1], [1]Dipartimento di Chimica and Nanostructured Interfaces and Surfaces (NIS) Centre, Università degli Studi di Torino, via P. Giuria 7, I-10125, Torino, Italy (stefano.pantaleone@unito.it), [2]Dipartimento di Chimica, Biologia e Biotecnologie, Università degli Studi di Perugia, Via Elce di Sotto 8, I-06123 Perugia, Italy, [3]Departament de Química, Universitat Autònoma de Barcelona, 08193 Bellaterra, Catalonia, Spain, [4]Osservatorio Astrofisico di Arcetri, Largo E. Fermi 5, I-50125 Firenze, Italy, [5]Université Grenoble Alpes, CNRS, Institut de Planétologie et d'Astrophysique de Grenoble (IPAG), F-38000 Grenoble, France.

Phosphorus is an element of primary importance for all living creatures, being present in many biological activities in the form of phosphate (PO_4^{3-}). However, there are still open questions about the origin of this specific element and on the transformation which allowed it to be incorporated in biological systems. The most probable source of prebiotic phosphorus is the intense meteoritic bombardment during the Archean era, few million years after the solar system formation, which brought tons of iron-phosphide materials (schreibersite) on the early Earth crust [1]. It was recently demonstrated that by simple wetting/corrosion processes from this material various oxygenated phosphorus compounds are produced [2]. In the present work, the wetting process of schreibersite (Fe_2NiP) was studied by computer simulations using density functional theory, with the PBE functional supplemented with dispersive interactions through a posteriori empirical correction (D*0) [3,4]. Therefore, the two stable (110) and (001) Fe_2NiP surfaces were used simulating different water coverages, from which structures, water binding energies and vibrational spectra have been predicted. The computed (an-)harmonic infrared spectra have been compared with the experimental ones, thus confirming the validity of the adopted methodology and models (see Figure 1) [5,6]. Moreover, water reactivity was inspected in several possible deprotonation reactions, also increasing the number of water molecules in order to lead to the formation of phosphonic and phosphoric acids and their corresponding deprotonated forms.

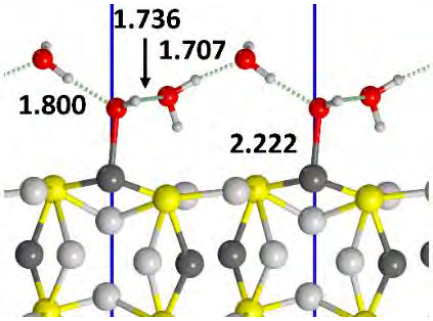

a) Structure

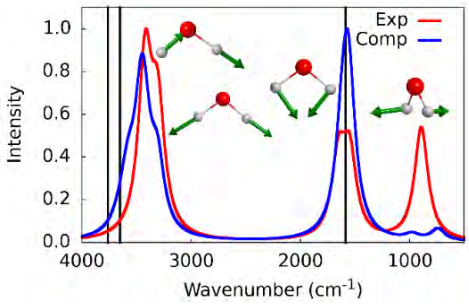

b) IR spectrum

Figure 1: PBE-D*0 optimized geometry of water monolayer on the (110) Fe_2NiP surface (left) and simulated vs experimental IR spectrum (at 125 K). Atom color legend: H in white, O in red, P in yellow, Fe in light grey, Ni in dark grey.

References:

[1] Gulick A. (1955) *Am. Sci.*, *43*, 479-489. [2] Pasek M. A. and Lauretta D. S. (2005) *Astrobiology*, *5*, 515-535. [3] Pantaleone S., Corno M., Rimola A., et al. (2021) *ACS Earth Space Chem.*, *5*, 1741-1751. [4] Pantaleone S., Corno M., Rimola A., et al. (2022) *J. Phys. Chem. C*, *126*, 2243-2252. [5] La Cruz N. L., Qasim D., Abbott-Lyon H., et al. (2016) *Phys. Chem. Chem. Phys.*, *18*, 20160-20167. [6] Qasim D., Vlasak L., Pital A., et al. (2017) *J. Phys. Chem. C*, *121*, 13645-13654.

SPECTROSCOPIC AND NANOSCALE MINERALOGICAL INVESTIGATION OF RYUGU RETURNED SAMPLES. M. Ferrari[1], S. De Angelis[1], L. Folco[2], M.C. De Sanctis[1], E. Mugnaioli[2], A. Raponi[1], G. Filacchione[1], M. Ciarniello[1], E. La Francesca[1], M. Masotta[2], L. Rossi[1], E. Ammannito[3], M. Pedone[3]. [1]INAF-IAPS, Via del Fosso del Cavaliere 100, 00133, Rome (marco.ferrari@inaf.it); [2]Dep. Earth Science, University of Pisa,Via Santa Maria, 53, 56126, Pisa; [3]ASI, Via del Politecnico, 00133, Rome.

Introduction: The JAXA/Hayabusa2 mission collected 5.4 g of samples from two different sites (i.e., A and C) on the surface of C-type asteroid (162173) Ryugu [1; 2]. This asteroid is characterized by a low albedo and by the presence of hydrous and carbonaceous materials [3]. The Ryugu surface spectra collected by the Hayabusa2/NIRS 3 spectrometer reveal a narrow absorption feature at 2.72 µm [4] resembling that observed on the surface of Ceres by the Dawn/VIR spectrometer [5; 6]. Laboratory analysis of returned grains confirmed that Ryugu samples contain hydrated silicates, carbonates, and organics and have spectroscopic similarities to CI chondrites [7]. MicrOmega hyperspectral microscope observation [8] revealed the presence of a band at 3.06 µm, indicating the possible presence of NH-bearing phases in most of the returned grains [9]. This ammonium-related absorption feature was confirmed by FTIR measurements [10]. The 3.06 µm band was also observed in the spectra of Ceres by telescopic observations [11] and by the Dawn/VIR spectrometer that accurately characterized its distribution on the dwarf planet's surface [12]. Current interpretations of Ceres spectra suggest that the most likely mineralogical phases hosting ammonium are phyllosilicates [13; 14], but the presence of ammonium salts has also been inferred in specific areas of the Cerean surface [15; 16]. Hydrated silicates represent the main reservoir of water in Ryugu samples and their presence is indicative of extensive aqueous alteration of its parent body, likely similar to the alteration path that occurred on Ceres. Even if phyllosilicates are the most likely carriers, the specific ammonium-bearing phase determining the 3.06 µm band on Ryugu samples and on the surface of Ceres is not fully constrained, nor are the processes that led to ammonium enrichment on these C-type bodies.

Sample selection: Our selection criterion of the samples among those available in the first allocation (2022A) was the presence of the absorption at 3.06 µm as observed in the spectroscopic data obtained from the preliminary screening by FTIR and MicrOmega. In particular, we have considered:

1. Similarities of the 3.06 µm absorption between Ryugu samples and Ceres spectra, in terms of wavelength range and band center position;
2. The presence of surface features or morphological structures suggests some mineralogical diversity.

Through the first allocation, we obtained two samples: A0198 and C0091 (Fig. 1). The preliminary FTIR data provided by JAXA collected on particle C0091 show the presence of a remarkable absorption close to 3.06 µm. On the contrary, the spectroscopic data collected on particle A0198 show a shallow absorption ascribed to the presence of ammonium and several surface features that comply with our scientific requirements. Moreover, the two assigned samples were collected at different sites which will allow us to make further considerations.

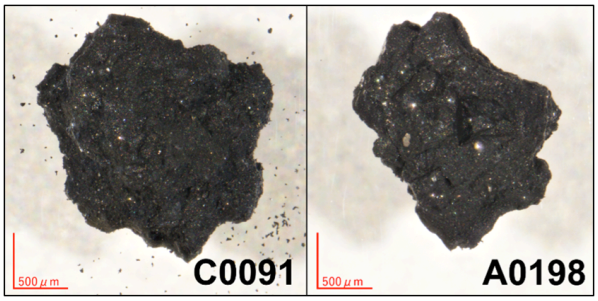

Fig.1 Assigned samples with the allocation 2022A.

Objectives and research plan: With this work, we aim to contribute to the definition of the physical and mineralogical characteristics of the Ryugu asteroid in order to understand the initial stages of formation and evolution of C-type bodies; particular attention will be given to the identification of the ammonium-bearing phase(s) and its/their interplay with hydrated silicates. In addition, we aim to define Ryugu's path of alteration and its similarities with Ceres.

The following laboratory analyses will be used to characterize the samples:

- VIS-IR imaging spectroscopy (0.4–5 µm) will be carried out with the SPectral IMager (SPIM) facility [17] on whole samples. Data will allow a first characterization of the mineralogic composition of their external surface, including an assessment of the presence of water, organic matter, and ammonium in addition to the minerals. Furthermore, by using the SPIM facility (i.e., the Dawn/VIR replica), we can perform a compelling comparison between the data collected on the samples with those provided by the Dawn/VIR spectrometer on Ceres;

- X-ray microscopy (XRM). This non-destructive technique will provide 3D image maps of the morphology, texture, structure, and composition of the whole samples with submicrometer resolution; data will also enable the location of regions of interest (ROIs) within the samples to be analyzed by transmission electron microscopy (TEM);
- Raman μ-spectroscopy, to obtain compositional maps of the surface of the samples at the micrometric scale;
- Focused ion beam-field emission gun-scanning electron microscopy (FIB-FEG-SEM) will be used to identify the main mineralogical phases ad to extract the electron-transparent lamellae for TEM analyses;
- Transmission Electron Microscopy (TEM), electron diffraction, and energy-dispersive X-ray spectroscopy (EDS) will be used to identify cryptocrystalline mineral phases and crystal defects through high-resolution techniques.

In addition, the two samples will be imaged with a resolution of 20 μm/px and spectrally characterized in reflectance in the VIS range from 0.43 to 0.73 μm by using the fISPEx breadboard instrument available in IAPS [18].

Conclusions: The notable similarities of the spectra of some Ryugu samples with Ceres' average spectrum [19] sparked scientific curiosity. To date, interpretation of remotely sensed data coupled with spectroscopic investigation of analogs has not enabled a full understanding of the mechanisms of ammonium enrichment and the nature of the mineral assemblage hosting ammonium on the surface of C-Type objects. Furthermore, studies on meteorites have not provided morphological and compositional information on the mineral phases that preceded the alteration of their progenitor body. For this reason, spectroscopic measurements and nanoscale mineralogical investigations on Ryugu returned samples represent a unique opportunity to definitively establish the link between ammonium and its host phase(s).

References: [1]Yada, T. et al. (2021) Nat. Astron.; [2] Watanabe, S. et al. (2019) Science; [3] Kitazato, K. et al. (2019) Science; [4] Kitazato, K. et al. (2021) Nat. Astron.; [5] De Sanctis, M.C. et al. (2011) Space Sci. Rev.; [6] De Sanctis, M.C. et al. (2015) Nature; [7] Tachibana, S. et al. (2022) 53rd LPSC, #1265; [8] Bibring, J.-P. et al. (2017) Astrobiology; [9] Pilorget, C. et al. (2022) Nat. Astron.; [10] Kebukawa, Y. et al. (2022) 53rd LPSC, #1271; [11] King, T.V. et al. (1992) Science; [12] Ammannito, E. et al. (2016) Science; [13] Ferrari, M. et al. (2019) Icarus; [14] De Angelis, S. et al. (2021) J. Geophys. Res. Planets; [15] De Sanctis, M.C. et al. (2016) Nature; [16] Raponi, A. et al. (2019) Icarus. [17] Coradini, A. et al. (2011) EPSC-DPS Joint meeting, #1043. [18] Filacchione, G. et al., 2022, SPIE 12188, id.1218809. [19] Raponi, A. et al. (2021) Life.

ProDisCo: A Systematic Comparison Between Measured Molecular Abundances in Comets and Protoplanetary Disks.

M. Lippi[1], L. Podio[1], C. Codella[1]
[1]INAF – Osservatorio Astronomico di Arcetri (manuela.lippi@inaf.it).

Comets are cryogenically preserved relics from the formation of the Solar System, accumulated from the material around the young Sun, about 4.6 billion years ago. Different dynamical models predict their birth at different distances from the protosun, and their successive dispersion into their present reservoirs: the Oort cloud, primary source of long period and dynamically new comets, and the Kuiper Belt, main source of Jupiter Family comets [1,2,3].

Once relocated in their reservoirs, comets have remained mostly frozen until today, with their composition only marginally altered by the diverse thermal and physical processes experienced during their lifetime (e.g., multiple transits in the inner solar system for short period comets or cosmic rays weathering), preserving thus signatures of primordial interstellar chemistry and/or thermal processing at the solar nebula location where they formed.

A systematic comparison between the chemical composition measured in comets with that of planet formation regions can thus reveal key clues on the physical, chemical, and evolutionary processes in act during the formation of our and other planetary systems.

From this perspective, nuclei that incorporated material from the colder regions of the protoplanetary disk are expected to show higher abundances of hypervolatile ices and molecules which can form easily through low-temperature surface processes (e.g., hydrogenation), as well as higher deuteration and dust mainly in the amorphous state. In contrast, bodies that collected material from areas closer to the protosun should be dominated by species which form easier via gas-to-gas chemistry, lower deuteration, and crystalline dust signatures. The composition of a comet should also partially reflect the evolution of the protoplanetary disk in time [4].

Indeed, comets show properties like the pre-stellar ice's ones as well as diverse features that can only be explained considering high temperature/radiation processing of the material before its incorporation in the nuclei [5]. This stimulate the debate whether the material is inherited from the proto-star nebula or if a full chemical reset takes place during the formation of the Solar System.

The ProDisCo project: The ProDisCo project combines diverse expertises in the same working group to examine and compare relative chemical abundances observed both in comets and star forming regions. More in details, we plan to use archival data that were not fully exploited in the past, together with new results from observations performed with state-of-the-art instruments (e.g., James Webb Space Telescope, ALMA, VLT/CRIRES+). The collected data will be analysed using appropriate statistical techniques (e.g., exploratory data analysis, multivariate statistic), to retrieve the most information from the data.

The search for correlations will be focused (but not limited) to:

(1) **CO, CH_3OH and H_2CO:** keys to study the physical and chemical conditions at different distances from the protosun and the formation of organics [6,7,8]

(2) **CH_4, C_2H_6, C_2H_2:** commonly observed in the warm molecular layer of Sun-like protostars [9], their relative abundances can be influenced by the level of impacting UV/X/cosmic rays radiation

(3) **HCN and NH_3:** also correlated to formation temperatures, are considered as precursors to formation of ammoniated salts, recently observed in comet 67P and thought to be a main component in comets [10,11]. The recent detection of salts in the disk around Orion Source I [12] opens intriguing scenarios of possible inheritance from primordial material.

Preliminary results in the literature show potential correlations amid comets and star formation regions (see Fig. 2), but are limited to a few targets. Our objective is to create a reliable statistics and to find a more systematic way to compare these astronomical objects.

The results we aim to obtain are expected to increase our understanding of the formation and evolution of planetary systems, bringing new insights and making a deep impact in both comet and star forming regions fields.

References: [1]. Gomes, R., et al., 2005, Nature, 435, 466 – [2]. Morbidelli, A., et al., 2007, AJ, 134, 1790 – [3]. Walsh, K. J. & A. Morbidelli, 2011, A&A, 526, A126 – [4]. Eistrup, C., et al., A&A,613, 2018 – [5]. Mumma, M. J. & S. B. Charnley, 2011, Ann. Rev. Astron. Astroph., 49,471 – [6]. Podio, L. et al., 2020, A&A 642, L7 – [7]. Hiraoka, K, et al. 2005, ApJ, 620, 542 – [8]. Ceccarelli, C., et al., 2022, Protostars and Planets VII, in press – [9]. Schwarz, K. R., Bergin, E. A., Cleeves, L. I., et al. 2018, ApJ, 856 – [10]. Mum-

ma, M. J., et al., 2017, DPS, 49, 414.19 – [11]. Altwegg, K., et al., 2020, NatAs, 4, 533 – [12]. Ginsburg, A., et al. 2019, ApJ, 872, 54 – [13]. Öberg, K. I. and Bergin, E. A., Physics Reports, 893, 1–48, 2021 – [14]. Lippi, M., et al., 2021, AJ, 162, 74 – [15]. Drozdovskaya, M. N., et al., 2019, MNRAS, 490, 50 – [16]. Podio, L. et al., 2020, A&A 642, L7

Additional Information: This project is funded by the European Union under the "NextGenerationEU" program, in the context of the "Piano Nazionale di Ripresa e Resilienza (PNRR)".

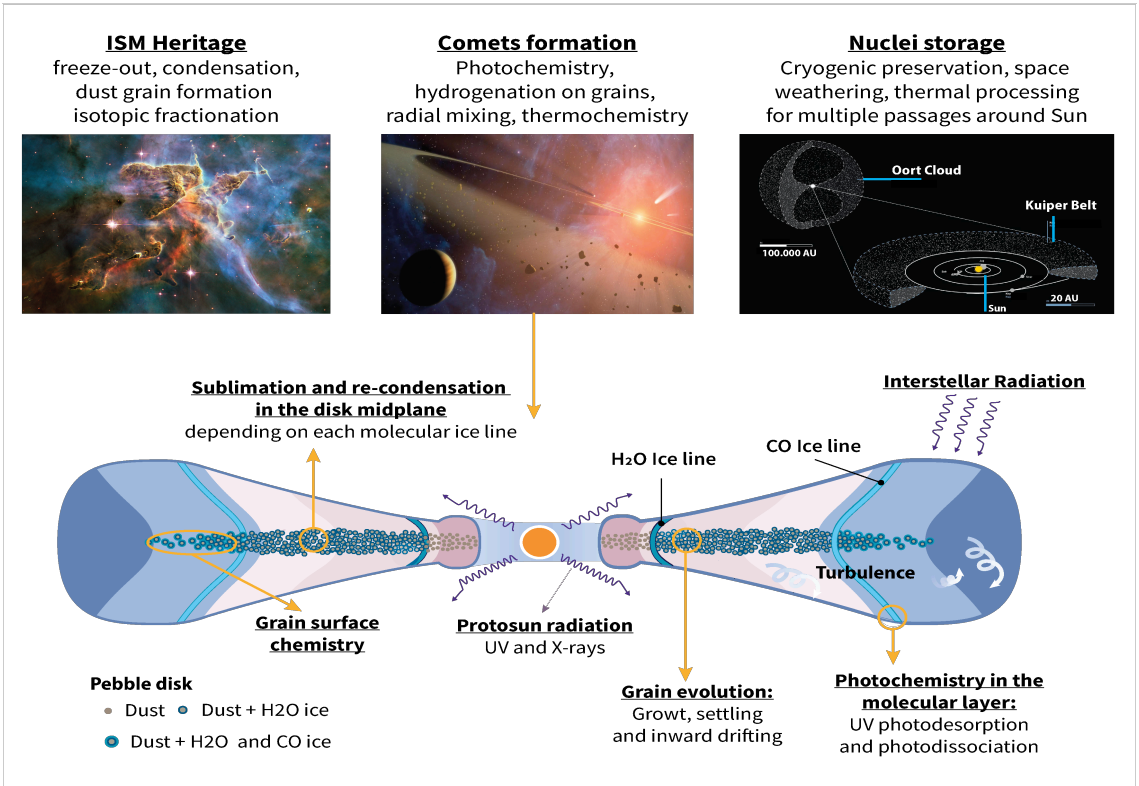

Fig. 1: Upper panel: different stages of life for cometary material from interstellar medium (ISM) to our Solar System. Lower panel: schematic view of some of the chemical and physical processes active in protoplanetary disks, where comets are supposed to form (adapted from [13]).

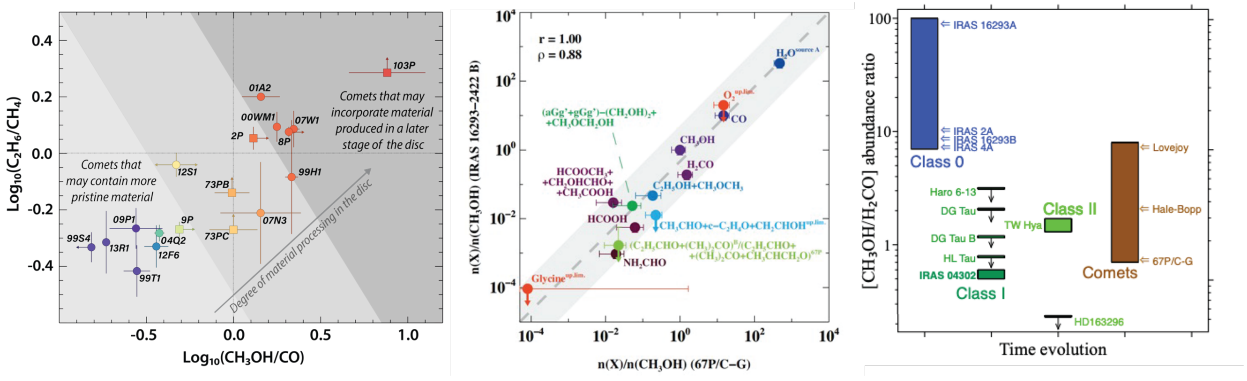

Fig. 2: Chemical diversity in comets [14] (left). Correlations observed between abundances of CHO bearing molecules in IRAS 16293-2422 B and comet 67P [15] (center) and between Class II disks and comets [16] (right).

VIS-IR imaging spectroscopy of Martian Meteorites. S. De Angelis[1], E. La Francesca[1], P. Manzari[2], M. Ferrari[1], M.C. De Sanctis[1], F. Altieri[1], E. Ammannito[2], J. Brossier[1], E. Bruschini[1], M. Formisano[1], A. Frigeri[1], L. Rossi[1]. [1]National Institute of Astrophysics, INAF-IAPS, via Fosso del Cavaliere, 100, 00133, Rome (Italy) (simone.deangelis@inaf.it); [2]Italian Space Agency – ASI-Rome.

Introduction:

The study of Martian Meteorites in the laboratory provides fundamental clues about the formation and evolution of Mars. Spectroscopic and geochemical investigations furnish insight both regarding the planet composition and evolution, as well as information related to secondary processes (i.e. aqueous alteration) [1,2] SNCs meteorites have compositions that are mafic to ultramafic [1,2] essentially basalts or basaltic cumulates. Nakhlites can be characterized by different levels of aqueous alteration and by the presence of phyllosilicates and other secondary minerals [1,2,3,4]
Reflectance spectroscopic measurements, by using the VIS-IR hyperspectral imaging technique, have been performed in the C-Lab @INAF IAPS on a series of Martian meteorites, in the form of small fragments.
Four shergottites, two nakhlites and one brown chassignite sample have been investigated in the VIS-IR range (0.35-5.1 μm) by means of the SPIM facility [5,6].

Setup and samples description: meteorites chips and fragments have been investigated with the Spectral Imager (SPIM) instrument in use at C-Lab laboratory at INAF-IAPS. The facility consists in an imaging spectrometer operative in the 0.35-5.1 μm-range [5,6], based on the laboratory spare of VIR instrument onboard Dawn mission [7]. The setup consists of two bidimensional focal planes, a CCD (0.35-1 μm) and an HgCdTe (1-5.1 μm) both hosted, together with the spectrometer, inside a liquid N_2 cooled Thermal Vacuum Chamber. The entry slit is 9x0.038 mm corresponding to a single acquired image on the sample of 256 px, with spatial resolution of 38 μm/px on the target. The sample to analyze is placed outside the TVC on a 3-axis motorized stage: by moving the target at 38 μm-steps and acquiring consecutive frames it is possible to construct an hyperspectral cube of 876 spectral bands and the desired number of lines.

Different Martian meteorites have been analyzed with the described setup. These are four Shergottites, two Nakhlite specimens and a Chassignite (see table 1). The samples were in form of chips and small fragments, most of them of very few mm in size (about 2-3 mm) and irregular. The largest sample (Shergottite NWA12269) was about 14x5 mm, embedded in an epoxy resin and with a cut plane surface suitable to be scanned.

Sample	*Classification*
NWA 12269	Shergottite
DaG 489	Shergottite
Sueilila 002	Shergottite
Zagami	Shergottite
NWA 998	Nakhlite
NWA 10153	Nakhlite
NWA 2737	Chassignite

Table 1. The analyzed samples and relative classification.

Measurements and Results: An example of acquired image is shown in figure 1. A composite RGB image is shown concerning the NWA10153 Nakhlite specimen. The image has ben constructed by acquiring 70 consecutive frames at 38-μm steps (dimension along vertical axis).

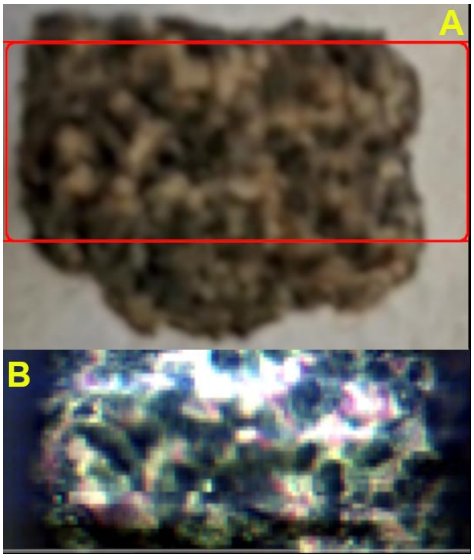

Fig.1. Photo (A) and RGB image (0.7-0.55-0.44 μm) (B) extracted from the hyperspectral cube acquired on the NWA10153 Nakhlite sample.

A selection of representative spectra extracted from the cube is shown in fig.2. A certain spectral (and compositional) variability is observed when looking at

the spectra. These are mainly dominated by pyroxene and olivine absorptions, as indicated by (i) the 1-μm band that appears shifted in the 0.9-1.1-μm range and with variable shape and width, (ii) the VIS reflection peak that occurs at slightly different locations in the 0.6-0.9-μm range, (iii) the second pyroxene band occurring near 2.2-2.3 μm, indicating a Ca-rich (augite) composition. Additional absorption bands are related to the presence of hydrated minerals/phyllosilicates (bands at ~2.7 μm and 3 μm) plus some amount of adsorbed water. Moreover almost all spectra are also characterized by the presence of the carbonate absorption at 3.4-3.5 and 4 μm. Finally in a number of spectra absorption bands occur near 3.1, 3.17 and 3.22 μm: a further in-depth investigation will be done in order to attribute such bands.

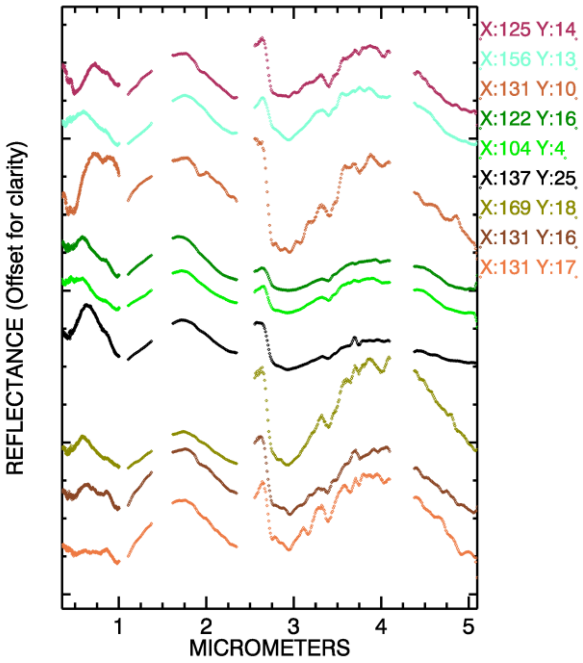

Fig.2. Selection of representative spectra of NWA10153, extracted from the cube. Data at 1.5 and 2.5 μm are cut because of instrumental artifacts, while data at 4.2 μm are cut because of CO_2 absorption.

Conclusions and Future Work:

High spatial resolution spectroscopic analyses of Martian meteorites in the visible and near-infrared are a powerful tool to investigate in detail meteorite composition. Such investigations can provide important clues on the formation and thermal history of these Martian samples and of their parent body, and moreover provide laboratory reference data for supporting the interpretation of future remote-sensing and rover data. Future investigations will concern for example the characterization of phyllosilicate and carbonate phases in Nakhlites, as well as the use of additional techniques such as Raman microscopy to better characterize the samples.

References: [1] Udry A. et al. JGR Planets 125 2020. [2] Treiman A H et al PSS, 48 1213 1230 2000 [3] Hicks L.J. et al. Geoc. Et Coscmoc. Acta, 136 194 210 2014. [4] Bishop J. L. et al. 80th Met. Soc. 6115 2017. [5] Coradini A. et al., Vol. 6, EPSC-DPS2011-1043, 2011. [6] De Angelis S. et al., Rev.Sci.Instr. 86, 093101, 2015. [7] De Sanctis M.C. et al., Space Sc. Rev., 163:329–369, 2011.

Acknowledgements: Scientific activities with SPIM are funded within the ExoMars program by the Italian Space Agency (ASI) grant 2017-48-H.0.

MULTI-COLLECTOR ^{40}AR-^{39}AR DATING IN PLANETARY GEOSCIENCES: DATING TERRESTRIAL IMPACT STRUCTURES. G. Di Vincenzo[1], L. Folco[2], J. Gattacceca[3] and P. Rochette[3], [1]Istituto di Geoscienze e Georisorse - CNR (via Moruzzi 1, 56124 Pisa, Italy, gianfranco.divincenzo@igg.cnr.it), [2]Dipartimento di Scienze della Terra, Università di Pisa (Via S. Maria 53, 56126 Pisa, Italy, luigi.folco@unipi.it), [3]CEREGE (CNRS, Aix Marseille Univ, IRD, INRAE, CEREGE, 13545 Aix-en-Provence, France, gattacceca@cerege.fr and rochette@cerege.fr).

Introduction: The ^{40}Ar–^{39}Ar method [1] is a variant of the conventional K–Ar method and is based on the natural decay of ^{40}K to ^{40}Ar, where ^{39}Ar is produced by fast neutron irradiation and is used as a proxy for the parent ^{40}K. The proportion of ^{39}Ar derived from ^{39}K during irradiation is determined by irradiating together with unknown samples, minerals with known age. The ^{40}Ar–^{39}Ar method represents one of the most versatile and powerful geochronological tools to constrain timescales of geological processes, which can be applied to a wide range of geological problems and to rocks ranging in age from a few thousand years to the oldest rocks available. The ^{40}Ar–^{39}Ar method is routinely applied to planetary sciences, and can be used to constrain the timing of volcanic and metamorphic processes on asteroids or planets, with a strong effectiveness in dating impact events in the solar system [2]. After a renewed interest in the 90s, due to the development of laser extraction techniques (e.g. [3]), the ^{40}Ar–^{39}Ar method is experiencing a third youth thanks to the recent improved precision acquired through a new generation of multi-collector noble gas mass spectrometers ([4–5] and references therein). The new generation of mass spectrometers allows analysis of much smaller samples (down to tens of times smaller with respect to old generations mass spectrometers), with an analytical precision improved by up to one order of magnitude.

Tektites, and their submillimeter equivalents microtektites, are siliceous natural glasses which represent a component of the distal ejecta produced by hypervelocity impacts on Earth of large asteroidal/cometary impactors. Given their generally appreciable K contents and the minor amount or lack of unmelted mineral clasts from the source rocks, tektites are in principle suitable candidates to date impact events by the ^{40}Ar-^{39}Ar method. Knowledge of accurate and precise ages of impact structures is important, as it can be used to constrain the impact flux on Earth and to establish a causative link between impact events and sudden mass extinctions and climate crisis [6].

Dating terrestrial impact structures: Different impact glasses have been investigated in order to test the analytical performances of the multi-collector noble gas mass spectrometer coupled with laser extraction systems installed at IGG-CNR (Pisa, Italy).

Moldavites. Central European tektites (moldavites) are genetically related to the meteorite impact event that produced the ~24-km diameter Ries crater (Germany) during the Langhian, representing one of the youngest large impact structures on Earth ([7] and references therein). Moldavites are known from several areas, including southern Bohemia, western Moravia and the Cheb Basin in the Czech Republic, Lusatia in Germany, and Horn area in Austria. These glasses are typically anhydrous, generally free of inclusions and contain significant K contents (K_2O up to ~4 wt%), which make them well suited to be dated by the ^{40}Ar-^{39}Ar method. Despite the numerous geochronological studies over the last decades and the potential implications for stratigraphic, paleontological and paleoclimatic studies, the age of the Ries impact is still debated [8,9,10]. In this study [11] the age of the Ries crater is addressed by investigating moldavite samples from southern Bohemia by multi-collector ^{40}Ar–^{39}Ar laser dating. Data were obtained relative to the key Fish Canyon sanidine (FCs) and Alder Creek sanidine (ACs) reference materials, over a period of nearly two years and in four irradiations of different duration (neutron flux in the range of 0.5 to 15 MWh). Results, completed through the laser step-heating and total fusion techniques, demonstrate an excellent intrasample and intersample reproducibility of moldavites and prove that analytical performances of moldavites in terms of uncertainties on the ^{40}Ar*/^{39}Ar$_K$ ratios are in line with those achievable by the FCs and ACs reference minerals. Using the most recent astronomical calibration for the ACs reference material [12] yields an ultraprecise age of 14.7495±0.0045 Ma (±2σ - ±0.016 Ma, including all external uncertainties, i.e. age of the reference material and ^{40}K decay constant), which reconciles geochronological and paleomagnetic data.

Atacamaites. Atacamaites are centmeter-sized impact glasses identified over an area of ~650 km^2 in the Atacama Desert (Chile) [13]. Their glassy nature, aerodynamic shapes, elevated formation temperature and low water content, resemble features characteristic of tektites but their small size, heterogeneity, oxidation state and a significant contamination by the impactor (an iron meteorite based on Ni, Co and Cr contents), differentiate them from typical tektites. An associated

impact crater has not been identified so far, suggesting that it may consist of a small, km-sized, crater. Their age is referred to the Late Miocene on the basis fission track data. Glass aliquots of ~15 mg from the 0.35-0.50 millimetre grain size were analyzed by the laser step-heating technique using an old generation mass spectrometer. Results yielded concordant age spectra with mean ages of ~6.5 Ma and large analytical uncertaties of ±0.2–0.1 Ma (±2σ) due to atmospheric Ar contents >>60%. Aliquots of only a few milligrams which were analysed by the laser step-heating technique using a new generation multi-collector mass spectrometer, yielded concordant segments with age of ~6.6 Ma and analytical uncertainties as low as ±36–30 ka. Furthermore, in order to verify grain-to-grain reproducibility, invidual fragments were analysed by the laser total fusion technique using the same instrument. Using both step-heating and total fusion results and relative to the ACs reference material, yields a pooled, high precision, mean age of 6.580±0.012 Ma (±2σ - ±0.014 Ma, including all external uncertainties).

Transantarctic Mountain Microtektites. Demonstrating that microtektites found at several locations throughout East Antarctica [14] consist of a homogeneous class of geologic objects belonging to the Australasian tektite/microtektite strewn field is fundamental to define the actual extent of the largest and youngest known tektite field on Earth produced by an asteroidal impact ~0.8 Ma ago. In this study [15] new ^{40}Ar-^{39}Ar analyses were performed by multi-collector noble gas mass spectrometry on individual microtektites from key locations in the Transantarctic Mountains (Antarctica). Results suggest that particles are heavily contaminated by at least one excess Ar component (parentless ^{40}Ar, e.g., see [16]), which is not correlated with size nor with bulk chemical composition, and precludes a straightforward interpretation of ^{40}Ar–^{39}Ar data. Analysis of laser step-heating and total fusion data in three-isotope correlation diagrams yields indistinguishable isochron ages, with a pooled mean of 800±89 ka (95% confidence level). Results improve by more than one order of magnitude previously published ^{40}Ar–^{39}Ar age determinations [14], thus strengthening the southward extension of the Australasian field and implying a launch distance of nearly 12,000 km from the putative impact location in Indochina [17]. Results also reveal a contrasting behavior between microtektites from the Transantarctic Mountains, highly contaminated by excess Ar, and Australasian macroscopic tektites, weakly or negligibly contaminated ([18] and refrences therein). Excess Ar is commonly considered a troublesome drawback of the ^{40}Ar–^{39}Ar dating method, however in the investigated microtektites from the Transantarctic Mountains it may potentially provide additional constraints on the microtektite formation model. The excess Ar detected and its possible distribution within the spherules was acquired necessarily when microtektites were still hot and possibly while traveling, as molten droplets, through a plume which contained Ar with an isotope composition higher than that of modern atmosphere (most likely due to vaporized target). The contrasting contents of excess Ar between microtektite versus macroscopic tektites may therefore reflect displacement in different environments.

References: [1] Merrihue C., Turner G. (1966). *J Geophys Res* 71 (11), 2852–2857. [2] Jourdan F. (2012) *Aust J Earth Sci* 59, 199-224. [3] Kelley S.P. (1995) In: Potts P.J., Bowles J.F.W., Reed S.J.B., Cave M.R. (Eds.), Microprobe Techniques in Earth Sciences, Mineralogical Soc. Series 6. Chapman & Hall, London, pp. 123–143. [4] Mixon E.E., Jicha B.R., Tootell D., Singer B.S. (2022). *Chem Geol* 593, 120753. [5] Phillips D., Matchan E.L., Dalton H., Kuiper K.F. (2022). *Chem Geol* 597, 120815. [6] Kelley S.P. (2007) *J Geol Soc Lond,* 164, 923–936. [7] Di Vincenzo G. and Skála R. (2009) *Geochim Cosmochim Acta* 73, 493–513. [8] Schmieder M., Kennedy T., Jourdan F., Buchner E., Reimold W.U. (2018). *Geochim Cosmochim Acta* 220, 146–157. [9] Rocholl A., Bohme M., Gilg H.A., Pohl J., Schaltegger U., Wijbrans J. (2018). *Geochim Cosmochim Acta* 220, 146–157. [10] Schmieder M., Kennedy T., Jourdan F., Buchner E., Reimold W.U. (2018) *Geochim Cosmochim Acta* 220, 146–157. [11] Di Vincenzo G. (2022). *Chem Geol* 608, 121026. [12] Niespolo E.M., Rutte D., Deino A.L., Renne P.R. (2017). *Quat Geochronol* 39, 205–213. [13] Gattacceca J., Devouard B., Barrat J.-A., Rochette P., Balestrieri M.L., Bigazzi G., Ménard G., Moustard F., Dos Santos E., Scorzelli R., Valenzuela M., Gounelle M., Debaille V., Beck P., Bonal L., Reynard B., MWarner M. (2021). *Earth Plane Sci Lett* 569, 117049. [14] Folco L., Rochette P., Perchiazzi N., D'Orazio M., Laurenzi M.A., Tiepolo M. (2008) *Geology* 36, 291-294. [15] Di Vincenzo G., Folco L., Suttle M.D., Brase L., Harvey R.P. (2021) *Geochim Cosmochim Acta* 298, 112–130. [16] Kelley S.P. (2002). *Chem Geol* 188, 1–22. [17] Sieh K., Herrin J., Jicha B., Angel D.S., Moore J.D.P., Banerjee P., Wiwegwin W., Sihavong V., Singer B., Chualaowanich T. and Charusiri P. (2019). *PNAS* 12, 1– 8. [18] Jourdan F., Nomade S., Wingate M.T.D., Eroglu E., Deino A. (2019). *Meteorit Planet Sci* 1–19, 13305.

EARLY DIFFERENTIATION OF PLANETESIMALS: INSIGHTS FROM MELTING EXPERIMENTS OF AN L6 ORDINARY CHONDRITE. M. Masotta[1], S. Iannini Lelarge[1], L. Folco[1], L. Pittarello[2], L. Mancini[3]
[1]Dipartimento di Scienze della Terra, Università di Pisa, Via Santa Maria 53, Pisa, Italy (matteo.masotta@unipi.it), [2]Natural History Museum Vienna, Mineralogisch-Petrographische Abteilung, Burgring 7, 1010 Vienna, Austria, [3]Elettra-Sincrotrone Trieste, S.S. 14 - km 163.5, Area Science Park, 34149 Basovizza, Trieste, Italy

Introduction: Planetary differentiation in small bodies is believed to be ruled by several partial end-states that were dominated by variable degrees of melting and fractionation of the metallic and silicate phases. Studying the melting behaviour of undifferentiated chondritic materials is pivotal for reconstructing differentiation processes occurring during the early evolution of planetesimals and, eventually, leading to the formation of rocky planets and partially differentiated asteroids. In this study, we present results from melting experiments performed at 1 GPa, using an L6 ordinary chondrite (DAV 01001).

Results: At the temperature of 1100 °C, the initial chondritic texture is preserved and melting of silicate minerals is not observed, while the opaque phases (kamacite, taenite and troilite) react forming two immiscible liquid phases, a FeNi metal phase and a S-rich phase. Melting of the silicate domain initiates at 1200 °C and slightly increases with temperature, yielding to a progressive obliteration of the chondrules and textural re-equilibration of the silicate assemblage (re-crystallization at mineral-melt interfaces and within the melt). No substantial textural changes are observed for the FeNi metal and S-rich phase upon further temperature increase, with the FeNi metal phase typically forming spherical or cruciform blebs enveloped by the S-rich phase. The non-modal melting of the silicate mineral assemblage (in the order: plagioclase > high-Ca pyroxene > low-Ca pyroxene > olivine) and subsequent re-crystallisation determines the evolution of the silicate melt from a dominantly trachy-andesitic composition at 1200 °C, to basaltic trachy-andesitic at 1300 °C and andesitic at 1400 °C. The composition of the silicate melt produced in the experiments shows analogies with the trachy-andesitic and andesitic bulk compositions of some anomalous achondrites, whereas the compositional variation of the silicate minerals compares well with that of several achondrite groups, such as pallasites, acapulcoites, lodranites, ureilites, brachinites and IAB inclusions.

Discussion: At the experimental conditions, the FeNi metal and S-rich liquids are always immiscible and the surface tension-dominated regime causes the FeNi metal to be preferentially wet by the S-rich phase, remaining thus insulated from the silicate domain. Under such circumstances, the partitioning of siderophile elements into the metal phase is expected to be limited by the presence of the S-rich phase, which acts as a chemical barrier reducing the exchange of these elements between the silicate and FeNi metal phases. This is consistent with the "excess" of siderophile elements in the Earth's mantle, relative to the abundance expected from complete core-mantle equilibration. Overall, melting experiments suggest that small degrees of melting and re-crystallisation under magmatic conditions could have been dominant processes at the onset of planetesimal differentiation, explaining the formation of both differentiated (crustal-like) and undifferentiated (mantle-like) lithologies. The absence of evidence for silicate-metal fractionation suggests that, in the lack of differential stress or strain (possibly induced by impact processes or spin rotation) and particularly when silicate melt is present interstitially, the efficiency of metal-sulphide segregation into a core may be severely limited in small planetesimals.

Glass of possible impact origin from Pica (Chile)

G. Giuli[1], G. Pratesi[2], M.Morelli[3], F. Capaccioni[4], M. Di Martino[5], A. Di Michele[6], S. Nazzareni[6], M. Barbieri[7] [1]School of Science and Technology-Geology division, University of Camerino, Via Gentile III da Varano, 62032, Camerino (MC); [2]Dipartimento di Scienze della Terra, Università di Firenze, Via G. La Pira 4, 50121 Firenze, Italy; E-Mails: g.pratesi@unifi.it; [3]Fopndazione Parsec e Museo di Scienze planetarie, Via di Galceti 74, 59100, Prato, marco.morelli@fondazioneparsec.it; [4]Istituto di Astrofisica e Planetologia Spaziali, Istituto Nazionale di Astrofisica (INAF), Rome, Italy, fabrizio.capaccioni@iaps.inaf.it.; [5]Istituto Nazionale di Astrofisica, Osservatorio Astronomico di Torino (OATo), Torino, mario.dimartino@inaf.it; [6]Dipartimento di Fisica e Geologia, Università di Perugia, Via Pascoli, 06123 Perugia, Italy; E-Mails: alessandro.dimichele@unipg.it, sabrina.nazzareni@unipg.it; [7]Instituto de Astronomía y Ciencias Planetarias, Universidad de Atacama (UDA), Copayapu 405, 1531772 Copiapo', Chile, mauro.barbieri@uda.cl

Introduction: Impact glasses are features associated with many terrestrial impact craters or impact structures that can provide important clues for dating impact events or even discovering new impact structures [1]. Also large airbursts have been proposed to be able of melting of the soil surface by radiation [2,3]. Airbusts have been invoked in order to explain the formation of some anomalous silicate glasses like the Libyan Desert Glass. Other examples include Pleistocene scoriaceous glasses from Australia [4] and northern Africa. However, as French and Koeberl point out [1], it is often difficult to ascribe an impact origin to such glasses, which closely resemble non-impact glasses such as fulgurites, volcanic glasses or even metallurgical slags. The origin and mechanism of formation of these glasses is thus strongly debated. Hence, proving or disproving the impact origin of these glasses has implications for estimating the flux of airburst producing bolides to the Earth surface.

The enigmatic Pica Glass: Massive glassy formations (called Pica Glass) were recently discovered in Chile near the town of Pica [5,6]. These glasses have been found in several oucrops forming a line as long as 70 km, lying on the surface along the eastern margin of the Tamarugal–Llamara basin in the Atacama Desert. They have been variously interpreted by several authors as fulgurites, impact glasses, or glasses resulting from large fires melting the surface sediments (See Ropert et al., and references therein). Also, they have been interpreted as the consequence of a major airburst [5, 7]. Preliminary results found by our group strongly suggest the presence of a meteoritic component in the glass, thus indicating that the melt originated from an impact or an airbust.

Meteoritic components?: We accurately analysed by FESEM, 9 thin sections made from samples coming from the 4 studied glass outcrops.

The samples consist of a vescicular silicate glass (ca 54 wt% SiO2) embedding many clasts of the sand from which the melt probably originated. In addition, we found the ubiquitous presence of sulphide blebs (from micron to 30 micrometers size) whose composition is, within error, identical to troilite. A small fraction of these troilite blebs contains also appreciable amounts of Ni. In three out of four outcrops spherules consisting of a fine intergrowth of Fe phosphide and native iron has been found; these spherules have diameters up to 12 micrometer in size and are usually mantled by troilite.

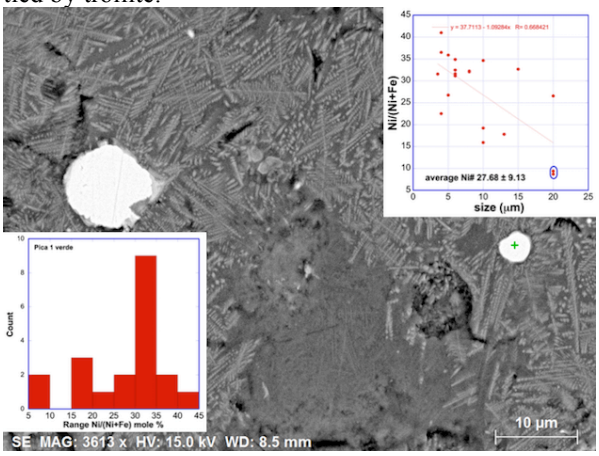

Fig. 1 Fe-Ni spherules partially mantled by troilite

In two out of four outcrops a suite of metallic spherules have been found with diameters from 4 up to 20 micrometer and Ni/(Ni+Fe) ratios ranging from 0 to 0.4 (average 0.278 ±0.09).

Other phases of possible meteoritic provenance include merrillite (found in samples from two out of four outcrops) and apatite-(Cl) (found in samples from three out of four outcrops). Remarkably, in one sample also two chondrules have been found embedded in the glass which consisted of euhedral diopside crystals, troilite, merrillite, and recristallised mesostasis.

Despite other mechanisms could be invoked for the formation of reduced phases, we suggest that the phases we detected are of meteoritic provenance. In particular, despite extensive fires in presence of a reducing agent may be invoked for the formation of metallic Fe spherules, the ancient fire hypothesis [6] would not explain the presence of Fe-Ni alloys.

Several issues should be further addressed to better interpret these finds: namely why crystalline phases with so diverse melting temperature persisted in the glass, and the unicity of such an occurrence (no other

impact glass has so far been reported bearing so many phases interpreted as relicts of the projectile). In our opinion, the mineralogy of the clasts interpreted here as relicts of the projectile, the presence of chondrules, and the presence of numerous Fe-Ni spherules (including two non spherical fragments of kamacite with troilite inclusions) may point to a projectile of ordinary chondritic composition, in contrast to the hypothesis of Schultz et al [7] that instead invokes a cometary projectile.

References: [1] French B.M., Koeberl C. (2010) EarthSci.Rev.98,123–170. [2] Wasson J.T., (2003) Astrobiology3, 163–179. [3] Boslough M.B.E., Crawford D.A. (2008) Int. J. Impact Eng.35, 1441–1448. [4] Haines P.W., Jenkins R.J.F., Kelley S.P., (2001) Geology29, 899. [5] Blanco N., Tomlinsson A.J. (2013) Carta Guatacondo. Región de Tarapacá. Carta Geológica de Chile. [6] Ropert P, Gattacceca J, Vallenzuela M, Devouard B., Lorand JP, Arriagada C., Rochette P., Latorre C., Beck P. (2017) Earth and Planetary Science Letters, 469, 15-26. [7] Schultz P.H., Harris R.S., Perroud S., Blanco N., Tomlinson A.J. (2021) Geology, 50, 205-209.

Cavezzo: fall, recovery and analysis of the first Italian meteorite found by PRISMA

D. Gardiol[1], D. Barghini[1,2], S. Bertocco[3], A. Carbognani[4], M. Di Carlo[5], M. Di Martino[1], C. Falco[1], G. Pratesi[6,7], W. Riva[1,8], G. M. Stirpe[4], C. Volpicelli[1], and the PRISMA team, [1]INAF – Osservatorio Astrofisico di Torino, via Osservatorio 20, 10025 Pino Torinese (TO), daniele.gardiol@inaf.it, [2]Università di Torino - Dipartimento di Fisica, Torino, [3]INAF – Osservatorio di Astrofisica e Scienze dello Spazio, Bologna, [4]INAF – Osservatorio Astronomico di Trieste, [5]INAF – Osservatorio Astronomico d'Abruzzo, Teramo, [6]Università di Firenze, Dipartimento di Scienze della Terra, Firenze, [7]INAF – Istituto di Astrofisica e Planetologia Spaziali, Roma, [8]Osservatorio Astronomico del Righi, Genova.

Introduction: PRISMA, the first Italian fireball network, has achieved a major milestone by recovering the first Italian "pedigree" meteorite on the 4th January 2020 near Cavezzo (MO) less than three days after the fall. This was the first recovery of this type in Italy.

Fall: Video recordings of a bright bolide were captured by eight PRISMA cameras on the 1st January 2020 at 18:26:53 UTC. The meteoroid entered the atmosphere at 12.8 ± 0.2 km/s with an inclination angle of about 68°. The meteor shone from 76 km to 22 km of height, reaching a magnitude of -9.5. The bolide was seen by hundreds of witnesses, that provided visual reports. At a height of about 32 km and 30 km the meteoroid experienced two fragmentation episodes. The low altitude reached and the final velocity of about 4 km/s indicated the high probability of a meteorite fall.

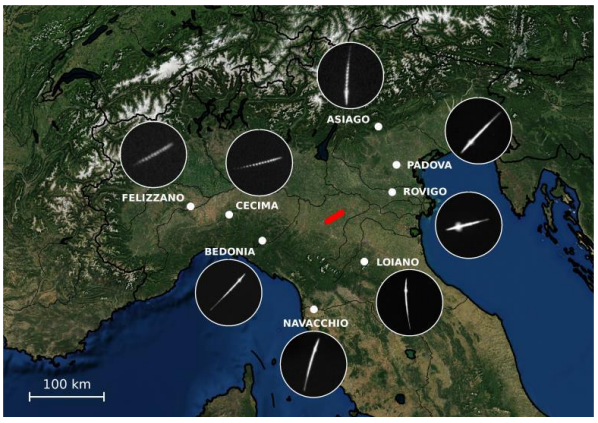

Fig. 1 – The bolide visible trajectory and the eight PRISMA cameras that recorded the event [1]

Strewn-field: A strewn-field of about 6 km² was identified by computations from PRISMA observations. The total final mass was estimated in about 1.5 kg. Due to intense winds of that night the area of probable fall was shifted towards S-E with respect to ground trajectory. PRISMA informed and reached the attention of the inhabitants of the region by press releases and local media. The area is located in the municipality of Cavezzo, in province of Modena, between the towns of Rovereto sulla Secchia and Disvetro.

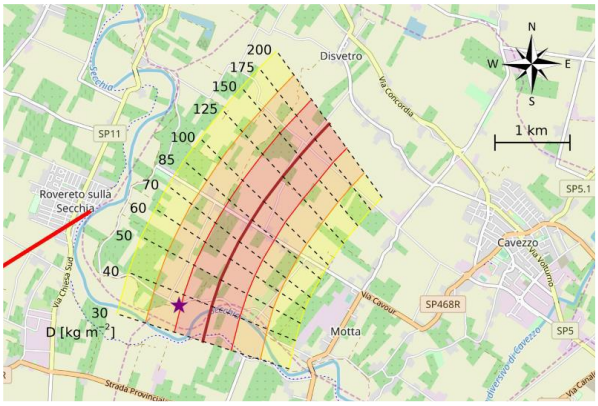

Fig. 2 – The computed strewn-field and the place were the fragments were found (purple star) [1]

Orbit: The computed orbit is compatible with one object only among known NEOs, namely 2013 VC_{10}. It is an Apollo type asteroid observed for 54 days only in 2013, with an estimated size of 10 m and an orbital period of about 2 years.

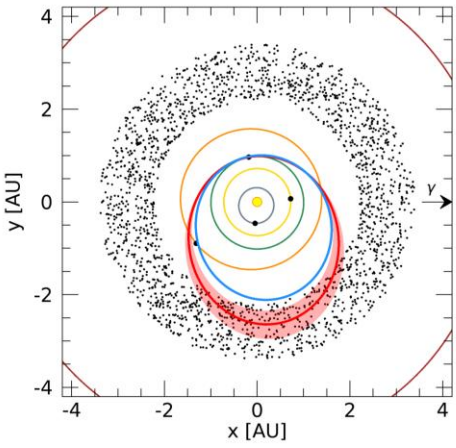

Fig. 3 – The orbit of the Cavezzo meteoroid (red) compared with the orbit of 2013 VC_{10} (blue) [1]

Recovery: Three days after the event, on the 4th January, around 3 PM local time, Mr. Davide Gaddi was walking with his dog Pimpa over the embankment of the Secchia river floodwater detention basin and was attracted by a small dark shiny stone. He then recovered a second larger fragment. They looked like freshly fallen meteorites. He suddenly informed the PRISMA Project Office with an email. A meeting with a scouting group already on site was immediately organised, and by 5 PM the recovery was confirmed by Romano Serra to whom the two fragments were given. Mr. Gaddi eventually decided to donate them to INAF for scientiric analysis.

Fig. 4 – Mr. Davide Gaddi with his dog Pimpa show the exact place were they found the first fragment

Analysis: The meteorite has been classified as a L5-anomalous chondrite. On 5th September 2020 it was approved with the name "Cavezzo". In fact, the two recovered fragments F1 (3.12 g) and F2 (52.19 g) were found to be quite different in their petrology, modal mineralogy and oxygen isotopes composition. In particular, F1 may be xenolitich material representing a previously unsampled port ion of the L-chondritic parent body [2]. Gamma activity measurement were performed soon after the fall. The detection of many short lived radionuclides confirmed the recent fall of the sample [3].

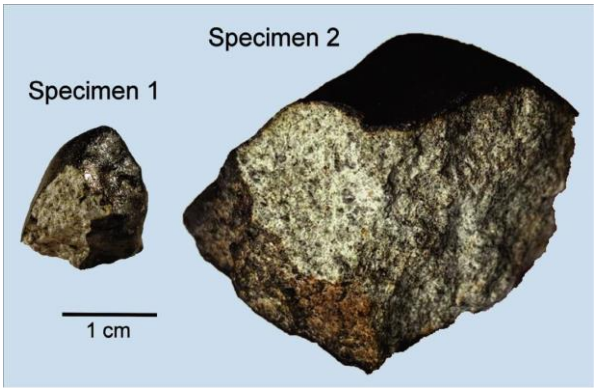

Fig. 5 – The two recovered fragments of the Cavezzo meteorite [2]

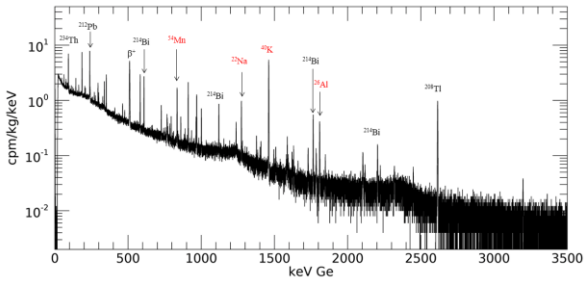

Fig.6 – The gamma emission spectrum of the Cavezzo meteorite [3]

References:

[1] Gardiol D. et al. (2021) *MNRAS, 501*, 1215–1227.
[2] Pratesi G. et al. (2021) *MAPS, 56*, 1125–1150.
[3] Bizzarri I. et al (2023) *Applied Radiation and Isotopes*, (accepted)

CARBON PHASES IN UREILITES WITH INCREASING THE DEGREE OF SHOCK: THE EXAMPLE OF FIVE FRONTIER MOUNTAIN UREILITES.

A. Barbaro[1], M. C. Domeneghetti[2], A.M. Fioretti[3], M. Alvaro[2] and F. Nestola[1]
[1]Department of Geosciences, University of Padova, I-35131 Padova, Italy (barbaroanna08@gmail.com ; fabrizio.nestola@unipd.it), [2]Department of Earth and Environmental Sciences, University of Pavia, 27100 Pavia, Italy (chiara.domeneghetti@unipv.it; matteo.alvaro@unipv.it), [3]Institute of Geosciences and Earth Resources, National Research Council, I-35131 Padova, Italy (anna.fioretti@igg.cnr.it)

Introduction: Carbon is an essential ingredient for life as we know it. Therefore, its primary occurrence and evolution in the early Solar System, and especially within the first differentiated planetesimals, is of vital interest. Carbon phases occur in different kinds of meteorites, spanning from differentiated to undifferentiated ones. In particular, among the differentiated meteorites, carbon is present in iron meteorites and in ureilites. Ureilitic meteorites (achondrites) consist of ultramafic rocks, mainly composed of olivine, pigeonite, minor carbon (graphite and diamond) and Fe-Ni compounds [1, 2, 3]. and are believed to come from the same parent body, the Ureilitic Parent Body (UPB). The analysis of mafic silicates of ureilites suggested that the parent body diameter should be close to 180 km (Warren 2012). Moreover, the investigation of small asteroidal bodies, possibly linked to ureilitic daughter bodies [formed after the catastrophic disruption of the UPB] by Jennisken et al. (2010), assessed that the original diameter of the UPB was < 200 km.

Recent studies on ureilites [4, 5, 6, 7] indicate that the coexistence of large monocrystalline diamonds, nanodiamonds together with nano-graphite is consistent with a transformation of graphite enhanced by the catalysis of Fe-Ni phases during impact shock events.

Sample and methodology: FRO 95028, FRO 01089, FRO 97013, FRO 01088 and FRO 01012 ureilitic samples with different shock degrees were analysed by the multhimetodological approach reported by [4, 5, 6, 7]. In particular, we performed scanning electron microscopy [equipped with energy dispersive spectroscopy (SEM-EDS)], micro-X-ray diffraction (XRD), and micro-Raman spectroscopy (MRS) to characterize the carbon phases and to observe if there is any correlation between the degree of shock recorded by silicates and the presence of the different carbon polymorphs. The shock level of the investigated samples ranges from U-S2 (low shock degree) to U-S6 (very high shock degree) [8].

Results and Discussion: the XRD results demonstrate that all investigated samples contain nano-graphite. FRO 95028, with the lowest (S2) shock degree, contains nanodiamond, while samples from S3 to S6 contain both nano- and micro-diamond. XRD results support the shock formation of micrometer-diamonds with the assistance of (Fe, Ni)-alloys as catalysts at pressure >10 GPa (S3 shock level recorded by silicates). The formation of polycrystalline diamond is already allowed at pressure between 5-10 GPa. The powder diffraction patterns of each of the selected fragments revealed asymmetry on the highest peak of graphite and on the highest peak of diamond, suggesting respectively the presence of "compressed graphite" and stacking disorder on the diamond; these features are both considered markers of impact event(s) [9, 10]. Temperature estimated by a graphite-thermometer based on MRS data [11], provided values in the range of 1291 to 1398°C ±120°C, revealing that there is not a considerable variation of the graphite temperature with the increasing degree of shock.

Conclusions: the results of this work demonstrate that:

(i) the formation of polycrystalline diamond, as demonstrated by the results obtained in FRO 95028 low shock ureilite (S2), is allowed at pressure between 5-10 GPa.

(ii) the micrometer-diamonds found in FRO 01089, FRO 97013, FRO 01088 and FRO 01012 formed by shock event with the assistance of (Fe, Ni)-alloys as catalysts at pressure >10 GPa (S3 shock level recorded by silicates).

(iii) the application of graphite geothermometer based on MRS data [11] does not show any obvious correlation between temperature and shock stage between low-medium and high shock ureilitic samples.

Acknowledgments: This research was funded by the PNRA 2018 00247-A project to F. Nestola.

References: [1] Berkley J. L. and Jones J. H. (1982) J. Geophys. Res. 87:A353–A364. [2] G. P. Vdovykin (1970) Space Sci. Rev. 10:483–510. [3] Goodrich C. A. (1992) MAPS 27:327–352. [4] Nestola F. et al. (2020) PNAS 41:25310–25318. [5] Barbaro A. et al. (2020) Minerals 10:1005. [6] Barbaro et al. (2021) GCA 309:286-298. [7] Barbaro et al. (2022) Am. Min. 107 (3): 377–384 [8]Stöffler D. et al. (2018) MAPS 53(1):5-49. [9] Nakamuta Y. and Aoki Y. (2000) MAPS 35(3): 487-493. [10] Murri M. et al. (2019) Sci. Rep. 9(1):1-8. [11] Cody G. D. et al. (2008) Earth Planet. Sci. Lett. 272:446–455.

THE CHONDRITIC IMPACTOR ORIGIN OF THE Ni-RICH COMPONENT IN AUSTRALASIAN TEKTITES/MICROTEKTITES. L. Folco[1,2], and P. Rochette[3], [1]Dipartimento di Scienze della Terra, Università di Pisa, Italy; [2]Centro per la Intergrazione della Strumentazione della Università di Pisa, CISUP, Pisa Italy. (luigi.folco@unipi.it), [3]CEREGE, Centre Europeen de Recherche et d'Enseignement des Geosciences de l'Environnement, CNRS, Université Aix-Marseille (France).

Introduction: Impact melt rocks produced by hypervelocity impacts of asteroidal/cometary bodies onto Earth's crust can incorporate small amounts of meteoritic material, resulting in a distinct chemical signature relative to the local or average continental crust values. The identification of this signature is a geochemical challenge due to the important dilution (in the order of ~1:100). Nevertheless, it can provide important clues on the impactor type, thereby enabling investigation of the flux of different kinds of impactors to Earth, their orbital evolution from their source regions and the collisional/disintegration history of their asteroidal/cometary parent bodies.

The nature of the impactor that generated the Australasian tektite/microtektite (high velocity ejecta of impact melts) strewn field, i.e., the largest Cenozoic strewn field (15% of the Earth's surface), the youngest (0.79 Myr old, [2, 3] on Earth, and the only one without an associated impact crater so far, is an outstanding issue. In our previous work [4], we identified a chondritic impactor signature in 77 Australasian microtektites (size range: 200–700 µm) from within 3000 km of the hypothetical impact location in Indochina (~17 N, 107 E; [5]), based on Ni, Co and Cr concentrations above continental crust values (i.e., up to 680, 50 and 370 µg/g, respectively; LA-ICP-MS data). We also shows that the Cr/Ni versus Co/Ni ratios are consistent with mixing between crustal compositions and an LL chondrite. An impactor signature of broadly chondritic composition was proposed earlier by [6] based on the Cr and Ir elemental ratios in Australasian tektites enriched in Ni (100–340 µg/g). Nonetheless, these results were recently questioned by [7, 8], who linked the high concentrations of high siderophile elements (HSE) and Ni, Co and Cr in Australasian tektites to a mafic terrestrial component, namely basalts of the Bolaven Plateau in souther Laos according to [8].

Ni occurs abundantly in mafic, mantle and mantle-derived rocks (i.e., peridotites and basalts). In these rocks, it is coupled with Mg in Mg-olivine, Mg-pyroxene, and spinel, in concentrations up to 3000 µg/g, e.g. [9]. Using a large geochemical data base of Australasian tektites and microtektites from the literature, we have studied the relationship between Ni and Mg to solve the question. Data show conclusive evidence that Ni-rich component is a genuine signature of a chondritic impactor and not of a contribution of terrestrial mafic-ultramafic terrestrial target rocks.

Results: The plots in the figure below show the concentrations of Ni (µg/g) versus Mg (wt%) for 126 tektites [6, 10, 11, 12, 13] and 234 microtektites [4, 14, 15, 16, 17, 18, 19, 20], along with terrestrial mafic and ultramafic rocks [21], including Indochina volcanic rocks [8, 22].

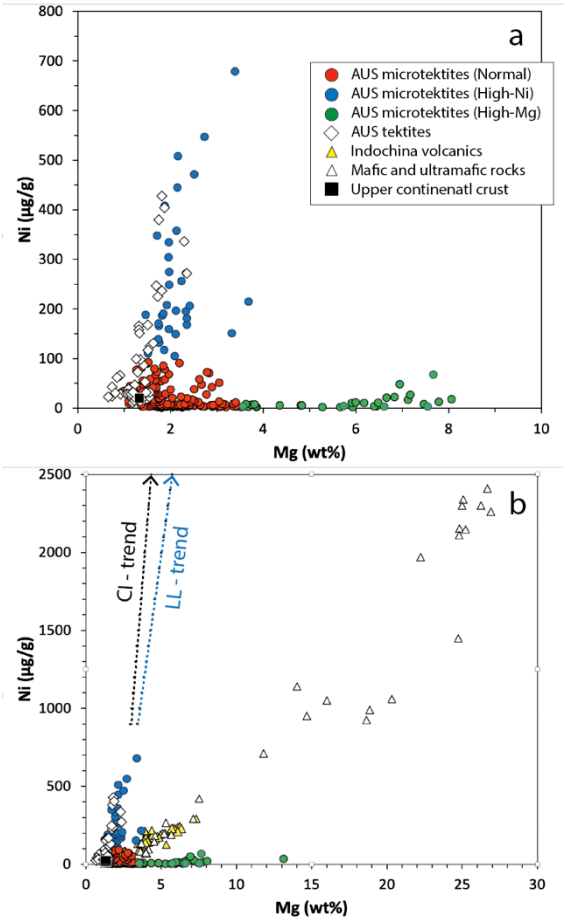

Tektites show a positive correlation between Ni and Mg (a) with Ni concentrations that are one order of magnitude higher than crustal values. High-Ni microtektites extend this trend, but Ni does not increase from crustal values with Mg in High-Mg (up to ~13 wt% Mg) microtektites. Terrestrial mafic and ultramafic rocks and Indochina volcanics show a positive relationship between Ni and Mg, but plot along a distinct

trend with a lower Ni/Mg ratio (b). The positive Ni vs Mg trend observed in tektites and High-Ni microtektites aligns along a mixing trend with chondrites, likely LL-chondrites.

Discussion: The relation between Mg and Ni concentrations provides conclusive evidence that Ni-rich component is a genuine signature of a chondritic impactor and not of a contribution of terrestrial mafic-ultramafic terrestrial target rocks. This strengthens our previous conclusion that the Australasian strewnfield was produced by the impact of a large asteroid, possibly of LL-chondrite composition [4].

The compositions of the High-Mg microtektites likely resulted from disequilibrium melting that prevented melt homogenization followed by melt fragmentation – a nugget effect. Note that Mg-rich microtektites are rare in the Australasian microtektite collection and that Mg-olivine and Mg-pyroxene grains, about the size of the microtektites themselves, are dominant mineral phases in ordinary chondrites. Moreover, the effects of compositional heterogeneity at the micrometer-size scale in the precursor are likely diluted in the large tektite sample volumes (several hundred mg up to some g in mass) analyzed by conventional emission spectroscopy or INAA.

Had the Australasian tektite/microtektite strewnfield generated by the impact of a LL-chondrite body, all the four known large impacts occurred on Earth around 1±0.2 million years ago were produced by stony asteroids with ordinary chondritic composition. Beside the Australasian strewfield, they include Bosumtwi (Ghana; 1.03 ± 0.02 million year old; 11 km in diameter [1]), Zhamanshin (Kazakhstan; 0.9 ± 0.1 million year old; 14 km in diameter [23]) Pantasma (Nicaragua; ~0.8 million years old; 14 km in diameter) [24].

Ordinary chondrite projectiles are responsible for a significant number of terrestrial impact craters [25]. This abundance could be related to the original position of their parent bodies close to the main resonance in the inner part of the Main Asteroid Belt which generates a bias in the impactor population towards inner main belt objects. However it would be intersting to explore if the high incidence of large impactor of ordinary chondritic composition around 1 million years ago was simply background flux or the result of a dynamic process in the Main Asteroid Belt.

References: [[1] Goderis S. (2013) In Impact Cratering - Processes and Products (eds. G. R. Osinski and E. Pierazzo). Wiley-Blackwell, Oxford, 223–239. [2] Jourdan F. et al. (2019) *Meteorit. Planet. Sci., 10,* 2573-2591. [3] Di Vincenzo G. et al. (2021) *GCA*, 298, 112–130. [4] Folco L. et al. (2018) *GCA, 222,* 550–568. [5] Ma P. et al. (2004) *GCA, 68*, 3883–3896. [6] Goderis S. et al. (2017) *GCA 217,* 28–50. [7] Shirai N. 2016) *LPS, 47th,* #1847. [8] Sieh K. (2019) *PNAS, 117(3)*, 1346-1353. [9] Gall L. et al. (2017) *GCA, 199*, 196–209. [10] Amare K. and Koeberl C. (2006) *Meteorit. Planet. Sci.*, 41, 107–123. [11] Mizera J. et al. (2016) *Earth-Sci. Rev. 154,* 123–137. [12] Son T. H. and Koeberl C. (2005) *Meteorit. Planet. Sci., 40,* 805–815. [13] Zak K. et al. (2019) *Meteorit. Planet. Sci.,* 54, 1167–1181. [14] Folco L. et al. (2008) *Geology*, 36, 291–294. [15] Folco L. et al. (2009) *GCA, 73*, 3694–3722. [16] Folco L et al. (2010) *EPSL, 293,* 135–139. [17] Folco L. et al. (2016) *Polar Sci., 10,* 147–159. [18] Brase L. E. et al. (2021) *Meteorit. Planet. Sci.*, 56, 829-843. [19] Soens B. et al. (2021) *Geosci. Front., 12,* 801153. [20] van Ginneken M. et al. (2018) *GCA, 228,* 81–94. [21] Condie K. C. (1993) *Chem. Geol., 104,* 1-37. [22] Hung K. T. (2010) *Ann. Soc. Geol. Pol., 80,* 185–226. [23] Mizera J. et al. (2012), *J. Radioanal. Nucl. Chem., 293,* 359–376. [24] Rochette P. et al. (2021) *Comm. E&E, 2,* 94. [25] Tagle R. and Berli J. (2008) *Meteorit. Planet. Sci., 43,* 541–559.

THE BRACHINITES AND BRACHINITE-LIKE UNGROUPED ACHONDRITES CONNECTION: INSIGHTS FROM SPINELS MINERAL-CHEMISTRY. Cuppone[1] T., Pratesi[1] G., Carli[2] C. . [1]Dipartimento di Scienze della Terra, Università degli Studi di Firenze, Firenze, Italy, [2]Istituto di Astrofisica e Planetologia Spaziali - INAF, Roma, Italy (tiberio.cuppone@unfi.it).

Introduction: Among primitive achondrites, brachinites are an olivine-rich meteorites group displaying equilibrated textures and homogenous mineral phase compositions [1]. Brachinite-like ungrouped achondrites (UAB) share many similarities with brachinites [2], although textural and compositional features allow to infer about a different origin for their parent body(ies) [3]. Both represent oxidized meteorite groups and their genetic relationship remains still unknown. In this work we have analyzed 4 brachinites, NWA 4969, NWA 6308, NWA 11756, NWA 12733, and 8 brachinite-like ungrouped achondrites, Al Huwaysah 010, Miller Range 090206-090405, NWA 5400 together with three of its paired (NWA 5363, NWA 6077 and NWA 6292) and NWA 6112. Two more samples are under analyses (the brachinite NWA 13489 and the UAB NWA 14635). For some of these meteorites, a wide literature exists (MIL206-405 and 5400's group), while for most of remaining few or none works are available. We performed a complete petro-mineralogic survey, focusing on spinels mineral-chemistry, in order to highlight potential relationships between the two achondrite groups. Spinel is a common accessory phase in terrestrial, lunar , martian and asteroidal ultramafic rocks. Moreover, being one of the first phase to crystallize (together olivine) from a basaltic magmas and allowing the incorporation of many multivalent cations (i.e. Fe, Cr, Mn, Ti, V) within its crystalline structure, can provide a useful tool for inspection of pristine source composition and its oxidation state.

Methods: Back-scattered electron (BSE) images and X-ray elemental maps on meteorite epoxy mounts, as well as electron microprobe analyses (EMPA), were acquired by means of Zeiss Evo MA15 (at the MEMA center of University of Firenze) and a JEOL-JXA 8230 (at LaMA, UniFI IGG-CNR). EMPA data were acquired on olivine, low and high-Ca pyroxenes, feldspar, troilite, chromite, kamacite and taenite. Mineral modal abundances were calculated using FIJI ImageJ2 tool [4]. Closure temperatures were determined using olivine-spinel and two-pyroxene thermometry, where both pyroxenes available. Oxygen fugacity were calculated from these closure temperatures, following Gardner-Vandy formulation [5].

Results: *Petrography and modal abundances*. All analyzed samples display equilibrated textures with well developed 120° triple junctions between silicate phases and mean grain size varying between 400-800 µm. Olivine is the major phase, with modal abundances from 60 to 92 vol% and Fa values spanning a wide range (17.5-34.3 mol%). High-Ca pyroxene (from 1.0 to 11.2 vol%) and spinel (from nearly 0 to 1.0 vol%) are invariably present. Low-Ca pyroxene is quite common (1.0-21.7 vol%), while plagioclase is rare (0.1-4.6 vol%). Cl-apatite and merrillite are common accessories. Sulphides and FeNi (from 4 to 20 vol%) alloys are ubiquitous although often altered. All samples display, even if with different degrees of development, the classical reduction rim bordering olivines, formed by low-Ca pyroxene and sulphide.

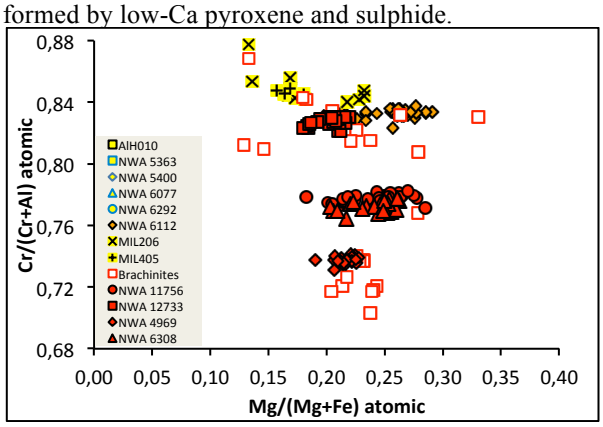

Fig 1 – #Mg and #Cr spinel compositions for brachinites and ungrouped achondrites brachinite-like

Mineral chemistry. Overall, analysed spinels cover a wide compositional range (#Cr=0.73-0.88 and #Mg=0.13-0.37), with UABs group spanning a narrower #Cr range (0.79-0.88), but wider in #Mg with respect to brachinites (Fig. 1).

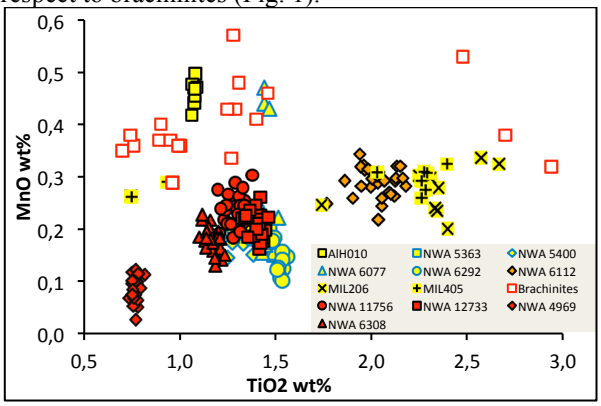

Fig 2 – TiO_2 vs MnO wt% plot for brachinites and ungrouped achondrites brachinite-like.

For many samples are well visible horizontal reduction trends (increasing #Mg for nearly constant #Cr), as described for ureilite chromites [6]. By plot-

ting spinel minor element contents (especially Ti, Mn and Zn), it is possible to separate the compositional fields for each meteorite (Fig. 2). Our brachinites display a good compositional match with brachinites described in literature, especially for some elements (Ti, V and Zn). Conversely, UABs display a noticeable chemical signature, which allow to distinguish between them and brachinites, with the exception of NWA 5400 pairing group, whose components overlap invariably with NWA 12733 brachinite.

Discussion: a first geothermometric analysis shows lower olivine-chromite equilibrium temperature with respect to what found in literature, although a direct comparison can be done for few samples owing to the paucity of thermometric data for brachinites/UABs. Consequently, our calculated oxygen fugacities are not directly comparable with what stated by other authors [3,5,7], but the obtained fO_2 values range is comparable, from IW-1.3 to -2.1 log unit, and, even more importantly there is a clear positive relationship between Fa olivine contents and the oxygen fugacity (Fig. 3).

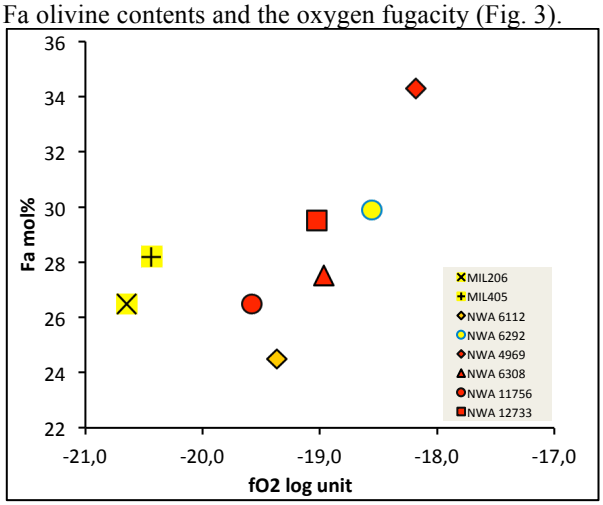

Fig 3 – fO_2 *vs Fa mol% wt% plot for brachinites and ungrouped achondrites brachinite-like.*

Future analyses: ICP-MS for bulk minor and trace elements and Cr isotopic systematics are in progress together with the complete petro-mineralogic characterization for the last two of our samples set (NWA 13489 and NWA 14635). For the future, we are planning in situ LA-ICP-MS analyses on spinels and XANES spectroscopy to determine valence of transition elements in order to constraint O_2 fugacity independently from the thermodynamic formulation.

References: [1] Keil K. (2014) *Chemie der Erde*, 74, 311–329. [2] Day J.M.D. et al., (2012) *Nature Geosc.*, 5, 614-617. [3] Crossley S.D. et al., (2020), *Meteoritics & Planet. Sci.*, 55, 1-23. [4] Schindelin et al., (2012) *Nature*, 9, 676-682. [5] Gardner-Vandy K.G. et al., (2013) *Geochimica et Cosmochimica Acta*, 122, 36-57. [6] Goodrich C.A. et al., (2014) *Geochimica et Cosmochimica Acta*, 135, 126-169. [7] Goodrich C.A. et al., (2017) *Meteoritics & Planet. Sci.*, 52, 949-978.

Acknowledgements: This work is supported by the ASI-INAF agreement n.2018-16-HH.0, OLBODIES project. We thank Natural History Museum Bern and the National Institute for Polar Research for the meteorite samples (AlH010 and MIL206/405 respectively).

PROTOPLANETARY DISKS AROUND SOLAR-ANALOGUES: FACTORIES OF PRE-BIOTIC MOLECULES?

C. Codella[1] and L. Podio[1]
[1] INAF, Osservatorio Astrofisico di Arcetri, Largo E. Fermi 5, 50127, Firenze, Italy

Scientific Context: About 4.5 Gyr ago, a molecular cloud turned into the Sun and its Solar System [1]. How have planets formed in the Solar System? And what chemical composition they inherited from their natal environment? Is the chemical composition passed unaltered from the earliest stages of the formation of the Sun to its disk and then to the planets which assembled in the disk? Or does it reflects chemical processes occurring in the disk and/or during the planet formation process?
A viable way to answer these questions is to observe protoplanetary disks around young Sun-analogues, and compare their chemical composition with that of the early Solar System, which is imprinted in comets [1]. The impacting images recently obtained by millimetre arrays of antennas such as ALMA provided the first observational evidence of ongoing planet formation in 0.1-1 million years old disks, through rings and gaps in their dust and gas distribution. The chemical composition of the forming planets and small bodies clearly depends on the location and timescale for their formation and is intimately connected to the spatial distribution and abundance of the various molecular species in the disk.

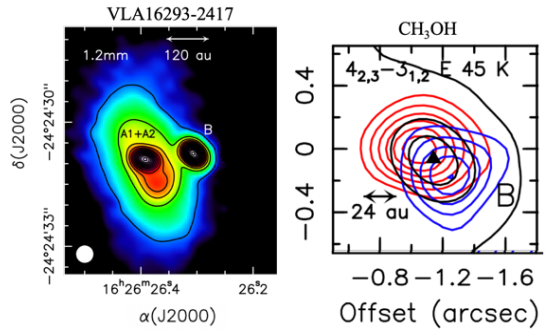

Figure 1. The VLA16293-2417 multiple protostellar system as imged in the context of the FAUST ALMA Large Program (adapted from [3]). Left panel: Continuum dust emission at 1.2mm showing the A1+A2 binary system surrounded by a circmbinary disk, and the B protostar. Right panel: Zoom-in around B: Spatial distribution of the red- and blue-shifted CH_3OH-E emission due to the $4_{2,3}$-$3_{1,2}$ transition revealing a disk rotating around the protostar (black triangle) on 50 au scale.

The chemical characterisation of the protostellar envelope, and, in particular of the protoplanetary disks is therefore crucial. A special attention has to be devoted to (i) the so-called interstellar Complex Organic Molecules (iCOMs, i.e. mainly O-bearing species with at least 6 atoms, such as CH_3OH, CH_3COH, and NH_2CHO), which are considered the building blocks of a pre-biotic chemistry, and (ii) smaller, molecular species essential for the iCOMs formation, such as HCOOH, and H_2CO.

The ALMA-FAUST and the ALMA-DOT projects: *We will present results on the chemical composition of protoplanetary disks based on two ALMA programs:*

1. the FAUST (Fifty AU STudy of the chemistry in the disk/envelope system of Solar-like protostars Large Program [2], which focuses on the ealiest phases (10^4-10^5 yr) of the Sun-analogues and their chemical diversity down to scales of 50 au, where planets are expected to form. The goal of FAUST is to investigate the variety of chemical composition of the envelope/disk system. Figure 1 shows as an example the image of CH_3OH emission rotating around the VLA16293-2417B protostar revealing the presence of a chemical rich accretion disk [3].

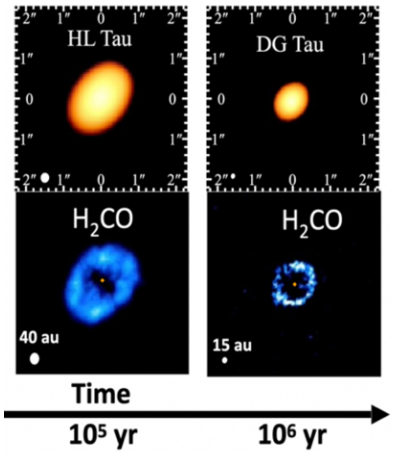

Figure 2. Example of observations sampling the chemical composition of protoplanetary disks with ages of 10^5-10^6 yr on Solar-System scale (10-40 au) using the ALMA interferometer in the context of the ALMA-DOT project [4,5].

2. the ALMA-DOT program (ALMA chemical survey of Disk-Outflow sources in the Taurus star forming region) focused on evolved disks [4,5], with an age of 10^5-10^6 yr. Thanks to the ALMA images at 20 au resolution,

ALMA-DOT recovered the radial and vertical distribution and abundance of, among others, simple organics (H_2CO and CH_3OH) which are key for the formation of prebiotic compounds. Enhanced H_2CO emission in the cold outer disk (see Fig. 2), outside the CO snowline, suggests that organic molecules may be efficiently formed in disks on the icy mantles of dust grain.

The chemical rich disk of HH212: Which are the next steps expected once the data obtained in the context of ALMA-FAUST and ALMA-DOT will be exploited? In other words, what happens when a disk is imaged at higher spatial resolutions, i.e. down to 10 au? A prototypical, so far unique, example is represented by the edge-on disk of about 10^4 yr around the HH212 protostar [6,7]. Several iCOMs, such as CH_3OH, CH_3CHO, and NH_2CHO, has been imaged with ALMA (Fig. 3). These species are clearly associated with the dust dik (orange scale in Fig. 3). A lack of emission is observed along the equatorial plane, plausibly due to the high opacity of the dust emission. On the other hand, a stratified distribution of the iCOMs is found, with the outer emission radius increasing from about 24 au for NH_2CHO, to 36 au for CH_3CHO, 40 au for CH_3OH, and finally to 48 au for H_2CO (see Fig. 3). Intriguingly, the increasing order of the outer emission radius of NH_2CHO, CH_3OH, and H_2CO is consistent with the decreasing binding energies of these species, supporting that they are thermally desorbed from the ice mantle on dust grains.

Conclusions: Thanks to the advent of high-spatial resolution and high-sensitivity telescopes such as IRAM-NOEMA and ALMA, we are living a golden age in astrochemistry. Several iCOMs are imaged in young (10^4 yr) accretion disks. On the other hand, the detection of iCOMs in evolved protoplanetary disks (with ages close to 1 Myr) is more challenging given that most of the molecules are frozen on ices in the disk midplane and only a relatively low column density remains gaseous. However, recent observations of CH_3OH in a few disks [5,8,9] announce that iCOMs will be revealed in protoplanetary disks in a close future. This paves the way to the comparison with the iCOMs abundances in objects of the Solar System, more specifically in comets, which are fossils of the primitive planetary system around our Sun.

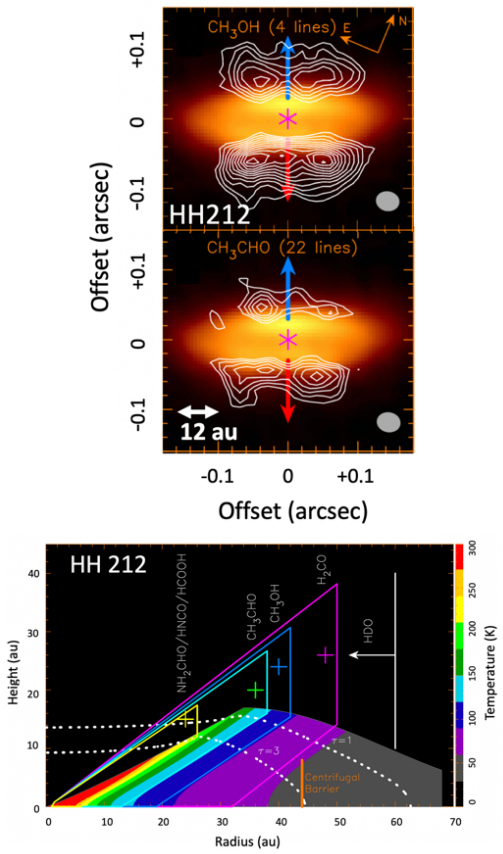

Figure 3. Spatial distribution of iCOMs as observed in the HH212 protostellar disk with ALMA on 10-12 au spatial scale [6,7]. *Upper panels:* CH_3OH and CH_3CHO (white contours) images overlayed on the dust continuum emission (orange). Blue and red arrows indicate the jet direction. *Lower panel:* Stratification of iCOMs (e.g. CH_3OH, CH_3CHO, and NH_2CHO), plotted on the temperature structure. The crosses mark the outer radius and vertical height as derived from the observations.

References: [1] Ceccarelli C., Codella C., Balucani N., et al. (2022) Chapter of the Protostars & Planets VII conference (arXiv:2206.13270) [2] Codella C., Ceccarelli C., Chandler C., Sakai N., Yamamoto S., & the FAUST team (2021) FrASS, 8, 227 [3] Codella C., Lòpez-Sepulcre, A., Ohashi, S., & the FAUST team (2022) MNRAS, 515, 543 [4] Podio L., Bacciotti F., Fedele, D. & the ALMA-DOT team (2019) A&A, 623, L6 [5] Podio L., Garufi, A., Codella, C., & the ALMA-DOT team (2020) A&A, 642, L7 [6] Lee C.-F., Codella C., Li, Z.-Y., Liu, S.-Y. (2019) ApJ, 876, L63 [7] Lee C.-F., Codella C., Ceccarelli C., Lòpez-Sepulcre, A. (2022) ApJ, 937, 10 [8] Walsh C., Loomis R.A., Öberg K.I., et al. (2016) ApJ, 823, L10 [9] Booth A.S., Walsh C., Terwisscha van Scheltinga J., et al. (2021) Nature Astronomy, 5, 684

KINEMATICS PERTURBATION IN THE PROTOPLANETARY DISK OF AS 209: SIGNATURE OF A GIANT PROTOPLANETS AT 100 AU

D. Fedele[1], F. Bollati[2] and G. Lodato[3] - [1]INAF, Osservatorio Astrofisico di Arcetri, L.go Fermi 5, 50125 Firenze, davide.fedele@inaf.it; [2]Dipartimento di Scienza e Alta Tecnologia, Università degli Studi dell'Insubria, Via Valleggio 11, 22100, Como; [3]Dipartimento di Fisica, Università degli Studi di Milano, Via Giovanni Celoria, 16, I-20133 Milano

Introduction: AS 209 is a Solar-like pre-main-sequence star in the Ophiucus star forming region at a distance of 121 pc from the Sun. The age of the star is estimated to be between 0.5 and 1.5 Myr. Interferometric observations of the millimeter dust continuum with ALMA revealed a characteristic ring-like structure with a 30 au wide dust gap centered at 100 au and multiple narrow dust rings inward of 50 au ([1],[2]). Figure 1 shows the ALMA continuum image at 870 μm. Such a structure hints at the presence of a giant protoplanet orbinting at 100 from the star. The characteristic ring-like structure is indeed a natural outcome of hydrodynamical simulations of disk-planet interaction. The planet hypothesis still lacks of a direct detection confirmation. Further support to the proposed scenario can come from the analysis of the disk velocity field as the presence of a giant planet is expected to perturb the gas kinematics. We report on a new analysis of the gas kinematics as traced by ALMA observations of the J=2-1 rotational transitions of ^{12}CO and ^{13}CO.

Results: The velocity maps of ^{12}CO and ^{13}CO obtained with ALMA show substantial devitation from a Keplerian profile. This can be seen in Figure 2 that shows one velocity channel of ^{12}CO emission line. The gas follows the Keplerian profile in the inner disk (for radial distances < 100 au) but not in the outer disk region. The veolicty deviations spread at all azimuths in a spiral-like shape.

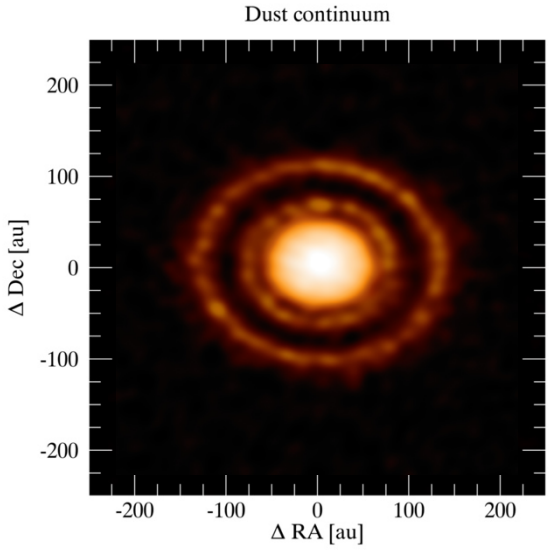

Figure 1: ALMA dust continuum image of AS 209. A prominent dust gap is detected at 100 au from the star. The gap is nearly 30 au wide (Fedele et al. 2018)

Remarkably, the ^{12}CO isovelocity curves in the southern region reveal a wiggling profile. Multiple mechanisms are able to produce such a velocity perturbation (or kink) in disks: gravitational instability (e.g., [3]), the vertical shear instability (e.g., [4]) and planet-disk dynamical interacion (e.g., [5]). The shape and the strength of the observed kink in AS 209 are not consistent with the first 2 hypothesis and the observations reinforce the embedded protoplanet hypothesis. These results point to the presence of an embedded planet that perturb the gas kinematics.

Analysis: To test the embedded planet hypothesis we compared the observed kink with semi-analytic model by [6]. The spiral wake induced by an embedded planet is mostly re gulated by the planet's mass (M_P) and by the disk scale height at the planet position (h_P = h/r) at the planet orbital radius r_P (e.g., Rafikov et al. 2002). The disk scale height is known from prvious analysis of the spectral energy distribution (h_P = 0.12). After testing different configurations, we imposed an orbital radius of 100 au, i.e. spatially coincident with the previously detected gap. The simulations of the semi-analytic models produce several of the observed findings. Based on our analysis we estimate a planet mass of a few Jupiter masses.

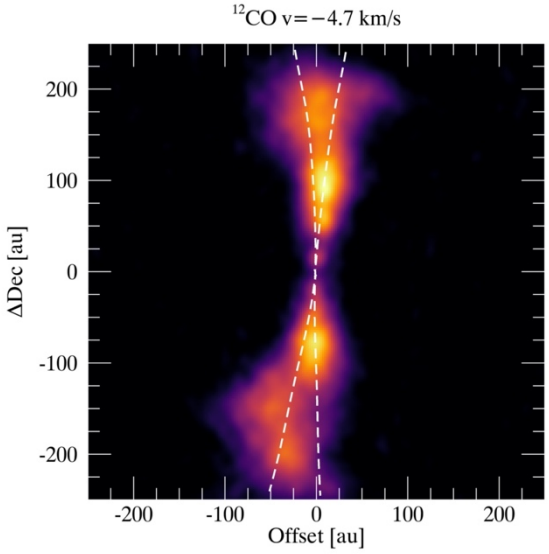

Figure 2: ALMA observations of CO J=2-1. The figure shows the velocity channel along the disk minor axis. The dashed lines indicate the expected Keplerian profile. A deviation from Keplerian profile is clearly detected (Fedele et al. submitted)

References:
[1] Fedele, D. et al. (2018), A&A, 610, 24
[2] Zhang et al. (2018) ApJ, 869, 47
[3] Longarini et al. (2021), ApJ, 920, 41
[4] Barraza-Alfaro at el. (2021) A&A, 653, 113
[5] Pinte et al. (2018), ApJ, 860, 13
[6] Bollati et al. (2021), MNRAS, 504, 5444
[7] Rafikov (2002), ApJ. 569, 997

BURIED FAULTS, SEDIMENTARY SEQUENCES AND PLAYA ENVIRONMENTS G. Schmidt[1], F. Salvini[1], E. Luzzi[2], A. T. Selepeng[3], and F. Franchi[3], [1]GeoQuTe Lab, Department of Science, Università degli studi Roma Tre, Rome, Italy genewalter.schmidt@uniroma3.it, [2]Bay Area Environmental Research Institute (BAERI), NASA Ames Research Center, Moffett Field, CA, USA, [3]Department of Earth and Environmental Science, Botswana International University of Science and Technology, Palapye, Botswana.

Introduction: Across the surface of Mars evidence of past lacustrine and evaporitic environments has been found within basins and craters, where often layered sedimentary deposits and hydrated minerals are observed. However, the intensity, duration and precise phases of aqueous processes during their deposition remain unresolved mostly for our inability to model subsurface structures. Although several geological processes and locations on Earth have been previously proposed as examples to describe these deposits on Mars, we lack a strong visualization of what water activity might have looked like during evaporitic stages within basins and craters. Here we propose to investigate the shallow subsurface of the Makgadikgadi Pans of Botswana as a potential analogue for understanding groundwater upwelling on Mars.

Purpose: The purpose of this work is to identify buried faults and areas of relative water saturation within the lacustrine sediment of the Makgadikgadi Pans by means of electrical resistivity surveys. This work represents the first electrical resistivity survey of the pan floor, which provides a framework of the relationship between faults, groundwater movement, and sediment thickness within infilled basins/craters on Mars. The hydrogeological processes active in the pans, may help to explain the formation of layered deposits and hydrated minerals on the surface of Mars, how they may have interacted with flowing water, and whether they might have hosted life.

Geological Setting: The pans are found within the Makgadikgadi Basin, a fault-boundeddepression located at the southwestern end of a northeast-southwest set of graben linked with the East African Rift [1] (Fig. 1A). The basin is an evaporitic environment rich in hydrated minerals and groundwater activity, and is infilled by a sedimentary succession of basal conglomerates and gravels are commonly overlain by clay beds and sandstones capped by unconsolidated sands [2].

On Mars, specific locations proposed as ideal analogs to the Makgadikgadi Pans are Oyama crater (Fig. 1B), Becquerel crater (Fig. 1D) and Meridiani Planum (Fig. 1C). These locations encompass an area of Mars where a regional paleo-hydrological system characterized by groundwater upwelling was sustanined for a signficiant period [3].

Methods: Electrical resistivity methods are applied for imaging faults previously identified with airborne geophysics and buried under lacustrine sediments to generate 2D Electrical Resistivity Tomography (ERT) [1]. This method allows the detection of low electrical resistance in void space produced by any faults and associated fractures in the overlaying water saturated sediment. Survey lines extend one kilometer in length and image 100-120 m of subsurface. Remote sensing techniques and satellite images were used to identifiy faults terminating at the pan shorlines, and identify regions of interest on Mars.

Discussion: Four ERT survey lines were placed over inferred faults (red circles Fig. 1A). Line C crosses the shoreline of the Ntwetwe Pan (Fig. 2). At the edge of the shoreline, the depth to bedrock drops 140 m (Fig. 2B) and at least 90 m in the ERT survey (Fig. 2D). This step matches with the vertical displacement of many of the Makgadikgadi Basin faults measured previously [4] and is thus considered to be a normal fault. A wedge of low resistivity (0.0 – 2.0 Ω·m) just below the surficial calcrete, probably indicates ingression of pan saline water in the drier shoreline sediments on the hanging wall side (Fig. 6D). The high resistivity values of the Karoo Supergroup here (30.0 – 200 Ω·m) are strikingly apart from the low <1.0 Ω·m values of the sediment infill (i.e. Makgadikgadi Group).

Areas within Arabia Terra have similar features, particularly the abundance of sedimentary infill and faulting (both observable and buried). Oyama crater (Fig. 1B) has a large N-S striking fault that cuts across it. On the hangingwall surface of the fault, in the center of Oyama, clay mineral signatures were identified [5]. Becquerel crater (Fig. 1D) was proposed to have had a protracted water level due in part to discharged water from buried faults, and also has clay and hydrated sulfate mineral signatures [6]. Furthermore, abundant silcrete (i.e. duricrust) in the area of ERT survey line D formed from groundwater processes and may be related to opaline deposits found on the floor of Becquerel crater [6]. Southwest from Arabia Terra (Fig. 1C), Meridiani Planum was proposed to have been the site of extensive fluid expulsion [3].

References:

[1] Schmidt G. et al. (2022) *Tectonophysics*, 229678. [2] Haddon I. G., & McCarthy T. S. (2005) *Jour. African Earth Sci.* 43(1-3). [3] Andrews□Hanna, J. C. et al. (2010) *JGR: Planets*, 115(E6). [4] Eckardt F. D. et al. (2016) *Quat. Intl.,* 404. [5] Loizeau, D. et

al. (2012) *Plan. Space. Sci.,* 72. [6] Schmidt, G. et al. (2022) *JGR: Planets*, 127(9).

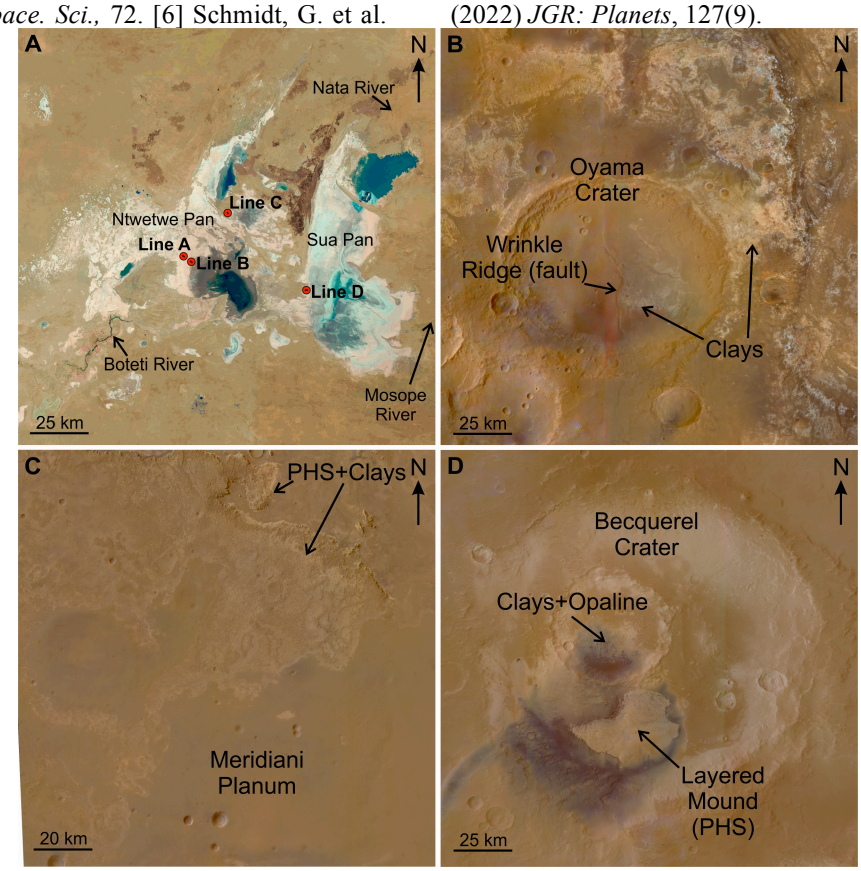

Figure 1. The Makgadikgadi Pans (Botswana) and several locations within Arabia Terra (Mars) that share various similarities. A) Landsat 8 images of the pans from October 2021 (-20.8°, 25.5°). Red circles indicate ERT survey line locations (Lines A, B, C, D). B) HRSC colorized mosaic of Oyama crater (23.5°, -20.1°) with the central wrinkle ridge and regions of clays (Loizeau et al., 2012; 2015; Tanaka et al., 2014). C) HRSC colorized mosaic of Meridiani Planum (-0.8°, 0.9°) with areas of hydrated minerals indicated (Flahaut et al., 2015). D) HRSC colorized mosaic of Becquerel crater (-8.0°, 21.5°) with areas of hydrated minerals indicated (Schmidt et al., 2022a).

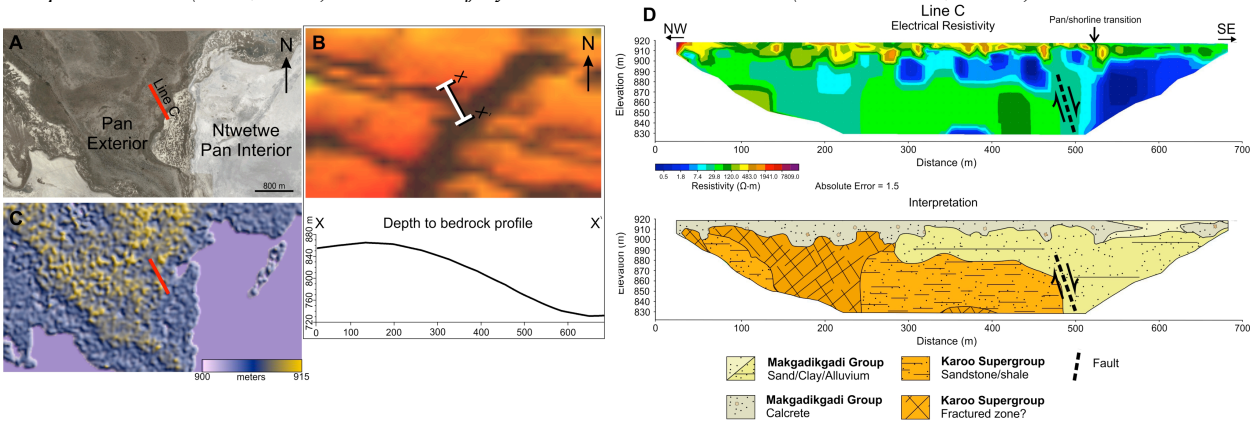

Figure 2. Example of an ERT survey interpretation. A) Location of ERT survey line C. B) Aeromagnetic depth to bedrock C) Surface topography. D) ERT profile of line C and stratigraphic interpretation. Line C shows the shore-line transition between the pan exterior (NW) and pan interior (SE).

METHANE ON MARS: POSSIBLE GEOMORPHIC INDICATORS OF METHANE EMISSION IN THREE IMPACT CRATERS. E. Mariani[1] and P. Allemand[1], [1]Université Claude Bernard Lyon 1, LGL-TPE, France (elettra.mariani@unich.it)

Introduction: From 1999 methane was detected in the atmosphere of Mars through terrestrial ground-based observations, then from 2004 by the instrument PFS (Planetary Fourier Spectrometer) on board of Mars Express (from 2004). In 2012 NASA MSL mission's Curiosity rover also detected methane plume emissions in Gale crater. Other detections were realised by the ACS (Atmospheric Chemistry Suite) and NOMAD (Nadir and Occultation for MArs Discovery) on board of ESA-Roscosmos ExoMars Tracer Gas Orbiter in 2018 and after. After the Global dust storm in 2018 the concentration of methane decreased drastically (10 to 100 time lower [5]) and TGO stopped detecting it, as opposed to the Curiosity rover, which continues to this day to detect plumes of methane [8][9]. The topic stirs much debate in the scientific community, not only for its astrobiological implications but also regarding possible theories that reconcile current and past observations from the orbiters and the Curiosity rover [5][15]. In the attempt to bring some clarity the purpose of this work is to map possible paleoindicators of methane emissions, considering presence of possible reservoirs of methane in the subsurface of Mars active until now (i.e. Gale crater, Mars [14].

Methods: The aim of this study is to compare the geology and geomorphology three impact craters (Gale, Gusev and Vernal crater) in which methane has been detected from orbit and/or from ground. We draw geological and geomorphological maps using satellite and in situ hyperspectral data (for Gusev, Spirit - for Gale, Curiosity), as well as high-resolution Context Camera (CTX) and HiRISE images (MRO mission) were also considered. Digital Elevation Models (DEM) were calculated from the highest resolution images that are available.

Results: Fig. 1 shows the geomorphological map of Gusev crater (Mars) based on CTX, HiRISE and CRISM images in addition to Spirit rover observations in Columbus Hills area. This crater is located at the dicothomy boundary between north and south hemisphere of Mars. It is also filled with both volcanic sediments from Apollinaris Patera from north and fluvial-lacustrine sediments from Ma'adim Vallis from south. The potential candidate areas for fossil methane emissions are marked by Swollen terrain unit and Columbus Hills unit where besides mounds and knobbed terrain, it was detected opaline silica mineralogical traces that corresponds to possible methane indicators [11].

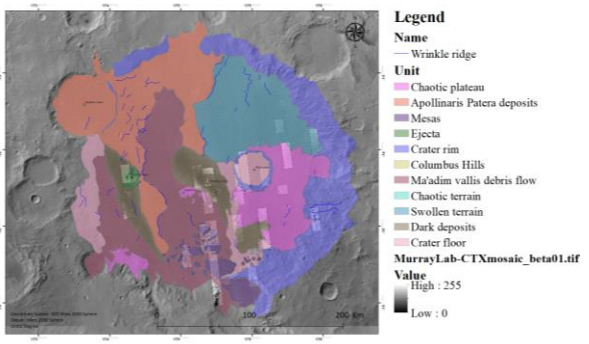

Fig. 1. Geomorphological map of Gusev crater (Mars).

A similar configuration units and paleo-geomorphological indicators have been found and mapped in Vernal crater (Mars) (Fig. 2). This crater is located in SW of Arabia Terra and by its configuration it's seems to be filled by volcanic deposits in the North and lacustrine deposits in the south [1].

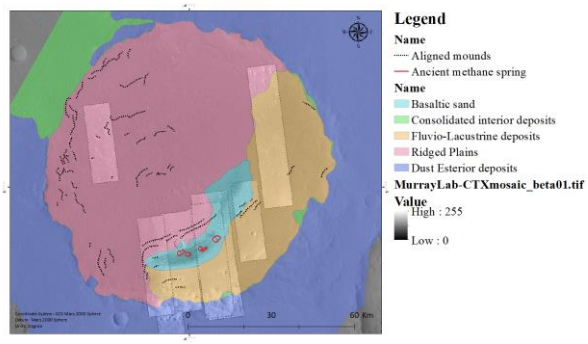

Fig. 2 Geomorphological map of Vernal crater (Mars) SW of Arabia Terra.

The division of these two environments is well delimited by allined mound that limits the volocanic deposits and well cemented basaltic sands which contains mounds feature-like (Fig. 3) that represents possible methane indicators for fossil methane emissions and traces of opaline silica materials. Unlike Gale crater (Mars) where there was and it is still detected methane spikes and presence of sulfates [6] [8], Gusev and Vernal crater (Mars) present similar units and mineralogical traces. Opaline silica, in fact, occurs in several locations on Mars and confirm the presence of aqueous environments. This trace is very important because it infers the possible interaction between water and mafic (Mg- and Fe-rich, silica poor) rocks which rapidly reacts with olivine and pyroxene (presence confirmed by CRISM images in the areas selected as possible methane spots for ancient emissions in Gusev and Vernal crater, Mars) and it could have been precipitated in hydrothermal or lacustrine evaporitic environment, which

corresponds to the past environments found in these two impact craters (Gusev and Vernal crater) [2].

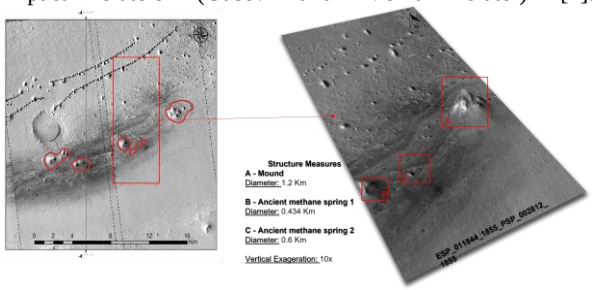

Fig. 3. Digital Elevation Model (DEM) of a stereo pair HiRISE ESP_011844_PSP_002821_1855 of mounds that have been classified as ancient methane spring also by Allen C.C. et al., 2007.

In this project it was also mapped Gale crater (Mars), in order to try to compare and understand the difference between ancient methane spikes (which mechanism was responsible for mound structure-like formations and developmente of all the past detections of methane in the atmosphere of Mars) and recent emissions of methane (registered in Gale crater by the rover MSL Curiosity). The area of Fig. 4 is where the MSL (Mars Science Laboratory) rover Curiosity's TLS (Tunable Laser Spectrometer) detected methane spikes until now. Gale crater (Mars) is located in a deep fault potential area due to it's closeness to the dichotomy boundary between north and south hemisphere and from its composition surface consisting mostly of sulfates.

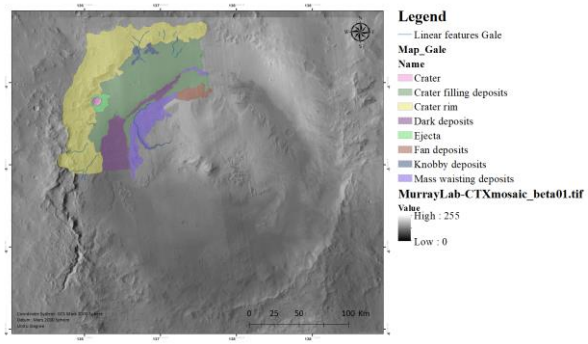

Fig. 4 Geomorphological map of methane spike emissions area delimited by Luo et al., (2021) from MSL rover detections from 2021 until nowadays.

This configuration could allow the presence of a methane reservoir formed in the past (when there were conditions that allowed the formation of this hydrocarbon gas) that over time, unlike other spots such as Gusev and Vernal crater has not been depleted; but on the contrary continues to gradually emit methane. These emissions occur mainly at night [15] and then disappear during the day. This may be explained by a near-surface production is occurring widely across Mars, it must be accompanied by a fast methane destruction or sequestration mechanism, or both. [13][15]. Both of these possibilities are already the subject of new studies to try to solve this issue.

Moreover the area represent the extend of the methane spikes detected since nowadays and it's possible to see from the map (Fig. 4) that the morphologies and units are really similar to the ones found in Gusev and Vernal such as Dark terrains, Mounds and Knobby terrains. By the current studies made on this topic and the geomorphological and mineralogical analysis made in this research it it possible to hypothesize that methane was formed in the past on Mars and stored in reservoirs all over the subsurface. Two types of "methane emission spots" can be seen in this work: the first encompassing Gusev and Vernal crater (Mars), indicate spots where the methane reservoir in the Martian subsurface has been depleted over time and left fossil traces of minerals such as opaline silica and paleostructures such as mounds that allow us to reconstruct their geological history. The second type, concerns points such as Gale crater (Mars) where the reservoir has not been depleted, on the contrary it continues to emit methane that fails to exceed a certain limit in the Mars atmosphere to be detected even by orbiters around the planet due to some mechanism of instantaneous destruction of this gas in the atmosphere. Unfortunately, there is still not enough data to allow the solution of this puzzle, but from the minimal concentration of methane recorded from 2018 to date by TGO, it is possible to infer that there are multiple points such as Gale crater on the surface of Mars that still emit methane from subsurface reservoirs [6][7]. In addition, to conclude, it seems that for now, the MSL rover Curiosity in Gale crater (Mars) provides the ground truth limit for methane detections on Mars nowadays. While TGO measurements provides the boundary conditions for methane detections in the atmosphere of Mars.

References: [1] Allen C.C. et al., (2007). [2] Encrenaz et al., (2008) *Advances in Space Research., 42(1),* 1-5. [2] Hauber E. et al., (2011) *Encyclopedia of Astrobiology. Springer, Berlin, Heidelberg.* [4] Komatsu G. et al., (2011) *Planetary and Space Science, 59 (2-3), 169-181.* [5] Korablev O. et al. (2019) Nature, 568(7753), 517–520. [6] Luo et al., (2021) *Earth and Space Science, 8, e2021EA001915* [7] Max M.D. et al., (2013). *Energy Resources for Human Settlement in the Solar System and Earth's Future in Space (pp. 99–114).* [8] Moores et al., (2019) *Geophysical Research Letters, 46*(16), 9430–9438 [9] Oehler D.Z. et al., (2017) *Astrobiology, 17(12), 1233–1264.* [10] Pozzobon R. et al., (2019) *Icarus, 321, 938–959.* [11] Ruff S.W. et al., (2020) *Astrobiology, 20*(4), 475–499. [12] Skinner J.A. et al. (2009) Marine and Petroleum Geology, 26(9), 1866–1878. [13] Smrzka et al., (2021) *Chemical Geology, 580,* 120357. [14] Webster et al., (2020) *Astronomy & Astrophysics, 641,* L3. [15] Webster et aòl., (2021) *Astronomy & Astrophysics, 650,* A166.

Application of the Minimum Noise Fraction technique to Exomars/TGO-NOMAD LNO channel nadir data: SNR enhancement evaluation

Fabrizio Oliva[1,*], Emiliano D'Aversa[1], Giancarlo Bellucci[1], Filippo Giacomo Carrozzo[1], Luca Ruiz Lozano[6-7], Ozgur Karatekin[7], Frank Daerden[2], Ian R. Thomas[2], Bojan Ristic[2], Manish R. Patel[3], Jose-Juan Lopez-Moreno[4], Ann Carine Vandaele[2], Giuseppe Sindoni[5].

[1]IAPS/INAF, Rome, Italy. [2]IASB-BIRA, Brussels, Belgium. [3]School of Physical Sciences, The Open University, Milton Keynes, U.K. [4]IAA-CSIC, Granada, Spain. [5]ASI, Rome, Italy. [6]UCLouvain, Louvain-la-Neuve, Belgium [7]ROB, Brussels, Belgium.

*Corresponding Author, (fabrizio.oliva@inaf.it)

Introduction. The Nadir and Occultation for MArs Discovery (NOMAD, [1]) is a spectrometers' suite, on board the Exomars Trace Gas Orbiter (TGO) spacecraft, devoted to the characterization of trace gases in the Martian atmosphere. In particular, the infrared Limb, Nadir and Occultation (LNO) channel of NOMAD allows to acquire data in nadir observing geometry at high spectral resolution in the infrared spectral range (2.2 – 3.8 μm), hence probing the whole atmospheric column down to the surface. However, its data are characterized by a moderate/low signal to noise ratio (SNR), mostly limited by the instrument's operative temperature.

In this study we apply to LNO nadir data the Minimum Noise Fraction (MNF) technique ([2,3,4]), commonly exploited for surface features classification in remotely sensed hyperspectral imaging datasets ([2,5,6,7]), to test its effectiveness in enhancing the dataset SNR.

The MNF technique. The MNF algorithm consists of two consecutive Principal Component (PC) transforms (see [8] for a comprehensive review). The first PC transform, known as *noise whitening* process, projects the data in a space in which the noise is rescaled and decorrelated from the signal, producing a noise covariance matrix that has unit variance and no band-to-band correlations. The second PC transform projects back the *noise-whitened* data in the original space, providing eigenvalues for the data reconstruction that are ordered with increasing noise. This allows to discard the noisiest ones and obtain an enhanced SNR.

Synthetic dataset analysis. As first step of the analysis, we apply the MNF on a synthetic dataset in order to evaluate the theoretical performances of the technique on features on which we have control from a spatial, spectral and SNR point of view. For this test we build a spectral cube (i.e. an array of data with two spatial dimensions and a third spectral one) in which a spectral absorption band on a specific spectral channel, crafted as a Gaussian with given amplitude and width, is only located in a circular spatial region in which it has a radial gradient of intensity. Random noise is added to these spectra to simulate SNR values as low as 5, i.e. reproducing some of the most critical noise conditions in LNO data. By applying the MNF we define a criterion to derive an adequate number of eigenvalues for the data reconstruction. This consists in increasing this number until spectral artifacts, introduced by the MNF itself and deriving from casual correlation of the spectral fluctuations, are statistically reabsorbed in the reconstructed noise. Moreover, such a test allows to verify the spatial coherence of the reconstructed data, which preserve the radial gradient of the band's intensity present in the original dataset.

LNO dataset preliminary analysis. After the synthetic dataset validation, we evaluate the MNF performances on specific LNO spectral orders covering different wavelength ranges, in order to assess the SNR improvement for studies related to the Martian surface and aerosols/clouds (e.g. [9]) and to trace gases. We select orders 121 (3647 – 3676 nm), 134 (3293 – 3319 nm) and 189 (2335 – 2353 nm) covering diagnostic features of CO_2/HCl/HDO, H_2O/CH_4 and CO_2 ice/CO respectively.

A major difference with respect to the synthetic dataset case is that we cannot use the same criterion for the evaluation of the number of MNF eigenvalues, since it is not possible to know a priori if a spectral feature pertaining to a specific wavelength is present in a given observation and, hence, if it is a MNF spectral artifact or not. Therefore, while following the same concept, we update the criterion as follows. For each order we arrange the data as a stack of all available orbits, storing the noise (observations with incidence angle $\theta \geq 90^{o}$) in a separated spectral cube for the MNF noise statistics computation. Then, in order to have control on the MNF spectral artifacts, we add to the data cube a line of noise and increase the number of

eigenvalues in the reconstruction until the average SNR on this line's observations drops below 1.

The SNR gain we get in this preliminary analysis allows to spot H_2O lines in order 134 and to better characterize CO lines and CO_2 ice features in order 189. However, it is still not enough to spot HDO and HCl lines in order 121, or CH_4 lines in order 134.

Further investigation is planned to enhance the SNR gain and for the processing of different spectral orders covering other species' spectral signatures.

References. [1]Neefs, E., et al., 2015. *Appl. Opt. 54*, 8494–8520. **[2]**Green, A.A., et al., 1988. *IEEE Transactions on Geoscience and Remote Sensing, Vol. 26*, No. 1, pp. 65–74. **[3]**Lee, J.B., Woodyatt, A.S. and Berman, M., 1990. *IEEE Transactions on Geoscience and Remote Sensing, Vol. 28*, No. 3, pp. 295–304. **[4]**Boardman, J.W. and Kruse, F.A., 1994. *ERIM, Ed., Proc. 10th Thematic Conference on Geological Remote Sensing, San Antonio*, 407-418. **[5]**Amato, U., et al., 2009. *IEEE Geosci. Remote Sens. Lett. 2009, 47*, 153–160. **[6]**Bjorgan, A. and Randeberg, L.L., 2015. *Sensors 2015, 15*, 3362-3378. **[7]**Luo, G., et al., 2016. *Canadian Journal of Remote Sensing, 42:2*, 106-116. **[8]**Jolliffe, I.T., and Cadima, J., 2016. *Phil. Trans. R. Soc. A, 374*:20150202.20150202 **[9]**Oliva, F., et al., 2022. *Journal of Geophysical Research: Planets, 127*, e2021JE007083.

Acknowledgments. ExoMars is a space mission of the European Space Agency (ESA) and Roscosmos. The NOMAD experiment is led by the Royal Belgian Institute for Space Aeronomy (IASB-BIRA), assisted by Co-PI teams from Spain (IAA-CSIC), Italy (INAF-IAPS), and the United Kingdom (The Open University). This project acknowledges funding by the Belgian Science Policy Office (BELSPO), with the financial and contractual coordination by the ESA Prodex Office (PEA 4000103401, 4000121493), by Spanish Ministry of Science and Innovation (MCIU) and by European funds under grants PGC2018-101836-BI00 and ESP2017-87143-R (MINECO/FEDER), as well as by UK Space Agency through grants ST/V002295/1, ST/V005332/1, and ST/S00145X/1 and Italian Space Agency through Grant 2018-2-HH.0. This work was supported by the Belgian Fonds de la Recherche Scientifique—FNRS under Grant No. 30442502 (ET_HOME). The IAA/CSIC team acknowledges financial support from the State Agency for Research of the Spanish MCIU through the "Center of Excellence Severo Ochoa" award for the Instituto de Astrofísica de Andalucía (SEV-2017-0709). US investigators were supported by the National Aeronautics and Space Administration. Canadian investigators were supported by the Canadian Space Agency. Open Access Funding provided by Istituto nazionale di astrofisica within the CRUI-CARE Agreement.

WATER CYCLE AND AEROSOLS AT MARS WITH THE NOMAD SPECTROMETER ONBOARD EXOMARS TRACE GAS ORBITER. G. Liuzzi[1], G. L. Villanueva[2], S. Faggi[2,3], S. Aoki[4], A. C. Vandaele[5], and the NOMAD team. [1]Università degli Studi della Basilicata, Via dell'Ateneo Lucano 10, 85100 Potenza (PZ), Italy, giuliano.liuzzi@unibas.it, [2]NASA Goddard Space Flight Center, 8800 Greenbelt Rd., 20771 Greenbelt, MD, USA, [3]American University, 4400 Massachusetts Avenue, 20016 Washington DC, USA, [4]Department of Complexity Science and Engineering, Graduate School of Frontier Sciences, The University of Tokyo, 5-1-5 Kashiwanoha, Kashiwa, Chiba 277-8561, Japan, [5]Royal Belgian Institute for Space Aeronomy, 3 Avenue Circulaire, 1180 Brussels, Belgium.

Introduction: The science operations of the ExoMars Trace Gas Orbiter (TGO) began in April 2018, and since then a lot of scientific results have been obtained in particular by the two spectrometers onboard the spacecraft, namely the Atmospheric and Chemistry Suite (ACS) and the Nadir and Occultation for MArs Discovery (NOMAD [1], [2]), whose main objective is to provide a novel, complete view of the vertical structure of the atmosphere of Mars, from the lower troposphere to the upper mesosphere up to 150 km of altitude. In this work we focus on the achievements made using the NOMAD observations, with particular attention on the retrieval of the vertical distribution of aerosols, water vapor and the D/H ratio in water, which are documented in several publications to date.

Data and methods: We have collected all the NOMAD observations from April/2018 to June/2022 in Solar Occultation (SO) Geometry, which allow for the observation of the vertical structure of the atmosphere at very high vertical sampling (<1 km in most cases) at very specific locations. Within the course of 2 months, these observations cover most latitudes and thus enable global mapping of the properties of several atmospheric constituents. Each occultations lasts only a few minutes, yet can be made up of 50 to >1000 spectra, depending on the angle between the orbit and the surface. NOMAD is a grating spectrometer covering the spectral interval 2.2-4.3 μm, yet at each occultation it observes a specific set of diffraction orders, each one covering a narrow spectral interval (20-35 cm^{-1}), selected through a specific filter called the AOTF. The spectral response of the AOTF is quite complex, and together with the ILS and other properties of the SO channel, it has been exhaustively characterized and documented [3], [4]. Water vapor and HDO concentrations have been retrieved from a set of observations comprising several diffraction orders, in order to maximize both the spatial coverage and the sspectral accuracy of the retrieved information. Each spectrum has been analyzed independently of the others by an Optimal Estimation approach implemented via the use of the Planetary Spectrum Generator (PSG, [5], [6], and by accounting in full the instrumental calibration. To retrieve aerosol (namely dust, water ice, CO_2 ice and their particle sizes) we have resorted a different and more complex scheme, which is based on the aggregation of simultaneously measured diffraction orders, to build a broadband spectrum covering the largest spectral interval, and using PSG to retrieve the above mentioned properties. In total we have analyzed more than 8000 occultations and a total of ~5,000,000 spectra for H_2O and D/H, and a total of ~1,500,000 broadband spectra for aerosols, and obtained a full 2.5 Martian Years (MYs) climatology for these parameters, mostly in form of time vs. altitude, which we present in this work.

Results: The analyzeed data cover a global dust storm in MY34, which has dramatic effects over th vertical distribution of water vapor and water ice. Water vapor shows very complex structures during the dust storm, being detectable at altitudes up to 120 km. There are also many other structures associated to the reinforcement of the meridional circulation at Ls 280, which result in temporary enhancements of the water vapor content at high southern latitudes [4], [7]–[9]. The D/H shows similar interesting patterns, and is an excellent indicator of the altitude of the hygropause: the analysis conducted in this work hass in fact demonstrated that the H fractionation in the atmosphere of Mars is mostly controlled by Rayleigh distillation up to 70 km of altitude, and the retrieved D/H evidences this trend, with a variability that depends on the rate of H_2O condensation and cloud formation. This is confirmed by the independent retrieval of water ice, which is shown to follow the patterns of water and D/H. During the MY34 global dust storm, water ice clouds are observed to dramatically vary in structure, and the altitude at which they form has been seen to increase up to 110 km [10]. We have evidenced the interplay between dust and water ice, and shown that there exist a direct relation between the particle sizes of water ice crystals f mesospheric clouds and the amount of water vapor available in the upper atmosphere. We also show the details of the seasonal cycle of water ice abundance, particle sizes and altitude. Finally, we will show the first detections of CO_2 ice clouds. While those are, in the big picture, unrelated to the water cycle, their spo-

radic detection with NOMAD [11] has been useful to reveal exotic dynamics, which sometimes involve water ice [12]. We will show how NOMAD detections are useful to put to the test current cloud formation theories and how they inform microphysical models in terms of the interplay between different aerosols.

References:

[1] A. C. Vandaele *et al.*, "NOMAD, an Integrated Suite of Three Spectrometers for the ExoMars Trace Gas Mission: Technical Description, Science Objectives and Expected Performance," *Space Science Reviews*, vol. 214, no. 5, Aug. 2018, doi: 10.1007/s11214-018-0517-2.

[2] E. Neefs *et al.*, "NOMAD spectrometer on the ExoMars trace gas orbiter mission: part 1—design, manufacturing and testing of the infrared channels," *Applied Optics*, vol. 54, no. 28, p. 8494, Oct. 2015, doi: 10.1364/AO.54.008494.

[3] G. Liuzzi *et al.*, "Methane on Mars: New insights into the sensitivity of CH4 with the NOMAD/ExoMars spectrometer through its first in-flight calibration," *Icarus*, vol. 321, pp. 671–690, Mar. 2019, doi: 10.1016/j.icarus.2018.09.021.

[4] G. L. Villanueva *et al.*, "The Deuterium Isotopic Ratio of Water Released From the Martian Caps as Measured With TGO/NOMAD," *Geophysical Research Letters*, vol. 49, no. 12, p. e2022GL098161, 2022, doi: 10.1029/2022GL098161.

[5] G. L. Villanueva, M. D. Smith, S. Protopapa, S. Faggi, and A. M. Mandell, "Planetary Spectrum Generator: An accurate online radiative transfer suite for atmospheres, comets, small bodies and exoplanets," *Journal of Quantitative Spectroscopy and Radiative Transfer*, vol. 217, pp. 86–104, Sep. 2018, doi: 10.1016/j.jqsrt.2018.05.023.

[6] G. L. Villanueva *et al.*, *Fundamentals of the Planetary Spectrum Generator*. 2022. Accessed: Jun. 07, 2022. [Online]. Available: https://ui.adsabs.harvard.edu/abs/2022fpsg.book...V

[7] A. C. Vandaele *et al.*, "Martian dust storm impact on atmospheric H 2 O and D/H observed by ExoMars Trace Gas Orbiter," *Nature*, p. 1, Apr. 2019, doi: 10.1038/s41586-019-1097-3.

[8] S. Aoki *et al.*, "Water Vapor Vertical Profiles on Mars in Dust Storms Observed by TGO/NOMAD," *Journal of Geophysical Research: Planets*, vol. 124, no. 12, pp. 3482–3497, 2019, doi: 10.1029/2019JE006109.

[9] S. Aoki *et al.*, "Global Vertical Distribution of Water Vapor on Mars: Results From 3.5 Years of ExoMars-TGO/NOMAD Science Operations," *Journal of Geophysical Research: Planets*, vol. 127, no. 9, p. e2022JE007231, 2022, doi: 10.1029/2022JE007231.

[10] G. Liuzzi *et al.*, "Strong Variability of Martian Water Ice Clouds During Dust Storms Revealed From ExoMars Trace Gas Orbiter/NOMAD," *Journal of Geophysical Research: Planets*, vol. 125, no. 4, Apr. 2020, doi: 10.1029/2019JE006250.

[11] G. Liuzzi *et al.*, "First Detection and Thermal Characterization of Terminator CO2 Ice Clouds With ExoMars/NOMAD," *Geophysical Research Letters*, vol. 48, no. 22, p. e2021GL095895, 2021, doi: 10.1029/2021GL095895.

[12] A. Määttänen *et al.*, "Nucleation studies in the Martian atmosphere," *Journal of Geophysical Research: Planets*, vol. 110, no. E2, 2005, doi: 10.1029/2004JE002308.

Structural mapping and stress analysis to unravel the polyphasic tectonic history of the Claritas Fossae, Mars

E. Balbi[1], P. Cianfarra, G. Ferretti, L. Crispini and S. Tosi[2], [1]Università degli studi di Genova, Dipartimento di Scienze della Terra dell'ambiente e della Vita (DISTAV), Corso Europa 26, 16123 Genova, Italy (evandro.balbi@edu.unige.it); [2]Università degli studi di Genova, Dipartimento di Fisica (DIFI), Via Dodecaneso 33, 16146 Genova, Italy

Introduction: The Claritas Fossae (CF) is an elongated, intricated system of scarps and depressions located to the south of Tharsis. It develops with a nearly N-S trend and exceeds 1000 km of length and 150 km of width (Figure 1).

Authors have proposed several tectonic settings to explain the origin of the CF, including local extensional, regional strike-slip and contractional settings [1-4]. In this way, the geo-tectonic framework of CF is still debated. In this work, we aim at providing new clues about the formation and evolution of the CF by a geostatistical analysis of the mapped morphotectonic structures. We show the preliminary results of the inversion method to find the stress (σ_1, σ_2, σ_3) that likely generated the mapped structures and possibly suggests a poly-phased tectonic history at the CF.

Methodology: The structural mapping was conducted through photo-geologic interpretation of satellite image mosaics to identify the regionally sized morphotectonic structures (orders of tens to hundreds of km) outcropping in the study area. We used subsets of the study area extracted from two different datasets: the *Mars MGS MOLA - MEX HRSC Blended DEM Global v2* and the *THEMIS Day/NightIR Controlled Mosaic v2*. These datasets represent the best compromise between resolution of the images and scale of the targets, allowing us to filter out faint structures with limited dimensions. In GIS environment (QGIS 3.18_Zurich) we further processed and enhanced the original dataset through *ad hoc* image processing tools. We prepared eight shadow images according to as many lightening conditions (every 45° of azimuth and common elevation of 45°) from the original MOLA DEM. This allows reducing the bias due to a single direction of the light that tend to enhance the visibility of structures nearly perpendicular to the synthetic lighting direction and to reduce those trending nearly parallel [5]. We also performed tone contrast enhancement by look-up-table stretching and applied High-pass Laplacian filters to the shadow images [6] and to the THEMIS Day/Night IR subset.

Geostatistical analysis included: i) azimuthal analysis by polymodal Gaussian fit [7] to identify the main azimuthal trends; ii) spatial analysis of the found azimuthal trends [8] to quantify the regional rotations; and iii) sinuosity computation (quantified as the ratio between the length of the feature and the Euclidean distance between its tips) to cluster the mapped faults and fractures into sets.

Eventually, the stress field has been derived through the Monte Carlo direct inversion method implemented in Daisy 3 software (freely available at https://host.uniroma3.it/progetti/fralab/Downloads/Daisy_App/) following the methodology described in [9]. This approach allows detecting the occurrence of one or more stress tensor that could be linked to the mapped structures. The inversion algorithm considers both fractures and faults. Slip data are necessary to constrain the stress tensor, but these are hardly achievable from remote sensing approach. Here we propose a method to infer the kinematic of the faults by the intersection between the main/master fault and the associated fractures. The software uses a convergent methodology [10] of fault and fracture inversion and provides the best attitude of the stress components with an estimate of the associated error [11]. This error is quantified by the MAD (mean angular deviation) factor. A solution with MAD higher than 30° is considered not reliable [12].

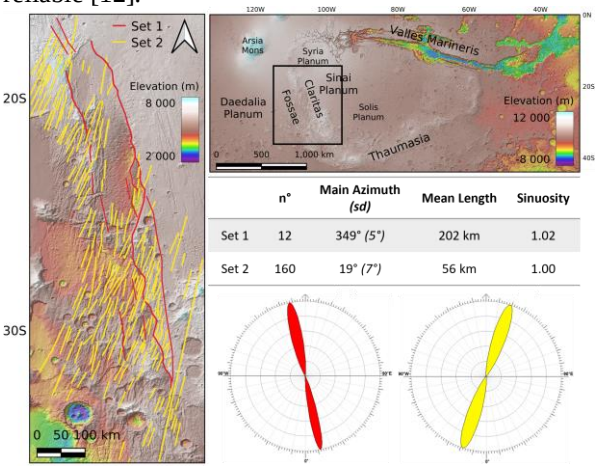

	n°	Main Azimuth (sd)	Mean Length	Sinuosity
Set 1	12	349° (5°)	202 km	1.02
Set 2	160	19° (7°)	56 km	1.00

Figure 1: Structural map of the CF with highlighted the two identified sets. Number of structures, main azimuth, mean length and mean sinuosity are shown in the table for both sets. Rose diagrams show the polynomial Gaussian fit of the azimuth by frequency (upper part of the rose diagram) and by cumulative length (lower part) for both sets.

Preliminary Results and Conclusions: Geostatistical analyses of the mapped structures showed the presence of 2 main azimuthal family sets in the study area (Figure 1). The first one (Set 1, red structures in

Figure 1) is characterized by main azimuth of 349°, mean length of 202 km, mean sinuosity of 1.02 (almost straight) and spatially cluster along a narrow NNW-SSE trending band (few km wide). Set 1 follows the steep swarm of scarps etching the topography at the eastern side of the CF. Within this deformation band, mapped structures often show en-echelon pattern with left stepping. This spatial arrangement suggests a strike-slip component associated to the main regional deformation band. We consider the structure of Set 1 as the surface expression of a regional/crustal fracture zone (e.g., the envelope of main and secondary faults with their associated damage zones) characterized by a strike-slip component of its kinematic history. The second system (Set 2, yellow structures in Figure 1) features a total of 160 structures, with a main azimuth of 19°, mean length of 55 km and mean sinuosity of 1.00 (straight). Although minor azimuthal rotation exists in the second family set (as quantified by the higher *sd* of the main peak), a nearly constant angular relationship between Set 1 and Set 2 exists along the entire length of the CF fracture zone (>1000 km) with an average value of 30°. If we consider the structures of Set 2 as fractures related to the strike-slip component of motion along the regional CF fracture zone, the value of 30° can be used to quantify the transtensional component along the CF by using the method proposed by [9] (Figure 2). In pure strike-slip setting the fractures develop at 45° from the main fault plane. In transpressional setting this angle increases and is >45° and becomes 90° for pure compressional kinematics. In transtensional setting the angle decreases and is <45° and becomes 0° in pure extensional fault kinematic [13]. In our study area, at the CF the measured angle between Set 1 (main fault/shear zone) and Set 2 (fractures) is 30° and suggests a right-lateral, strike-slip regime with 29% of Transtension (Figure 2).

Fault and fracture inversion looking for one stress solution provided a reliable solution with MAD = 6.5°, characterized by an extensional tectonic setting (vertical σ_1) with a NE-SW Shmax (σ_2) and a WNW-ESE Shmin (σ_3). An inversion looking after two solutions was performed as well and achieved results are reliable with an even smaller MAD of <4.5°. The two stress tensors suggest i) a right-lateral, strike-slip event (vertical σ_2) characterized by NNE-SSW trending Shmax (σ_1) and WNW-ESE trending Shmin (σ_3); ii) an extensional event characterized by an ESE-WNW trending Shmin (σ_3).

Refinement of the structural mapping and further analyses considering the cross-cutting relationships between the structures belonging to different family sets will support the identification of the relative chronology between the two tectonic events that likely affected the tectonic evolution of the CF.

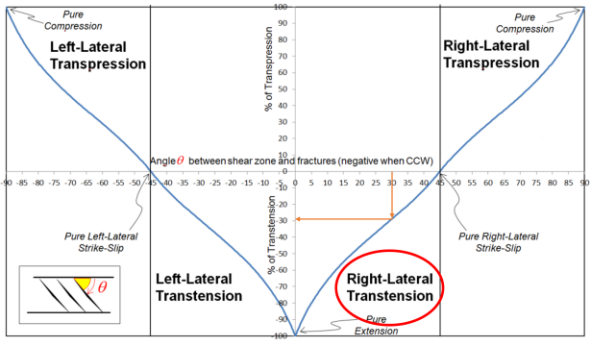

Figure 2: Diagram showing the angular relationship between the main shear zone and the related fractures (redrawn after [14]). Details in the text.

References: Use the brief numbered style common in many abstracts, e.g., [1], [2], etc. References should then appear in numerical order in the reference list, and should use the following abbreviated style:

[1] Hauber E. and Kronberg P. (2005) *JGR, 110*, E7. [2] Yin A. (2012) *Lithosphere 4(6)*, 553-593. [3] Dohm J. et al. (2018) *GSF, 9(4)*, 1085-1098. [4] Balbi E. et al. (2022) *EPSC2022-1041* [5] Wise D. et al. (1985) *GSA, 96(7)*, 952. [6] Drury S. A. (1987). Image interpretation in geology. [7] Cianfarra P. and Salvini F. (2016) *Rend. Fis. Acc. Lincei 27(19)*, 229–241. [8] Rossi C. et al. (2020) *J. Maps 16(2)*, 6-16. [9] Cianfarra P. et al. (2022) *Tectonics, 41(6)* [10] Tarantola A. (2005) Inverse problem theory and methods for model parameter estimation, SIAM [11] Cianfarra P. et al. (2022) *Geosciences, 12(2)*, 101. [12] Pinheiro M. R. and Cianfarra P. (2021) *Geosciences, 11(7)*, 270. [13] Cianfarra P. and Salvini F. (2015) *Pageoph, 172(5)*, 1185-1201. [14] Rossi C. et al. (2018) *Tectonophysics, 749*, 72–87

DID MARSIS FIND LIQUID WATER BENEATH THE MARTIAN SOUTH POLAR LAYERED DEPOSITS? R. Orosei[1], J. Baniamerian[2], G. Caprarelli[3], B. Cosciotti[2], S. E. Lauro[2], E. Mattei[2], E. Pettinelli[2], K. Primm[4], F. Soldovieri[5] and D. E Stillman[6], [1]Istituto Nazionale di Astrofisica (Istituto di Radioastronomia, Via Piero Gobetti 101, 40129 Bologna, Italy, roberto.orosei@inaf.it), [2]Università degli Studi Roma Tre, [3]University of Southern Queensland, [4]Planetary Science Institute, [5]Consiglio Nazionale delle Ricerche, [6]Southwest Research Institute.

Introduction: The Mars Advanced Radar for Subsurface and Ionosphere Sounding (MARSIS) was built to probe the Martian subsurface down to depths of kilometers by transmitting electromagnetic pulses in the MHz frequency range [1]. Echoes coming from a depth of about 1.5 km, stronger than surface reflections, were repeatedly detected in a 20 km wide area centered at 193°E, 81°S. Quantitative analysis of such echoes yielded values of the relative dielectric permittivity at the base of the South Polar Layered Deposits (SPLD) greater than 15, matching that of water-bearing materials [2].

Reanalysis of observations presented in [2], using signal processing procedures previously applied to terrestrial polar ice sheets, confirmed that the properties of MARSIS echoes match those of reflections from subglacial lakes, while the analysis of subsequent observations revealed the presence of other wet areas nearby [3]. Because of the very low temperatures expected beneath the SPLD, it was proposed that the waters are hypersaline perchlorate brines, known to form at Martian polar regions and thought to survive for an extended period of time on a geological scale at below-eutectic temperatures [3].

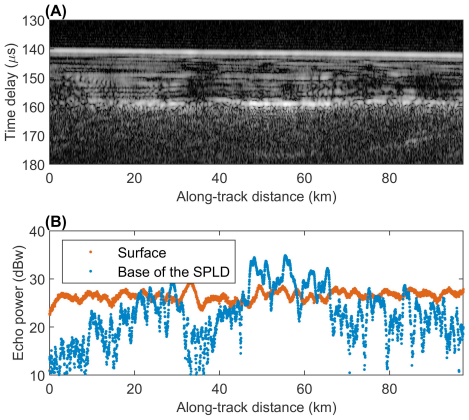

Fig. 1: (A) Radargram for MARSIS orbit 10737. The bottom reflector at about 160 μs corresponds to the interface between the SPLD and the bedrock. (B) Surface and basal echo power for the radargram in (A). Red dots mark surface echo power values, while blue ones mark subsurface echo power (from [2]).

Because of its significance in the study of the biologic potential of Mars, the identification of liquid water has been closely scrutinized by the scientific community at large, and several counter-arguments and alternative interpretations of MARSIS measurements have been proposed over the last four years. Here we aim at providing a summary of the existing literature on the topic, and at assessing the current status of the debate.

Points of Debate: Criticism of the identification of liquid water in MARSIS observations has been focused along four main lines of reasoning, namely that the base of the SPLD is too cold even for brines to survive over geologic time scales; that the geologic context of the area where strong echoes were detected does not support the presence of water bodies; that other materials can produce the same strong reflections seen in MARSIS data without the need for liquid water; and that certain geometric effects can result in exceptionally strong echoes through electromagnetic resonances.

Thermal State of the SPLD: One of the earliest comments to [2] is that it would take an unrealistically high heat flow from the interior of Mars to reach the temperatures needed by brines at the base of the SPLD. The model presented in [4] is based on the solution of Fourier's law of thermal conduction for constant surface temperature and SPLD thickness, for a thermal conductivity corresponding to either pure water ice or a mixture of water ice and up to 20% dust. They find that the minimum geothermal heat flux required to melt ice at the base of the SPLD is greater than 72 mW/m^2, several times the values expected for Mars. These findings were revisited in [5], by studying the effect of an added surface layer a few meters thick made of CO_2 ice and/or uncompacted water ice, and reaching the same conclusions presented in [4]. These studies, however, do not explore the effect of low-conductivity materials potentially present in the SPLD such as clathrates.

Geologic context: A first attempt to map subglacial topography and to compute the subglacial hydraulic potential surface was made by [6] using MARSIS data published in [2], which have a horizontal resolution of a few to several kilometers. They found that the high reflectance area did not coincide with any predicted lake location. A subsequent analysis of the surface above the bright reflector using infrared data and high-resolution images did not find evidence for surface modification linked to postulated lake locations

[7]. However, more recently [8] described an anomaly in the surface topography similar to those found above terrestrial subglacial lakes of comparable size. A similar finding was reported shortly afterwards by [9].

Dielectric properties of dry materials: The cause of strong echoes detected by MARSIS at the bottom of the SPLD is, in the interpretation presented in [2], the high relative permittivity of water-bearing materials, resulting in a high reflection coefficient. It has been alternatively proposed that other materials could cause strong reflections thanks to their high conductivity. According to [10], potential basal materials with suitably high conductivity include clays, metal-bearing minerals, or saline ice. Conductivity values reported in [10] had been measured at temperatures that are above those expected at the bottom of the SPLD, however. Shortly afterwards, [11] measured the dielectric properties of smectites at 230 K, finding values large enough to cause bright radar reflections. [12] noted however that the experimental setup used by [11] could be inadequate for measurements at low temperatures.

A comprehensive survey by [13], including published data, simulations, and new laboratory measurements, demonstrated that the dielectric properties of clay, hydrated salts, and saline ices do not generate strong basal reflections at MARSIS frequencies and Martian temperatures. More recent laboratory measurements found that a mixture of sediments and brines at 197 K with a salt-bulk sample concentration of about 6 wt% is capable of producing the echoes observed by MARSIS [14]. Gray hematite with a concentration of 33.2–59.0 vol% could also cause the observed radar returns, but require concentrations 2–3 times larger than anywhere currently detected [14].

Electromagnetic modelling: A survey of basal echo power over the entire SPLD by [15] found other locations of strong reflections exceeding surface echo power. Because some of them are located much closer to the surface, and thus at much lower temperatures, [15] conclude that their origin is not related to the presence of water. Similarly, an estimate of surface echo power in MARSIS observations over lava flows by [16] found scattered spots of high reflectivity that would produce echoes stronger than surface ones if they were located beneath the SPLD. It was already noted in [2] that bright basal echoes could result from the presence of a CO_2 ice layer on the surface, and indeed the brightest basal reflector found by [15] is known to be located below a CO_2 ice sheet. Further, the uncertainty in estimates of surface brightness presented in [16] is unknown.

Another possible mechanism to produce bright radar reflections at the bottom of the SPLD was recently proposed by [17], who employed a one-dimensional numerical model of electromagnetic propagation within a plane parallel stratigraphy to show that echoes from two or three CO_2 ice layers, each several meters thick and embedded in water ice at the bottom of the SPLD, could interfere constructively to produce the strong radar echoes seen by MARSIS. A thorough exploration of the parameter space of the numerical model used in [17] found however that no arrangement of CO_2 ice layers is capable of causing the strongest echoes detected by MARSIS, and that the decrease of echo power with increasing frequency observed in measurements could not be produced by the model [18]. Such decrease was explained by [19] as due to the presence of a significant fraction of dust within the SPLD, increasing attenuation and thus the basal permittivity needed to produce the observed echoes.

Summary: The current debate on the origin of bright radar echoes observed by MARSIS and originating at the bottom of the SPLD is yet to reach a conclusion, although some geologic evidence, all experimental work and most electromagnetic modelling favour the presence of brines, possibly as interstitial fluid in sediments. More work is needed to better constraint the thermal state of the SPLD, and more observations are required to characterize other bright basal reflectors found across the SPLD.

Acknowledgements: This work was supported by the Italian Space Agency (ASI) through contract ASI-INAF 2019-21-HH.0. This research has made use of NASA's Astrophysics Data System.

References: [1] Picardi G. et al. (2004) *Planet. Space Sci., 52,* 149-156. [2] Orosei R. et al. (2018) *Science, 361,* 490–493. [3] Lauro S. E. et al. (2021) *Nature Astronomy, 5,* 63–70. [4] Sori M. M. and Bramson A. M. (2019) *GRL, 46,* 1222–1231. [5] Egea-González I. et al. (2022) *Icarus, 383,* 115073. [6] Arnold N. S. et al. (2019) *JGR (Planets), 124,* 2101–2116. [7] Landis M. E. and Whitten J. L. (2022) *GRL, 49,* e98724. [8] Arnold N. S. et al. (2022) *Nature Astronomy, 6,* 1256–1262. [9] Sulcanese D. et al. (2023) *Icarus, 392,* 115394. [10] Bierson C. J. et al. (2021) *GRL, 48,* e93880. [11] Smith I. B. et al. (2021) *GRL, 48,* e93618. [12] Schroeder D. M. and Steinbrügge G. (2021) *GRL, 48,* e95912. [13] Mattei E. et al. (2022) *Earth and Planet. Sci. Letters, 579,* 117370. [14] Stillman D. E. et al. (2022) *JGR (Planets), 127,* e2022JE007398. [15] Khuller A. R. and Plaut J. J. (2021) *GRL, 48,* e93631. [16] Grima C. et al. (2022) *GRL, 49,* e96518. [17] Lalich D. E. et al. (2022) *Nature Astronomy, 6,* 1142–1146. [18] Orosei R. et al. (2022) *Icarus, 386,* 115163. [19] Lauro S. E. et al. (2022) *Nature Communications, 13,* 5686.

HIGH-RESOLUTION COMPOSITIONAL MAP AND SUBSURFACE INVESTIGATION OF A MARTIAN VALLEY CLOSE TO OLYMPIA PLANUM.

Pianeti e Satelliti – Analisi di superfici; Presentazione orale

N. Costa[1-2] (nicole.costa@studenti.unipd.it), M. Massironi [1-3], L. Penasa [1-3], J. Nava [1], R. Pozzobon [1-3], S. Ferrari [1-4].
[1] Geosciences Department of University of Padova, Via Gradenigo, 6, 35131, Padova, Italy
[2] Institute for Space Astrophysics and Planetology, IAPS-INAF, Via Fosso del Cavaliere, 100, 00133, Roma, Italy
[3] Observatory of Padova, OAPD-INAF, Vicolo dell'Osservatorio, 5, 35122, Padova, Italy
[4] Centre of Studies and Activities for Space, CISAS, Via Venezia, 15, 35131, Padova, Italy

Introduction:

The Martian Polar Caps stratification is well-visible along steep scarps at the edge of the caps, where layers are exposed by the blowing and erosion of katabatic winds [1]. In particular, the North Polar Cap stratigraphy proposed by Tanaka et al. was built on the interpretation of morphology and compositional-based data like MOC, CTX and CRISM [3], whereas Putzig et al. provided a radar-based polar stratigraphy [4].

In our study we selected a 140 km wide and 500 m high scarp in the North-Western part of the North Polar Cap, facing Olympia Planum, to carry out a throughout stratigraphic analysis (Figure 1). The exposed stratification is the upper part of finely-layered and laterally continuous sequence of icy and dusty strata, named North Polar Layered Deposits [2]. Its periodicity is the result of fluctuations in the ancient Martian climate due to orbital variations [2].

The aim of our work is to relate the composition and stratigraphy of the visible layered deposits with the subsurface radar reflectors, using data acquired by the NASA Mars Reconnaissance Orbiter instruments.

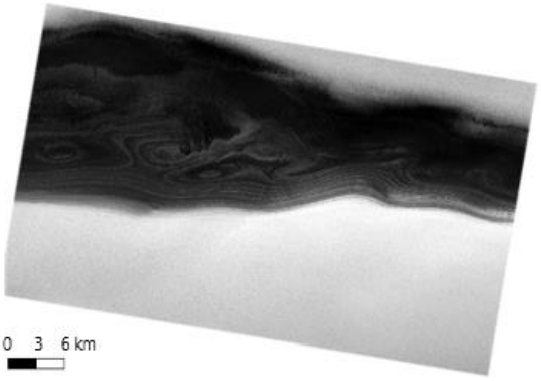

Figure 1. CTX image shows the study valley of the North Polar Cap.

Data selection:

We started with the surface image interpretation using data from the Context Camera (CTX) and the High Resolution Imaging Science Experiment (HiRISE). They allowed us to understand geomorphology and the stratigraphy of the study area. After that, we performed band ratios on a Compact Reconnaissance Imaging Spectrometer for Mars (CRISM) hyperspectral cube, followed by spectral analysis. Shallow Radar (SHARAD) was employed for interpretation of the polar subsurface.

Multi-score data-set made possible the junction of radargram-based stratigraphy with the stratification exposed along the scarp with its compositional variation.

Stratigraphy and composition:

The scarp investigated in this work displays two Tanaka et al. units: at the top Planum Boreum 3 unit and at the bottom Planum Boreum 1 [3]. The two units of different thickness (less than decameter thick and meters thick, respectively [3]) are composed of ice and dust, but in different amount. In particular, layers of the two units are composed by different amount of dry ice, water ice and basaltic dust [3].

According to Putzig, this stratification is part of the upper part of the radar-based packet-inter-packet sequence of Unit G [4].

Spectral analysis:

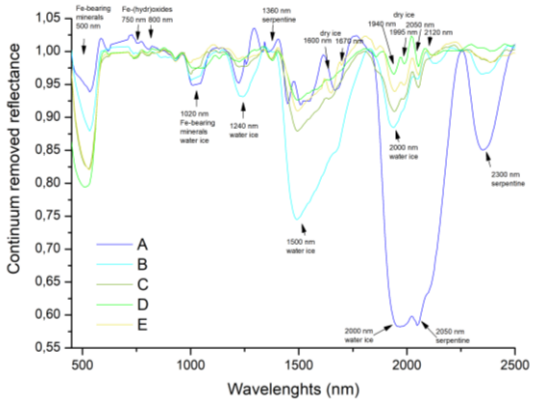

Figure 2. Spectra taken in representative areas within the study region. Continuum is removed.

Figure 2 shows five spectra obtained by spectral analysis done in the interesting part of the valley.

We distinguished three classes based on the similarity of the spectra:

1) spectrum A: shows absorption bands at 1, 1.5 and 1.95 μm, related to water ice;
2) spectra C, D and E: display multiple absorption bands at 1.65 and 2.06 μm with different depths but indicating a variable amount of CO_2 ice. All of them have weaker water-ice absorption bands with respect to A;
3) spectrum B: seems to be transitional between spectrum A and the three-spectra group.

Furthermore, all spectra present absorption bands corresponding to femic mineral and their alteration forms, like at 0.50 and 2.30 μm. These bands have different depths depending on groups previously mentioned: we registered a variable content of femic minerals in dry-ice-rich spectra (C, D and E) and aqueous alteration in spectra richer in water ice (A and B).

Spectral indexes:

CAT Analysis Toolkit (CAT) allow us to create spectral indexes and false colour images in order to underlie the presence and absence of specific categories of minerals, like ices (CO_2 or H_2O ice), femic minerals or phases and hydrated minerals.

An example of RGB is a false-colour image composed of:

- BDI1000VIS index in red to highlight presence of Fe-bearing minerals;
- BD1500_2 index in green to indicate water ice;
- BD1435 index in blue to show where dry ice is.

This work is essential to have an idea of the general composition of the area and have afterward driven the geological map drawing.

Geological Mapping:

CRISM and CTX data and their derivates (i.e. spectral indexes maps) are at the basis of our geologic and stratigraphic map because they provided morphological, compositional, albedo and stratigraphic information. In the map twenty-two subunits were found and they could be subdivided into five units:

- high-albedo and water-ice-rich unit (WI);
- unit composed of water ice and femic dust (WF);
- unit characterized by an alternation of pure-dry-ice layers and strata richer in femic minerals (DI and DF);
- surficial and relatively recent wind-transported sediments (aeolian deposits);
- landslides deposits produced by summer interstitial ice sublimation (gravitational deposits).

Correlation between geological units and radar reflectors:

At this point, we tried to correlate units represented in the geological map with radargram reflectors.

Usually, in radargrams, differences in signal reflectance are due to variations of the dielectric constant among layers. This is caused by different amount of water ice or dust: strong and bright signals for H_2O ice rich layer stacks, weak and dark signals for strata with a higher amount of dust [4] [6].

An example of correlation is reported in Figure 3 where the lines constitute lower contacts of the geological units. Dashed contacts are those that could not be correlated with surface data.

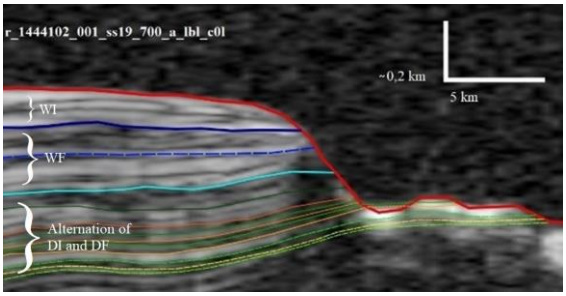

Figure 3. Correlation between geological units and radar reflectors. Vertical axis is in time.

Conclusions:

A detailed compositional analysis of exposed stratification in the Martian North Polar Cap has been carried out and correlated with the subsurface radargram layers.

Our work has also highlighted the variable content of femic dust and aqueous alterations in the icy layers.

Acknowledgments:

We acknowledge support from the EU's H2020 research and innovation program under grant agreement N° 871149 (GMAP).

References:

[1] Masse, M. et al. (2012), Earth and Planetary Science Letters, 317, doi: 10.1016/j.epsl.2011.11.035;

[2] Byrne, S. (2009), Annual Review of Earth and Planetary Science, 37, doi: 10.1146/annurev.earth.031208.100101;

[3] Tanaka, K. et al. (2008), Icarus, 196(2), doi: 10.1016./j.icarus.2008.01.021;

[4] Putzig, N. et al. (2009), Icarus, 204(2); doi: 10.1016/j.icarus.2009.07.034;

[5] Viviano-Beck, C. et al. (2014), Journal of Geophysical Research, 119(6), doi: 10.1002/2014JE004627;

[6] Lauro, S. et al. (2012), Icarus, 219(1), doi: 10.1016/j.icarus.2012.03.011.

The debate on the formation of large martian ripples.

H. Yizhaq[1], L. Saban[2], O. Vinent Duran[3], K. Kroy[4], K. Tholen[5], T. Pähtz[6] and I. Katra[7].
[1]Blaustein Institutes for Desert Research, Ben-Gurion University of the Negev, Sede Boqer Campus, 8499000, Israel (yiyeh@bgu.ac.il). [2]Geography and Environmental Development, Ben-Gurion University of the Negev, Beer Sheva, 8410501, Israel (sabal@post.bgu.ac.il). [3]Department of Ocean Engineering, Texas A&M University, College Station, TX, USA (oduranvinent@tamu.edu). [4]Institute for Theoretical Physics, Leipzig University, Leipzig, Germany (klaus.kroy@uni-leipzig.de). [5]Institute for Theoretical Physics, Leipzig University, Leipzig, Germany (tholen@itp.uni-leipzig.de). Institute of Port, Coastal and Offshore Engineering, Ocean College, Zhejiang University, 866 Yu Hang Tang Road, 310058 Hangzhou, China (tpaehtz@gmail.com). [7]Geography and Environmental Development, Ben-Gurion University of the Negev, Beer Sheva, 8410501, Israel (katra@bgu.ac.il).

Introduction:
Aeolian sand ripples formed due to the interaction between wind and loose sand and they are ubiquitous both on Earth and Mars. Terrestrial normal ripples forming in unimodal fine sand are quite small with wavelengths smaller than 30 cm and height in the order of 1 cm. Surprisingly, on Mars, these ripples are much larger with wavelengths of an order of 1-3 m and height of a few cm with smaller decimeter superimposed ripples (see Fig.1; [1-2]). Since the discovery of these large martian ripples, there is an ongoing scientific debate about their formation and two main theories have been suggested to explain their formation [3-5]. The first theory views the large martian ripples as impact ripples that grew larger due to the lower dynamic pressure on Mars [6]. It was shown by CFD simulations under typical martian atmospheric conditions that the shear stress over large ripples is lower than the fluid threshold needed to dislodge grains from the crests, thus enabling further growth of ripples [7-8]. As the spaces between the primary ripples become larger enough, smaller ripples can develop between them and migrate over windward slopes of the large ripples [6]. This hypothesis can explain the observed coexistence of small and large ripples [9]. Within this framework, the large ripples are a consequence of small ripples coalescence.

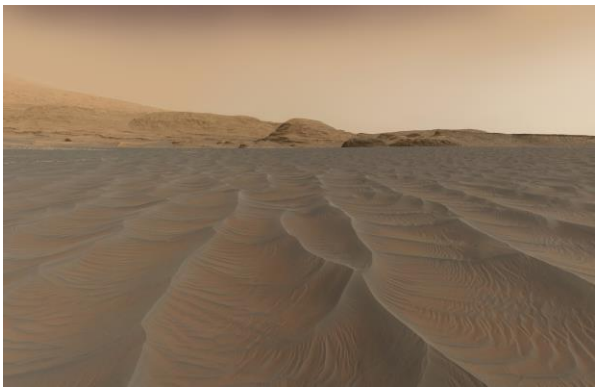

Fig. 1 Multi-scale ripples on Mars as imaged by the NASA MSL Curiosity rover in Gale crater. The wavelength of the large ripples is about 1.8 m with small impact ripples between them. The picture shows the amazing complexity of the pattern due to multidirectional wind and different formation mechanisms (https://an.rsl.wustl.edu/msl/mslbroser/an3.aspx).

According to the second theory, the large martian ripples are wind drag (fluid) ripples or hydrodynamic ripples that are similar to subaqueous ripples that form due to the large kinematic viscosity of the martian atmosphere. This hypothesis argues that these two ripple sizes have distinct size distributions and lack bedforms in the ~20–80 cm range, indicating two different formative mechanisms that can overlap [10]. According to the new model of Duran et al. [11], the large ripple form due to hydrodynamic instability and their size scale with the thickness of viscous sublayer ν / u_* where ν is the kinematic viscosity and u_* is the shear velocity. It is important to note that these large meter-scale ripples do not have crests covered with very coarse grains like terrestrial or martian megaripples, which their formation is attributed to the sorting mechanism and to the development of armoring layer at the crests [12-13]. However, in a recent study [5] it was found that the grains size distributions of the small and the large ripples are different. Large ripples observed by Curiosity in the Gale crater have larger sand grains than the smaller ripples. They concluded that the large martian ripples are more similar to terrestrial megaripples. This recent work indicates that we still lack a full understanding of the large martian ripples.

Here we present a detailed experimental study about the formation of impact and hydrodynamic ripples in a boundary layer wind tunnel for different grain sizes of sand. These results can shed light on the formation of the large martian ripples.

Methods: The aeolian experiments were performed using an open circuit wind tunnel at the Ben-Gurion University consisting of three parts: an entrance cone, a test section, and a diffuser [14]. The cross-sectional area of the tunnel is ~0.7 × 0.7 m and the working length is 7 m for measurements in the test section. The boundary layer in the wind tunnel is ~22 cm above the tunnel bed. Glass beads of three fractions have been used in the

experiments and their grain size distributions are shown in Fig. 2.

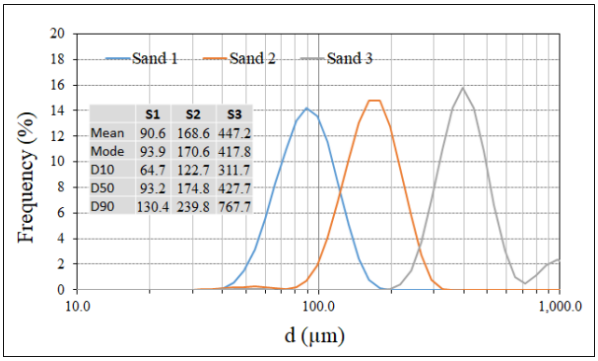

Fig. 2 Statistical analyses of sand samples (glass beads) used for the wind tunnel experiments, including grain size distribution with mean, mode, median (d_{50}), d_{10} and d_{90} as the values (grain diameters) where 10% and 90% of the population resides below this point, respectively.

Results: Fig. 3 shows the results of the size fractions Sand 1 and Sand 2 with $d_{50} = 90$ μm and $d_{50} = 170$ μm, respectively.

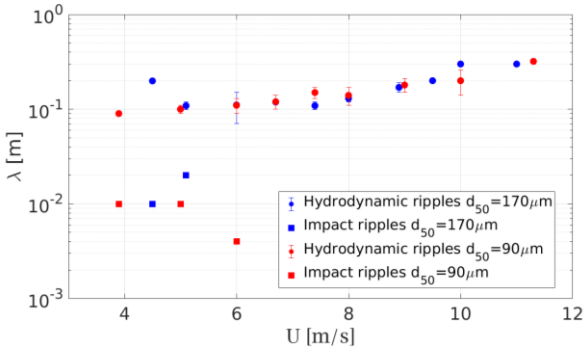

Fig. 3 The wavelengths of the impact ripples (squares) and hydrodynamic ripples (circles) as a function of the wind velocity (measured at 25 cm height) for the size fractions of $d_{50} = 90$ μm and $d_{50} = 170$ μm. The impact ripples exist only for low wind velocities. For the large fraction Sand 3 ($d_{50} = 447$ μm) only impact ripples formed.

Figs. 4 and 5 shows typical ripple patterns for the two size fractions developed during the wind tunnel experiments under two wind velocities.

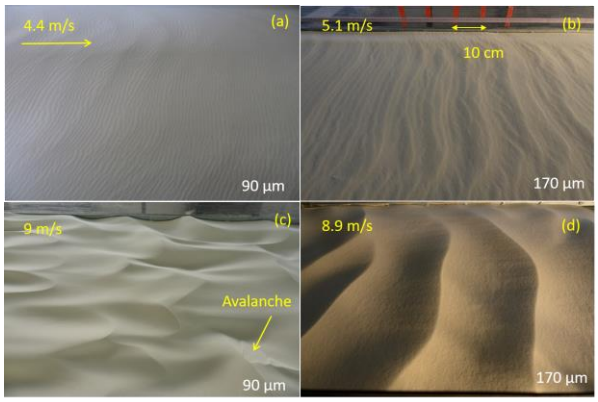

Fig. 4 Hydrodynamic ripples and impact ripples for $d_{50} = 90$ μm (a and c) and for $d_{50} = 170$ μm (b and d). For wind velocity of 9 m/s, the hydrodynamic ripples show a complex pattern similar to subaqueous ripples. For lower wind velocities, there is a coexistence of impact and hydrodynamic ripples as shown in Fig. 5 and has been observed on Mars (Fig. 1).

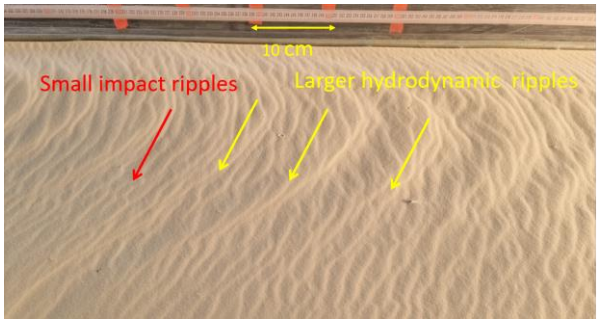

Fig. 5 Two size ripples. Coexistence of small impact ripples after 40 minutes ($\lambda \approx 1$ cm) and larger hydrodynamic ripples ($\lambda \approx 12$ cm). The wind velocity was 4.5 m/s from left to right ($d_{50} = 170$ μm). For larger wind velocities only the hydrodynamic ripples exist.

References: [1] Lapotre, M. G. A., et al., (2016) *Science*, 353, 6294, 55–58. [2] M. G. A., et al., (2018) *GRL*, 45, 10, 229-239. [3] Lorenz, R., (2020) *JGR Planets* 125, doi:10.1029/2020JE006658. [4] Lapotre, M. G. A., et al., (2021) *JGR Planets*, 126, e2020JE006729. [5] Gough et al., (2021) *JGR Planets* 10.1029/2021JE007011. [6] Sullivan et al., (2020) *JGR Planets* v. 125 no. e2020JE006485. [7] Simanovich et al., (2019) *JGR Planets 124*, (1), 175–185. [8] Yizhaq et al., (2021) *Planets* 126, e2020JE006515. [9] Yizhaq et al., 2022 Geociences, 12, 422. 10.3390/geosciences12110422 [10] Ewing et /https://doi.org al., (2017) *JGR Planets*, 122, 2544–2573. [11] Vinent Duran, O. et al., (2019) *Nat. Geoscience*, 12(5), 345–350. [12] Lämmel, M. et al., (2019) *Nat. Phys.* 14, 759–765. [13] Tholen, K. et al., (2022). *Nat.Comm.*https://doi.org/10.1038/s41467-021-26985-3 [14] Schmerler, E. et al., (2016) *Aeolian Research*, 22, 37-46.

Study of the dust lifting and electrification physics by means of martian analogues

G. Franzese[1] (gabriele.franzese@inaf.it), F. Esposito[1], F. Cozzolino[1], S. Silvestro[1], G. Mongelluzzo[1], C. Porto[1], C. I. Popa[1].
[1] *Osservatorio Astronomico di Capodimonte, Istituto Nazionale di Astrofisica, Napoli, Italy.*

Introduction:

Wind driven phenomena are the major factors able to shape martian surface. The planet boundary layer hosts indeed frequent dust storms and dust devils that leads to widespread sand mobilization and dust erosion. Dust so injected in the atmosphere plays a crucial role on the martian climate, remaining in suspensions even for weeks and regulating the atmospheric thermal gradient and surface albedo, due to the redeposition. For these reasons, martian landed missions are putting increasing efforts on the monitoring of near surface atmospheric conditions and dust activity, in order to determine the possibilities of the planetary climate to sustain present or past life.

The exact threshold conditions able to initiate the dust lifting process are still highly debated in literature, being the current modelling not completely in agreement with the high frequency of martian dust events. To solve these uncertainties new and more exhaustive surveys are needed, and terrestial data can be precious in this optics. As on Mars, dust storms and devils are indeed common phenomena also in the terrestrial arid areas. So far, despite the environmental differences (mostly in atmospheric pressure and composition), the scientific literature has confirmed a common lifting physics on the two planets. Terrestrial phenomena represent hence a good opportunity to increase our knowledge of the martian counterparts. Besides, on Earth dust lifting is always coupled with grain triboelectrification, that can lead to the formation of huge atmospheric electric fields. The same mechanism is expected to happen on Mars, where it could cause electric discharges, affecting the atmospheric composition and leading to local enhancement of oxidants (Atreya et al 2006). Hence, even if there is still no direct evidence of the presence of a martian electric circuit, due to the lack of a proper in situ instrumentation, dust electrification is expected to be the main atmospheric charging mechanism (Harrison et al. 2016). Laboratories and on field data indicate how the charge acquired from grains depends mainly on their composition and size distribution, however we still lack a general model able to predict the charge value and hence the E-field magnitude (Farrell et al. 2004; Zhang et al. 2018).

Along the past decade our team have acquired a vast experience in the study of terrestrial analogues of martian dust phenomena with numerous field missions in terrestrial deserts. In particular, different extensive campaigns have been developed in the Sahara Desert deploying a fully equipped meteorological station coupled with an environmental electric field and a dust concentration monitoring. These data represent some of the most comprehensive lifting process surveys and has given an empirical indication of how the dust storm E-field can act as a feedback on the lifting, potentially regulating the amount of airborne grains (Esposito et al. 2016). In addition, the data have allowed a preliminary characterization of the dust devil induced electric field (Franzese et al. 2018).

Franzese et al. 2018 has indeed showed how the E-field is one of the main recognizable features of the dust devil occurance: its magnitude is directly related to the rotatory and vertical wind of the vortex and to its core pressure drop, closely mirroring also the variation of the airborne dust concentration. However, the analysis was affected by a high uncertainty related to lack of knowledge of the distance of passage (impact parameter d) of the events from the station that led to a size/distance degeneracy of the results. For this reason, currently we are reanalyzing the acquired data to take into account of the impact parameter following the method suggested in Franzese et al. 2020.

Fig. 1 shows one of the preliminary results of this analysis, were the relation between the induced E-field and the core pressure drop (dP) has been corrected using the impact parameter d. Using the Rankine model to describe the dP trend ($\propto 1/d^2$), Fig. 1 suggests how the vortex charge configuration can be roughly described as a dipole distribution ($E \propto 1/d^3$).

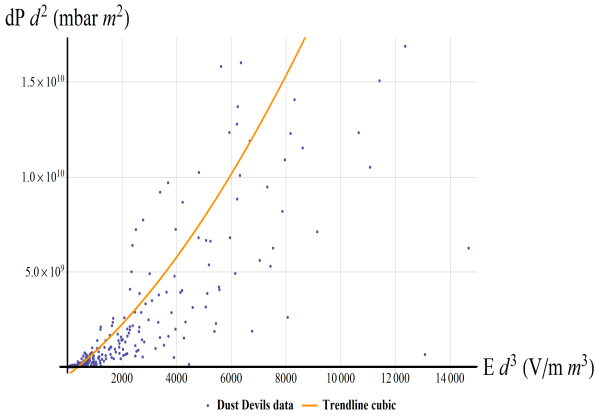

Fig. 1 Relation between the dust devil induced E-field and the core vortex pressure drop dP, taking into account the impact parameter d.

The authors are hence working on a dipole like model able to fit the acquired E-field time series to obtain information on the average charge per grain and the relative position of the positive and negative charge layer. Indeed, a proper characterization of the terrestrial phenomena represent the first fundamental step for the understanding of the martian counterparts. To complete fitful this purpose, new extensive field and laboratory surveys are required to improve the modeling of both lifting and electrification mechanisms. In this optics our scientific team foreseen further field missions for the study of lifting processes as part of the Earth Mars and Moon (EMM) proposal, to which we are members. Next missions aim to characterize the vertical profile on the charge distribution and electric field, taking measurements at different heights. EMM has been financed in the field of the PNRR programme.

Moreover, in this same view, our team have also proposed the Dust Charging Knowhow (DuCK) project that aims to improve the current saltation modelling including the contribution of the grain charging and external electric field. The DuCK project has been financed through the INAF mini grant programme, and will be achieved in collaboration with the colleagues of the Key Laboratory of Mechanics on Disaster and Environment in Western China (Lanzhou University).

References:

[1] Atreya, S.K., Wong, A.S., Renno, N.O., Farrell, W.M., Delory, G.T., Sentman, D.D., Cum-mer, S.A., Marshall, J.R., Rafkin, S.C., Catling, D.C., 2006. Oxidant enhancement in martian dust devils and storms: implications for life and habitability. Astrobiol-ogy6 (3), 439–450.

[2] Esposito, F., Molinaro, R., Popa, C. I., Molfese, C., Cozzolino, F., Marty, L., ... & Ori, G. G. (2016). The role of the atmospheric electric field in the dust□lifting process. *Geophysical Research Letters*, *43*(10), 5501-5508.

[3] Farrell, W.M., Smith, P.H., Delory, G.T., Hillard, G.B., Marshall, J.R., Catling, D., Cummer, S.A., et al., 2004. Electric and magnetic signatures of dust devils from the 2000–2001 MATADOR desert tests. J. Geophys. Res., Planets109 (E3).

[4] Franzese, G. et al. (2018) Electric properties of dust devils. *Earth and Planetary Science Letters*, 2018, 493: 71-81.

[5] Franzese, G., et al. (2020). Resolution of the size/distance degeneracy of the dust devils signals observed with a stationary meteorological station. *Aeolian Research*, *44*, 100594

[6] Harrison, R. G., Barth, E., Esposito, F., Merrison, J., Montmessin, F., Aplin, K. L., ... & Zimmerman, M. (2016). Applications of electrified dust and dust devil electrodynamics to Martian atmospheric electricity. *Space Science Reviews*, *203*(1), 299-345.

[7] Zhang, H., & Zheng, X. (2018). Quantifying the large-scale electrification equilibrium effects in dust storms using field observations at Qingtu Lake Observatory. *Atmospheric Chemistry and Physics*, *18*(23), 17087-17097.

A preliminary study of Ganymede's energetic ion environment to be investigated with JUICE. C. Plainaki[1,2], S. Massetti[2] , X. Jia[3] , A. Mura[2], E. Roussos[4], A. Milillo[2] and D. Grassi[2], [1]Agenzia Spaziale Italiana –ASI, Via del Politecnico, 00133, Rome, Italy christina.plainaki@asi.it, [2]INAF-IAPS, Via del Fosso del Cavaliere 100, 00133, Rome, Italy, [3]Department of Climate and Space Sciences and Engineering, University of Michigan, Ann Arbor, MI 48109-2143, USA, [4]Max Planck Institute for Solar System Research, Justus-von-Liebig-Weg 3, 37077 Göttingen, Germany

Introduction: The topic of the current work is the investigation of the radiation environment around Ganymede. We apply a single-particle Monte Carlo model [1], [2], [3] to obtain 3-D distribution maps of the H^+, O^{++}, and S^{+++} populations at the altitude of ~500 km and to deduce surface precipitation maps. We perform these simulations for three distinct configurations between Ganymede's magnetic field and Jupiter's plasma sheet (JPS), characterized by magnetic and electric field conditions similar to those during the NASA Galileo G2, G8, and G28 flybys (i.e., when the moon was above, inside, and below the centre of Jupiter's plasma sheet). Our results provide a reference frame for future studies of planetary space weather phenomena in the near-Ganymede region and surface evolution mechanisms [3]. In fact, recent observations from both ground- and space-based telescopes, e.g. [4], [5], have confirmed the idea by [6] that the properties of the ices on the surface of Ganymede are strongly linked to exogenic factors, in particular to the energetic ion precipitation patterns.

Model: The main characteristics of the single-particle Monte Carlo model applied in this study are summarized in the following Table. Note that R_G stands for Ganymede's radius. For further details the reader is referred also to [1], [2].

Parameter	Value or description	Notes and references
Type of model	Single-particle Monte Carlo model	energetic ion trajectories are traced for the full three-dimensional ion velocity distribution
Dimension of the simulation box	$\pm10 \times \pm10 \times \pm10$ R_G centred to the moon	*Inner box:* $\pm3 \times \pm3 \times \pm3$ R_G centred to the moon
Spatial resolution	0.1 R_G	*Inner box:* 0.05 R_G
Background magnetic field configuration	Magnetic and electric field data are from [7] and [8] global MHD models of Ganymede's magnetosphere	To track particles, the Boris-Buneman Lorentz force integrator over gridded magnetic and electric field data interpolated within each cell was applied
Energetic ion spectrum	H^+, O^{++} and S^{+++} spectra by [9] were considered as a test case	Discrete energies covering the range from 1 to 3000 keV were considered. The simulation results are scaled *a posteriori* to the observed values.
Ion velocity distribution	Test particles are launched with a defined initial energy but random initial direction	A thick planar "source surface" perpendicular to the moon's orbit, located between X = -6 R_G and X = -7 R_G was placed upstream of Ganymede

Results and Discussion: For all the considered configurations between Ganymede and JPS, both for the H^+ (Figure 1) and O^{++} circulation in Ganymede's magnetosphere, there is a significantly increased flow in the anti-Jupiter low-latitude and equatorial surface regions of the leading side of Ganymede. This asymmetry in the flux above the Jupiter and anti-Jupiter facing sides tends to decrease approaching the surface, because of the shielding given by the closed magnetic field configuration and the strong magnetic field around the equator belt. The asymmetry in the fluxes above the Jupiter and anti-Jupiter facing sides is in general expected for all types of ions and is due to the ion cyclotron motion and finite Larmor radius effects (see also discussion in [2]).

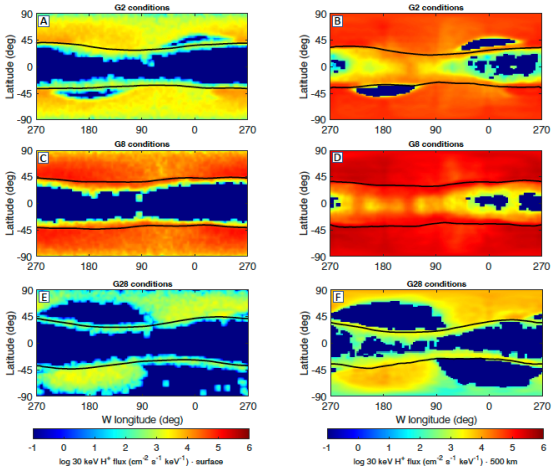

Figure 1: 30 keV H^+ flux precipitating at the surface (left panels A, C, and E) and at the altitude of 500 km (right panels B, D, and F) for 3 different configura-

tions of the moon's magnetic field: panels A and B correspond to science case (i) (Ganymede above the centre of the JPS), panels C and D to science case (ii) (Ganymede near the centre of the JPS), panels E and F to science case (iii) (Ganymede below the centre of the JPS). Superimposed are the Open-Closed Field boundaries (black lines). The W longitude system has been used meaning the leading hemisphere is at long = 90° and long = 0° is at the Jupiter-facing hemisphere apex [3].

Longitudinal variations in the width of the equatorial shielded regions of Ganymede at the altitude of 500 km are found in the simulations of all three ion populations. The widest latitudinal shielding occurs above the trailing hemisphere (plasma upstream) for ions with low initial magnetic rigidity. Our results show that the extent of the shielded region changes dramatically in the first 500 km from the moon's surface indicating the influence of the geometry of the magnetic field in the ion motion in both the plasma upstream and downstream regions. In particular, above the low latitude regions of the leading hemisphere, the heavy ion flux is highest at the altitude of 500 km and it decreases dramatically towards the surface.

In Figure 2 we show the ratio between the flux at the surface and the one at 500 km (with direction towards the surface), for Oxygen ions of initial energy equal to 30 keV, in the configuration where Ganymede in near the centre of JPS. One can see that the flux at the altitude of 500 km is always higher than the one at the surface (ratio smaller than 1), as expected in case of a magnetized body. For 30 keV O^{++} the differences are somehow smaller at the low latitude regions of the leading hemisphere (ratio of the order of 0.4-0.5); this is indeed the region where reconnection plays a role in the accessibility of the equatorial leading hemisphere surface.

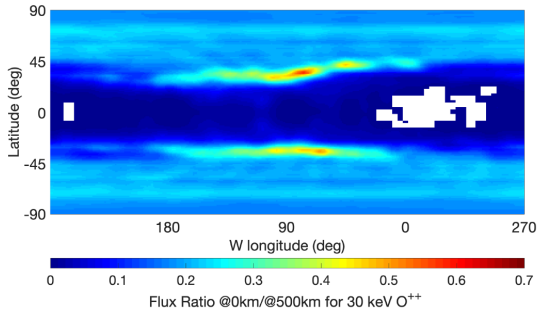

Figure 2: Ratio of the flux at the surface towards the flux at 500 km (with downwards direction) for Oxygen ions of initial energy equal to 30 keV, for the configuration when Ganymede is near the centre of the JPS (linear scale) [3].

In Figure 3 we show the XZ projection of the 3-D ion distribution of S^{+++} at initial energy equal to 30 keV. Note that X is along the ambient flow direction (and Ganymede's orbital motion), Z is along the Jupiter's spin axis). The regions of lower flux, especially evident on the right panel of Figure 3, depend on the S^{+++} magnetic rigidity and the configuration of the moon's magnetic field with respect to JPS. Our results are in agreement with simulations in other works, e.g., [1][10]

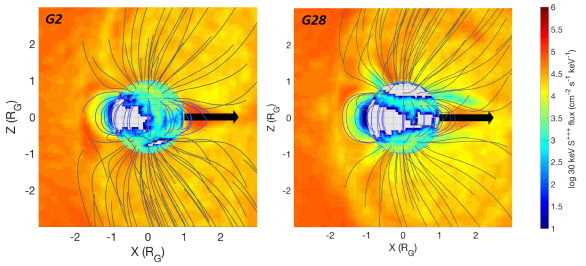

Figure 3: Circulation maps of S^{+++} at initial energy equal to 30 keV in science case (i) (Ganymede above the centre of the JPS; left panel) and (iii) (Ganymede below the centre of the JPS; right panel), in the XZ plane. The GPhiO coordinates have been used: X is along the ambient flow direction (and Ganymede's orbital motion), Z is along the Jupiter's spin axis, and Y points toward Jupiter (in units of Ganymede's radii). The black arrow shows the direction of Ganymede's orbital velocity [3].

References:

[1] Plainaki, C., Milillo, A., Massetti, S., et al. 2015, Icarus,245,306. [2] Plainaki, C., Massetti, S., Jia, X., Mura, et al. 2020, ApJ, 900, 74. [3] Plainaki, C., Massetti, S., Jia, X., Mura, A. et al. 2022, ApJ, 940 186. [4] Ligier, N., Paranicas, C., Carter, J., et al. 2019, Icarus, 333, 496– 515. [5] Mura, A., Adriani, A., Sordini, R., et al. 2020. Journal of Geophysical Research: Planets, 125, e2020JE006508. [6] Khurana, K. K., Pappalardo, R. T., et al. 2007, Icar, 191, 193, doi; 10.1016/j.icarus.2007.04.022. [7] Jia, X., Walker, R. J., Kivelson, M. G., et al. 2008, JGR, 113, A06212. [8] Jia, X., Walker, R. J., Kivelson, M. G., et al. 2009, JGR, 114, A09209. [9] Paranicas, C., Paterson, W. R., Cheng, A. F., et al. 1999, JGR, 104, 17459. [10] Toth, G., Jia, X., Markidis, S., et al. 2016, JGRA, 121, 1273, doi:10.1002/2015JA021997

Observability of Callisto's exosphere with MAJIS/JUICE

E. D'Aversa[1], G.Sindoni[2], F.Oliva[1], M.Lopez-Puertas[3], G.Gilli[3], C.Plainaki[2], F.Tosi[1], G.Piccioni[1], G.Filacchione[1], A.Migliorini[1], F.Altieri[1] , D.Grassi[1].

[1]INAF-IAPS (Via del Fosso del Cavaliere 100, 00133, Rome, Italy; emiliano.daversa@inaf.it), [2]Agenzia Spaziale Italiana, Rome, Italy, [3]IAA,CSIC, Granada, Spain.

Introduction: The surface of the icy Galilean satellite Callisto is known to sustain a significant neutral atmosphere, whose properties are however still poorly constrained by direct observations. The only direct detection refers to the CO_2 non-LTE 4.3 μm emission, measured by the NIMS instrument onboard the NASA Galileo spacecraft during a limb scan acquired in a close flyby passage ([1]). Ionised components detected through their UV emissions ([2]; [3]) helped in establishing an atmospheric composition dominated by O_2 and H_2O, with minor contributions by CO_2 and CO, but the actual abundances and their spatial and temporal variability remain poorly known. Here, we report about the capabilities of the MAJIS instrument onboard the ESA JUICE spacecraft [4], due to launch in April 2023 and reach the Jupiter system in July 2031, to contribute to this study field.

MAJIS (*Moon And Jupiter Imaging Spectrometer*) is a dual-channel, visible to infrared mapping spectrometer, covering the 0.50-5.54 μm spectral range [5].

Near-IR non-LTE emissions at Callisto: In this work we consider the following emissions expected to fall within the MAJIS spectral range: the CO_2 complexes at 4.3 μm and 2.3 μm, the H_2O complex also at 2.3 μm, the O_2 emission at 1.27 μm, and the CO bands at 4.7 μm and 2.3 μm. We evaluated the intensities of such emissions for reference abundances of the molecular species and for limb-viewing geometry, by taking advantage of the KOPRA algorithm [6], feeded in its turn by molecular levels population calculated using the GRANADA algorithm [7]. An example of resulting emissions is shown in Figure 1.

Molecules detectability: The simple comparison of the emission intensities with the MAJIS NESR (noise equivalent spectral radiance) levels for different exposure times (Figure 1) suggests the possibility to observe CO_2 4.3 μm emission with good SNR, as well as the H_2O complex also at 2.3 μm. On the other hand, being realistic MAJIS exposures typically shorter than 10 s, both O_2 and CO detections seem challenging, at least at the single-pixel level.

A detection limit for each species has been evaluated for an exposure duration of 10 s and by spectrally integrating the signal across the emission bands (spectral summing). They are expressed in terms of surface number density in Table 1. For both CO_2 and H_2O such limits are well below the predicted density levels, although spatial and temporal variability can strongly affect the actual results.

As far as O_2 is concerned, the detection of its emission at 1.27 μm is challenging within the 10 s exposure time limit. The application of spectral summing can be crucial in this case. If on one hand it impacts the steady time for the observation geometry, on the other hand, it is expected to decrease the detection limit to $3.4 \cdot 10^9$ cm^{-3}, value compatible with the O_2 surface density predicted by some atmospheric models [8].

The CO detection is the most critical, since the stronger bands at 4.7 μm are below the 10 s NESR level by about one order of magnitude. The spectral summing is effective in this case in decreasing the surface density detection limit to about $3.4 \cdot 10^7$ cm^{-3}, but it is still above the value predicted by models by a factor of 2 [9]. The spatial/temporal coadding of several observations can in principle help reducing CO detection limit further, but its feasibility will depend on the available opportunities for observing the atmosphere in the same conditions.

Table 1- Molecular detection limits from spectrally integrated emissions in 10 sec exposure MAJIS limb geometry.

species	*surface number density*
CO_2	$6.2 \cdot 10^6$ cm^{-3}
H_2O	$6.6 \cdot 10^6$ cm^{-3}
O_2	$3.4 \cdot 10^9$ cm^{-3}
CO	$3.4 \cdot 10^7$ cm^{-3}

Observing opportunities: The possibility for MAJIS to scan the Callisto's limb with adequate spatial resolution can only be achieved during the flybys occurring in the Jovian tour mission phase. In the current trajectory plan (CReMA 5.0, [10]), 21 such events are planned, and the best vertical resolution achievable under reasonable assumptions about the spacecraft pointing capabilities is 2.1 km/px. The possibility to observe the dayside limb of Callisto in several opportunities is of course valuable in order to gather insights about eventual spatial and temporal variations of the discussed species. On the other hand, a significant degree of redundancy is found among the observing conditions of several flybys, in terms of accessible latitudes and local solar times, which can help in reducing

detection limits by coadding homogeneous observations.

Acknowledgements

This work is supported by the Italian Space Agency (ASI-INAF grant 2018-25-HH.0). IAA researchers acknowledge financial support from the State Agency for Research of the Spanish MCIU through the Center of Excellence Severo Ochoa" award to the Instituto de Astrofísica de Andalucía (SEV20170709).

References:

[1] Carlson, R. W. 1999. "A Tenuous Carbon Dioxide Atmosphere on Jupiter's Moon Callisto." *Science* 283 (5403): 820–21

[2] Kliore, A. J. 2002. "Ionosphere of Callisto from Galileo Radio Occultation Observations." *Journal of Geophysical Research*. doi: 10.1029/2002ja009365.

[3] Cunningham, N.J., J.R. Spencer, P.D. Feldman, D.F. Strobel, K.France, and S.N. Osterman. 2015. "Detection of Callisto's Oxygen Atmosphere with the Hubble Space Telescope." *Icarus*. Doi: 10.1016/j.icarus.2015.03.021.

[4] Grasset, O., M.K. Dougherty, A. Coustenis, E.J. Bunce, C. Erd, D. Titov, M. Blanc, A. Coates, P. Drossart, L.N. Fletcher, H. Hussmann, R. Jaumann, N. Krupp, J.-P. Lebreton, O. Prieto-Ballesteros, P. Tortora, F. Tosi, T. Van Hoolst, "*JUpiter ICy moons Explorer (JUICE): An ESA mission to orbit Ganymede and to characterise the Jupiter system*", 2013, Planet.Sp.Sci., 78, doi:10.1016/j.pss.2012.12.002.

[5] Guerri I., Fabbri A., Tommasi, L., Taiti, A., Amoroso, M., Mugnuolo, R., Filacchione, G., Fonti, S., Piccioni, G., Saggin, B., Tosi, F., Zambelli, M., 2018. "*The optical design of the MAJIS instrument on board of the JUICE mission*". Proc.of SPIE Vol. 10690 106901L-1. doi: 10.1117/12.2312013.

[6] Stiller, G.P., T.von Clarmann, B.Funke, N.Glatthor, F.Hase, M.Höpfner, A.Linden. 2002. "Sensitivity of Trace Gas Abundances Retrievals from Infrared Limb Emission Spectra to Simplifying Approximations in Radiative Transfer Modelling." *Journal of Quantitative Spectroscopy and Radiative Transfer*. https://doi.org/10.1016/s0022-4073(01)00123-6.

[7] Funke, B., M. López-Puertas, M. García-Comas, M. Kaufmann, M. Höpfner, and G. P. Stiller. 2012. "GRANADA: A Generic RAdiative traNsfer AnD Non-LTE Population Algorithm." *Journal of Quantitative Spectroscopy and Radiative Transfer*. https://doi.org/10.1016/j.jqsrt.2012.05.001.

[8] Vorburger, A., P. Wurz, H. Lammer, S. Barabash, and O. Mousis. 2015. "Monte-Carlo Simulation of Callisto's Exosphere." *Icarus*. https://doi.org/10.1016/j.icarus.2015.07.035.

[9] Liang, Mao-Chang. 2005. "Atmosphere of Callisto." *Journal of Geophysical Research*. https://doi.org/10.1029/2004je002322.

[10] ESA SPICE Service, JUICE Operational SPICE Kernel Dataset, https://doi.org/10.5270/esa-ybmj68p.

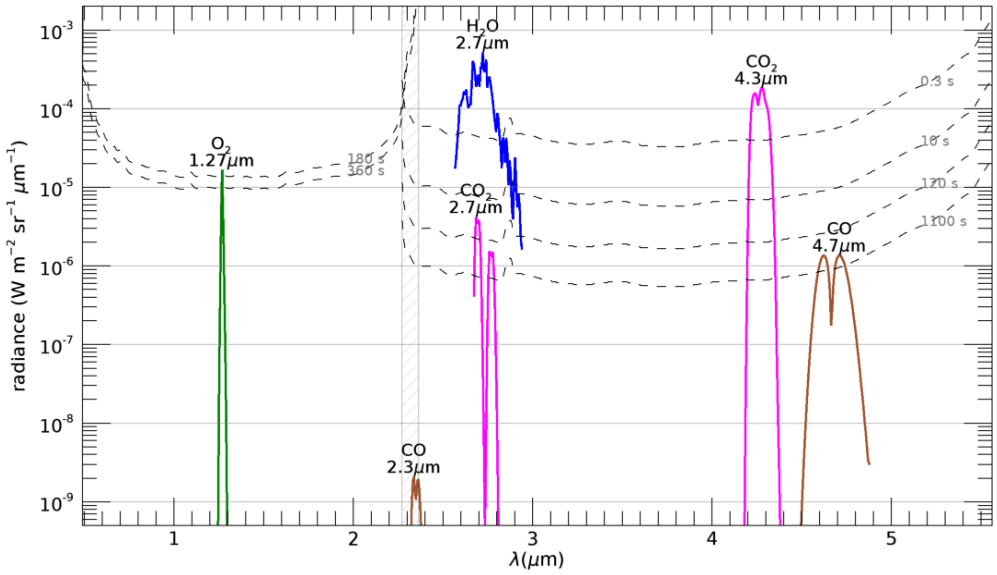

Figure 1- Intensities of molecular non-LTE emissions in the MAJIS spectral range, calculated for Callisto limb-grazing geometry for the following surface densities: $5 \cdot 10^9$ cm^{-3} for O_2, $1.2 \cdot 10^9$ cm^{-3} for H_2O, $3.6 \cdot 10^8$ cm^{-3} for CO_2, and $1.5 \cdot 10^7$ cm^{-3} for CO. Dashed curves represent MAJIS NESR levels for different exposure durations.

COMBINING REMOTE SENSING AND LABORATORY ANALYSIS TO SEARCH FOR ORGANICS ON THE SURFACE OF EUROPA S. Pagnoscin[1,2], J. R. Brucato[1,2], A. Lucchetti[3]
[1]Department of Physics and Astrophysics, University of Firenze, Italy, [2]INAF - Astrophysical Observatory of Arcetri, Firenze Italy (silvia.pagnoscin@unifi.it, john.brucato@inaf.it), [3]INAF Astronomical Observatory of Padova, Padova, Italy.

Introduction: Europa is one of the most intriguing objects we can find in our Solar System. What attracts scientists comes from beneath its surface, a possible subsurface global ocean containing twice as much water as all of Earth's oceans. This makes the satellite one of the main targets in searching for extraterrestrial life being water one of the first ingredients necessary for life to emerge and persist. However, the importance of Europa does not just come from its possible hidden salty water reservoir but also from its geological complexity showed up by a surface crisscrossed by ridges, faults, throughs and others. This suggested the presence of a certain activity presumably connected with what is hidden in its interior. The energy, necessary to support the presence of liquid water and to generate geological features comes from Jupiter that acts on its satellites producing intense tidal stresses. In addition, thermal models suggested that tidal dissipation can be even distributed in the mantle making it thermally and volcanically active supporting connection between ocean and ice crust and the existence of another form of energy due to water-rock interaction in the ocean floor namely hydrothermal activity. This latter has important astrobiological consequences being hydrothermal vent possible candidate sites for the origin of life in which prebiotic reactions can synthesize molecules crucial to life itself such as amino acids, the building blocks of proteins. In particular, previous investigations[1] on the survivability of these molecules under Icy Moon's oceans environments determined how Aspartic Acid and Threonine could be associated with hydrothermal activities due to their short lifetime if compared with primordial origin time scales. Thus, if founded on the surface of the satellite, the two molecules could be identified as traces of recent activities such as hydrothermal vent or the presence of an active biota. In this scenario we selected a region on the surface of Europa, named Tyre Macula, characterized by the largest impact feature of the satellite, to investigate possible signatures associated with these two amino acids and their survivability under Europa's surface conditions with remote sensing and laboratory analyses.

Remote Sensing: Remote sensing investigation was conducted using data from NASA's Galileo Mission (1989-2003) that was equipped with several instruments including a Solid-State Imaging Camera (SSI) and a Near Infrared Mapping Spectrometer (NIMS). In this work, SSI data were used to generate a geological map (Figure 1) distinguishing different units[2] with the software QGIS and Mappy plug-in[3]. NIMS data were used to generate a spectral map and obtain spectra from different geological units with ISIS3. In particular, we focused our attention on three different geological units, Ridged Plains, Chaos Terrains and Low Albedo Plains, which composition was previously inferred[4] and thus reproduced in our laboratory.

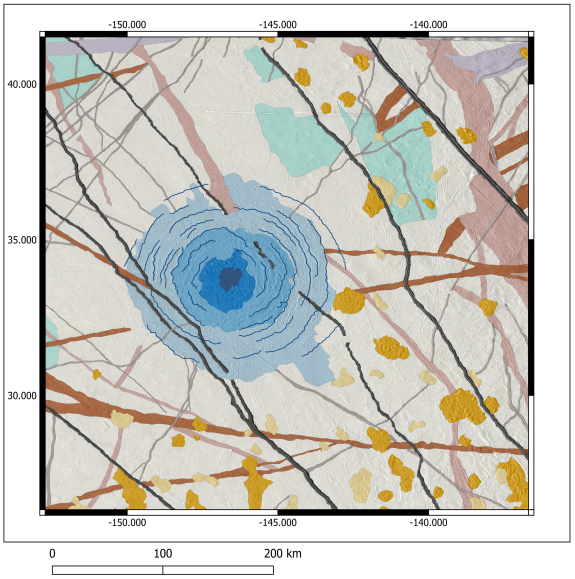

Figure 1. Geological map of Tyre Macula with recognized geological units. The three investigated are Ridged Plains (white), Chaos Terrains (orange) Low Albedo Plains (green).

Laboratory analysis: Laboratory analysis was conducted in the Astrobiology Laboratory of INAF-Astrophysical Observatory of Arcetri with the aim of reproducing Tyre Macula's surface which is mainly made of water ice and other compounds like hydrated salts coming from the ocean below such as Hexahydrite, Mirabilite and Bloedite[4,5]. We prepared samples using mixtures of salts with abundances determined in previous works[4,5] and analyzed them though diffuse reflectance spectroscopy under Europa's environmental condition to compare laboratory spectra with spacecraft's ones. Laboratory setup includes an FT-IR spectrometer equipped with a vacuum

chamber interfaced with a cryostat to simulate space environments and an UV lamp that simulates solar irradiation. Organics have been included into mixtures to investigate possible signature of Aspartic Acid and Threonine.

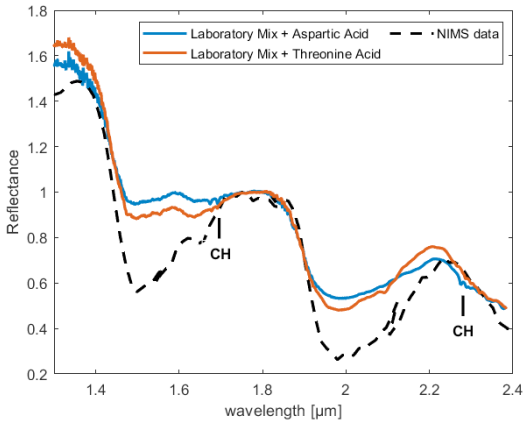

Figure 2. NIR spectra (1.3-2.4 μm) of laboratory Ridged Plains analogue with Aspartic Acid (blue), with Threonine (red) and NIMS Ridged Plains (black dashed line). Features associated with amino acids can be seen around 1.7 μm and 2.3 μm and are due to CH bonds.

Results: Laboratory analysis let us conclude that Aspartic Acid and Threonine have interesting features in the NIR spectrum (Figure 2) due to CH bonds but those cannot be distinguished by Galileo Mission data due to low resolution and instrumental issues. In addition, we saw that 7 hours UV laboratory irradiation, that correspond to 4000 Europa's day-night cycles, do not affect the two amino acids, which show a great photo-stability. Moreover, even if Europa is sourrounded by a crowded particle environment, Tyre Macula is located in a region of the icy moon subjected by a low flux of energetic particles[6]. Thus, it makes sense to search for the two amino acids in that region by future missions (NASA's Europa Clipper and ESA's JUICE) to prove the presence of recent activity that can be associated with hydrothermal vent but also with an active biota. Further investigation on signatures produced by other amino acids should be carried on to let future missions distinguish different species.

References: [1] Truong N. et al. (2019) *Icarus, 329, 140-147*. [2] Greeley R. et al. (2000) *Journal of Geophysical Research, 105(E9), 22559–22578*. [3] Penasa L. et al. (2020) EPSC2020-1057. [4] Dalton III J. B. et al. (2012) *Journal of Geophysical Research: Planets, 117(E3)*. [5] Dalton III J. B. et al. (2007) *Geophysical research letters, 34(21)*. [6] Nordheim T. A. et al. (2018) *Nature Astronomy, 2(8), 673-679)*.

THE JUPITER'S HOT SPOTS AS OBSERVED BY JIRAM-JUNO: LIMB-DARKENING IN THERMAL INFRARED

D. Grassi[1], A. Mura[1], A. Adriani[1], G. Sindoni[2], C. Plainaki[2], F. Tosi[1], A. Olivieri[2], G. Piccioni[1], P. Scarica[1], F. Biagiotti [3,1], and the JIRAM-Juno team, [1]INAF-IAPS (Via del Fosso del Cavaliere, 00133, Rome, Italy), [2]Agenzia Spaziale Italiana (Via del Politecnico, 00133, Rome, Italy), [3]Università di Roma "Sapienza"

Introduction: The Jupiter InfraRed Auroral Mapper (JIRAM) instrument on board the Juno spacecraft performed repeated observations of the Jupiter North Equatorial Belt (NEB) around the time of 12th Juno pericenter passage on April 1st 2018. The data consist in thermal infrared images (the JIRAM filter has a band pass centred around 4.8 μm) and show, among other atmospheric features, two bright hot-spots (Fig. 1).

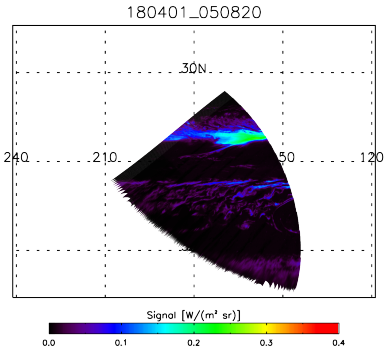

Fig. 1. Example of JIRAM mosaic considered for the study

Methods: Images of the same areas at different emission angles were used to constraint the trend of the limb darkening function (Fig. 2).

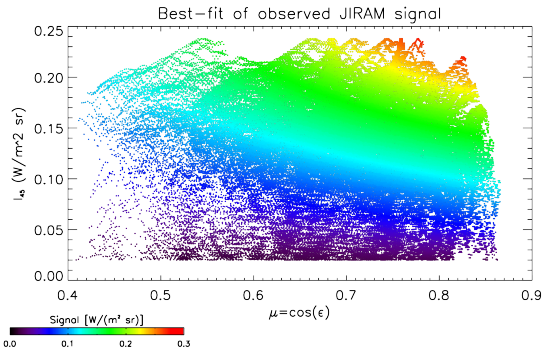

Fig. 2. Observed trend of JIRAM signal as a function of emission angle ε and estimated signal at the reference emission anlge of 45°. The latter quantity is taken as a proxy of absolute opacity of the cloud.

Comparison against simulated observations computed for different emission angles, total opacities, single scattering albedo ω_0 and asymmetry parameter g suggest that $\omega_0 \sim 0.9$ and $g \sim 0.32$ provide best match with data, with the latter parameter only weakly constrained by JIRAM observations. Then, we computed the ω_0 and g resulting from different size distributions (exploring the effective radius r_{eff} and variance v space), taking into account the complex refractive indices of ammonium hydrosulphide by [1] and [2].

Results: Our analysis suggests that neither sets of refractive indices are consistent with JIRAM observations. A more reasonable agreement is found once tholines are adopted, with an effective radius of 0.6 μm. This value is broadly consistent with the mean radius of Hot Spot's particles estimated by [3] on the basis of Galileo Entry Probe data. While a composition of pure tholine is not realistic for Jupiter conditions, our results indicate that scattering properties of clouds are largely dominated by optical properties of contaminants, as already suggested in [4]. Indeed, a thin (0.01 of total radius) coating of such compound over a NH_4SH particle can effectively mask the optical properties of the latter. An effective radius of 0.4 μm for these coated particles produces the ω_0 and g derived from JIRAM data (Fig. 3).

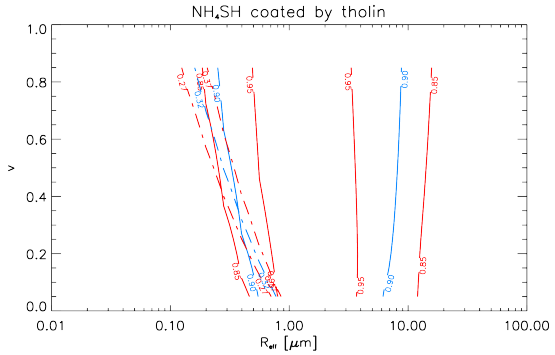

Fig. 3. Curve levels for ω_0 (solid curves) and g (dashed curves) in the r_{eff} – variance space. Blue curves present the values that best fits the trends in Fig.2, red curves the corresponding uncertainities.

References: [1] Howett C. J. A. et al., (2007) *J. Opt. Soc. Am.* B 24, 126-136. [2] Ferraro J. R et al. (1980) *Applied Spectroscopy*, 34 (5), 525-533. [3] Ragent B. et al, (1998), *J. Geophys. Res.*, 103 (E10),

22891– 22909. [4] Grassi D. et al. (2021) *MNRAS*, 503(4), 4892-4907.

Acknowledgments: This work was supported by the Italian Space Agency through ASI-INAF contract 2016-23-H.1-2018.

We thank N. Ignatiev (Institute for Cosmic Research of the Russian Academy of Sciences, Moscow) for the permission to use his radiative transfer subroutines and his kind help in code development.

We are grateful to Angioletta Coradini (1946-2011), our late collaborator and director, for her foresight and determination that made possible the realization of JIRAM and its operation on board the Juno mission.

WATER DESORPTION FROM LUNAR SAMPLE ANALOGUES TO SUPPORT THE ESA PROSPECT INSTRUMENT DEVELOPMENT. J. R. Brucato[1], M.A. Corazzi[1,2], G. Poggiali[1], T. Fornaro[1], S. Pirrotta[3], J. I. Mortimer[4], P. Reiss[5], and D. J. Heather[5] [1]INAF-Arcetri Astrophysical Observatory (L.go E. Fermi 5, 50125 Firenze, Italy, john.brucato@inaf.it), [2]University of Firenze, Dept Physics and Astronomy (via Sansone 1, 50019 Sesto Fiorentino, Firenze, Italy), [3]Italian Space Agency (via del Politecnico snc, 00133 Roma, Italy), [4]School of Physical Sciences, The Open University Walton Hall, Milton Keynes, Buckinghamshire, UK, [5]ESA/ESTEC, Keplerlaan 1, PO Box 299, 2200 AG Noordwijk, The Netherlands.

Introduction: The presence of water on the lunar surface is a scientific topic that has gathered a renovated interest thanks to the indirect observations of various recent missions [e.g. 1,2] and by renewed analysis of Apollo lunar samples [3]. Understanding the presence and character of water on the Moon is directly linked to understanding the evolution of the Solar System. The most probable mechanisms for the origin of water, predomininatly found in polar regions, are comet or asteroid impacts and solar-wind proton implantation. The formation of hydroxyl groups by proton implantation has been only marginally studied in laboratory, where lunar regolith dust analogues have been implanted with a stream of charged particles consisting of protons or deuterium. The nature of polar regolith, which has never been sampled or studied in situ, and which may contain a volatile component, is of particular interest. The development of a platform for resource utilization and in-situ exploration is ongoing in Europe and contributions to robotic missions in collaboration with Roscosmos targeting the lunar polar regions are underway. The PROSPECT instrument package developed by ESA [4], including the elements ProSEED and ProSPA, will assess the resource potential of the lunar surface by drilling, extracting and chemically processing samples of lunar regolith before performing chemical and isotopic analysis on the derived products. The first platform targeted for this package is the Russian Luna-27 (Luna-Resource) mission to be launched in 2025. The sample processing and analysis functions of the miniaturised chemical laboratory will quantify the resource potential of volatiles in the lunar regolith [5]. This is performed by extracting those volatiles via pyrolysis or combustion and then determining the composition, the yield and the isotopic systematics of those volatiles. Here, we present the results of a laboratory study in preparation of PROSPECT, including the TPD (Temperature-Programmed Desorption) curves of water desorbed from analogues of lunar soil.

Laboratory measurements: The experimental apparatus was assembled at INAF-Arcetri Astrophysical Observatory and TPD profiles were obtained by placing the lunar sample analogues in a customized sample holder of the cold finger. Water vapour was condesed on the surface of the analogues under high vacuum (~10^{-9} mbar). Firstly, water vapor is introduced to the vacuum chamber and trapped on a cryostat cold finger at 9 K. The cold finger is then heated at a constant rate (1.21 K/s), and as the molecules desorb, they enter a mass spectrometer and are detected. TPD experiments have been performed on a range of natural and synthetic mineral separates (olivine, spinel, enstatite, quartz), as well as on the NU-LHT-2M lunar regolith simulant. All materials were first cleaned, then crushed to <5 μm grain size, and loaded onto the cold finger in a layer with thickness of 100 μm. The resulting temperatures of desorption and calculated desorption energies were compared to reference measurements without sample. Desorption energies allow us to derive ice losses from very low ice content samples (<1% starting ice content).

Results: From the TPD profiles obtained from different percentages of deposited water, we evaluated the desorption temperature T_{des} and the binding energies E_{des}/K_b. From these experiments and in combination with thermal modelling, the loss of water during sampling can be assessed. The Figure 1 shows the TPD curves of pure H_2O (18 m/z) desorbed both from the bare cold finger of the cryostat (blue curve with a temperature peak at 141.2 K) and from micrometric grains of olivine (yellow curve), spinel (green curve), enstatite (red curve), quartz (pink curve), and lunar simulant NU-LHT-2M (black and blue curve).

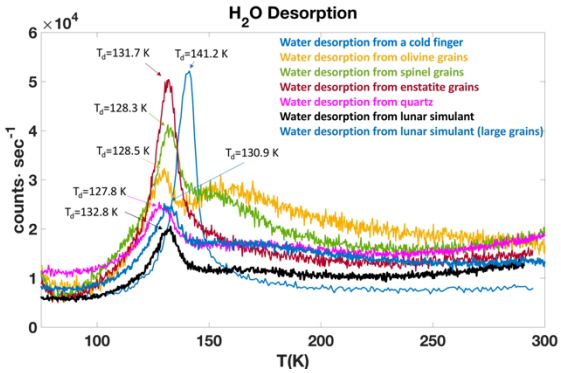

Figure 1: TPD curves of water ice desorbed from the bare cold finger (nickel-plate), and from different olivine, spinel, enstatite quartz minerals, and lunar simulant NU-LHT-2M.

When the molecules desorbed directly from the bare cold finger, only one desorption peak was obtained at 141.2 K. On the other hand, when the same number of molecules (i.e. same partial pressures) condensed on the micrometric grains, two different desorption peaks appeared. TPD measurement shows that as the temperature increased, the water molecules began to desorb from the bare cold finger at around 110 K until reaching the desorption

peak at 141.2 K. In the presence of the olivine substrate, we observed that water molecules desorb at a lower temperature 128.5 K, while the rest of the water ice desorbs in a wider temperature range, which shows a peak at 166.4 K. This result reveals that the water remains trapped by the olivine grains showing a desorption drift. Similar behavior also occurs in the presence of other minerals such as spinel (green curve), and quartz (pink curve). In the case of the lunar simulant (black curve), the ~40% of the water molecules desorbed at 132.8 K and the rest of desorbing water ice showed a gradual desorption drift.

The results show that water desorbs at temperatures well below the 350-400 K range derived by Lunar Reconaissance Orbiter [6]. This could be due to a different heating rate between laboratory and diurnal heating on the Moon. However, the laboratory data show no significant changes of desorption energies among various mineral phases and NU-LHT-2M simulant.

Acknowledgments: This work has been funded by ESA, and was conducted and led by members of the PROSPECT Science Team, in support of the development of ESA's PROSPECT package.

References: [1] McConnochie T.H., Buratti, B.J., Hillier J.K., and Tryka K.A. (2002) *Icarus, 156,* 335–351. [2] Feldman W.C., Maurice S., Binder A.B., Barraclough, B.L., Elphic R.C., and Lawrence D.J. (1998) *Science, 281,* 1496. [3] Anand M, Tartèse R., and Barnes J.J. (2017) *Phil. Trans. R. Soc. A, 372,* 20130254. [4] Heather, D.J. et al. (2021), this conference. [5] Heather, D. et al. (2021) The ESA PROSPECT payload for Luna 27: development status, 52nd Lunar and Planetary Science Conference. [6] Hendrix A.R., Hurley D.M., FarrellW.M., Greenhagen B.T., Hayne P.O., Retherford K.D., Vilas F., Cahill J.T.S., et al. (2019) *Geophys. Res. Lett.,* 46, 2417-2424.

DIELECTRIC SPECTROSCOPY ANALYSES OF LUNAR REGOLITH SIMULANTS FOR THE RADAR DETECTION OF WATER ICE ON THE MOON. C. H. Martella[1*] , B. Cosciotti[1] , S. E. Lauro[1] , E. Mattei[1] , F. Tosi[2], and E. Pettinelli[1]. [1]Mathematics and Physics Department of Roma Tre University, Via della Vasca Navale 84, 00146 Roma, [2]INAF-IAPS, Via del Fosso del Cavaliere 100, 0133 Rome (chloe.martella@uniroma3.it).

Introduction: The presence of water ice in permanently shadowed regions (PSR) of the Moon has been suggested since 1960s [1,2], but the first detection came in 2009 when the instrumentation onboard the NASA LCROSS mission observed near-infrared absorbance and UV emissions attributed to water vapour and water ice in the plume produced by the impact of a rocket onto the Cabeus crater [3]. Further observations indicated the presence of water ice and volatiles in PSRs. However, it is still up for debate whether the water ice is mostly distributed in thick layers (superficial or buried), broken and mixed with the regolith, or in the form of icy soil (permafrost). Spectral evidences in lunar cold traps, where the superficial temperature is <110K, indicate superficial water ice of >~ 100nm thickness. The concentration is predicted to be 0.1%-2.0% by mass if the water ice is combined with the lunar regolith, and it can cover up to 10% of the surface when exposed [4]. The Ground Penetrating Radar (GPR) is one of the geophysical techniques that can potentially be employed to detect water ice and volatiles in the lunar polar regions. To assess whether water ice can be distinguished from regolith in radar data, an intensive laboratory activity is required to study the dielectric properties of lunar regolith analogues. Here, with the goal of understanding the role of temperature and chemical composition, we measured real and imaginary part of permittivity of severals lunar regolith analogues from 200 to 350 K at 1 MHz.

Facility set-up and measurements: We present the results of dielectric investigations of 6 commercial lunar regolith simulants, see Table 1 [5,6,7] to define the radar response of the regolith in the lunar-like conditions. We performed the dielectric measurements in the temperature range 200-350K with a climatic chamber over the frequency spectrum 20Hz-1MHz using a LCR meters (Agilent HP4284A). The analogues are oven dried at 105°C for 24 hours and then measured filling a parallel plate capacitive cell. The entire temperature range was covered using two different cycles: the first one from room temperature down to 200 K, the second one from room temperature up to 350 K.

EXOLITH	Type of analogue
LHS-1	*Lunar Highland simulant*
LHS-1D	*Lunar Highland Dust simulant*
LMS-1	*Lunar Mare simulant*
LMS-1D	*Lunar Mare Dust simulant*
OFF PLANET RESEARCH	
OPRH2N	*General Nearside Highland simulant*
OPRH3N	*General Farside Highland simulant*

Table 1. The six commercial lunar regolith simulants that we dielectrically tested at varying physial conditions for the radar detection of water ice.

Results and discussion: The temperature dependence of dielectric parameters can reveal certain mechanisms that contribute to the electromagnetic (EM) behavior at high and low temperatures. Figure 1 and 2 show that the real part of dielectric permittivity of the regolith analogues is temperature independent over the examined temperature range. For the whole set of simulants under test, it ranges from 1.9 to 3.4, in good agreement with the dielectric measurements carried out on the Apollo-returned regolith samples [8].

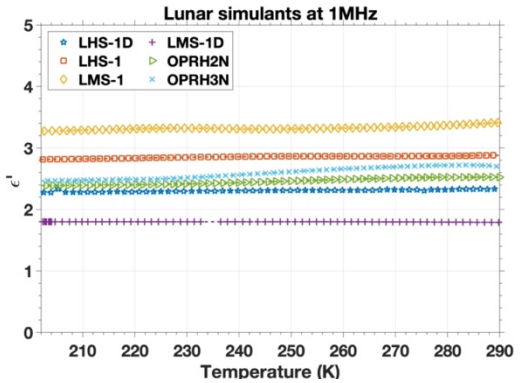

Figure 1: Real part of dielectric permittivity of lunar regolith simulants measured with the LCR meter setup in the temperature range 200-290K. The uncertainties are less than few percent of the measurements and are not visible in the plot.

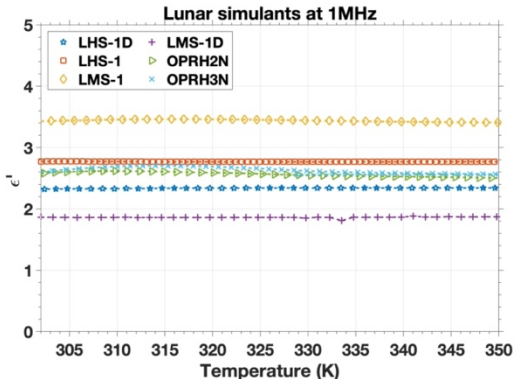

Figure 2: Real part of dielectric permittivity of lunar regolith simulants measured with the LCR meter setup at 1MHz in the temperature range 300-350K. The uncertainties are less than few percents of the measurements and are not visible in the plot.

We evaluate the activation energy from the imaginary part of permittivity as a function of temperature through the Arrhenius model (Eq. 1), where ε'' is the imaginary part, A is a constant, E is the activation energy, k_b is the Boltzmann constant, and T is the temperature. The activation energy E varies slightly between $0.0160\ eV \pm 0.0083\ eV$ and $0.131\ eV \pm 0.024\ eV$, suggesting that the imaginary part of regolith analogues is temperature independent. They can be tested in a limited temperature range and EM parameters can be extrapolated through the application of models and linear regressions.

$$\varepsilon'' = A\, e^{-\frac{E}{k_b T}}$$

Equation 1

Upcoming analysis: We plan to follow up the dielectric measurements of regolith simulants mixed with water ice at different proportions and configurations.
In addition, we are also planning to undertake acoustic investigations of regolith analogues to combine seismic and electromagnetic thechnique for the water ice detection in the lunar polar regions.

Acknowledgements: We acknowledge support from the research project: "*Moon multisEnsor and LabOratory Data analYsis* (MELODY)" (PI: Dr. Federico Tosi), selected in November 2020 in the framework of the PrIN INAF (RIC) 2019 call.

References: [1] Watson, K., Murray, B., & Brown, H. (1961). *On the possible presence of ice on the Moon. Journal of Geophysical Research, 66, 1598–1600.* [2] Arnold, J. R. (1979*). Ice in the lunar polar regions. Journal of Geophysical Research, 84, 5659–5668.* [3] Colaprete A. et al. (2010). *"Detection of water in the LCROSS ejecta plume". In: science 330.6003, pp. 463–468*. [4] Hayne P. O. et al. (2015*) "Evidence for exposed water ice in the Moon's south polar regions from Lunar Reconnaissance Orbiter ultraviolet albedo and temperature measurements". In: Icarus 255, pp. 58–69.* [5] Exolith Labs, U. of C.F *LMS-1 Lunar Mare Simulant Spec Sheet (2021).* [6] Exolith Lab, U. of C.F *LHS-1 Lunar Highland Simulant Spec Sheet (2021).* [7] Simulants, Feedstocks, and Additives [WWW Document], (2021*). URL https://www.offplanetresearch.com/simulants-feedstocks-and-additives (accessed 9.5.21).* [8] Alvarez, R. (1974). *Dielectric comparison of lunar and terrestrial fines at lunar conditions. Journal of Geophysical Research, 79(35), 5453-5457.*

ALTERATION OF ORGANIC MATTER ON CERES: RESULTS FROM LABORATORY STUDIES ON THE COMPLEX GEO-CHEMICAL HISTORY OF THE INNERMOST DWARF PLANET .

M.C. De Sanctis[1], G.A. Baratta[2], J.R. Brucato[3], S. De Angelis[1], Ferrari M.[1], D. Fulvio[4], M. Germanà[2], V. Mennella[4], M.E. Palumbo[2], S. Pagnoscin[3,5], G. Poggiali[3,6], C. Popa[4], C. Scirè[2], G. Strazzulla[2], R.G. Urso[2]

[1]INAF-IAPS, Rome, Italy,[2] INAF-Astrophysical Observatory of Catania, Catania, Italy, [3] INAF-Astrophysical Observatory of Arcetri, Florence, Italy, [4]INAF- Astronomical Observatory of Capodimonte, Naples, Italy, [5]Department of Physics and Astrophysics, University of Firenze, Italy, [6]LESIA-Observatoire de Paris, Meudon, France

Introduction: Ceres is the largest object in the Solar System asteroid belt and experienced extensive water-related processes with a complex geological and chemical history[1]. Its surface is characterized by dark materials, phyllosilicates,nammonium-bearing minerals, carbonates, water ice and salts. Local concentration of aliphatic organics have been detected by Dawn mission [2-4] in addition to a global presence of carbon [5] (fig.1). The origin, evolution, and persistence of the organic matter on Ceres is a matter of debate, given the strong spectral signature observed, corresponding to a "large quantity of aliphatic material (up to 10% according to some modelling [4]) mixed with phyllosilicates, carbonates and salts.

Hence, in this study we conducted a series of laboratory measurements of physicochemical interactions of organic material and minerals present on Ceres investigating the transformations induced by ultraviolet radiation, neutral atoms and fast ions in conditions that simulate the environment of Ceres.

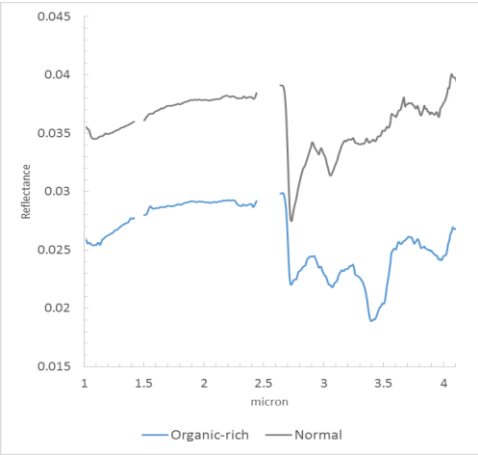

Fig.1 Example of organic rich area vs background material on Ceres from VIR on Dawn mission.

Laboratory studies:: We prepared mixtures of materials resembling the Ceres surface composition using an Mg-phyllosilicate, a carbonate, a darkening agent, and an NH_4-bearing clay. The latter was produced following the procedure described by [6]. Spectral proprieties of the ammoniated clays were fully characterized in previous works [6,7]. In this work, we added organic molecules to the mixture in order to understand how organic molecules degrade on Ceres. In particular, how aliphatic molecules degrade by energetic processing with fast ions (keV-MeV) and UV photons [8,9]. Moreover, the physico-chemical properties of the materials exposed to flux of neutral atoms were investigated [10].

The project is carried out by several INAF institutes and laboratories. In detail: INAF-IAPS (Institute for Space Astrophysics and Planetology) is in charge of preparation of analogues mineral mixtures and comparison with observations. INAF-Astrophysical Observatory of Arcetri subsequently doped the mixture with several organic investigating UV photostability in Ceres'conditions and the influence of temperature. INAF-Astronomical Observatory of Naples studied irradiation with atoms and temperature effect while INAF-Catania Astrophysical Observatory performed irradiation with fast ions. Finally, results of laboratory measurements were compared with data obtained by VIR instrument on board Dawn mission.

Results: In this section we report the main results found after having irradiated the samples representative of the Ceres surface rich in aliphatic organics.

UV radiation: In the Arcetri laboratory, we mixed undecanoic acid and Cerere analogue sample (ratio 1:80 organic:mineral). We irradiated the sample in the vacuum chamber at room temperature using an UV-enhanced Newport Xenon lamp to simulate the solar radiation. The simulant was irradiated at increasing fluence up to irradiation time of about 7 hours and the degradation process was monitored in real time with diffuse FTIR spectroscopy. In Fig.2 the reflectance spectra of the simulant as prepared and after UV irradiation at 180, 2280, and 21180 s are showed. The bands area of NH_3 at 3 μm and aliphatic CH_2/CH_3 at 3.4 μm is decreasing as the irradiation fluence increases with time. Each band area, which is proportional to the number of functional groups, was evaluated at different irradiation time and the degradation rate was obtained by fitting the band areas vs irradiation time using an exponential function. The degradation cross section of the aliphatic band at 3.4 μm, which is the probability that chemical bonds are broken by UV radiation was 5.85×10^{-21} cm^2. In presence of mineral simulant, the degradation rate of aliphatic compounds

xtrapolated to the estimated UV flux at the surface of Ceres gives a half-lifetime of 215 days.

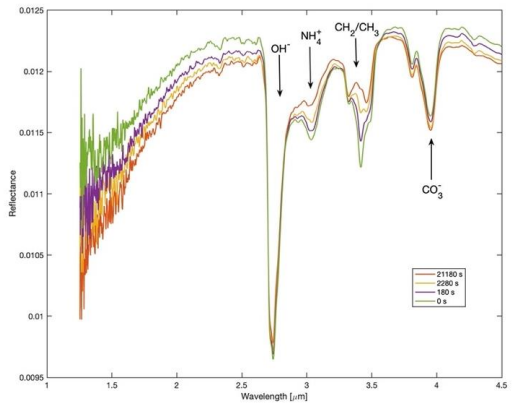

Figure 2 Diffuse reflectance spectra of the simulant as prepared (0 s) and after UV irradiation at 180, 2280, and 21180 s

Energetic ions: At INAF-Catania three pellet samples made of a mixture of minerals and undecanoic acid (80:1) have been irradiated under vacuum at room temperature by 200 keV H+, He+, and N+ ions, respectively. At selected step of irradiation, the samples have been analyzed by diffuse reflectance IR spectroscopy at room conditions using a FTIR Bruker (Vertex 70) spectrometer. The spectra show that the intensity of the 3.4 μm feature decreases as the irradiation fluence (ions/cm2) increases (Fig. 3). For each experiment, the values of the area of the 3.4 μm feature have been plotted versus the irradiation dose (eV/16u) and were fit by an exponential curve. For the three experiments considered the value of the destruction cross section of the 3.4 μm feature is σ[3.4μm] = 0.04 ± 0.01 16u/eV.

Atomic H treatment: The Ceres analogue was exposed at room temperature to a beam of atomic H with a Maxwellian distribution of temperature at 300 K [11]. The beam was produced by microwave excited dissociation of molecular hydrogen. The sample was exposed to increasing fluence of atomic H and corresponding spectral changes were studied in-situ by FTIR transmission spectroscopy. In Figure 2 we report the evolution of the organic bands due to C-H bond stretching. The decrease of the band intensity with the atomic H exposure indicates an abstraction of H from the simulant. From the trend of the integrated optical depth as a function of time, a H abstraction rate of 1.4×10-4 s-1 was obtained. Considering the value of the H atomic flux in the experiment the rate corresponds to a cross-section of 8.3×10-19 cm2. Assuming undecanoic acid as the representative organic material on Ceres' surface, the result of this experiment suggests that atomic hydrogen also contributes to the degradation of organics on Ceres.

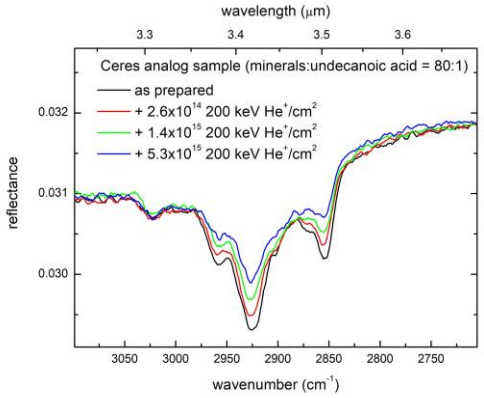

Figure 3: Diffuse IR reflectance spectra of Ceres analog sample after irradiation with 200 keV He+ ions at room temperature.

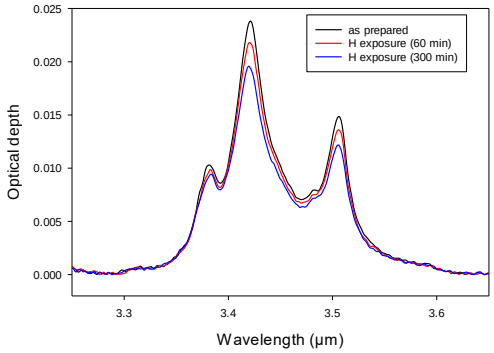

Figure 4 Transmission spectra of the simulant aliphatic bands as prepared (To) and after 60 and 300 min of atomic H exposure.

Conclusions: The experiments indicate that organic matter should degrade on Ceres, given the radiation environment of the body. However, the signature of the aliphatic organic is well detectable, suggesting that the organic matter is extremely recent or is preserved/re-constituted by unidentified processes.

Acknowledgements: This work is support by INAF Main Stream programme, grant 1.05.01.86.08 Evoluzione ed alterazione del materiale organico su Cerere (ref. Maria Cristina De Sanctis).

References: [1] De Sanctis et al., 2016, Nature 536, 54; [2] De Sanctis et al., 2011, Space Sci. Rev.163, 329; [3] De Sanctis et al.,2017, Science, 355, 719;[4] De Sanctis et al., 2019, MNRAS 482; [5] Marchi et al., Nature Astr., 2019. [6] Ferrari et al.,2018, Icarus, 321;[7] De Angelis et al., 2021,JGR, 126;[8] Baratta et al. 2002, A&A, 384, 343-349;[9] Brucato et al. 2006, A&A, 455, 395-399 [10] Mennella et al. 2003, ApJ, 587, 727-738.

Preliminary results on the infrared H_2-H_2 and H_2-He experimental collision induced absorption coefficients

S. Stefani[1], F. Vitali [1,2], G. Piccioni[1], D. Grassi[1] and M. Snels[3]
[1] IAPS-INAF, via del fosso del cavaliere 100, 00133 Rome Italy , [2] Università degli studi ''Sapienza'' piazzale Aldo Moro, 00185 Rome Italy, [3] ISAC-CNR via del fosso del cavaliere 100, 00133 Rome Italy
stefania.stefani@inaf.it

Introduction: The atmosphere of Jupiter is mainly composed by molecular hydrogen and helium. The H_2-H_2 and the H_2-He Collision Induced Absorption (CIA) represent one of the most important gaseous opacity sources in the infrared range from 1 to 5 μm, a range widely used by remote sensing instruments devoted to study its atmosphere. For this reason a proper modelling along experimental data are of paramount importance in order to accurately perform absolute retrieval of abundances of minor species and estimation of the atmospheric physical conditions from the observed radiance. In addition, a poor modelling of the CIA can alter the slopes of the synthetic spectra, impacting the retrieved mixing ratios of ammonia or aerosol properties, among the others. To overcome these limitations, we performed measurements of the CIA bands at the same or close to the physical conditions of the actual vertical atmospheric profile of Jupiter. In this work we report the preliminary results of this study.

Experimental Setup: The experimental setup employed to record spectra in the spectral range from 1 to 6μm, consists of a special chamber coupled with a Fourier Transform InfraRed (FT-IR) spectrometer. The FT-IR allows to acquire spectra in the same spectral range with resolution set from 0.06 to 10cm^{-1}. The chamber, shown in figure 1, is composed by two stainless steel concentric vessels; the inner one containing the gas or mixture of gases under test and the external one in vacuum ensuring the thermal insulation from the inner cell to the outer laboratory environment. Inside the internal vessel is installed a multi-pass optical cell characterized by an optical path of about 3.2 m. For a more detailed description of the cell, please refer to [1].

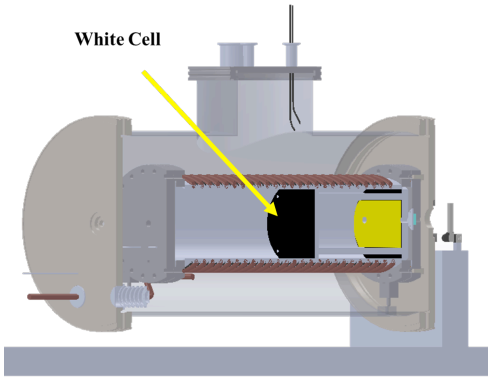

Figure 1: sketch of the PASSxS. In jellow the multi-pass optical cell is shown

Results and discussion: The infrared transmittance of the H_2-H_2 and the H_2-He is obtained at the gas pressure and temperature according to the (p,T) of the Jupiter atmospheric vertical profile [2], shown in figure 2.

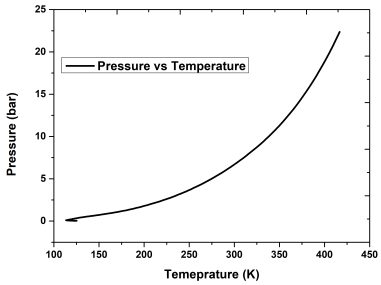

Figure 2: p, T Jupiter atmospheric vertical profile

In figure 3 (top), results of the H_2-H_2 CIA Absorption Coefficients (AC) acquired at different pressure and temperature are shown, while a comparison between measured and simulated [3] AC with relatively good agreement is shown on bottom.

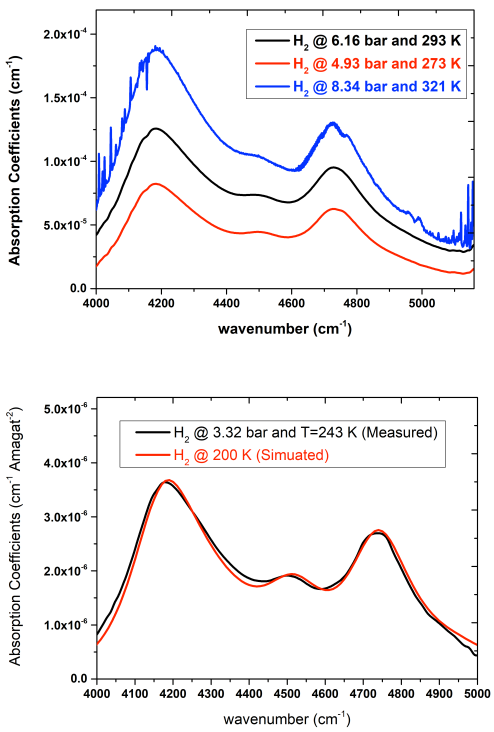

Figure 3: On top: H_2-H_2 CIA absorption coefficients at 6.16 bar and 293K (black curve), 4.39 bar and 273K (red curve) and 8.34 bar and 321 K (blue curve). On bottom: comparison between simulated (red curve) and measured (black curve) CIA absorption coefficients

In figure 4, the H_2-He measured AC at the typical mixing ratio of Jupiter (86% H_2 and 14% He) are shown, in comparison to a measurement acquired at the same condition of P and T of pure hydrogen. A qualitative comparison of the two spectra shows that He reduces the total absorption (opacity) and changes the shape of the spectrum.

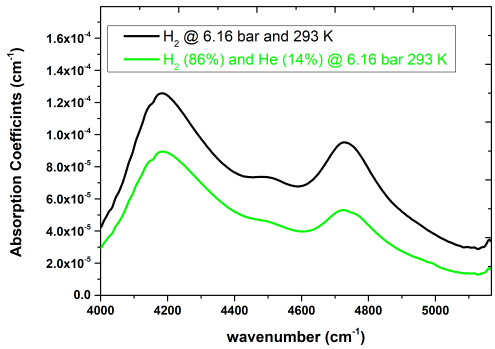

Figure 4: H_2-H_2 (black curve) and H_2-He AC of CIA (green curve)

Conclusions: Preliminary H_2-H_2 and H_2-He absorption coefficients of CIA acquired at the Jupiter atmospheric vertical profile, have been experimentally measured and compared to the models. A relatively good agreement with the model published by [3] has been reported. For what concerns the mixing H_2-He with a concentration of 86%-14% typical of the Jupiter atmosphere, the model seems to be consistent with the experimental data but the study is still going on.

Acknowledgements: we wish to thank the financial support by the Italian Space Agency (ASI), through the ASI-INAF contracts JUNO 2016-23-H.0 and JUICE 2018-25-HH.0.

References:

[1] M. Snels and al. (2021), AMT 14, 7187–7197, https://doi.org/10.5194/amt-14-7187-2021
[2] A. Seiff and al. (1998), JGR 103 (E10): 22857–22889. doi:10.1029/98JE01766.
[3] A. Borysow (2002), A&A 390, 779-782, DOI: 10.1051/0004-6361:20020555

HYPERVELOCITY IMPACTS ON COMET INTERCEPTOR DUST IMPACT SENSOR AND COUNTER FOR DUST SHIELD AND DETECTION SYSTEM ASSESSMENT.

S. Ferretti[1,2], V. Della Corte[2], A. M. Piccirillo[1,2], I. Bertini[1,2], S. Fiscale[1], A. Longobardo[2], L. Inno[1], A. Rotundi[1,2], E. Ammannito[3] and G. Sindoni[3], [1]Dipartimento di Scienze e Tecnologie, Università degli Studi di Napoli "Parthenope", CDN, IC4, 80143 Naples, Italy, (stefano.ferretti@assegnista.uniparthenope.it), [2]Istituto di Astrofisica e Planetologia Spaziali, Istituto Nazionale di Astrofisica, Via del Fosso del Cavaliere, 100, 00133 Rome, Italy, (vincenzo.dellacorte@inaf.it), [3]Italian Space Agency (ASI), via del Politecnico snc, 00133 Rome, Italy.

Topic: *Instrumentation.*

Introduction: Essential details on the formation and evolution of the early Solar System are encoded in the dust ejected by cometary nuclei. Multiple short-period comets have already been studied in situ [1], but multiple perihelion passages modified their pristine condition. Dynamically new comets (DNCs) remain pristine bodies since they never visited the inner Solar System stationing in the Oort cloud, more than 2000 A.U. from the Sun.

Comet Interceptor (CI) is the first F-class space mission selected by the European Space Agency to study a DNC or an interstellar object passing through the inner Solar System for the first time [2]. The Dust Impact Sensor and Counter (DISC) is an instrument included in the Dust Field and Plasma (DFP) suite, part of the payload dedicated to characterize the dust that CI will observe in the coma of its target. DISC will measure hypervelocity impacts (HVIs) of cometary dust particles 1–400 μm in size at speeds in the range 10–70 km/s, i.e. the speed range of the flyby. It aims to: 1) characterize the dust particles mass distribution in the range 10^{-15}–10^{-8} kg; 2) retrieve information on dust structural properties from impacts duration [3].

DISC design: DISC is a 121×115.5×46 mm^3 aluminum box containing the detection system and its electronics (Fig. 1). The sensing element consists in a 100×100×0.5 mm^3 aluminum plate with three piezoelectric traducers (PZTs) at its corners. Far from the impacted area, the shockwaves induced by HVIs become acoustic Lamb waves that propagate reaching the PZTs. The resonant vibration is processed by two electronic boards, mounted under the sensing plate, returning individual particles momentum.

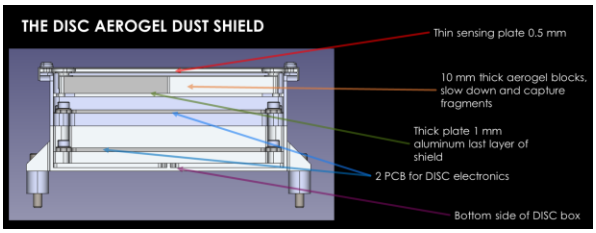

Fig. 1: DISC sectional drawing showing the sensing element, dust shield, and electronics mounting.

DISC electronics and the spacecraft (S/C) surface beneath it need to be shielded from hazardous dust particles possibly perforating the sensing plate. For this aim, we designed a never-used-before dust shield: four 12 mm-thick aerogel blocks inserted in a 1.5 mm-thick aluminum frame are mounted underneath the DISC sensing surface.

DISC impact detection system is derived from the GIADA Impact Sensor subsystem, used onboard Rosetta space probe to measure low-velocity dust impacts [4]. In order to ensure that the measurement concept is suitable for CI, i.e. at HVIs regime, two aspects need to be verified, namely DISC capability to:

- survive the expected coma dust environment;
- measure the momentum of dust particles with 10^{-15}–10^{-8} kg in mass and impacting at speed in the range 10–70 km/s.

Dust shield assessment: To check for the DISC survival in the expected coma dust environment, we tested the dust shield performance using a two-stage Light-Gas Gun (LGG) (Open University, Milton Keynes) shooting mm-sized particles of different materials at speeds around 5 km/s [5,6]. This facility allowed us to test DISC resistance to momenta in the range 10^{-2}–10^{-1} kg·m/s and to energies of the order of 10^2 J. The dust shield proved to survive at impacts with energies of about 200 J released by a 3 mm nylon bead at 5.5 km/s, with failure when impact energies are greater than 400 J. DISC resistance to higher-energy particles will be improved using the aerogel thickness of 2 cm. This thickness was selected comparing the experiment results with experimental ballistic limit equation (BLE) of similar configuration [7]. The performed tests show that with our design the resistance to HVIs, with respect to the limits expressed by BLE, is improved up to 30%.

These experiments showed that DISC is compatible with the foreseen coma dust environment. Integrating a thick aerogel layer in the design will reduce the risk of failure due to the expected hyper speed particles to low enough values even for the S/C more exposed to the dust flux. The S/C beneath DISC unit, in addition, is further protected by DISC lower layers.

DISC performance: DISC will have to measure momenta in the range 10^{-11}–10^{-3} kg·m/s [8]. The LGG facility allows to reach high momentum values by shooting heavy particles. However, the collision dynamics for mm-sized objects of common terrestrial materials is very different from equivalent cometary dust particles, thus a different strategy to simulate the foreseen impact momentum range is needed.

The expected HVI effects can be replicated using the apparatus that we assembled at INAF-IAPS in Roma, that includes a high-power pulsed laser beam (Fig. 2). Indeed, according to the late stage equivalence, laser intensity, beam dimension, and pulse duration can be tuned to match a particle's impact pressure, section, and shock duration, respectively [9]. Laser intensities of 10^{9}–10^{10} W/cm^2 can generate surface pressures from kbar to Mbar, corresponding to cometary dust particles colliding at 3–6 km/s. Using the Nd:YAG laser (λ = 1064 nm), emitting τ = 6 ns pulses with pulse energy of E_{pulse} = 1.2 J, we can cover a momentum range of 10^{-10}–10^{-5} kg·m/s.

Real dust particle impacts close to CI foreseen HVIs can be performed using a Van der Graaf (VdG) gun, i.e. an electrostatic accelerator that can shoot µm-sized dust particles up to 20 km/s [10]. This facility allows to reproduce momenta of 10^{-9}–10^{-7} kg·m/s, which partly overlap with laser simulated shots momentum range. VdG real impacts will be used to calibrate our high-power laser pulses facility and verify their representativity of cometary dust HVIs.

The expected energy range for dust impacts that will occur during CI flyby is 10^{-7}–10^{2} J; the highest values of the range are not simulated by the laser apparatus. However, the wide energy/pulse duration range, with some attenuators and pulse reducers, allows to cover the mJ energy range.

The setup dedicated to laser simulated HVIs is reported in Figure 2. A polarizer attenuator splits the laser beam and allows to tune its power. A couple of mirrors prevents backwards reflections from reaching the laser aperture. A beam expander enlarges the laser beam before entering the vacuum chamber, where it is then focused by a plano-convex lens on the DISC breadboard mounted on a 3-axis translational stage. The vacuum chamber is fundamental to prevent plasma generation in air around the focus.

By properly tuning the laser parameters, this strategy allows to achieve representative simulations of cometary dust HVIs that will occur during the CI flyby. In addition to assessing DISC performance, simulating similar impacts many times provides statistics to calibrate DISC detection system and individual dust particle momentum measurements methodology with great accuracy.

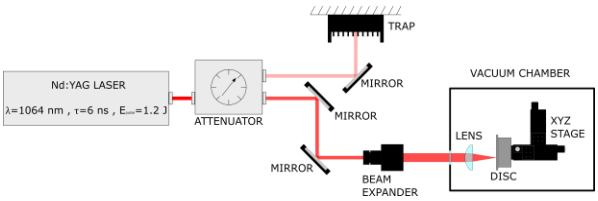

Fig. 2: Optical setup for high-power pulsed laser simulated dust particle hypervelocity impacts.

Summary: DISC dust shield mechanical resistance to cometary dust HVIs was tested by shooting different mm-sized particles at about 5 km/s using a LGG facility. Momenta of 10^{-2}–10^{-1} kg·m/s and energies of the order of 10^{2} J were released during collisions. The tests demonstrated that the DISC dust shield can survive impacts with kinetic energy expected during the DNC close encounter and allow the instrument operability and measurement requirements compliance.

A dedicated optical setup was realized and used to extend the tested impact parameters ranges through high-power laser pulses simulations of foreseen CI HVIs. Such experiments play a fundamental role for accurate calibration of the instrument.

Acknowledgments: We thank the Italian Space Agency (ASI) within the ASI-INAF agreements I/024/12/0 and 2020-4-HH.0. We also thank Dr M. Sylvest and Dr M. Patel for the experiments with the Light-Gas Gun at the Open University, Milton Keynes.

References: [1] Keller H. U. and Kührt E. (2020) *Space Sci. Rev., 216(1),* 1–26. [2] Snodgrass C. and Jones G. H. (2019) *Nat. Commun., 10(1),* 1–4. [3] Della Corte V. et al. (2021) *LPSC LII,* Abstract #2332. [4] Esposito F. et al. (2002) *Adv. Space Res., 29(8),* 1159–1163. [5] McDonnell J. A. M. (2006) *Int. J. Impact Eng., 33(1–12),* 410–418. [6] Hibbert R. et al. (2017) *Procedia Eng., 204,* 208–214. [7] Ryan S. et al. (2010) *Hypervelocity Impact Symposium,* (No. JSC-CN-19432). [8] Di Paolo F. et al. (2021) *LPSC LII,* Abstract #1238. [9] Pirri A. N. (1977) *Phys. Fluids, 20(2),* 221–228. [10] Friichtenicht J. F. (1962) *Rev. Sci. Instrum., 33(2),* 209–212.

The spectral and chemical changes of atmosphere-less surfaces induced by ion bombardment

R. G. Urso[1], G. A. Baratta[1], C. Scirè[1], O. Sohier[1], G. Strazzulla[1], M. E. Palumbo[1]. [1]INAF-Osservatorio Astrofisico di Catania, via Santa Sofia 78, 95123 Catania (Italy) riccardo.urso@inaf.it

Introduction: Atmosphere-less bodies in the Solar System are continuously bombarded by solar particles and cosmic rays that release their energy to the surface materials, inducing changes in their physical and chemical properties. In particular, energetic ions induce spectral changes, causing the alteration of the slopes in the ultraviolet (UV), visible (Vis), and near-infrared (NIR) spectra of small bodies [1] as well as the change in the profile of NIR spectral bands revealed in frozen volatile-rich surfaces [2]. The understanding of how ion bombardment alters surface layers in space is thus necessary to avoid misleading considerations on the properties and composition of underlying pristine materials.

Laboratory experiments are a fundamental tool to comprehend the effects induced by energetic charged particles on solid-phase materials and to study the destruction of pristine frozen compounds [3, 4, 5]. Furthermore, advanced analysis on laboratory analogues extend the available information, in most cases limited to remote sensing observations [6].

Methods: We present recent results obtained by means of ion irradiation experiments on both frozen samples and complex organic compounds to simulate the alteration of materials at the surface of Solar System small bodies induced by solar particles and galactic cosmic rays. All experiments were performed in high vacuum chambers (pressure $\leq 10^{-8}$ mbar) connected to ion accelerators capable to accelerate ions to tens or hundreds of keV. In particular, irradiation was performed with fast H^+ and He^+ ions as they are the most abundant charged particles in the spectra of solar particles and cosmic rays. The analyses were performed by means of Fourier-Transformed Infrared spectroscopy (FT-IR), a non-destructive analytical tool that allows the comparison with infrared astronomical observations and space mission data collected on atmosphere-less bodies.

Results: Our experiments show that significant spectral alterations are induced in both the NIR and mid-IR spectra of samples by ion irradiation. We first attributed the detected IR features to the related compounds. After the attribution, we followed the variation of the IR band areas as the irradiation dose increases to obtain quantitative information on the destruction of deposited compounds and on the formation of new species. In particular, Fig. 1 (top panel) shows the destruction of methanol (CH_3OH), a compound revealed on the surfaces of small bodies in the outer Solar System, such as Arrokoth [7], VE95, and Pholus [8]. Radicals and molecular fragments produced by the ion-induced destruction of CH_3OH and of the other deposited compounds present in the mixtures (e.g., H_2O, CO, CH_4, NH_3) recombine in short times (picoseconds or less) forming various new molecular species, including precursors of complex organics of astrobiolical relevance. In particular, we revealed the presence of aldehydes, e. g. formaldehyde (H_2CO) and acetaldehyde (CH_3CHO) and we give information on their abundance in ices exposed to ion bombardment [9].

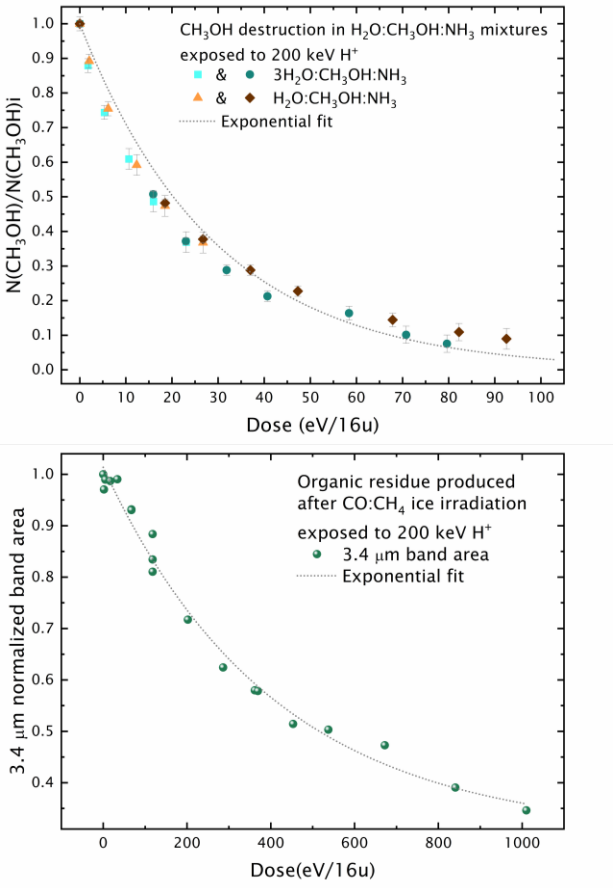

Figure 1: the effects of ion irradiation on the destruction of methanol (top panel) and on the 3.4 μm band of a organic material produced after irradiation and warm-up of a $CO:CH_4$ ice (bottom panel).

Ion irradiation of ices causes the production of complex organic materials that are considered laboratory analogues of the materials responsible for the red slopes observed at the surfaces of outer small bodies [8, 9, 10]. We also investigate the effects of irradiation on the alteration of such complex organics by following the changes in the 3.4 μm band (Fig. 1, bottom panel), in order to support the interpretation of observations of this IR feature on main belt asteroids and we give information on their chemical composition.

Conclusions: The experimental results we obtained show that ion irradiation causes the destruction of pristine frozen compounds that are revealed at the surface of small bodies in the outer Solar System. Complex organic materials that might be present at the bodies surfaces are also affected by ion irradiation. The extent of alteration can be revealed by the analysis of the 3.4 μm band. The changes induced by ion irradiation depend on the dose and thus on the timescales of exposure in space. Changes would be detectable in timescales that span between 10^7 and 10^9 years and that are thus compatible with the lifetime of small bodies in the Solar System.

References: [1] Brunetto, R., Barucci, M. A., Dotto, E., Strazzulla, G. (2006) ApJ, *644*, 646–650. [2] Urso, R. G., Baklouti, D., Djouadi, Z., Pinilla-Alonso, N., Brunetto, R. (2020) ApJL, 894, L3. [3] Baratta, G. A., Leto, G., Palumbo, M. E. (2002) A&A, 384, 343. [4] Islam, F., Baratta, G. A., Palumbo, M. E. (2014) A&A, 561, A73. [5] Strazzulla, G., Baratta, G. A., Johnson, R. E., Donn, B. (1991) Icarus 91, 101. [6] Urso, R. G., Vuitton, V., Danger, G. et al. (2020) A&A, 644 A115. [7] Grundy, W. M., Bird, M. K., Britt, D. T., et al. (2020) Science, 367, 6481. 101. [8] Barucci, M. A., Merlin, F., Dotto, E., Doressoundiram, A., de Bergh, C. (2006) A&A, 455, 725. [9] Urso, R. G., Hénault, E., Brunetto, R. et al. (2022) A&A, in press. [10] Cruikshank, D. P., Roush, T. L., Bartholomew, M. J. et al. (1998), Icarus, 135, 389

LOW TEMPERATURE REFLECTANCE SPECTRA OF NH_4^+ MINERALS IN THE VISIBLE AND NEAR-INFRARED (VNIR): EFFECT OF PHASE TRASITIONS FOR PLANETARY INVESTIGATION.

M. Fastelli[1], A. Zucchini[1], B. Schmitt[2], P. Beck[2], O. Poch[2], F. Frondini[1] and P. Comodi[1]
[1] Department of Physics and Geology, University of Perugia, I-06123, Perugia, Italy [2] Univ. Grenoble Alpes, CNRS, IPAG, 38000 Grenoble, France. (maximiliano.fastelli@gmail.com)

Introduction:

The interest in the detection of ammonia and ammonium-bearing minerals on the surface of ice bodies is related to their properties within subsurface brines for understanding the dynamics and composition of icy moons. After the *Galileo* mission to the Jovian moons, the *Cassini-Huygens* mission to Saturn, the *Dawn* mission that flyby Ceres and the *New Horizons* analyses of Pluto and its moons several questions were raised regarding the detection and the importance of ammonium minerals [1-6]

The surfaces of several icy bodies such as Ceres, Pluto and its moons were modelled using NH_4^+-bearingminerals to identify the spectral features located at ~1.65; ~2.21 and ~3.05 μm [7-8]. On these bodies, the presence of ammonium compounds has been associated with geological activity in the recent past, such as cryovolcanism, and the 'tectonic' exposure of ammonia-rich deposits or due to impact events [9]. In addition due to the reducing freezing temperature of water propriety [10], the presence of NH_4^+ minerals can also influence water density and modify the overpressure degree from a specific amount of freezing that triggers the emplacement of ammonia-rich cryolavas [11].

In this work, the low-temperature behaviour in relation to the phase transitions of a selected number of anhydrous and hydrated NH_4^+-bearing minerals in the 1-4.2 μm spectral range down to 65 K was analysed. This study is focused on understanding the effect of crystal-chemical modifications on the spectral features at temperatures like those presumed on the surface of icy moons. We intend to identify variations between the different mineral structures and their transformations at low temperatures to provide insights into the interpretation of remote-sensing data of icy bodies.

Results:

We analysed the reflectance spectra of a selected number of anhydrous and hydrated ammonium-bearing minerals containing different anions and water content.

All the samples were preliminary checked to evaluate the presence of ancillary phases and their purity using X-ray powder diffraction techniques (XRPD). Samples were sieved to obtain a controlled granulometry.

Reflectance spectra were collected at the Cold Surface Spectroscopy (CSS) facility (https://cold-spectro.sshade.eu) located at the Institut de Planétologie et d'Astrophysique (IPAG), Grenoble, France. The instrument used was the SHINE Spectro-Gonio Radiometer.

Spectra were collected in the 1-4.2 μm spectral range at different low temperatures between 65 and 290 K. The collected reflectance spectra show absorption features related to NH_4^+ group overtone and combinations in the 1-2.5 μm range. In particular, the bands located at ~1.09 μm ($3\nu_3$), ~1.3 μm ($2\nu_3 + \nu_4$), ~1.58 μm ($2\nu_3$), ~2.02 μm ($\nu_2 + \nu_3$) and ~2.2 μm ($\nu_2 + \nu_3$) could be useful to discriminate among these salts. The low temperature spectra, compared to those at room temperature, reveal fine structure displaying more sharper and narrower absorption bands. The selected NH_4^+-bearing minerals are subjected to reversible low temperature phase transitions, which is revealed in the spectra by a progressive growth and shift of the bands toward shorter wavelengths with an abrupt change of their depth.

Discussions:

The two main effects caused by low temperature are: (i) the wavelength shift of the absorption bands to higher frequencies as temperature decreases and (ii) phase trasitions related to NH_4^+ groups reorganizations.

As far as transformations are concerned, ammonium compounds are widely known and studied for their particular behaviour and properties at low temperatures. In the reflectance spectra of selected ammonium minerals, the effects of these structural variations affect the NH_4^+ and/or hydrogen bonds causing spectral changes and growth of additional bands. Of the samples analysed, the following show clear spectral evidence of transformations.

In mascagnite $(NH_4)_2SO_4$ a transformation occurs below 223 K, the structure becoming ferroelectric [12]. The most obvious changes of the mascagnite spectrum are at 1.8 μm with the growth of a new band and the change of spectrum slope at ~2.6 μm.

Salammoniac NH_4Cl spectra shows clearly the effect of the ordering of hydrogen bonds. Below 242 K an order-disorder phase transition (λ-transition) occurs [13] changing the overoall spectrum shape with the growth of new bands and drastic band position shifts.

Ammonium hydrogen phosphate $(NH_4)_2HPO_4$ undergoes to double-phase transition at ~246 K and ~174 K attributed to the different reorientation of NH_4^+ groups [14]. In this case, the two transitions do not

generate drastic changes but tend to modify the rate and slope of shift and/or increase of spectral band parameters.

Ammonium hydrogen sulphate $(NH_4)HSO_4$ undergoes two phase transitions: (i) at *T* ~270K from phase III to II, defined as second order in nature from para- to ferroelectric behaviour [15]. The second phase transition is clearly evidencedby an abrupt change in band positions and parameters and highlighted by shifts in position in the spectral features.

Conclusions:

To evaluate the remote sensing data and to distinguish between different types of ammonium-bearing minerals the bands considered in this work could be of great interest for the surface analysis of icy planetary bodies. The possibility of distinguishing which ammonium-bearing phase is present, has a great impact on the chemico-physical planetary models.

Cryogenic data can be useful for discriminating transient phases that impact the internal dynamics of ocean worlds [16]. Different mineralogical phases influence the buoyancy convection of the ductile region of the ice shell and impact on material resurfacing and subduction rate [17]. Finally, these data can be used as a proxy to determine the surface temperature of the bodies on which they will be detected.

In this perspective, this work provides a new set of spectral data useful for interpreting remote sensing data for present and future missions, such as New Horizons focused on the Pluto system, NASA's Europa Clipper and ESA's JUICE focused on the Jovian moons, and James Webb Space Telescope (JWST) on trans-Neptunian objects (TNOs).

Acknowledgements:

This work has been done in the frame of the Trans-National Access program of Europlanet 2024 RI which has received funding from the European Union's Horizon 2020 research and innovation programme under grant agreement No 871149.

References:

[1] Ammannito, E. and Ehlmann, B. (2022): 134-142. [2] Dalle Ore, C. M., et al. (2019) *Science advances 5.5* : eaav5731. [3] Fortes, A. D.(2000) *Icarus 146.2* 444-452. [4] Lacy, J. H., et al. (1975) *ApJ 198* L145-L148. [5] Matson et al. (2003) *The Cassini-Huygens Mission* 1-58. [6] Spencer, J., and Grinspoon, D. (2007). *Nature*, *445(7126)*, 376-377. [7] Cook, J. C. et al. (2023) *Icarus 389* 115242. [8] De Sanctis, M. C. et al. (2016) *Nature 536.7614* 54-57. [9] De Sanctis, M. C (2020). *Space Sci. Rev*, 216(4), 1-33. [10] Neveu, M. et al. (2017). *Geochim. Cosmochim. Ac. 212*, 324-371. [11] Martin, C. R., and Binzel, R. P. (2021). *Icarus*, *356* 113763. [12] Schlemper, E. O., and Hamilton, W. C. (1966) J. Chem. Phys., 44(12), 4498-4509. [13] Levy, H. A. and Peterson, S. W. (1952). Phys. Rev., 86(5), 766. [14] Hadrich, A. et al. (2000). *J. Raman Spectrosc. 31(7)* 587-593. [15] Swain, D. et al. (2012). *J. Phys. Chem. A, 116(1)*, 223-230. [16] Fortes, A. D., and Choukroun, M. (2010). *Space Sci. Rev., 153(1)*, 185-218. [17] Buffo, J. J. et al.(2020). *JGR: Planets, 125(10)*, e2020JE006394.

UV IRRADIATION EXPERIMENTS OF ORGANO-SULFATE MARTIAN ANALOG SAMPLES TO SUPPORT DETECTION OF ORGANICS ON MARS BY THE NASA MARS2020 AND ESA EXOMARS ROVERS

A. Alberini[1,2], C. Garcia Florentino[3], G. Poggiali[1,4], J. Brucato[1] and T. Fornaro[1]

[1]INAF-Astrophysical Observatory of Arcetri, largo E. Fermi 5, 50125 Florence, Italy (andrew.alberini@unifi.it), [2] Department of Physics and Astronomy, University of Florence, Via Giovanni Sansone 1, 50019 Sesto Fiorentino (Florence), Italy, [3]Department of Analytical Chemistry, University of the Basque Country UPV/EHU, P.O. Box 644, 48080 Bilbao, Basque Country, Spain, [4]LESIA – Observatoire de Paris PSL, Université PSL, CNRS, Sorbonne Université, Université de Paris, 5 place Jules Janssen, 92190 Meudon, France.

Introduction: The SHERLOC instrument onboard the NASA Mars 2020 Perseverance rover, currently operating on Mars at the Jezero crater, has detected fluorescence signals that can be interpreted as organic matter both in igneous rocks of the Crater Floor and in the sedimentary rocks of the Delta Front [1]. The most intense signals have been observed in association with sulfate minerals, which might have played an important role in the preservation of organic matter. Morevoer, Perseverance SuperCam suite include also a VIS-IR spectrometer [2] operating in the range 1.3–2.6 µm to investigate mineralogy of the site but also allowing some investigation on the possible presence of organic features.

This laboratory work investigates magnesium sulfate preservation of aromatic organic compounds plausibly present on Mars, such as the polycyclic aromatic hydrocarbons benzo[a]pyrene and dihydroxynaphthalene, and the carboxylic acids phthalic and mellitic acid, under martian-like UV irradiation.

Methods: Martian analog samples were prepared using an equilibrium adsorption method in which the organic compounds are dissolved in a proper solvent and mixed with the mineral for a time sufficient to reach the equilibrium state favoring the physico-chemical interactions between molecules and mineral surfaces as in natural processes of adsorption [3]. Then, the samples were dried in oven in mild conditions to simulate the deposition of any organic molecules on mineral as a result of planetary drying that occurred in the post-noachian geologic eras.

UV irradiation experiments were performed using an experimental setup assembled at the INAF-Astrophysical Observatory of Arcetri, in which the UV light emitted by a Xenon lamp (good simulator of the Solar spectrum) was focused on the sample through an optical fiber inserted directly in the sample chamber of a Vertex 70v FTIR interferometer (Bruker), equipped with a Diffuse Reflection Accessory to acquire diffuse reflectance spectra of the sample in situ during UV irradiation and follow the degradation kinetics in real time (Fig. 1) [3][4]. Experiments were conducted under a nitrogen flux at ambient temperature and pressure.

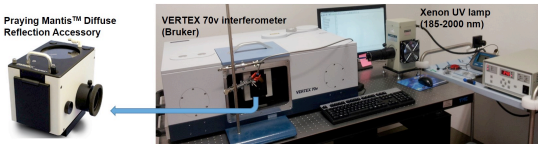

Fig. 1. *UV irradiation experimental setup at the INAF-Astrophysical Observatory of Arcetri*

Results: Investigations of the photostability of organics adsorbed on minerals are critical to understand whether the mineral has a photoprotective or photocatalytic role and thus suggest to Perseverance one class of minerals to analyze over others to have a higher probability of detecting organic molecules [5]. The effect of UV needs to be taken into account to get a better idea of the molecular targets to look for in natural surfaces highly degraded by UV and to test how quickly subsurface organic material can be altered by ambient UV once revealed by Perseverance's abrasion tool. Experiments done at the Arcetri Astrobiology Laboratory shed light on the behavior of magnesium sulfate toward the four molecules mentioned above. For example, in the case of benzo[a]pyrene adsorbed on magnesium sulfate, a photoprotective behavior of the mineral toward the aforementioned organic molecule was observed, as reported in Fig. 2.

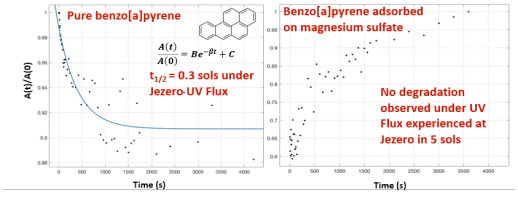

Fig. 2. *Degradation kinetics for the vibrational band at 1510 cm^{-1} of pure benzo[a]pyrene and benzo[a]pyrene adsorbed on magnesium sulfate.*

These experiments have the more general goal of creating a database of infrared spectroscopic features for molecular-mineral complexes, which will aid the

interpretation of spectroscopic data from the current Mars 2020 mission and the future ExoMars mission, and generally expand the availability of laboratory spectroscopes for the interpretation of spectroscopic data from planetary surfaces.

References:

[1] Scheller, E. L. et al. (2022) *Science*, eabo5204.
[2] Fouchet, T. et al. (2022) *Icarus*, 373, 114773
[3] Fornaro, T. et al., (2020) *Front. Astron. Space Sci.,* 7, 91.
[4] Fornaro, T. et al., (2018) *Icarus*, *313*, 38-60.
[5] Fornaro, T. et al., (2018) *Life*, 8, 56.

Simulating icy-world surfaces in the laboratory: NIR spectra of natron, mirabilite and epsomite dissolved in water. D. Fulvio[1], C. Popa[1], F. Tosi[2], S. De Angelis[2], M. Ciarniello[2], A. Mura[2], V. Mennella[1], and G. Filacchione[2], [1]INAF, Osservatorio Astronomico di Capodimonte, Salita Moiariello 16, 80131, Naples, Italy (daniele.fulvio@inaf.it), [2]INAF, Istituto di Astrofisica e Planetologia Spaziali, Via del Fosso del Cavaliere 100, 00133, Rome, Italy.

Introduction: Hydrated salts are thought to be among the possible surface components of several icy-world satellites (e.g., [1-6]). In this context, we have selected three hydrated salts of potential planetary interest – natron ($Na_2CO_3 \cdot 10H_2O$), mirabilite ($Na_2SO_4 \cdot 10H_2O$), and epsomite ($MgSO_4 \cdot 7H_2O$) – diluted them in H_2O and investigated the changes in their NIR reflectance spectra while frozing them at cryogenic temperatures simulating the ones found on the surface of icy-world satellites (down to 95 K). The main objectives of this laboratory study are to investigate: (i) the NIR spectral changes induced in the hydrated salt spectra by the mixing and melting with water, (ii) the changes induced by the freezing of the samples down to 95 K, and (iii) the spectral properties of binary mixtures of salts in water.

Laboratory Experiments: We used a Harrick Praying-Mantis accessory for diffuse reflectance spectra coupled to a liquid nitrogen cooled Reaction Chamber. This setup was inside the sample compartment of an FTIR spectrometer (Bruker Vertex 70v), operated in the NIR spectral range from 0.8 to 3.6 μm. An average of 250 scans with 4 cm^{-1} resolution was used. The samples were loaded in form of powder into a homemade stainless-steel sample holder, attached to the bottom of the Reaction Chamber. A thermocouple was employed for measuring the sample temperature while the experiments were performed. A gold coated commercial quartz-crystal microbalance (QCM hereafter) was used as substrate for the mineral samples and reflectance standard [7]. To limit atmospheric water condensation on the cooled sample, a dual stage purging system was implemented: a dry-air purging line was applied within the Praying-Mantis accessory while a dry-N_2 line was purging the Reaction Chamber during the experiments.

Coarse samples of natron, mirabilite, and epsomite were bought by Sigma Aldrich and grain powders in the size range 75–100 μm were obtained after grinding and sieving. Each selected powder was firstly loaded into the sample holder and demineralized water was therefore added on top of it. For all experiments we always started by measuring the mineral(s):water sample at room temperature (298 K) and after that the sample was frozen down to 95 K, while spectra were acquired at different intermediate temperatures.

Results: Table 1 summarizes the experiments performed in the context of the present study. The temperature dependence of NIR spectra of pure salts of natron, mirabilite, and epsomite dissolved in water will be discussed as well as spectra of the binary mixtures natron:epsomite, natron:mirabilite, and epsomite:mirabilite in water. The spectra of the present experiments will also be compared with previous experimental studies conducted on pure endmember salts [8-10]. Finally, in our analysis particular focus will be given to the changes of the absorption band minimum position with temperature.

mineral 1	mineral 2	Ratio mineral(s):water	T_{min}
natron	-	1 : 3	95 K
mirabilite	-	1 : 3	95 K
epsomite	-	1 : 3	95 K
natron	mirabilite	1 : 3	95 K
natron	epsomite	1 : 3	95 K
epsomite	mirabilite	1 : 3	95 K

1 Table 1: summary of the experiments discussed in the present study.

Conclusions: We will show that mixing of hydrated salts with water induces a complex phenomenology characterized by the formation of new bonds and absorption features. The shape and minimum position of the NIR features are temperature-dependent. The present laboratory study will be extremely useful to interpret the high-resolution data of Jupiter's icy satellites surfaces, available in the next future thanks to the MISE and MAJIS instruments aboard NASA Europa Clipper and ESA JUICE spacecraft, respectively.

Acknowledgment: The authors acknowledge financial support from the Mainstream INAF project: "Caratterizzazione delle superfici dei satelliti di Giove

mediante osservazioni di Juno-JIRAM e misure di laboratorio nell'infrarosso" (INAF Grant 1.05.01.86.11). This research has made use of NASA's Astrophysics Data System.

References: [1] Dalton J. B. et al. (2005) *Icarus, 177*, 472-490. [2] Durham W. B. et al. (2005) *JGR, 110*, E12010. [3] Carlson F. G. et al. (2009) *Europa's Surface Composition, pp. 283.* [4] McCord T. B. et al. (2010) *Icarus, 209,* 639-650. [5] Niles P. B. et al. (2013) *SSR, 174,* 301-328. [6] De Sanctis M. C. et al. (2017) *Science, 355,* 719-722. [7] Allodi M. A. et al. (2013) *SSR, 180,* 101-175. [8] De Angelis S. et al. (2017) *Icarus, 281,* 444-458. [9] De Angelis S. et al. (2019) *Icarus, 317,* 388-411. [10] De Angelis S. et al. (2021) *Icarus, 357,* 114-165.